Translation Report   T-A2049-26

AEROSTATIC [EXTERNALLY-PRESSURIZED **NASA** CR **71054**
GAS LUBRICATED] THRUST BEARINGS

N66-19622

by

Erwin Loch

Translated from a doctoral thesis submitted
to the Technical University of Graz, Austria

THE FRANKLIN INSTITUTE RESEARCH LABORATORIES

BENJAMIN FRANKLIN PARKWAY AT 20TH STREET, PHILA. 3, PA.

AEROSTATIC [EXTERNALLY-PRESSURIZED
GAS LUBRICATED] THRUST BEARINGS.

By

Erwin Loch

Translated from a doctoral thesis submitted
to the Technical University of Graz, Austria.

AEROSTATIC [EXTERNALLY-PRESSURIZED
GAS LUBRICATED] THRUST BEARINGS.

(Calculation and Experiments).

AEROSTATISCHE AXIALLAGER

(Berechnung und Versuche)

From the Faculty of Mechanical Engineering and Electrical Engineering

of the

Technical University of Graz, Austria

As a requirement for graduation to Doctor of Engineering

Thesis submitted by

Erwin Loch

A native of Innsbruck, Tirol (Austria)

Reviewer: Professor H. Winter

Co-Reviewer: Professor A. Steller

Summer 1962

The present research work was performed at the firm
Escher Wyss, A. G., in their Research Laboratories
at Zurich, Switzerland. This report is part of the
development program for aerodynamic* and aerostatic*
gas bearings.

The writer would like to thank especially Dr. C. Keller,
Director of the Escher Wyss Research Division, and his
assistant, Dr. W. Spillmann, who graciously approved the
publication of this paper.

Zurich, Summer, 1962.   Erwin Loch

* Editor's Note

The terms "aerodynamic" and "aerostatic" are used throughout
this thesis. In the United States however, the generally
accepted and preferred designations for these types of gas-
lubricated bearings are "self-acting" and "externally-
pressurized" respectively. This recommendation was made in
about 1958 by a Technical Coordination Committee formed to
review the research work in the field, sponsored by the
Office of Naval Research in conjunction with many other
agencies of the United States government.

Preface

This report is a translation of the doctoral thesis by Erwin Loch, on the subject "Externally-Pressurized, Gas-Lubricated Thrust Bearings", that was submitted to the Technische Hochschule, Graz, Austria in 1962.

It deals with the static and dynamic characteristics of single- and double-acting thrust bearings of many geometrical forms in such a thorough manner that it seemed very desirable to translate this important work into the English language to enhance its usefulness. The extensive theoretical analysis of these bearings included in the thesis is matched by the abundant experimental data taken from a series of tests performed in the research laboratories of Escher Wyss at Zurich, Switzerland.

We wish to express our thanks to Dr. Erwin Loch for authorizing this translation and for his kind assistance in bringing it to completion, and to Mr. Stanley Doroff, Fluid Dynamics Branch, Code 438, O.N.R., Washington for providing the necessary support.

The translation was done by Dr. Hans Figdor of the Franklin Institute's Science Information Service. Technical editing was done by Prof. Dudley D. Fuller. Typing by Mrs. Anna H. Karle.

<div align="right">

W. W. Shugarts, Jr., Manager
Friction & Lubrication Laboratory

</div>

Table of Contents

1. <u>Principally used designations</u>

A	caloric working equivalent	kcal/kpm
b	width of the compensation channel	m
d	smallest nozzle diameter	m
F_D	effective cross section surface of the inlet nozzles	m^2
F_L	bearing surface	m^2
g	acceleration of gravity	m/sec^2
G	flow of bearing gas	kg/sec
h	height of the bearing slit	m
H	head by the compressor of bearing gas	m
n	number of the inlet nozzles	
K	absolute axial force	kp
N	output	kpm/sec
p	absolute pressure	kp/m^2
r	radius of the bearing	m
R	gas constant	$m/°K$
s	depth of the compensating channel	m
t	time	sec
T	temperature	$°K$
v	local velocity	m/sec
w	radial velocity averaged over h	m/sec
Re	Reynolds number	
γ'	specific gravity	kg/m^3
η	dynamic viscosity	$kpsec/m^2$
$\varkappa$	adiabatic exponent	
λ	heat conductivity of the gas	$kcal/msec\ °C$
λ_r	coefficient of friction	
Ω	angular velocity	1/sec

Indices

a	flow outwards in the direction + r
i	flow inwards in the direction -r
B	condition prior to exposure to the throttling elements
1	inlet to the bearing slit
2	outlet from the bearing slit
I	carrying or loaded side of the bearing
II	non-carrying or unloaded side of the bearing

2. Short synopsis of the most important literature

Shires studies in a report (IX) the flow of air through long, narrow clearances with rectangular cross sections. Both laminar and turbulent flows were discussed. The results for different shapes of clearances showed a satisfactory agreement between theory and experiments as far as pressure profile, flow and temperature are concerned.
Basic parameters in the comparison were the friction coefficient λ and the Reynold number; the results were also compared with the laws found by Blasius for incompressible liquids. Shires concluded that, in laminar flow, the resistance coefficients λ are in good agreement with the incompressible flow whereas, in turbulent flow, the λ - values given by Blasius are, in general, not applicable.

The paper by Deuker and Wojtech (VII) describes the radial flow of compressible liquids between closely adjacent parallel circular discs. The kinetic energy term in the equation of flow was included in the investigations. By several successive transformations of the variable magnitudes, the equations are converted into an expression which can be graphically integrated. From the plurality of calculated velocity curves, a solution for the pressure profile in the bearing is determined. This paper includes both compressible and non-compressible cases. The author states that, in compressible flow, the change of state of the gas can be assumed as $p \gamma^m = $ constant, the polytropic exponent m changing with the radius. A simplification of the equations was achieved in the following way: For the flow in the immediate vicinity of the inlet nozzle, i.e., with small radii, an isentropic change of state of the gas in the clearance was assumed; in the other areas of the bearing, an isothermal change. The investigation referred to various conditions at the inlet for Mach numbers between 0 and 1.

Comolet (VIII) compiles, in the form of a small textbook, the two-dimensional flows of viscous liquids and gases for the longitudinal and radial flow between two fixed parallel plates. It is based on a polytropic change of state of the gas. The investigations are widely applicable, since also inertia forces, the effects of which are sometimes considerable, have been considered. The equations obtained allow the derivation of known results for the most simple cases. The experiments performed confirm the theoretical assumptions and define the range of applications of the suggested equations. For the radial-divergent clearance (flow from a source in the center of two parallel circular discs), the flow is laminar and isothermal whenever the Renumber at this location is smaller than 1100. This critical Renumber for the sudden change from laminar to turbulent flow is approximately one half the number found for the parallel clearance. Comolet traces this back to the fact that the divergent flow in the immediate vicinity of the gas feed, i.e., with small radii, has instability factors which do not occur in the parallel and convergent flow. In the case of thrust bearings where the flow is radially outward from a central chamber, Licht and Fuller (IV) derived the equations of laminar clearance flow for the pressure profile, the height of the clearance, the load capacity and the

flow. In doing this, they assumed that the change of state of the gas was isothermal. In the general energy equation, however, the increase of kinetic energy of the radial velocity and the influence of rotation were not taken into consideration. A comparison between the theoretical results and the measured values showed a good agreement within the range of the experiments.

Laub (X) discusses in his paper the mathematical interrelationships for similar bearings as (IV) and under the same conditions. Of great interest, in this connection, are the measuring technique used and the experimental setup. This paper includes a synopsis of the most important contributions in the field of aerostatic bearings.

Pigott and Macks (V) conducted experiments in a non-rotating thrust bearing which was fed by compressed air at temperatures up to 540° C. Simplified expressions were used in the description of the flow through the capillary nozzles used and the bearing clearance. The results were shown in the form of curves and compared to the experimental values in a wide range of temperatures and load capacities. In this connection, they confirmed the fact that the load capacity of gas bearings is increased with increasing temperature of the gas on account of the increased dynamic viscosity. In the range of very high temperatures, however, the theoretical and experimental values for the height of the clearance and throughput were no longer in agreement on account of distortion of the disc of the bearing. Besides, there is a short report on the occurrence of instabilities in the bearing, i.e., self-excited oscillations, in one of the experiments.

The authors Hughes and Osterle (VI) made a theoretical investigation of the influence of rotation in a revolving bearing disc on the load capacity of a static thrust bearing with laminar flow outward. This investigation had the following result: When the lubricant is a viscous liquid, the load capacity of the bearing changes considerably with increasing angular velocity; if, however, a gas flows through the bearing clearance, the influence of rotation on the load capacity is very small.

In another paper (XVI), Hughes and Osterle first defined the range of applicability for adiabatic and isothermal operating conditions with radial clearance flow, and then investigated the intermediary range with consideration of the heat transfer between gas and bearing discs. Based on a simplified model, it was found that the flow in the bearing clearance is in most cases, especially at high temperatures, predominantly isothermal. Besides, equations for the calculation of the radial temperature distribution were derived and the results of actual experiments were compared with the isothermal and adiabatic flow.

The report by Licht, Fuller and Sternlicht (XVII) discusses the problem of the pneumatic instability of an aerostatic thrust bearing. The appearance of self-excited vibrations is traced back to the compensation spaces which are in most cases arranged in the fixed bearing disc. By means of a method which corrects nonlinear distortions, the problem is opened to an analytical study. Confirmed by the experimental results, the authors could show in a thrust bearing with a central compensating space that the greatest stability of self-excited vibrations (air-hammer)

is reached with the lowest depths of the compensation space, the narrowest bearing clearances and the highest input pressures. Further considerations and experiments showed the advantage of nozzles with large cross sections and short boreholes (orifices) compared to nozzles with small cross section surfaces and long boreholes (capillaries).

Similar conditions and equations for the description of self-excited vibrations in aerostatic thrust bearings are the basis of the paper by Roudebush (XVIII). By means of a digital computer, highly systematical investigations on the influence of the various parameters (height of the clearance, pressure, compensating space, vibrating mass) on the stability of the bearing are performed. For some actual examples, the amplitudes of vibration are determined and represented as a function of time. The author emphasizes that the volume of the compensating space as well as the rigidity of the bearing are responsible for the pneumatic instabilities.

In the reference (XIX), the phenomenon of self-excited vibrations in aerostatic bearings is interpreted by means of a vectorial representation. Richardson makes a distinction between a static and a dynamic rigidity of the bearing. The result of his studies is that the relation between dynamic force and deflection of the bearing behaves like a static spring constant with a leading and trailing effect. While the restoring and deflecting force, respectively, of the sinusoidal motion of the bearing mass is trailing with the time, it is preceded by a negative damping force. The stability criterion was obtained from the condition of a positive damping. In order to illustrate the application of the derived equations, a comparison was made between two customary aerostatic bearings with compensating channel and nozzles opening directly into the clearance, respectively.

I would like to mention the papers (XX), (XXI) and (XXII) by the authors Licht and Elrod, without commenting on them; they relate, likewise, to the problem of self-excited vibrations in aerostatic bearings.

Gottwald and Vieweg (XXIII) made calculations and model experiments in static hydraulic and air bearings. In a conical bearing with annular clearance inlet and in a thrust bearing consisting of two circular discs with central inlet borehole, the mathematical interrelationships between the course of the pressure in the clearance, the flow volume, the load capacity and the moment of friction were determined partly analytically and partly graphically. The influence of the size of the nozzle borehole diameters on the stability of the bearing was especially emphasized in one chapter.

3. Review of the items covered in this study.

Based on the energy phenomena, an equation of general applicability for small disc clearances, for radial equilibrium of the compressible clearance flow with consideration of rotation is derived.

Furthermore, it will be shown that the heat transfer of a flowing gas between two discs in close vicinity to each other is very good and that, under certain conditions, the clearance flow is subject to an isothermal change of state.

All calculations and investigations have been extended to bearings
through which the flow is in two directions, i.e., outward and inward.
For the laminar, isothermal radial flow, the pressure distribution in
the bearing clearance and the throughput volume are derived by means
of a simple approximation (w, dw = 0, Ω = 0) and an extended approx-
imation (w.dw. $\neq$ 0, $\Omega \neq$ 0).

A discussion of the flow equations obtained shows the influence of
kinetic energy, of rotation of a disc, of gas-dynamic effects and
of labyrinth positions. This study is followed by a synopsis of the
observations on the conditions at the sudden transition from laminar
to turbulent flow, which have been made by various authors.

Based on the friction values for the turbulent clearance flow given
in the literature, the course of the pressures and throughput volumes
are calculated for the turbulent isothermal radial flow in a simple
case (w.dw= 0, Ω= 0)

Although the solution of the load capacity integral for the simple
approximation of the laminar isothermal radial flow in narrow clearances
for the positive r - direction had already been known, the result could
be evaluated in such a way that the carrying capacity of any bearing
whatsoever can be determined without calculations, by the introduction
of a dimensionless factor C_{ka} which depends only on the respective
radii and pressure ratio. The solution of the load capacity integral
of the laminar flow for the negative r - direction, which is, likewise,
characterized by a dimensionless factor, C_{ki}, as well as the integral
solution for the turbulent isothermal radial flow are added as novel
items.

Another chapter deals with the optimization and economical calculations
of the bearings. Various criteria lead to the establishment of the
optimum bearing geometry as far as the site of the gas inlet is concerned.
The minimization of the total power input for an aerostatic bearing yields
optimum values for the compensating space and the height of the clearance.
A comparison of the power losses illustrates the applicability of different
gases. For double-acting and symmetrically designed thrust bearings, an optimum
nozzle pressure ratio is defined and calculated by means of minimization of
the compressor output (bearing gas production).

The description of the individual throttle elements includes the properties
and basic calculations for cylindrical nozzles and apertures, capillary
nozzles, venturi nozzles and throttles with pressure-dependent, variable
cross sections. With the aid of theoretical studies and the results of
measurements, the advantages of venturi nozzles over regular cylindrical
nozzles will be shown (cf. also German Patent 1,070,452). Whereas the
present paper gives only a reference to the gas feed through surfaces of
porous material directly into the bearing clearance, the calculation and
design of such bearings is the subject of another paper.

Another chapter is devoted to the non-radial isothermal clearance flow.
If the influence of inertia of the gas and the disc rotation is disregarded,
the flow distribution can be represented as a potential function where the
correlation between ϕ, ψ and p, w deviates from that of the incompressible

flow. General relations between the pressure profile, the load capacity and the throughput volume are given. With the aid of a bearing with several individual nozzles which open directly into the bearing clearance, the influence of the number of nozzles on the carrying capacity and throughput volume is determined and compared to the respective measuring results.

From the equilibrium condition for the amount of gas which flows into the bearing through the inlet nozzles and escapes again through the clearance, dimensionless bearing characteristics are derived and are represented in the form of curves, as functions of gas and pressure parameters for laminar and turbulent clearance flow. The characteristics are applicable to feed systems with short cylindrical nozzles or apertures and any arrangements whatsoever of bearings and flows.

Several experimental results of heating of the bearing, bearing characteristics, pressure profile in the clearance, volume of throughput and load capacity in specially designed bearing testing equipment confirm the correctness of the theoretical derivations. Besides, a simple method is described for determination of axle shift actually occurring in a machine.

The derivation of the amplitude equation was taken from the literature on self-excited vibrations in aerostatic bearings and was applied to bearings with ring-shaped supporting surface. With the aid of some comparisons and measurements, the influences of feeding nozzles, the compensation volume and other parameters on the bearing stability are pointed out. All previous developments and theoretical efforts concerning the design of stable aerostatic bearings relative to self-excited vibrations tend to dimension the compensating spaces in the bearing in such a way that the vibration described above does not occur. Conversely, in the present paper, methods for damping the vibrations are suggested. The knowledge of the oscillating frequency of the bearing system allows the design of damping elements which can be installed in the bearing discs in the form of Helmholtz resonators. Finally, axial vibrations can appear without the presence of compensating spaces. The possibilities of removing these instabilities are discussed.

4. Design and mode of operation of aerostatic thrust bearings.

The bearings described in this report consist of at least two parallel discs which are separated from each other by the bearing clearance; one of them is fixed on the rotating machine shaft, the other in the casing either rigid or self-adjusting. The passage of the machine shaft through the fixed disc requires an annular supporting surface. In order to keep the bearing clearance permissible for safe operation as small as possible (low gas consumption), the bearing discs should be plane, parallel to each other and should have finely ground surfaces.

The bearing gas is under increased pressure p_B and is taken from a source located outside the bearing; it can be admitted to the bearing

clearance in different ways. Upon entering into the clearance, the gas stream is divided in such a way that one part flows outward, the other towards the inside in the direction of the shaft center.

In order to attain a load capacity as high as possible in the bearing, it is desirable to utilize the highest pressure p_B of the bearing gas which may be stored, e.g., in a container. In a bearing designed according to this requirement, the gas feeding duct should enter the bearing clearance with its whole cross section either directly or across an annular compensating channel. If the volume of the gas container is large enough to keep the pressure in the reservoir p_B constant even at a high rate of withdrawal, (large bearing clearance) and if the pressure loss in the feeding duct is disregarded, the pressure distribution and the average loadability $\bar{p}$, i. e., the carrying capacity of the bearing, is independent of the height of the clearance h. Such a bearing can be designed for one single load capacity only. Since any height of clearance can appear at the given axial force, the bearing is in an indifferent equilibrium. The through-put volume which is proportional to h^3 would assume undesirably high values at great heights of the clearance. Thus the bearing does not have either a defined or a limited gas consumption.

If the bearing just described is fed directly from the compressor (for example, a multiple-stage piston compressor) without an inter-polated gas reservoir and this compressor aspirates permanently the same amount of gas from the surroundings and pumps it into the bearing, a definite pressure p_B adjusts itself corresponding to the height of the clearance and depending on h. Since, for example, the flow volume is

$$G \sim (p_B^2 - p_2^2) \, h^3$$

for laminar isothermal clearance flow (equations 7.19 and 7.20), the average load capacity for $\dot{G}$ = constant is, therefore

$$p \sim p_B \sim \sqrt{p_2^2 + \frac{const}{h^3}} \, .$$

Thus the load capacity of the bearing decreases with increasing height of the clearance. Although such a bearing has a fixed equilibrium position, it has a definite and limited gas consumption. The bearing system described here can, however, only be used where no changes of load, or very slow ones, are to be expected. If there occurred suddenly an appreciable additional load, the bearing clearance would drop to zero on account of the compressibility of the medium in the feeding system, and only after a certain period of time, when the compressor has produced a higher pressure p'_B in the duct system, a clearance corresponding to the new load is formed. For reasons of design, the duct volume between compressor and site of inlet to the bearing cannot be brought to the desirable
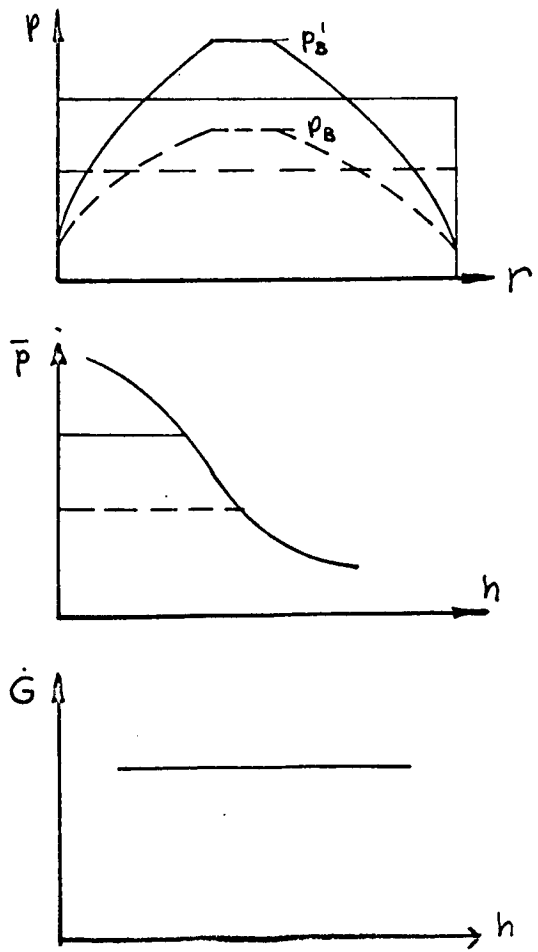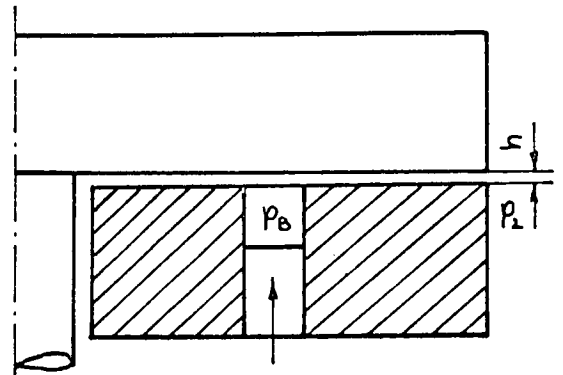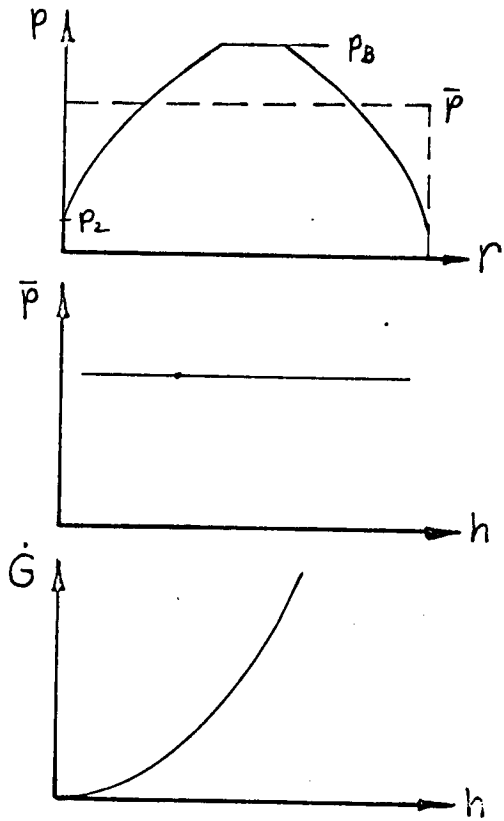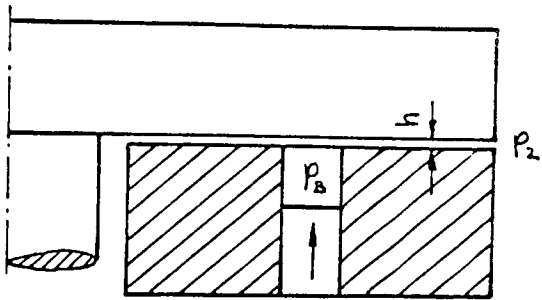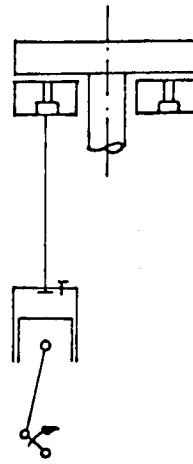
minimum value. Another disadvantage of this system appears when the bearing discs are in oblique position to each other. If the bearing is fed by only one single compressor, a major part of the gas would escape on the side of the wide bearing clearance and the pressure in the duct system would be reduced considerably. The conditions are considerably better in bearings which are in principle similar, but for incompressible liquids. The so-called supporting source bearings in large machine tools (vertical boring mills) have proven very satisfactory and result in a higher efficiency and better level course than hydrodynamic pivot bearings. They are designed in such a way that individual pockets which are separated from each other are arranged in the fixed bearing disc. The lubricant is fed under pressure into each pocket by a separate feeding system (including an oil pump). Since the pumps are adjusted in a way that they supply the same amount irrespective of the pressure, an oblique position of the faceplate, for instance by unilateral loading, is avoided. Likewise, the height of the bearing clearance remains automatically the same with all loads and r.p.m.

In aerostatic bearings, the supporting gas is led into the clearance across throttling elements. The throttle elements which remove the disadvantages described above may consist of individual nozzles which open directly into the bearing clearance or into a compensating space or are designed as continuous annular clearance. The throttles limit the volume of throughput at great heights of the clearance and thus achieve a maximum pressure p_1 and average pressure $\bar{p}$ dependent on the bearing clearance. The volume of throughput $\dot{G}$ increases first with increasing bearing clearance and reaches a constant value at the critical flow out of the throttles. The limitation of quantity induces, however, also a reduction of pressure; thus the highest available feeding pressure p_B will never be applied, but always only a lower pressure p_1.
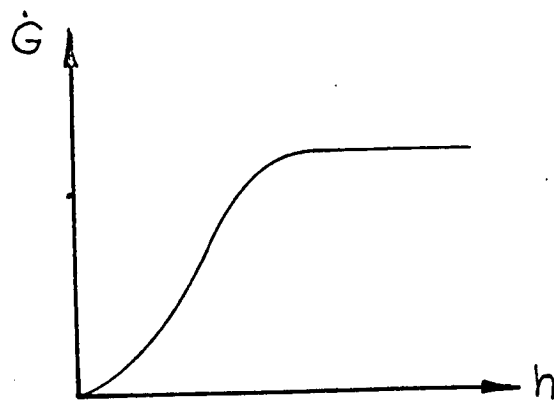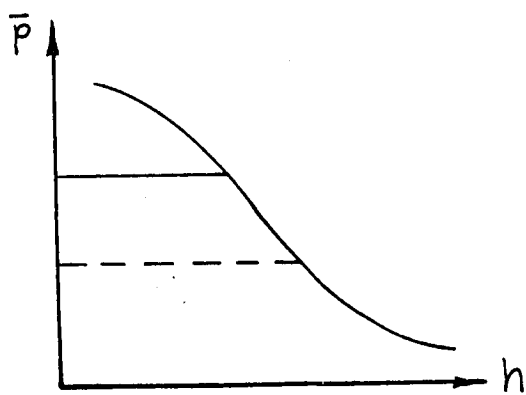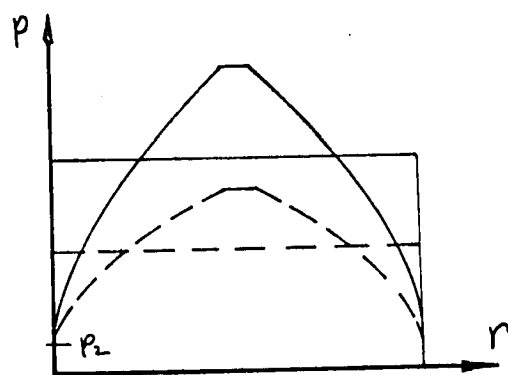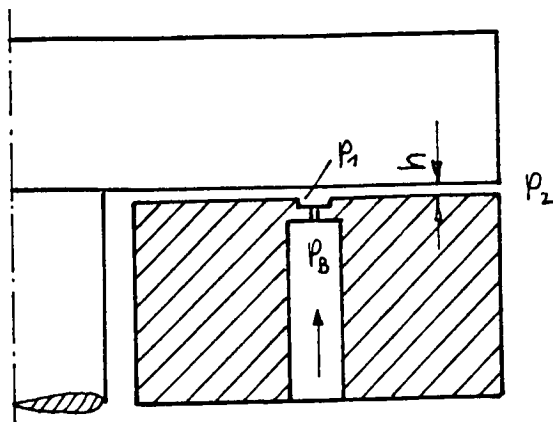
5.   Study of the energy.

The gas is admitted into the bearing clearance under the pressure p_1.
Besides, a torsional moment M_d, which is generally designated as
bearing friction moment, is introduced. This torsional moment gives
the bearing gas a circumferential speed v_φ (z), i.e., an angular
force and overcomes in addition the tangential shearing stress
components. The actual course of v_φ (z) will,
therefore, be adjusted in such a way that the
bearing friction moment is greater than the
counter-moment on the fixed bearing disc.
($M_d > M_o$). In order to facilitate the
analytical studies, a linear course,
however, of v_φ across the bearing
clearance h will be assumed.

$$V_\varphi = r\Omega \frac{z}{h}$$

(5.1)

This is, of course, only an approximation, since
in this case $M_d = M_o$; this means that no momentum
is left over for producing v_φ or the torsional
flow, respectively. The error which occurs when
it is assumed that the distribution of v_φ is
linear is small according to reference (I), p. 404
and to (II) at very narrow disc distances. A greater
deviation from this approximation occurs only at:

$$Re_h = \frac{h\Omega}{\nu} = \frac{h^2\Omega p}{\eta g RT} > 3$$

(5.1a)

Generally, however, Re_h is less than 3 in the
practical design of gas bearings. The height
of the clearance in the bearing should be as
small as possible on account of the gas con-
sumption. The lower limit of h_{min} for safe
operation must be selected more in considera-
tion of oblique position of the discs by errors
in assembly and by deformation rather than of the
roughness of the discs. Clearances of a width
between 15 and 30 x 10^{-6}m having proven satisfactory.
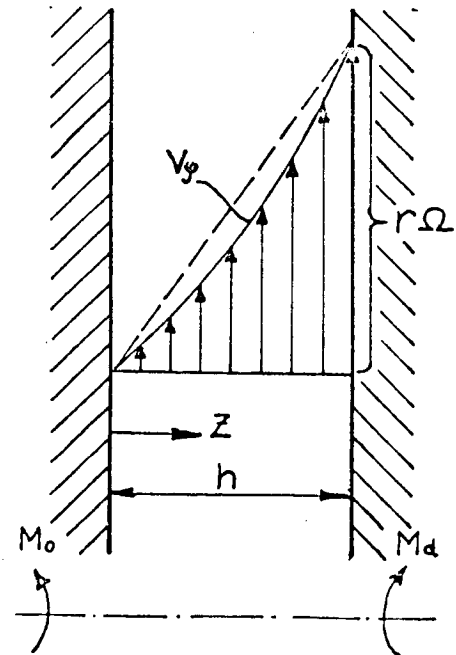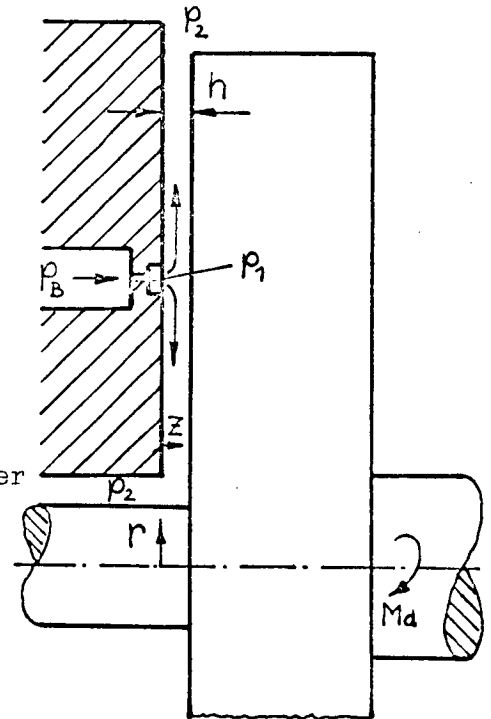
A centrifugal force which performs work when the flow is in radial direction acts upon the displaced gas particles between the rotating and the fixed disc. The exact connection between acceleration, the pressure and viscosity forces in radial direction can be derived from the Navier - Stokes equation for laminar flow. From

$$v_r = v_r \quad (r,z)$$

$$v_\varphi = v_\varphi \quad (r,z) \quad and$$

$$v_z = 0$$

the following can be concluded:

$$v_r \frac{\partial v_r}{\partial r} - \frac{v_\varphi^2}{r} = -\frac{1}{\rho}\frac{\partial p}{\partial r} + \nu\left[\frac{\partial^2 v_r}{\partial r^2} + \frac{\partial v_r}{r\,\partial r} - \frac{v_r}{r^2} + \frac{\partial^2 v_r}{\partial z^2}\right] . \qquad (5.2)$$

If one turns from this equation which applied to the annular element $2r\pi\,dr.dz$ to average values of the width of the clearance (annular element $2r\pi.h.dr$), this is transformed, if the following applies:

$$W = \frac{1}{h}\int_0^h v_r \, dz \qquad (5.2a)$$

into

$$\underbrace{\frac{w\,dw}{g}}_{} - \underbrace{\left\{\frac{1}{gh}\int_0^h \frac{v_\varphi^2(z)}{r}\,dz\right\}}_{}dr = \underbrace{-\frac{dp}{\gamma}}_{} + \underbrace{\frac{\eta}{\gamma}\left[\frac{d^2w}{dr^2} + \frac{dw}{r\,dr} - \frac{w}{r^2} + \frac{d^2w}{dz^2}\right]dr}_{-\,d\alpha_R} \qquad (5.3)$$

$\qquad\qquad\qquad\qquad\qquad\qquad\qquad\qquad$ Reibungsarbeit der Wand-
$\qquad\qquad\qquad\qquad\qquad\qquad\qquad\qquad$ schubspannungen in radi-
$\qquad\qquad\qquad\qquad\qquad\qquad\qquad\qquad$ aler Richtung

$\qquad\qquad\qquad\qquad\qquad\qquad$ Arbeit der Druckkräfte

$\qquad\qquad +\{\ \}\qquad$ Arbeit der Fliehkräfte

Beschleunigungsarbeit in radialer
Richtung (=Zuwachs an kinetischer
Energie)

(Reibungsarbeit......): friction effect of the shearing stresses in the wall in radial direction.
(Arbeit der Druck....): effect of the pressure forces
(Arbeit der Flieh...): effect of the centrifugal forces
(Beschleuingungsarbeit...): effect of acceleration in radial direction
$\qquad\qquad\qquad\qquad\qquad\qquad$ (= increase in kinetic energy).

In this connection, centrifugal force energy means that work is performed by a torsional moment M_d and that rotation of the gas is induced thereby. The centrifugal forces acting upon the gas particles thus work in radial direction. The equation No. 5.3 can, therefore, be written in the following way:

$$\frac{w\,dw}{g} - db + \frac{dp}{\gamma} + da_R = 0 \quad . \tag{5.4}$$

It is shown by equation No. 5.1 that the energy required for acceleration in circumferential direction is assumed to be so small that it can be disregarded. Equation No. 5.4 represents thus the energy equation of the flow in general form. It can, therefore, be used for the calculation on bearings with laminar as well as with turbulent flow if the respective members are introduced.

6. ## Radial temperature profile.

In order to obtain a general idea about the change of state of the gas during the flow through the clearance, an estimation with the aid of the laminar flow with heat exchange on the surfaces of the discs is attempted. According to the first principal theorem of thermodynamics, the following applies:

$$c_p\,dT = dq_{zu1} + dq_{zu2} + A\,da_R + A\frac{dp}{\gamma} \quad . \tag{6.1}$$

where c_p is the specific heat of the gases in kcal/kg °C; A is the caloric energy equivalent in Kcal/m kp: T means the average temperature across the width of the clearance in degrees K; dq_{zu1} is the heat introduced or removed by heat conduction relative to the unit of the weight of the throughput, in kcal/kg; dq_{zu2} is the heat of friction produced by the tangential shearing stresses, in kcal/kg; $A.da_R$ is the heat generated by radial shearing stresses on the walls, in kcal/kg; p means the static pressue of the gas in the clearance, in kp/m²; γ^* is the specific gravity of the gas, in kg/m³.

For the further studies in this connection, a simplification can be made by disregarding the first two members of the equation No. 5.4, since they are negligible in comparison to the two other members.

$$\frac{w \, dw}{g} - db \ll \frac{dp}{\gamma} + da_R \quad . \qquad (6.1a)$$

An estimation showing in which cases this approximation is valid
will be given in Chapter 8.1. Thus, if

$$\frac{dp}{\gamma} + da_R = 0 \qquad (6.2)$$

is introduced into equation No. 6.1, the first principal theorem
is reduced to:

$$c_p \, dT = dq_{zU1} + dq_{zU2} \quad . \qquad (6.3)$$

The amount of heat transmitted by a bearing disc per annular
surface element $2 \, r \, \pi \cdot dr$ to the gas or, conversely, from the
gas to the disc by heat conduction, relative to the unit of
the amount of gas flowing in radial direction is

$$\frac{dQ_{zU1}}{\dot{G}} = \frac{2 \, r \pi \, dr \, \alpha \, (T_w - T)}{\dot{G}} \quad . \qquad (6.4)$$

If it is assumed that both discs which determine the clearance
have the same wall temperature T_w, the following results:

$$dq_{zU1} = 2 \, \frac{2 r \pi \, dr \, \alpha \, (T_w - T)}{G} \quad . \qquad (6.5)$$

According to reference (III), for laminar flow in a plane, parallel
clearance with constant wall temperature, the heat transference
number α (Kcal/m^2 °C sec) is

$$Nu = \frac{\alpha \, h}{\lambda} = 3.75 \qquad (6.6)$$

where h is the height of the clearance (in m) and λ the heat
conductivity of the gas (in kcal/m °C sec). If this value of
α is used for the further calculations, it must be mentioned
that this is only an approximation, since in our case a flow
with change of the radial cross section is involved. Besides,
a v_φ component is superimposed to the radial flow; the influence
of this component on the value of α cannot be estimated here.
Consequently, the following applies:

$$dq_{2U1} = \pm \; 4.375 \; \pi \; \frac{\lambda (T_w - T) r}{h \dot{G}} \; dr \qquad . \qquad (6.7)$$

The sign "+" means: flow towards outside; the sign "-" means: flow towards inside.

In the equation No. 6.7, T_w is the wall temperature of the discs (in °K) and $\dot{G}$ is the throughput per second (kg/sec).

The second heat introduced, which is generated by the rotation of a disc, is found directly from the torsional moment. By the assumption of a linear v_φ distribution over the height of the clearance, it was already anticipated that the whole energy of the torsional moment is transformed into heat and that the energy which is required for the torsional flow v_φ is small and can be disregarded. The torsional moment for an annular element $2 \, r \, \pi \, . \, dr$ is
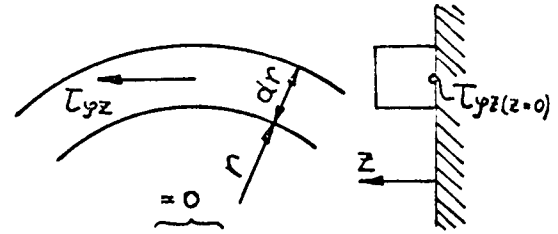
$$dM = 2 r \pi \; dr \; r \; \tau_{\varphi z (z=0)} = 2 \pi r^2 dr \; \eta \left[\frac{\partial v_\varphi}{\partial z} - \frac{\partial v_z}{r \partial \varphi} \right] \qquad .$$

$$(6.7a)$$

By introduction of the equation No. 5.1 into this formula, the following is obtained:

$$dM = 2 \pi r^2 dr \; \eta \; \frac{r \Omega}{h} \qquad . \qquad (6.7b)$$

The heat supplied relative to the throughput per second is:

$$dq_{2U2} = \frac{dQ_{2U2}}{\dot{G}} = \frac{A \, dM \, \Omega}{\dot{G}} = \frac{2 \pi r^2 dr \, \eta \, r \Omega^2 A}{h \dot{G}} = \pm \frac{2 \pi A \eta \, r^3 \Omega^2 dr}{h \dot{G}} \qquad . \qquad (6.8)$$

If the members No. 6.7 and No. 6.8 are introduced into the first principal theorem No. 6.3, the result is:

$$c_p \, dT = \left\{ \pm \; 15 \, \pi \; \frac{\lambda (T_w - T) r}{h \dot{G}} \pm 2 \pi \; \frac{A \eta \, \Omega^2 \, r^3}{h \dot{G}} \right\} dr \qquad . \qquad (6.9)$$

where "+" applies for the flow outwards (with increasing dr, T increases on input of heat); and "-" applies for the flow inwards (with decreasing dr, T increases on input of heat).

If we assume that there is a very good heat conduction in the bearing discs and that the wall temperature adjusts itself as constant over r, and if we use the following abbreviations:

$$M = \pm \frac{15 \pi \lambda}{h c_p \dot{G}}$$

$$N = \pm \frac{2 \pi A \rho \Omega^2}{h c_p \dot{G}} \tag{6.9a}$$

+: for flow outwards.   -: for flow inwards,

the equation No. 6.9 is transformed into:

$$\frac{dT}{dr} + MrT = Nr^3 + MT_w r \quad . \tag{6.10}$$

The general solution can be deduced from the homogeneous equation

$$\frac{dT}{dr} + MrT = 0 \tag{6.11}$$

$$T = C_{(r)} e^{-M\frac{r^2}{2}}$$

by variation of the constants $C(r)$:

$$\frac{dT}{dr} = C'_{(r)} e^{-M\frac{r^2}{2}} - M r C_{(r)} e^{-M\frac{r^2}{2}} \quad . \tag{6.12}$$

If No. 6.11 and No. 6.12 are introduced into the equation No. 6.10, the result is:

$$C_{(r)} = M T_w \int r e^{M\frac{r^2}{2}} dr + N \int r^3 e^{M\frac{r^2}{2}} dr + C_1 \quad . \tag{6.12a}$$

After integration, the following is obtained:

$$C_{(r)} = \frac{N}{M^2} \cdot e^{M\frac{r^2}{2}} \left[Mr^2 - 2\right] + T_w \cdot e^{M\frac{r^2}{2}} + C_1 \quad , \tag{6.12b}$$

Thus, the desired solution by introduction of $C(r)$ into equation No. 6.11 is:

$$T = T_w + \frac{N}{M^2} \left[Mr^2 - 2\right] + C_1 e^{-M\frac{r^2}{2}} \tag{6.13}$$

By introduction of the boundary conditions, $r = r_{1a}$, $T = T_{1a}$, and $r = r_{1i}$, $T = T_{1i}$, the course of the temperature for the outward flow is:

$$T = T_w - (T_w - T_{1a}) \cdot e^{-\frac{M}{2}(r^2 - r_{1a}^2)} + \frac{N}{M^2} \left[(Mr^2 - 2) - (Mr_{1a}^2 - 2) e^{-\frac{M}{2}(r^2 - r_{1a}^2)}\right] \tag{6.14}$$

and for the inward flow:

$$T = T_w - (T_w - T_{1i}) e^{\frac{M}{2}(r_{1i}^2 - r^2)} + \frac{N}{M^2} \left[(Mr_{1i}^2 - 2) - (Mr^2 - 2) e^{\frac{M}{2}(r_{1i}^2 - r^2)} \right] \qquad (6.15)$$

The derivation of the analogous equations for the turbulent clearance flow will not be given here, because this would not involve an essential contribution to the principal studies made in this paper.

The course of temperature in a bearing was calculated according to equations No. 6.14 and 6.15 for the adopted conditions. It is illustrated in Diagram 1. The case given here could, for example, occur in a machine in which the gas is heated by the shaft and the casing, and cooled by the bearing gas. It can be seen that the heat exchange between the bearing discs and the gas is very intensive. After the gas has flowed the very short distance Δr, the gas has reached the temperature of the wall and would remain constant up to the end of the clearance for $\Omega = 0$. The rotation causes heating of the gas which remains, however, very low on account of the reflux of the heat into the discs.

The basic assumption that the wall temperature remains constant may not be quite correct in all cases, since the discs are cooled or heated in the immediate vicinity of the gas inlet, depending on the temperature of the gas, are subject to heat supply by revolution along the entire bearing surface and thus radial temperature gradients occur within the bearing discs. But it can be seen from this estimation that the temperatures of the gas and of the wall are always almost the same for the clearance flow on account of the good heat exchange in the narrow clearance. To what value this wall temperature, remaining almost constant over r, adjusts itself, does not only depend on the temperature of the gas at the inlet into the bearing and the number of rotations per minute, but also on exterior conditions (such as introduction and removal of heat by the components of the bearing).

- - - - - - - -

Diagram 1.   (left) assumed   (right) calculated

(last line, 2nd col) t_w = constant over r.

assumed

$r_{2a} = 0,133$ m
$r_{1a} = 0,089$ m
$r_{1i} = 0,087$ m
$r_{2i} = 0,055$ m

$h = 20 \cdot 10^{-6}$ m

$\dot{G}_a = 3 \cdot 10^{-3}$ kg/s
$\dot{G}_i = 3 \cdot 10^{-3}$ kg/s
$\Omega = 2100$ 1/s
$t_{1a} = t_{1i} = 100\,°C$
$t_w = 300\,°C$
$t_w = $ constant over r

calculated

$M = 2,475 \cdot 10^4$
$N = 1,005 \cdot 10^7$
$\Delta r_a \cong 4\,mm$
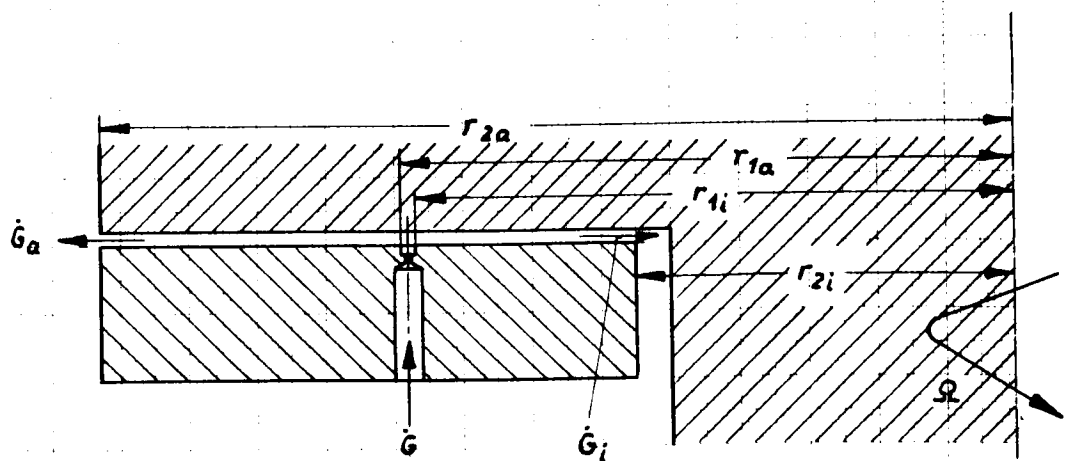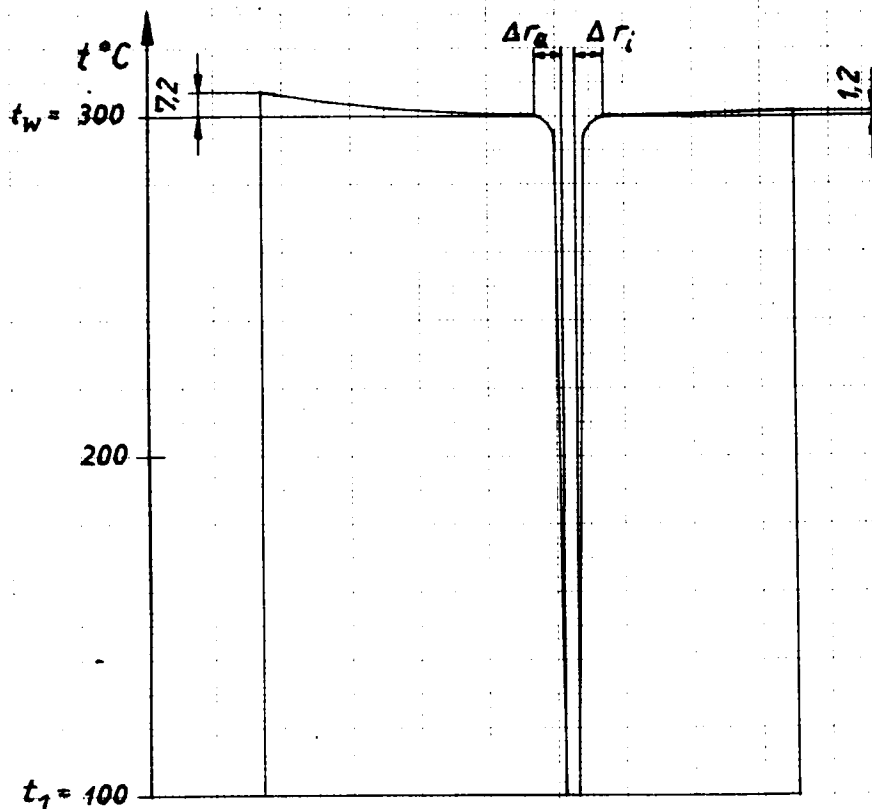$\Delta r_i \cong 4\,mm$
für $t_a = t_i \neq t_w$
$t_{2a} = t_w + 7,2\,°C$
$t_{2i} = t_w + 1,2\,°C$

On account of the intensive heat exchange between gas and discs, any hypothesis based on an adiabatic change of state of the gas during the clearance flow in bearing materials found in practice, i.e., of good heat conduction, can be eliminated. The further studies of the clearance flow rely, therefore, on an isothermal change of state of the gas.

7. **Laminar, isothermal clearance flow.**

It can be concluded from the explanations given in the preceding Chapter that the temperature of the gas in the bearing clearance depends, to a great extent, on the temperature of the bearing discs. Assuming an isothermal clearance flow, the temperature of the gas at the inlet into the bearing must not be used as a base for the calculation, but it must be governed by the wall temperature of the discs which is the resultant from the thermal equilibrium (heating by rotation, heat supply or removal by the shaft, outside cooling of the bearing discs, heat transport of the bearing gas, etc.) and remains constant.

In the following, equations for the calculation of the course of pressure and the throughput volume are derived for radial flow through narrow clearances. Since the derivations are based on different assumptions in each case, the range of validity of the equations obtained is limited.

7.1. **Simple approximation - Slow flow.**

Starting from the Navier - Stokes equation (No. 5.2), it is first assumed that the energies of the acceleration and centrifugal forces are small in comparison with the energies of the radial shearing stresses and pressure forces. An estimation on the permissibility of this approximation will be given in Chapter 8.1.

Thus equation No. 5.2 is reduced to the following:

$$-\frac{\partial p}{\partial r} + \eta \left[\frac{\partial^2 V_r}{\partial r^2} + \frac{\partial V_r}{r \partial r} - \frac{V_r}{r^2} + \frac{\partial^2 V_r}{\partial z^2} \right] = 0 \quad . \tag{7.1}$$

If the z-components are disregarded, the continuity equation for the case of incompressibility is

$$\frac{1}{r} \frac{\partial}{\partial r} \left(r V_r \right) = 0 \quad . \tag{7.1a}$$

or

$$\frac{1}{r}\left(V_r + r\frac{\partial V_r}{\partial r}\right) = 0 \ . \tag{7.1b}$$

We obtain by differentiation:

$$\frac{\partial^2 V_r}{\partial r^2} + \frac{\partial V_r}{r\partial r} - \frac{V_r}{r^2} = 0 \ . \tag{7.2}$$

If equation No. 7.2 is introduced into the second member of equation No. 7.1, only the following remains:

$$\frac{\partial^2 V_r}{\partial z^2} = \frac{1}{\eta}\frac{dp}{dr} \ . \tag{7.3}$$

The solution of this differential equation gives, with consideration of the boundary conditions

$z = 0, \quad v_r = 0 \qquad \text{and} \qquad z = h, \quad v_r = 0 :$

$$V_r = -\frac{1}{2\eta}\frac{dp}{dr}z(h-z) \ , \tag{7.4}$$

which is a parabolic distribution of the radial velocity in the clearance. The average value can be determined from:

$$w = \frac{1}{h}\int_o^h V_r\,dz = -\frac{h^2}{12\eta}\frac{dp}{dr} \ . \tag{7.5}$$

Another way of writing this equation

$$dp \pm \frac{12\eta\,w\,dr}{h^2} = 0 \tag{7.6}$$

or, with consideration of equation No. 6.2

$$da_R = \pm \frac{12\eta\,w\,dr}{h^2\gamma} \tag{7.7}$$

represents the decrease in pressure or the work on account of the radial viscous flow, respectively, where "+" applies to the outward flow and "-" to the inward flow. It is worth mentioning that the approximation equation No. 7.6 is analogous in form to the equation for the pressure drop in a channel of invariable width. The variability of w with r takes the widening and constriction, respectively, of the clearance in radial direction into consideration.

(7.7a)
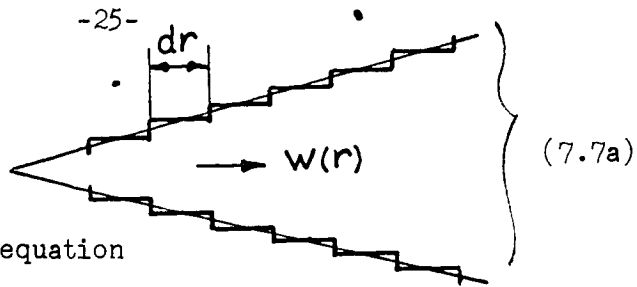
By using the continuity equation

$$\dot{G} = 2\pi r h \gamma w \qquad (7.8)$$

wherein $\dot{G}$ represents the throughput volume per second through the outer or inner bearing clearance, respectively, and the gas equation
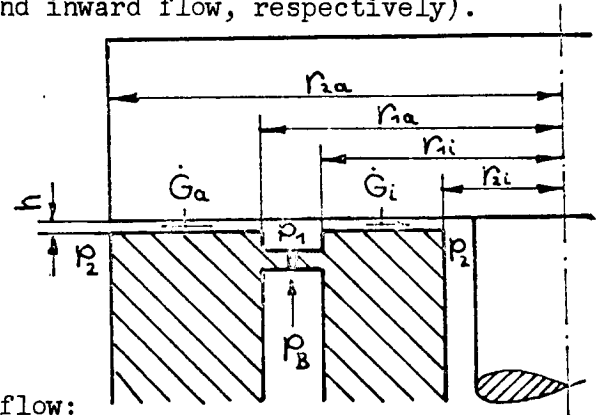
$$p = \gamma RT \qquad (7.9)$$

the equation No. 7.6 becomes:

$$p \cdot dp \pm \frac{6\eta RT \dot{G}}{\pi h^3} \frac{dr}{r} = 0 \quad . \qquad (7.10)$$

The integration gives the course of pressure over r (The indices "a" and "i" mean connection with the outward and inward flow, respectively). The boundary conditions are:

$r = r_{2a}$ $p = p_{2a}$

$r = r_{1a}$ $p = p_{1a}$

$r = r_{1i}$ $p = p_{1i}$

$r = r_{2i}$ $p = p_{2i}$

Thus the following applies to the <u>outward flow</u>:

$$p^2 = p_{2a}^2 + \frac{12\eta \dot{G}_a RT}{\pi h^3} \ln\frac{r_{2a}}{r} \qquad (7.11)$$

or

$$p^2 = p_{1a}^2 - \frac{12\eta \dot{G}_a RT}{\pi h^3} \ln\frac{r}{r_{1a}} \quad . \qquad (7.12)$$

If the throughput volume is eliminated, we obtain:

$$p^2 = p_{2a}^2 + \frac{p_{1a}^2 - p_{2a}^2}{\ln\frac{r_{2a}}{r_{1a}}} \cdot \ln\frac{r_{2a}}{r} \qquad (7.13)$$

or

$$p^2 = p_{1a}^2 - \frac{p_{1a}^2 - p_{2a}^2}{\ln\frac{r_{2a}}{r_{1a}}} \ln\frac{r}{r_{1a}} \quad . \qquad (7.14)$$

The following applies to the <u>inward flow</u>

$$p^2 = p_{2i}^2 + \frac{12\,\eta\,\dot{G}_i\,RT}{\pi\,h^3}\,\ln\frac{r}{r_{2i}} \qquad (7.15)$$

or

$$p^2 = p_{1i}^2 - \frac{12\,\eta\,\dot{G}_i\,RT}{\pi\,h^3}\,\ln\frac{r_{1i}}{r} \qquad (7.16)$$

and for eliminated amount of flow

$$p^2 = p_{2i}^2 + \frac{p_{1i}^2 - p_{2i}^2}{\ln\frac{r_{1i}}{r_{2i}}}\cdot\ln\frac{r}{r_{2i}} \qquad (7.17)$$

or

$$p^2 = p_{1i}^2 - \frac{p_{1i}^2 - p_{2i}^2}{\ln\frac{r_{1i}}{r_{2i}}}\cdot\ln\frac{r_{1i}}{r} \qquad (7.18)$$

The amount of flow can be given as:

$$\dot{G}_a = \frac{\pi\,h^3\,(p_{1a}^2 - p_{2a}^2)}{12\,\eta\,RT\cdot\ln\frac{r_{2a}}{r_{1a}}} \qquad (7.19)$$

and

$$\dot{G}_i = \frac{\pi\,h^3\,(p_{1i}^2 - p_{2i}^2)}{12\,\eta\,RT\,\ln\frac{r_{1i}}{r_{2i}}} \qquad (7.20)$$

As will be shown later, the accuracy of these approximation solutions is, in general, sufficient for the design and calculation of aerostatic thrust bearings. Thus, for instance, these equations are used in the papers (IV) and (V).

7.2 <u>Extended approximation</u>

In order to get an idea of the influence of the acceleration and inertia members, respectively, in the equations No. 5.2 and 5.4, respectively, an iteration is made in such a way that the term for the energy of the radial shearing stresses da_R according to equation No. 7.7, obtained from the simple approximation (Chapter 7.1) and by disregarding these members, is introduced into equation No. 5.4.

The member of the centrifugal force energy can be obtained, if the following assumption is made (see equation No. 5.1)

$$\frac{db}{dr} - \frac{1}{gh}\int_0^h \frac{V_\varphi^2(z)}{r}\,dz = \frac{1}{gh}\int_0^h \frac{1}{r}\left(r\,\Omega\,\frac{z}{h}\right)^2 dz \qquad (7.20a)$$

as:

$$db = \frac{r \, \Omega^2}{3 \, g} \, dr$$

(7.21)

Using the equations No. 7.7 and 7.21, equation No. 5.4 is transformed into:

$$\pm \frac{12 \, \eta \, w \, dr}{h^2 \, \gamma} + \frac{dp}{\gamma} + \frac{w \, dw}{g} - \frac{\Omega^2}{3 \, g} \, r \cdot dr = 0$$

(7.22)

In order to determine the pressure as a function of r, the variables w and γ must be expressed by $\dot{G}$ and p. Thus the continuity equation (cf. No. 7.8) reads:

$$w = \frac{\dot{G}}{2 \, \pi \, r \, h \, \gamma}$$

(7.22a)

and the gas equation (cf. No. 7.9)

$$\gamma = \frac{p}{RT}$$

(7.22b)

If equation No. 7.9 is introduced into equation No. 7.9. we obtain:

$$w = \frac{\dot{G} \, RT}{2 \, \pi \, h \, r \, p}$$

(7.22c)

and, differentiated:

$$dw = - \frac{\dot{G} \, RT}{2 \, \pi \, h} \left(\frac{dr}{r^2 \, p} + \frac{dp}{r \, p^2} \right)$$

(7.22d)

According to the studies made in Chapter 6, T remains almost constant over r. If the terms given above are introduced into equation No. 7.22, the following general differential equation results:

$$0 = \left(p - \frac{\dot{G}^2 \, RT}{4 \, \pi^2 \, h^2 \, g} \cdot \frac{1}{r^2 \, p} \right) dp + \left(\pm \frac{6 \, \eta \, \dot{G} \, RT}{\pi \, h^3} \cdot \frac{1}{r} - \frac{\dot{G}^2 \, RT}{4 \, \pi^2 \, h^2 \, g} \cdot \frac{1}{r^3} - \frac{\Omega^2}{3 \, g \, RT} \, r \, p^2 \right) dr$$

(7.23)

or, using the following abbreviations

$$a = \pm \frac{6 \, \eta \, \dot{G} \, RT}{\pi \, h^3} = \pm \alpha \, \dot{G}$$

(7.23a)

$$b = \frac{\dot{G}^2 \, RT}{4 \, \pi^2 \, h^2 \, g} = \beta \, \dot{G}^2$$

+: for outward flow
−: for inward flow

$$c = \frac{\Omega^2}{3 \, g \, RT}$$

(7.24)

$$\frac{dp}{dr} = - \frac{\frac{a}{r} - \frac{b}{r^3} - c \, r \, p^2}{p - \frac{b}{r^2 \, p}}$$

The integration of this equation in complete form is not feasible; if, however, two assumptions are made, a relatively simple solution can be found.

Assumption "a": In the clearance flow at large radii, it is permissible – since there is $p \gg b/r^2 p$ – to simplify the second term of the denominator in the equation No. 7.24 in such a way that r is replaced by a constant radius, e.g. the average value of the initial and final radius,

$$\bar{r} = \frac{r_1 + r_2}{2}$$

or that the whole member is omitted. In the flow at small radii, i.e. for the course of pressure in the immediate vicinity of a nozzle which opens directly into the bearing clearance, disregarding this member involves a certain error, which may be smaller or larger depending on the conditions prevailing in the bearing. But since the second member of the numerator in equation No. 7.24 is inversely proportional to r^3 and the second member of the denominator is inversely proportional to r^2 only, the former has a greater influence by far than the latter when the radii are very small. This fact will be illustrated in Chapter 8.1 by actual examples.

Assumption "b": In contrast to the equations given in (VI), appreciably simpler terms for the course of pressure are obtained, considering at the same time also the influence of inertia, if an interation is made in such a way that, for the pressure in the third member of the numerator of equation No. 7.24, the solution from the simple approximation (Chapter 7.1) is introduced.

If the equations No. 7.14 and 7.18 are used, respectively, and the assumption "a" is applied, equation No. 724 is transformed into:

$$\left(p - \frac{b}{\bar{r}^2}\frac{1}{p}\right)dp + \left(\frac{a}{r} - \frac{b}{r^3} - fr + kr\ln r\right)dr = 0 , \quad (7.25)$$

where the factors f and k for the outward flow are:

$$f_a = c\,p_{1a}^2 + k_a \ln r_{1a} \quad\quad (7.25a)$$

$$k_a = c\,\frac{p_{1a}^2 - p_{2a}^2}{\ln \frac{r_{2a}}{r_{1a}}}$$

and for the inward flow:

$$f_i = c\,p_{1i}^2 + k_i \ln r_{1i}$$

$$k_i = c\,\frac{p_{1i}^2 - p_{2i}^2}{\ln \frac{r_{1i}}{r_{2i}}} \quad\quad (7.25b)$$

If the equation No. 7.25 is integrated, the course of pressure becomes:

$$\frac{p^2}{2} - \frac{b}{\bar{r}^2}\ln p + a\ln r + \frac{b}{2r^2} - f\frac{r^2}{2} + k\frac{r^2}{2}\left(\ln r - \frac{1}{2}\right) + C_1 = 0 , \quad (7.26)$$

The boundary conditions being given, for the flow outwards, as:

$r = r_{1a}$, $p = p_{1a}$ or $r = r_{2a}$, $p = p_{2a}$, the following equation results:

$$\frac{1}{2}(p_{1a}^2 - p^2) - \frac{b}{r^2}\ln\frac{p_{1a}}{p} = a\ln\frac{r}{r_{1a}} - \frac{b}{2}\left(\frac{1}{r_{1a}^2} - \frac{1}{r^2}\right) - \frac{c}{2}p_{1a}^2(r^2 - r_{1a}^2) + \tag{7.27}$$

$$+ \frac{k_a}{2}r^2\ln\frac{r}{r_{1a}} - \frac{k_a}{2}\frac{r^2 - r_{1a}^2}{2}$$

or

$$\frac{1}{2}(p^2 - p_{2a}^2) - \frac{b}{r^2}\ln\frac{p}{p_{2a}} = a\ln\frac{r_{2a}}{r} - \frac{b}{2}\left(\frac{1}{r^2} - \frac{1}{r_{2a}^2}\right) - \frac{c}{2}p_{2a}^2(r_{2a}^2 - r^2) +$$

$$+ \frac{k_a}{2}\left(r_{2a}^2\ln\frac{r_{2a}}{r_{1a}} - r^2\ln\frac{r}{r_{1a}}\right) - \frac{k_a}{2}\frac{r_{2a}^2 - r^2}{2} \tag{7.28}$$

For the flow inwards: $r = r_{1i}$, $p = p_{1i}$ or $r = r_{2i}$, $p = p_{2i}$, and thus:

$$\frac{1}{2}(p_{1i}^2 - p^2) - \frac{b}{r^2}\ln\frac{p_{1i}}{p} = -a\ln\frac{r_{1i}}{r} + \frac{b}{2}\left(\frac{1}{r^2} - \frac{1}{r_{1i}^2}\right) + \frac{c}{2}p_{1i}^2(r_{1i}^2 - r^2) + \tag{7.29}$$

$$+ \frac{k_i}{2}\left(r^2\ln\frac{r_{1i}}{r} - \frac{r_{1i}^2 - r^2}{2}\right)$$

or

$$\frac{1}{2}(p^2 - p_{2i}^2) - \frac{b}{r^2}\ln\frac{p}{p_{2i}} = -a\ln\frac{r}{r_{2i}} + \frac{b}{2}\left(\frac{1}{r_{2i}^2} - \frac{1}{r^2}\right) + \frac{c}{2}p_{2i}^2(r^2 - r_{2i}^2) - \tag{7.30}$$

$$- \frac{k_i}{2}\left(r^2\ln\frac{r_{2i}}{r} - r_{2i}^2\ln\frac{r_{2i}}{r_{1i}} + \frac{r^2 - r_{2i}^2}{2}\right)$$

Flow volumes

   If the second boundary conditions are introduced into equations No. 7.27 and 7.29, quadratic equations for $\dot{G}$ are obtained. For the outward flow, the following applies: $A\dot{G}_a^2 - B\dot{G}_a + K = 0$, where A, B, and K mean the following:

$$A = \frac{\beta}{2}\left(\frac{1}{r_{1a}^2} - \frac{1}{r_{2a}^2}\right) - \frac{\beta}{r^2}\ln\frac{p_{1a}}{p_{2a}} ,$$

$$B = \alpha\ln\frac{r_{2a}}{r_{1a}} ,$$

$$K = \frac{1}{2}(p_{1a}^2 - p_{2a}^2) + \frac{c}{2}p_{1a}^2(r_{2a}^2 - r_{1a}^2) - \frac{k_a}{2}\left(r_{2a}^2\ln\frac{r_{2a}}{r_{1a}} - \frac{r_{2a}^2 - r_{1a}^2}{2}\right)$$

Thus the result is:

$$\dot{G}_a = \frac{B}{2A} + \sqrt{\frac{B^2 - 4AK}{4A^2}} . \tag{7.31}$$

In an analogous way, for the inward flow applies:

$D\dot{G}_i^2 + E\dot{G}_i - L = 0$, where D, E, and L have the following meaning:

$$D = \frac{\beta}{2}\left(\frac{1}{r_{2i}^2} - \frac{1}{r_{1i}^2}\right) + \frac{\beta}{r^2}\ln\frac{p_{1i}}{p_{2i}} ,$$

$$E = \alpha\ln\frac{r_{1i}}{r_{2i}} ,$$

$$L = \frac{1}{2}(p_{1i}^2 - p_{2i}^2) - \frac{c}{2}p_{1i}^2(r_{1i}^2 - r_{2i}^2) - \frac{k_i}{2}\left(r_{2i}^2 \ln \frac{r_{1i}}{r_{2i}} - \frac{r_{1i}^2 - r_{2i}^2}{2}\right)$$

and the flow volume is:

$$\dot{G}_i = -\frac{E}{2D} + \sqrt{\frac{E^2 + 4DL}{4D^2}} \qquad (7.32)$$

For the square roots only those signs are applicable which give positive throughputs.

8. Discussion of the flow equations.

8.1 Influence of the kinetic energy.

In order to estimate the individual members of the Navier – Stokes equation (No. 5.2) relative to each other, the quotient of the radial inertia force relative to the unit of volume 7_1 by the largest viscosity force 3 is established.

FROM

$$\frac{7_1}{3} = \frac{\rho \cdot w \frac{dw}{dr}}{\eta \frac{d^2 w}{dz^2}} \longrightarrow \frac{\rho w h^2}{\eta r} = R_{e1}^* \qquad (8.0a)$$

WHERE

$$\rho = \frac{p}{gRT} \qquad \begin{array}{c} and \\ und \end{array} \qquad \rho w = \frac{\dot{G}}{2r\pi hg} \qquad (8.0b)$$
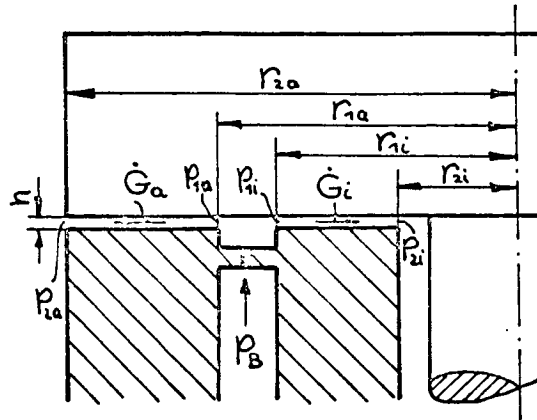
the comparative Reynolds number is determined as:

$$R_{e1}^* = \frac{\rho w h^2}{g\eta RTr} = \frac{\dot{G}h}{2\pi r^2 g\eta} . \qquad (8.1)$$

It can be seen that this influence of acceleration becomes the greater, the lower the radius and the higher the pressure and the clearance are.

Case 1. First, the course of pressure and velocity in a bearing which is equipped with an annular channel and where the flow is in both directions, along with the volume of throughput are calculated by means of the various equations derived in Chapter 7 for the data listed below. Since equation No. 7.24 cannot be solved, the comparative course of pressure was determined from the differential equations by step-by-step approximation by means of finite differences $\triangle p/\triangle r$.

$$
\begin{array}{llll}
r_{2i} = 0,055 \text{ m} & h = 20.10^{-6} \text{m} & R = 29,3 \text{ m/°C} & \\
r_{1i} = 0,087 & p_{1a} = 6,208.10^4 \text{ kp/m}^2 & T = 293 \text{ °K} & (8.1a) \\
r_{1a} = 0,089 & p_{1i} = 6,365.10^4 & \eta = 1,85.10^{-6} \text{ kp s/m}^2 & \\
r_{2a} = 0,133 & p_{2i} = p_{2a} = 1.10^4 & \Omega = 0 &
\end{array}
$$

Outward flow.

radius r (in m)	pressure p (atmospheres)			radial velocity w (in m/sec)
Calculated according to	differential equation No. 7.24	extended approximation, eq. No. 7.28	simple approximation equ. No. 7.13	continuity equation No. 7.8
0,089	6,208	6,208	6,208	15,2
0,090	6,125	6,133	6,120	15,3
0,095	5,707	5,705	5,694	15,6
0,100	5,278	5,296	5,256	16,0
0,105	4,834	4,825	4,796	16,7
0,110	4,368	4,345	4,330	17,7
0,114	3,972	3,945	3,920	18,8
0,118	3,545	3,515	3,491	20,4
0,122	3,071	3,030	3,007	23,0
0,126	2,520	2,391	2,359	28,4
0,128	2,205	2,163	2,139	30,8
0,130	1,836	1,786	1,754	36,9
0,131	1,617	1,565	1,546	41,5
0,132	1,357	1,317	1,304	49,0
0,133	1,000	1,000	1,000	63,4

(8.1b)

Throughput volume $\dot{G}_a$ (gr/sec)			
Calculated according to	(assumed) 1.200	(No. 7.31) 1.230	(No. 7.19) 1.231

Inward flow

radius r (in m)	pressure p (in atmospheres)			radial velocity w (in m/sec)
Calculated according to	differential equation No. 7.24	extended approximation, eq. No. 7.30	simple approximation equ. No. 7.17	continuity equation No. 7.8
0,087	6,365	6,365	6,365	14,0
0,086	6,288	6,287	6,287	14,4
0,084	6,133	6,130	6,122	15,1
0,082	5,970	5,962	5,955	15,9
0,080	5,798	5,785	5,772	16,8
0,076	5,422	5,403	5,378	19,0
0,072	4,992	4,986	4,923	21,9
0,068	4,491	4,457	4,389	26,0
0,064	3,889	3,813	3,749	32,4
0,060	3,120	2,980	2,918	44,5
0,058	2,612	2,432	2,360	56,8
0,057	2,298	2,177	2,012	67,9
0,056	1,905	1,824	1,592	87,2
0,055	1,000	1,000	1,000	141,4

(8.1c)

Throughput volume $\dot{G}_i$ (gr/sec)

Calculated according to	(Assumed)	(No. 7.32)	(No. 7.20)
	1.053	1.138	1.138

It can be seen that in bearings where the dimensions of the radii are large during clearance flow, the variation of the kinetic energy of the radial velocity has only a small and unimportant influence. The comparative Reynolds number is in this case $Re_1^* \ll 1$. All the equations derived in Chapter 7 yield practically the same result.

Case 2.

If an inlet nozzle opens directly into the clearance, the Reynolds number of the clearance flow in the immediate vicinity of the orifice is: $Re_1^* > 1$.

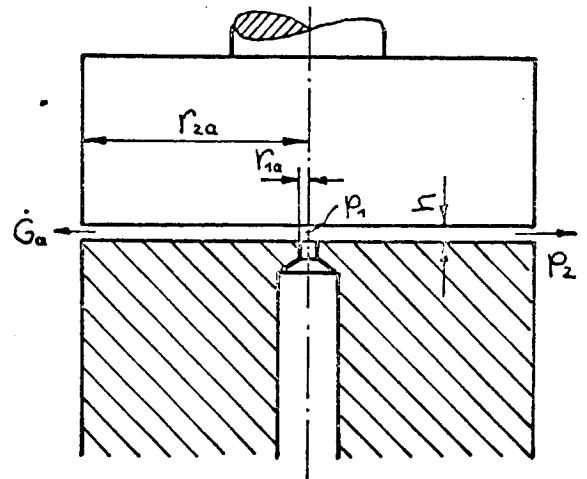At very small radii the following applies to equation No. 7.24:

$$crp^2 \quad \text{and} \quad \frac{a}{r} \ll \frac{b}{r^3} ,$$

i.e. the increments of centrifugal force and friction become small and negligible compared to the kinetic energy. The equation No. 7.24 is reduced to:

$$\frac{dp}{dr} = \frac{\dfrac{b}{r^3}}{p - \dfrac{b}{r^2 p}}$$

or, re-transformed into the original form

$$\frac{RT}{p} \, dp + \frac{wdw}{g} = 0.$$

This equation describes the friction-free flow in a radial diffuser. Its solution is:

$$RT \ln p + \frac{w^2}{2g} + C = 0 . \qquad (8.2)$$

The clearance flow at small radii is only interesting, in this connection, for the flow outwards. If one does not consider the cases where the gas in the bearing clearance reaches the velocity of sound which changes subsequently into supersonic speed (this case has been described in detail by reference (VII))and if one disregards the fact that the change of state of the gas for the flow in immediate vicinity of a nozzle is not, as assumed, isothermic (this error is, however, quite small), the pressure after entry into the clearance had to increase corresponding to diffuser flow, according to equation No. 8.2. The theoretical pressure profile, determined by means of stepwise approximation through finite differences $\Delta p / \Delta r$ for a bearing with the values

$$
\begin{aligned}
r_{1a} &= 1 \text{ mm} & h &= 20.10^{-6} \text{ m} \\
r_{2a} &= 68,5 \text{ mm} & R &= 29,3 \quad \text{m/°C} \qquad (8.2a) \\
p_2 &= 1.10^4 \text{ kp/m}^2 & T &= 293 \quad °\text{K} \\
G_a &= 0,177 \text{ gr/s} & \eta &= 1,9.10^{-6} \text{kp s/m}^2 .
\end{aligned}
$$

is plotted in Diagram 2 as a function of the pressure profile which were obtained from the two approximations No. 7.13 and 7.28, respectively. The

interaction of unfavorable factors such as (1) poor conditions at the inlet (on account of the difficulty to obtain clean nozzle edges), (2) flow in hydraulic and thermal take-off run, (3) occurrence of the highest possible Renumbers in each clearance flow, justifies the assumption that the flow does not undergo this high increase in pressure which had to be overcome within a few tenths of a millimeter.

Another problem, however, which is important for the design of the bearings comes up here: Which pressure p_1 at the inlet of the clearance is required in order to obtain that pressure profile which is described by the three equations (Diagram 2) identically in the area of large radii? For applying the pressure p_1 calculated theoretically according to equation No. 7.24 or equation No. 7.28, would not guarantee reaching the desired course of pressure. The simple approximation No. 7.13, on the other hand, gives too high values for p_1.

The radius r_k where the pressure reaches a maximum (beyond this there is no longer an increase of pressure in the flow) can be calculated from equation No. 7.24 for $\Omega = 0$. If it is assumed that $\frac{dp}{dr} = 0$, there is, as a consequence:

$$\frac{a}{r_K} - \frac{b}{r_K^3} = 0 , \quad \text{and, therefore:} \quad r_k = \sqrt{\frac{G_a h}{24 \pi g \eta}} \qquad (8.3)$$

The inherent maximum pressure p_K cannot be found from equation No. 7.24 in a simple way. The extended approximation No. 7.28 yields, as can be seen in Diagram 2, a value which is somewhat too low but still applicable. It can be assumed that the pressure profile between p_1 and p_k remains almost constant: thus one can establish the required pressure p_1.

A method of circumventing the questionable range between p_1 and p_k is the following: Next to the nozzle, a depression is provided of the magnitude r_k, on the side of the clearance. In this case, the radius r_1 is identical with r_k, and the pressure $p_1 \doteq p_k$. For the example given on page 33, the result is: $r_k = 1.58$ mm, $p_k = 6.775 \times 10^4$ kp/m^2 (cf. No. 7.28).
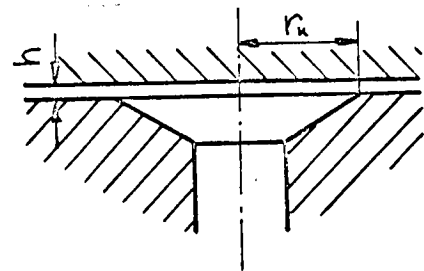
Diagram 3 (page 36) shows the course of the Reynolds numbers over r for the example mentioned above. In the area of small radii, Renumbers of over 1000 are reached, while Re_1^* increases beyond 10.
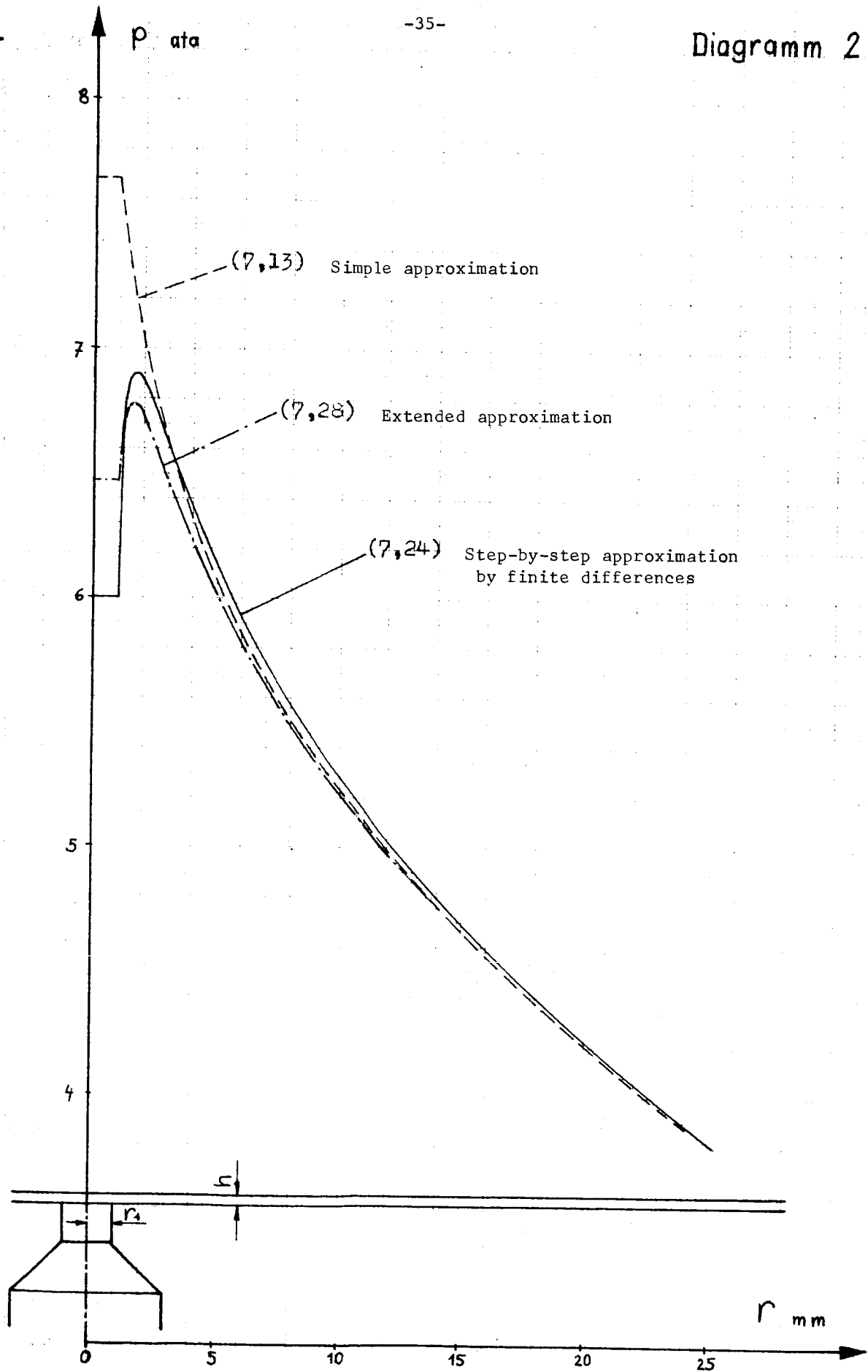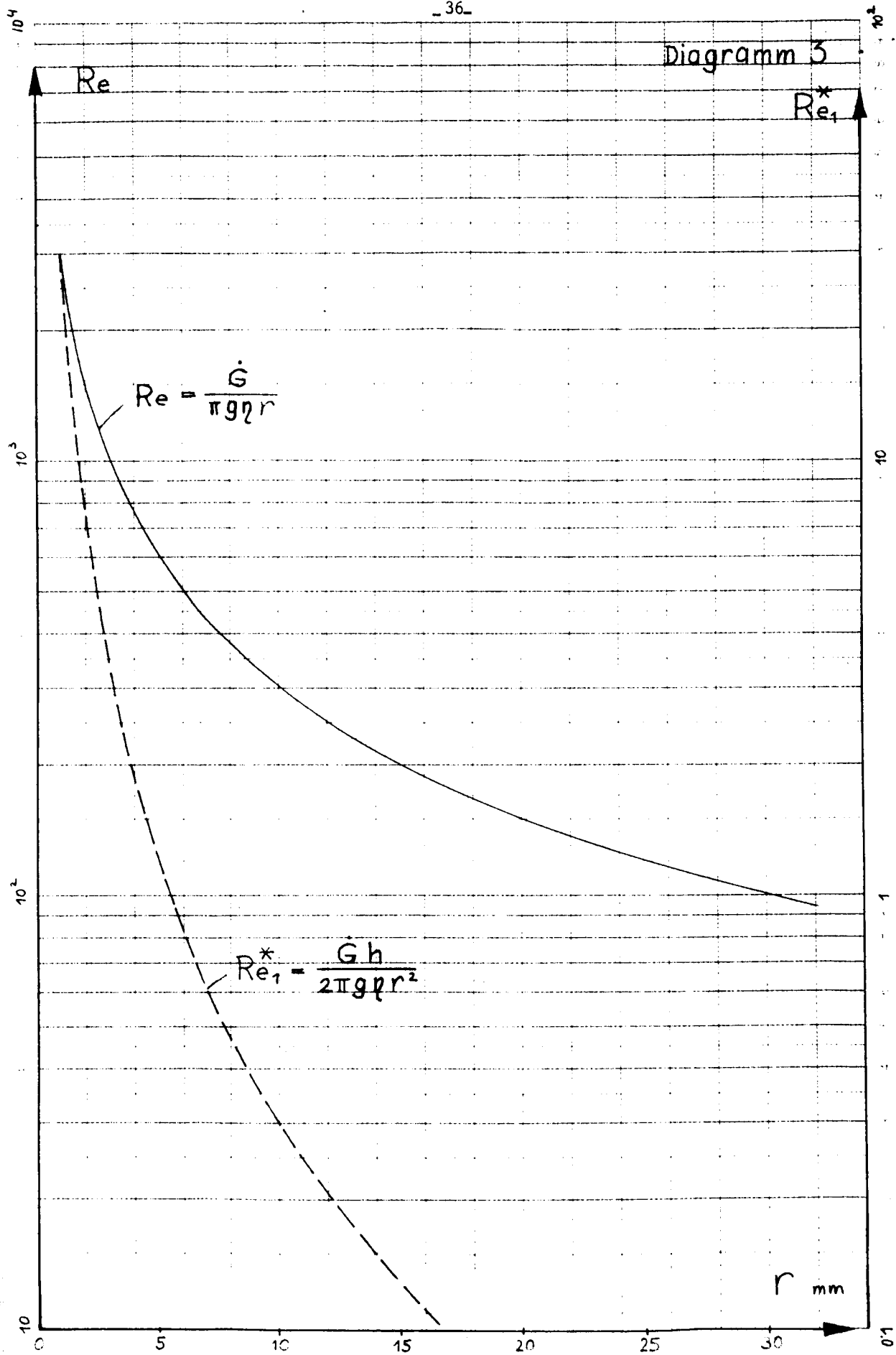
Diagramm 3

$$Re = \frac{\dot{G}}{\pi g \eta \, r}$$

$$Re_1^* = \frac{\dot{G}\, h}{2\pi g \varrho \, r^2}$$

8.2 Influence of rotation.

If, according to equation No. 5.2, the quotient of the centrifugal force ζ_2 relative to the unit of volume by the highest viscosity force ζ is written, the following applies according to equation No. 7.21:

$$\frac{\zeta_2}{\zeta} = \frac{\rho \, r \, \Omega^2}{3 \eta \frac{d^2 w}{d z^2}} \longrightarrow \frac{\rho \, r \, \Omega^2 h^2}{3 \eta w} = Re_2^* \qquad (8.3a)$$

or by

$$\rho = \frac{p}{g \, R \, T} \qquad \text{und} \qquad \rho w = \frac{\dot{G}}{2 \pi r g h} \qquad (8.3b)$$

the second comparative Reynolds number is given:

$$Re_2^* = \frac{r \, \Omega^2 \, p \, h^2}{3 \eta g R T w} = \frac{2 \pi h^3 r^2 \Omega^2 p^2}{3 g \eta R^2 T^2 G} \qquad . \qquad (8.4)$$

The influence of rotation depends in a high degree from the conditions of operation of the bearing; it increases quadratically with the factor p.r. Ω.

For the example on page 31, the pressure profile and the amount of flow was calculated with Ω = 1570 1/sec.

Outward flow		Inward flow	

Amount of flow $\dot{G}$(gr/sec)

calculated according to	No. 7.31	7.32	
	1.280	1.110	

Outward flow		Inward flow	
Radius r (m)	Pressure p (atmospheres)	Radius r (m)	Pressure p (atmospheres
calculated according to No. 7.28			No. 7.30
0,089	6,203	0,087	6,365
0,090	6,131	0,086	6,305
0,095	5,722	0,084	6,130
0,100	5,285	0,082	5,960
0,105	4,833	0,080	5,770
0,110	4,377	0,078	5,365
0,114	3,971	0,072	4,900
0,118	3,543	0,068	4,370
0,122	3,062	0,064	3,725
0,126	2,511	0,060	2,896
0,128	2,141	0,058	2,345
0,130	1,798	0,057	2,000
0,131	1,579	0,056	1,585
0,132	1,332	0,055	1,000
0,133	1,000		

In the case considered here, the influence of rotation is very small, as is shown by a comparison of the pressure profiles for $\Omega = 0$. (pp. 30 and 31). The comparative Reynolds numbers assume values which are: $Re^*_2 < 1$.

In reference (VI), the influence of rotation on the load capacity was studied in an aerostatic thrust bearing with outward flow. It is pointed out that a reduction or increase of pressure can occur in the bearing clearance, compared with a bearing with $\Omega = 0$, by the rotation of a bearing disc, depending on the conditions or the parameters, respectively r_{2a}/r_{1a}, p_{1a}/p_{2a} and $3\,\Omega^2 r^2_{1a}/10\,RT$. For the evaluation of each condition, only the boundary conditions for which the one case or the other may come true are to be established here. It can be concluded that in isothermal, laminar flow in outward direction for

$$\left(r_{2a}^2 - r^2\right)\left[p_{1a}^2 + \frac{p_{2a}^2 - p_{1a}^2}{2\ln\frac{r_{2a}}{r_{1a}}}\right] > \frac{p_{1a}^2 - p_{2a}^2}{\ln\frac{r_{2a}}{r_{1a}}}\left(r^2\ln\frac{r}{r_{1a}} + r_{2a}^2\ln\frac{r_{2a}}{r_{1a}}\right) \quad (8.4b)$$

the pressure in the bearing clearance, according to equation No. 7.28, is smaller in all places r which meet this condition when there is a rotation than the pressure which would occur without rotation. Analogously, in the flow inwards there is, according to equation No. 7.30, for

$$p_{1i}^2\left(r^2 - r_{2i}^2\right) > \frac{p_{1i}^2 - p_{2i}^2}{\ln\frac{r_{1i}}{r_{2i}}}\left(r^2\ln\frac{r_{1i}}{r} - r_{2i}^2\ln\frac{r_{1i}}{r_{2i}} + \frac{r^2 - r_{2i}^2}{2}\right) \quad (8.4c)$$

an increase in pressure compared to the bearing at rest. If the unequality sign is reversed in the conditions given above, the pressure in the clearance becomes greater (in the first case) and smaller (in the second case) than when no rotation takes place. At high pressure ratios p_1/p_2, rotation causes, as a rule, an increase of the load capacity in the part of the bearing where the flow is outwards and a reduction of load capacity in the part where there is an inward flow. (cf. the results given above). But since the influence of rotation in static gas bearings is, in general, very small, rotation is disregarded in calculation of bearings.

In an analogous way, an increase or reduction of the volume of throughput corresponds to a pressure reduction or pressure increase under the conditions given above with $r = r_{1a}$ and $r = r_{1i}$, respectively.

8.3 Gasdynamic influence.

For the laminar, radial clearance flow, the course of the radial velocity w averaged over the clearance is derived as a function of r first. This calculation is only an approximation, since the velocity distribution v_r over h had to be taken into consideration in an accurate investigation. In contrast with the studies made in Chapter 7, it is permissible to assume an adiabatic change of state for the clearance flow
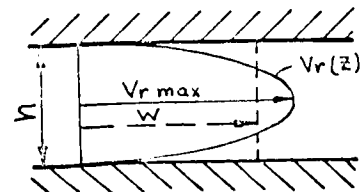
in the transsonic region. From the equation No. 7.22 it may be concluded that, for $\Omega = 0$, the following applies if the continuity equation No. 7.8 is considered:

$$\pm \frac{24\,\pi\,\eta\,w^2\,r\,dr}{hG} + \frac{dp}{\gamma} + \frac{w\,dw}{g} = 0 \quad . \tag{8.5}$$

Transformation of the second member:

The following equation applies to adiabatic change of state:

$$\frac{dp}{\gamma} = \mathscr{x}\,\frac{p}{\gamma}\cdot\frac{d\gamma}{\gamma} \quad . \tag{8.6}$$

The differentiated continuity equation No. 7.8 gives:

$$\frac{d\gamma}{\gamma} = -\left(\frac{dr}{r} + \frac{dw}{w}\right) \quad . \tag{8.7}$$

If equation No. 8.7 is introduced into equation No. 8.6, the result is:

$$\frac{dp}{\gamma} = -\mathscr{x}\,\frac{p}{\gamma}\left(\frac{dr}{r} + \frac{dw}{w}\right) = -\mathscr{x}\,RT\left(\frac{dr}{r} + \frac{dw}{w}\right) \quad . \tag{8.8}$$

The temperature, expressed by the adiabatic equation, becomes:

$$T = T_0 - \frac{A\,w^2}{2g\,c_p} \quad , \tag{8.9}$$

where $w \ne 0$, $T = T_0$. If equation No. 8.9 is introduced into equation No. 8.8, the following results:

$$\frac{dp}{\gamma} = -\mathscr{x}\,R\left(T_0 - \frac{A\,w^2}{2g\,c_p}\right)\left(\frac{dr}{r} + \frac{dw}{w}\right) \quad . \tag{8.10}$$

The introduction of equation No. 8.10 into equation No. 8.5 gives, with consideration of

$$\frac{A\,R}{c_p} = \frac{\mathscr{x} - 1}{\mathscr{x}} \tag{8.10a}$$

the differential equation for $w = w\,(r)$:

$$\frac{dr}{dw} = \frac{\mathscr{x}\,RT_0\,\frac{1}{w} - \frac{\mathscr{x} + 1}{\mathscr{x}}\,w}{\pm\,\dfrac{24\,\pi\,\eta\,r\,w^2}{hG} - \mathscr{x}\,RT_0\,\frac{1}{r} + \dfrac{\mathscr{x} - 1}{2g}\,\dfrac{w^2}{r}} \quad , \tag{8.11}$$

where the sign "+" applies to the outward flow and the sign "-" to the inward flow. If it is assumed that dr/dw = 0, it appears that the r-w function, as represented, runs parallel to the w-axis at a certain velocity, which is the velocity of sound

$$W_s = \sqrt{\frac{2\varkappa}{\varkappa + 1} g R T_o}$$ (8.11a)

and is obtained when the numerator is zero, since the denominator of the fraction on the right side of equation No. 8.11 cannot reach an infinite value. Thus the numerator of the fraction is positive for subsonic speeds, and negative for supersonic speeds.

Flow towards inside.

Since the third member of the denominator in equation No. 8.11 is, as a rule, small compared to the second, the entire denominator of the fraction remains negative. For $w < w_s$ the whole fraction becomes negative, from which it can be concluded that the velocity increases when the radius decreases. Velocity of sound can only be generated at the outlet of the clearance; supersonic velocities cannot occur in the clearance.

Flow towards outside

In a subsonic flow starting at $r = r_{1a}$, the course of the flow depends on the relative magnitude of the individual members of the denominator. For

$$\frac{24 \pi \eta r w^2}{h G} + \frac{\varkappa - 1}{2g} \frac{w^2}{r} > \varkappa R T_o \frac{1}{r}$$ (8.11b)

which is the regular case, the flow is accelerated on account of the great pressure reduction of the gas in spite of the fact that the clearance is to be considered geometrically as diffuser. If the pressure of the bearing gas is sufficiently high, velocity of sound can appear at the end of the clearance ($r = r_{2a}$) if the above condition is fulfilled.

Looking for the magnitude of the radius r_u of the bearing where velocity of sound is generated in the clearance - which changes over to supersonic velocity with increasing radius - one will find the answer in equation No. 8.11. Since dr/dw must be positive in order to fulfill the above condition and the numerator of the fraction is negative for $w > w_s$, it can be concluded that also the denominator of the fraction must assume a negative value. This is, however, only true if the following applies:

$$\varkappa R T_o \frac{1}{r} > \frac{24 \pi \eta r w^2}{h G} + \frac{\varkappa - 1}{2g} \frac{w^2}{r}$$ (8.11c)

For $r = r_u$ and $w = w_s$ the following applies:

$$\varkappa R T_o \frac{1}{r_u} \gtreqless \frac{24 \pi \eta r_u w_s^2}{h G} + \frac{\varkappa - 1}{2g} \frac{w_s^2}{r_u}$$ (8.11d)

from which the following can be derived by means of given values:

$$r_{\ddot{u}} \leqq \sqrt{\frac{\mathrm{æ}\,R T_0 - \frac{\mathrm{æ}-1}{2g}\,W_s^2}{\frac{24\,\pi\,\eta\,W_s^2}{h\,\dot{G}}}} \tag{8.12}$$

If the continuity equation No. 7.8 is considered for the respective place

$$\dot{G} = 2\pi\,r_{\ddot{u}}\,h\,W_s\,\gamma_{\ddot{u}} \tag{8.12a}$$

another equation results:

$$r_{\ddot{u}} \leqq \sqrt{\frac{\left(\mathrm{æ}\,R T_0 - \frac{\mathrm{æ}-1}{2g}\,W_s^2\right)h^2\,\gamma_{\ddot{u}}}{12\,\eta\,W_s}} \tag{8.13}$$

An example using the following values

$$
\begin{array}{llll}
T_0 = & 293 \ ^\circ K & \eta = & 1,85.10^{-6} \ \mathrm{kp\ s/m^2} \\
R = & 29,3 \ \mathrm{m/^\circ C} & h = & 50.10^{-6} \ \mathrm{m} \\
\mathrm{æ} = & 1,4 & \dot{G}_a = & 2,5.10^{-3} \ \mathrm{kg/s} \\
W_s = & 314 \ \mathrm{m/s} & &
\end{array}
\tag{8.13a}
$$

gives: $r_{\ddot{u}} = 3.0 \times 10^{-2}$ m.

Thus supersonic velocities can occur in the clearance only at radii which are smaller than, or equal to, $r_{\ddot{u}}$. This fact is very important for the design of aerostatic bearings with radial flow since, in the region of supersonic flow, the pressure in the bearing is greatly reduced and can even assume negative values relative to the surrounding pressure. It need not be specially emphasized that, in this case, the load capacity would be reduced correspondingly. In order to have a bearing with proper dimensions, r_{1a} must be larger than $r_{\ddot{u}}$.
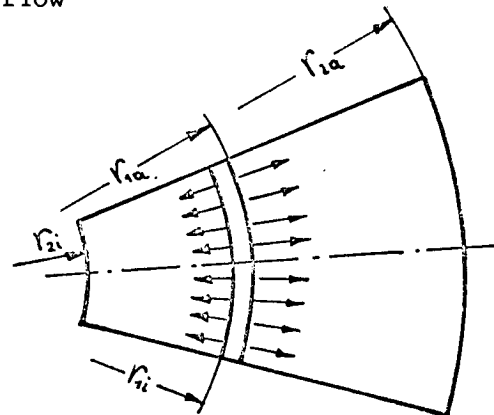
The compressible radial source flow from the center of two discs in close vicinity to each other is described in references (VII) and (VIII). With sufficiently great bearing gas pressures, sound velocity is reached at the beginning of the bearing clearance, i.e. at the opening of the inlet orifice. The radial diffuser formed by the two discs produces a further acceleration to supersonic flow and similar conditions as in a Laval nozzle can be observed here. The great pressure reduction in the supersonic region can go so far that the pressure in the clearance can become lower than the surrounding pressure. In such cases, there occurs a pressure impact which is connected with a sudden change from supersonic to subsonic speed.
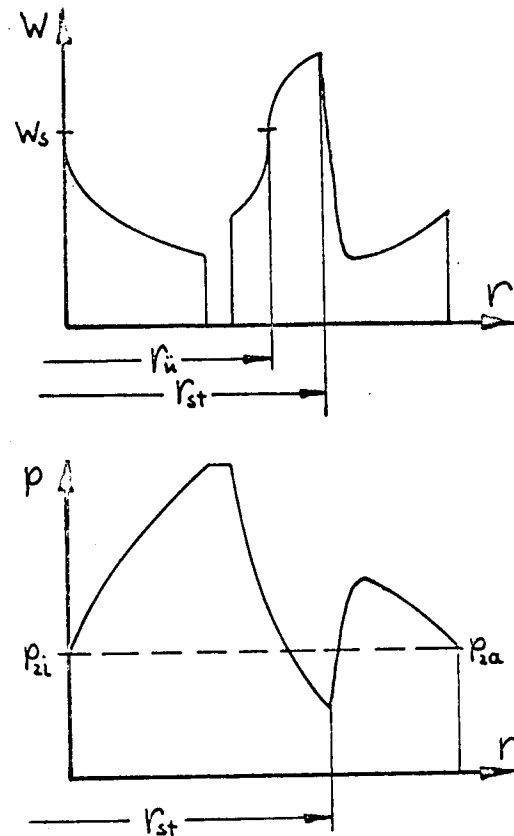
The Figures on the right side show: BOTTOM p. 41: section of a thrust bearing with bilateral flow. UPPER, this page: Course of the velocity; w_s = velocity of sound. Supersonic velocity for the outward flow between r_u and r_{st}. Pressure impact at r_{st}. Subsonic flow between r_{st} and r_{2a}, and also for the inward flow. LOWER, this page: CORRESPONDING PRESSURE PROFILE.

8.4 Conditions of separation.

With small heights of the clearance and large radii, the friction forces are so strong that, inspite of the enlarged cross section in the outward flow, there is a reduction of pressure rather than an increased pressure. Thus no positive pressure gradient is imparted to the layers in proximity to the wall, as it is the case with larger widths of the clearance, and a separation will hardly occur. The measured friction values for laminar and turbulent flow through narrow divergent clearances (IX) confirm this hypothesis.

8.5 Conditions at the transition from laminar into turbulent flow.

In the literature, the clearance flow is designated by a Reynolds number which is similar to Re_1^*, which is, however, formed with the hydraulic diameter of the radial clearance flow

$$d_h = \frac{4F}{U} = \frac{4 \cdot 2\, r \pi h}{2 \cdot 2\, r \pi} = 2h \qquad (8.13b)$$

and therefore reads:

$$Re = \frac{2hw}{\nu} = \frac{2h\gamma w}{g\eta} = \frac{2h p w}{g\eta RT} = \frac{\dot{G}}{\pi g \eta r} = \frac{2r}{h} Re_1^* \qquad (8.14)$$

At constant viscosity η and volume of flow $\dot{G}$, there is a hyperbolic relation between Re and the radius in such a way that the Renumber increases with decreasing r.

Although it is not necessary for the calculation, the friction coefficient λ_L for the clearance flow will be discussed here supplementarily. If the radial pressure decrease is defined as

$$dp = \lambda_L \frac{dr}{d_h} \frac{g}{2} w^2 \qquad , \qquad (8.14a)$$

where $d_h = 2h$ means the hydraulic diameter of the clearance flow, and $\varrho\, w^2/2$ the pressure head of the average radial velocity and if the above equation is equated to No. 7.6, then

$$dp = \lambda_L \frac{dr}{d_h} \frac{g}{2} w^2 = \frac{12\,\eta\, w\, dr}{h^2} \qquad (8.14b)$$

gives the following result: $\lambda_L = \frac{96}{Re.}$

For the flow of air through narrow clearances with constant rectangular cross sections, reference (VIII) gives a synopsis of the critical Re-numbers found by measurements. The transition value is, for example 1800 — 2000 in a channel with sharp edges at the inlet, but 2400 in a channel with rounded-off edges at the inlet opening. In reference (IX), values of 2120 — 3810 were found for clearance heights between h ≐ 50 — 250 x 10^{-6}m.

The results, reported in references (VIII) and (IX), of experiments on air flows through parallel clearances with expanded lateral borders suggest a connection between the critical Renumber and the degree of divergence of the channel. In the extreme case of the divergent clearance flow, i.e. in the flow between two parallel circular discs with eccentric gas feed across a nozzle, the transition point occurred, according to reference (VIII) already at Re = 1060. If one studies, for comparison, the calculated example on p. 31 and the Diagram 3, this low transition value can be easily understood. With small radii and high Renumbers, the flow starts as turbulent. It is a fact which is generally known that a change from turbulent to laminar flow takes place only at considerably lower Re-numbers than in the inverse case, i.e. transition from laminar to turbulent.

According to equation No. 8.14, it is to be expected, considering the variation of the Renumber over r, that the transition will be from laminar to turbulent in inward flow, but from turbulent to laminar in outward flow.

The flow in the bearings described in the present paper does not show, as a rule, high degrees of divergence or convergence on account of the geometrical shape (radial flow from a closed annular channel). Considering the poorly defined border line between laminar and turbulent flow, it is advantageous to avoid the transition region in the design of bearings. On the other hand, one can assume that, in the bearings mentioned above, there will be laminar flow when the highest Renumbers occurring there are below 2000, and turbulent flow when they are above 3000.

The experiments described above referred to fixed boundary walls of the clearance. In the practical operation of a bearing, the critical Renumbers are influenced by the rotation of a disc by the action of the v_φ components which are superimposed to the radial flow in such a way that there occurs an earlier transition from laminar into turbulent or, respectively, a delay at the transition from the turbulent to the laminar flow.

8.6 Influence of labyrinths in the bearing discs.

In a pair of discs of the testing setup (Figs. 1 and 2), experiments with recessed throttle labyrinths at the clearance outlets were performed in the region of laminar flow. The picture which follows shows the bearing discs used in the experiment and illustrates the size of the throttle sites. It was believed that there would be a greater pressure drop at the labyrinth sites than could be obtained in a smooth bearing clearance.

It was found, however, that the grooves produced a decrease in the load capacity of the bearing at an equal throughput volume, or an increased throughput volume at constant load capacity, compared to the bearing without labyrinth grooves. The fact that the smooth clearance induces the greatest resistance in laminar flow, has been verified again in this case. Only in the region of turbulent flow, baffle plates and labyrinths are effective.

Fig. 1. The pair of bearing discs with recessed throttle grooves (labyrinths) did not prove to be useful.

Resonator

Annular space
t = 1, b = 2.

Labyrinths

Feeding nozzle
d= 0.7 diameter.
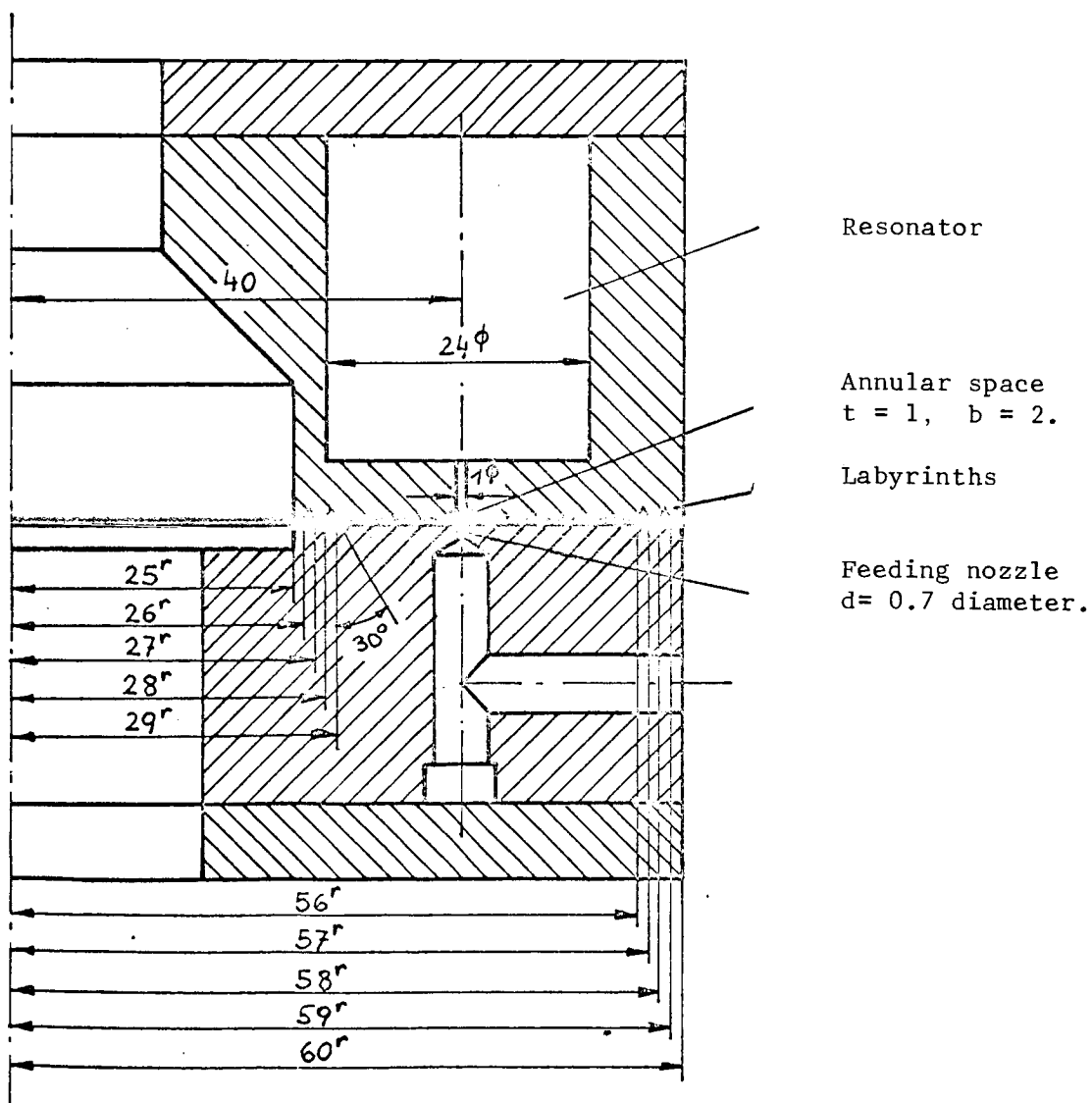
9. Turbulent, isothermal clearance flow.

Whereas the friction equation for the laminar clearance flow could be defined in a simple way by the introduction of the viscosity, the friction member da_R of the flow equation (No. 5.4) is governed by a more complex law in turbulent flow. It is useful to introduce a friction coefficient λ_T which depends on the Re-number and can be experimentally determined. The friction energy of the radial shearing stresses of the wall, therefore, becomes:

$$da_R = \pm\, \lambda_T \frac{dr}{d_h} \frac{w^2}{2g} = \pm\, \lambda_T \frac{w^2 dr}{4gh} \quad , \qquad (9.1)$$

"+" for outward flow: "-" for the flow inwards.

If the centrifugal force term of (No. 7.21) is not taken into consideration, the above equation in connection with equation No. 5.4 gives:

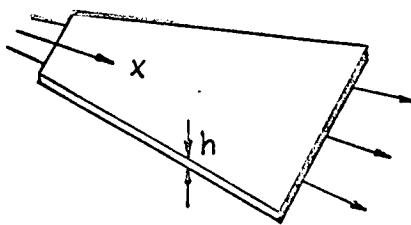$$\pm\, \lambda_T \frac{w^2 dr}{4gh} + \frac{dp}{\gamma} + \frac{w \cdot dw}{g} = 0 \quad . \qquad (9.2)$$

In reference(IX), measurements of air currents in narrow clearances with rectangular cross sections are reported. Three cases were studied which differ from each other by the shape of the channel.
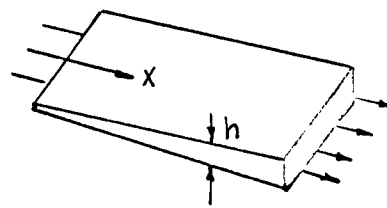
a) parallel plates,   b) parallel plates,   c) widening plates,
   parallel edge   widening edge   parallel edge
   boundaries.   boundaries   boundaries

Re = constant over x   Re ≠ constant over x   Re ≈ constant over x.

The λ_T values were given, for the cases a) and c), as a function of the Re-numbers. These values are, however, not generally applicable, because only the first two members of equation No. 9.2 were considered in the back calculation of λ_T, whereas the member w.dw/g was disregarded. The influence of this member was most comspicuous in case c). It was found that λ_T decreased in the experimemts with increasing divergence of the plates. Actually, the flow is slowed down, which causes a recovery of pressure which was considered to occur at the expense of a reduction of friction.

In the case b) where Re varies over the length of the clearance, neither local nor average λ_T values were determined in the paper quoted above.

The measurements for the case a) are illustrated in Diagram 4. Whereas the conformity with the theory is very good in the laminar region, the measured points in the turbulent area scatter somewhat more. In the paper mentioned above (IX) the influence of the roughness of the wall was not emphasized. The roughness measurements which I made in a finely ground thrust bearing disc are compiled on p. 49. I suppose that the plates used in the experiments described in reference (IX) had approximately the same average roughness ($R_m = 1.5 \times 10^{-6}$ m). Whereas the experimental points in (IX) are in rather good agreement in case a) for $h = 147 \times 10^{-6}$ m ($h/R_m \approx 98$) with the Law of Blasius for smooth boundary walls

$$\lambda_T = \frac{0.316}{\sqrt[4]{Re}}$$

(9.2a)

i.e., at this height of clearance, roughness does not have any influence yet, practically speaking, higher λ_T values were obtained at $h = 127 \times 10^{-6}$m ($h/R_m \approx 85$) on account of the greater relative roughness. It can be, furthermore, seen in Diagram 4 that the λ_T values for constant relative roughness tend towards constant values with increasing Re-numbers - which is a known fact, - these values depending only on the magnitude h/R_m.

In order to make an approximate calculation of a thrust bearing as far as course of pressure, load capacity and throughput volume are concerned, in the turbulent region, the term w.dw/g in equation No. 9.2 is disregarded and, besides, a constant value $\overline{\lambda}_T$ deduced from Diagram 4 based on an average Re-number and a known relative roughness is introduced for λ_T. It has already been estimated in Chapter 8.1 for the laminar flow, in which ranges it is allowable to disregard w.dw/g. In the later calculations, in most cases bearings are considered where the clearance flow occurs at large radial dimensions. Likewise, the ratios of the radii of the bearing between the inception and the termination of the flow

$$\frac{r_{1a}}{r_{1a}} \quad , \quad \frac{r_{1i}}{r_{1i}}$$

(9.2b)

as well as the ratios of the corresponding local Renumbers do not become very large. The λ_T value which is assumed disregarding an influence of roughness $\sim Re^{-\frac{1}{4}}$ does no longer change very much with r.

For example, for $\dfrac{r_{2a}}{r_{1a}}$ = 1.50 $\dfrac{\lambda_1}{\lambda_2}$ = 1.11
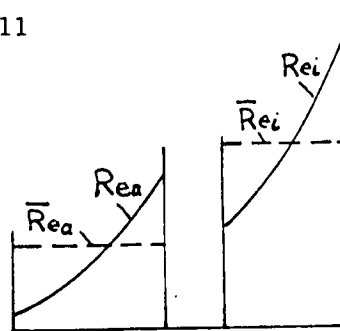
The average Reynolds numbers Re for which the corresponding λ_T values are to be determined are found for the outward flow from:

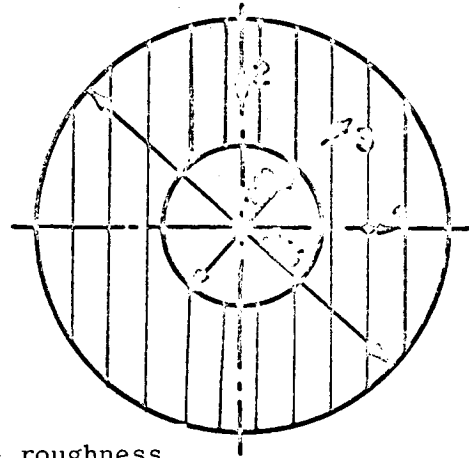$$\bar{R}_{ea} = \frac{\dot{G}_a \ln {}^{r_{2a}}\!/r_{1a}}{2\pi g \eta \, (r_{1a} + r_{2a})} \quad (9.2c)$$
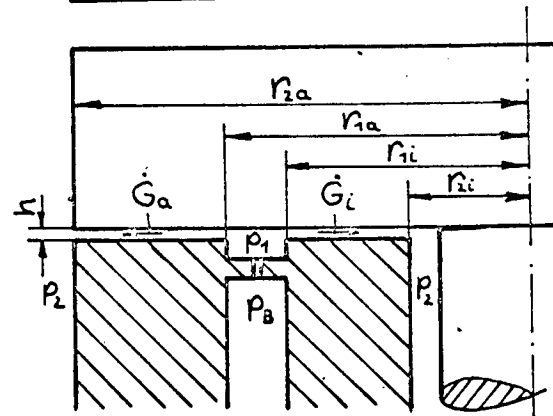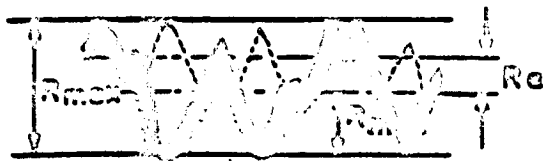
and for inward flow from:

$$\bar{R}_{ei} = \frac{\dot{G}_i \ln {}^{r_{1i}}\!/r_{2i}}{2\pi g \eta \, (r_{1i} + r_{2i})} \quad (9.2d)$$

The equation No. 9.2 is transformed by the simplifications described above to:

$$\pm \frac{\bar{\lambda}_r \, w^2 \, dr}{4 g h} + \frac{dp}{\gamma} = 0 \qquad (9.3)$$

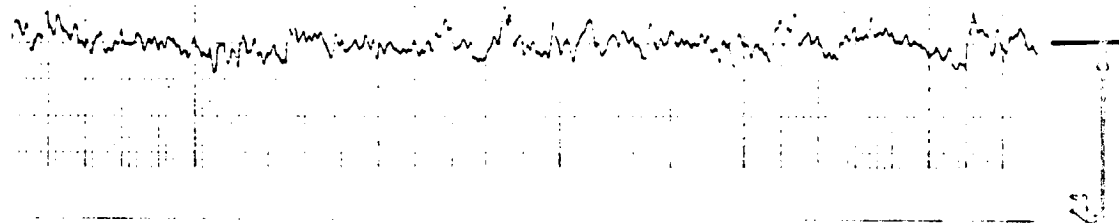Roughness measurement in

disc of a thrust bearing

(finely ground)

Rm = average roughness

$Rmax \doteq 2 Rm$ maximum depth of the roughness
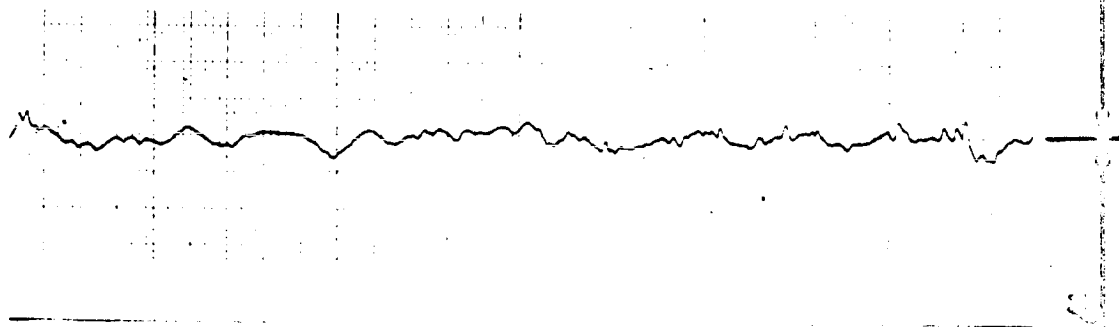
1:   in transverse direction to the $Rm = 1.0 \mu$
     direction of grinding

2:   in the direction of grindng $Rm = 1.5 \mu$

3:   45°: to the direction of $Rm = 1.5 \mu$

      grinding

Magnification, : horizontal 40, vertical 4000
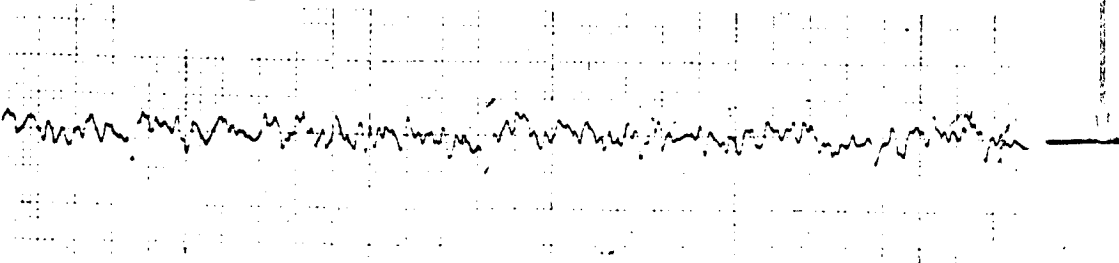
From the continuity equation No. 7.8 and the gas equation No. 7.9, the following can be concluded:

$$\pm \frac{\bar{\lambda}_T \dot{G}^2 RT}{16 \pi^2 g h^3} \cdot \frac{1}{r^2} + dp = 0 \tag{9,4}$$

after integration with consideration of the boundary conditions

$$
\begin{array}{llclll}
r = r_{1a} & p = p_{1a} & \text{oder} & r = r_{2a} & p = p_{2a} \\
r = r_{1i} & p = p_{1i} & \text{or} & r = r_{2i} & p = p_{2i}
\end{array} \tag{9.4a}
$$

the following is obtained for the flow outwards:

$$p^2 = p_{1a}^2 - \frac{\bar{\lambda}_{Ta} RT \dot{G}_a^2}{8 \pi^2 h^3 g}\left(\frac{1}{r_{1a}} - \frac{1}{r}\right) \tag{9,5}$$

or

$$p^2 = p_{2a}^2 + \frac{\bar{\lambda}_{Ta} RT \dot{G}_a^2}{8 \pi^2 h^3 g}\left(\frac{1}{r} - \frac{1}{r_{2a}}\right) \ . \tag{9,6}$$

If the volume of flow is eliminated, one obtains:

$$p^2 = p_{1a}^2 - \frac{p_{1a}^2 - p_{2a}^2}{\frac{1}{r_{1a}} - \frac{1}{r_{2a}}}\left(\frac{1}{r_{1a}} - \frac{1}{r}\right) \tag{9,7}$$

or

$$p^2 = p_{2a}^2 + \frac{p_{1a}^2 - p_{2a}^2}{\frac{1}{r_{1a}} - \frac{1}{r_{2a}}}\left(\frac{1}{r} - \frac{1}{r_{2a}}\right) \tag{9,8}$$

and for the inward flow:

$$p^2 = p_{1i}^2 - \frac{\bar{\lambda}_{Ti} RT \dot{G}_i^2}{8 \pi^2 h^3 g}\left(\frac{1}{r} - \frac{1}{r_{1i}}\right) \tag{9,9}$$

or

$$p^2 = p_{2i}^2 + \frac{\bar{\lambda}_{Ti} RT \dot{G}_i^2}{8 \pi^2 h^3 g}\left(\frac{1}{r_{2i}} - \frac{1}{r}\right) \tag{9,10}$$

and, when the volume of flow is eliminated:

$$p^2 = p_{1i}^2 - \frac{p_{1i}^2 - p_{2i}^2}{\frac{1}{r_{2i}} - \frac{1}{r_{1i}}}\left(\frac{1}{r} - \frac{1}{r_{1i}}\right) \tag{9,11}$$

or.

$$p^2 = p_{2i}^2 + \frac{p_{1i}^2 - p_{2i}^2}{\frac{1}{r_{2i}} - \frac{1}{r_{1i}}}\left(\frac{1}{r_{2i}} - \frac{1}{r}\right) \ . \tag{9,12}$$
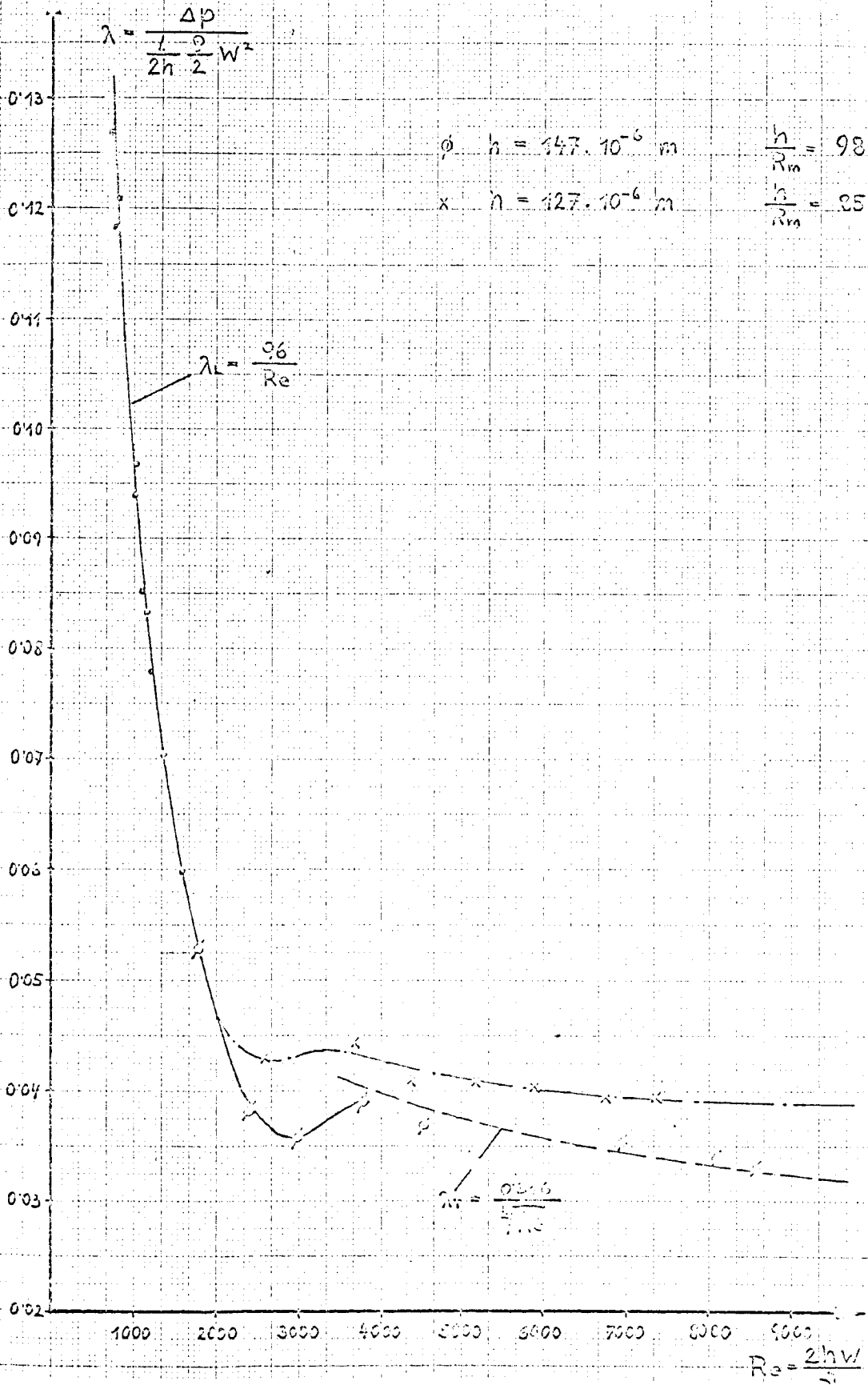
The amounts of flow are

$$\dot{G}_a = \sqrt{\frac{8 \pi^2 h^3 g \left(p_{1a}^2 - p_{2a}^2\right)}{\bar{\lambda}_{Ta} RT \left(\frac{1}{r_{1a}} - \frac{1}{r_{2a}}\right)}} \tag{9,13}$$

and

$$\dot{G}_i = \sqrt{\frac{8 \pi^2 h^3 g \left(p_{1i}^2 - p_{2i}^2\right)}{\bar{\lambda}_{Ti} RT \left(\frac{1}{r_{2i}} - \frac{1}{r_{1i}}\right)}} \tag{9,14}$$

Versuchsergebnisse aus [IX]

$$\lambda = \frac{\Delta p}{\frac{l}{2h} \cdot \frac{\rho}{2} W^2}$$

$\emptyset$ $h = 147 \cdot 10^{-6}$ m $\frac{h}{R_m} = 98$

x $h = 127 \cdot 10^{-6}$ m $\frac{h}{R_m} = 85$

$$\lambda = \frac{96}{Re}$$

$$\lambda_t = \frac{0.316}{\sqrt[4]{Re}}$$

$$Re = \frac{2hW}{\nu}$$

10. Load capacity.

The effective axial thrust K_{ges} which the bearing can take up can be determined from the difference between the force acting in the carrying bearing clearance and the force acting upon the backside of the movable bearing disc.

$$K_{ges} = K_I - K_{II} \qquad (10,1)$$

where K_I is the axial force of the carrying side of the disc, and K_{II} is the counter thrust of the non-carrying side. If the bearing is built in such a way that only one side can carry, the counter thrust is to be formed by the surrounding pressure p_2 and the area of the bearing (cf. the upper drawing.)
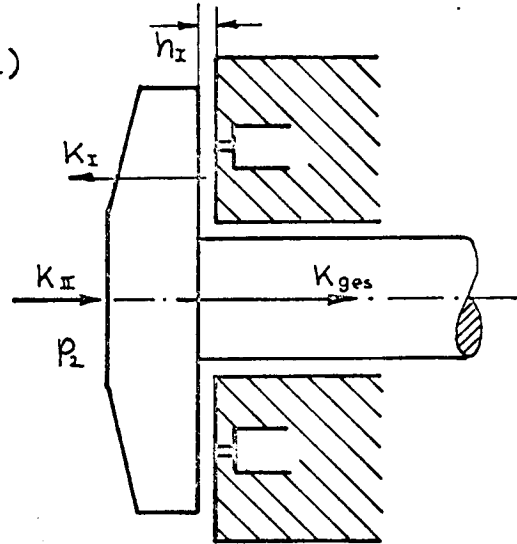
$$K_{II} = p_2 \cdot F_L \qquad (10,2)$$

where p_2 is the pressure surrounding the bearing and $F_L = (r_{2a}^2 - r_{2i}^2)$ is the bearing area of one side of the disc. In a bearing which can be loaded bilaterally and is built symmetrically the counter thrust is a magnitude which depends on the clearance h_{II}, or on the pressure in the clearance on the non-carrying side, respectively (cf. the lower drawing). Since, however, h_{II} is appreciably larger than h_I in a fully loaded bearing, the equation No. 10.2 can be applied here also in most cases.
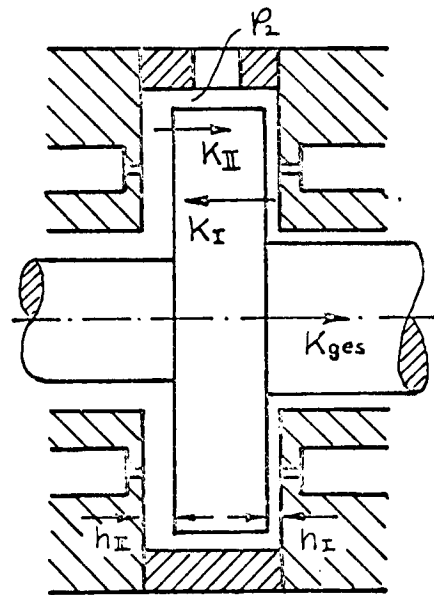
The axial force of the carrying bearing clearance can be obtained by integration of the absolute static pressure in the clearance over the whole bearing surface.

$$K_I = 2\pi \int_{r_{1i}}^{r_{1a}} p \cdot r \cdot dr \qquad (10.3)$$

An integration of equation No. 10.3 can be performed analytically only for the solution of the simple approximation (cf. Chapters 7.1 and 9.)

10.1 Radial isothermal laminar flow

If the approximation equations No. 7.14 and No. 7.18, respectively, are introduced into equation No. 10.3, the result for the outward flow is:

$$K_{Ia} = 2\pi\, p_{1a} \int_{r_{1a}}^{r_{2a}} r\, \sqrt{1 - \frac{1 - \left(\frac{p_{2a}}{p_{1a}}\right)^2}{\ln\frac{r_{2a}}{r_{1a}}}\ln\frac{r}{r_{1a}}}\ \cdot dr \qquad (10.4)$$

The results for the inward flow is:

$$K_{Ii} = 2\pi\, p_{1i} \int_{r_{2i}}^{r_{1i}} r\, \sqrt{1 - \frac{1 - \left(\frac{p_{2i}}{p_{1i}}\right)^2}{\ln\frac{r_{1i}}{r_{2i}}}\ln\frac{r_{1i}}{r}}\ \cdot dr \qquad . \quad (10.5)$$

Outward flow.

The solution of the integral for the outward flow was already given by references (IV) and (X), but will be repeated here for the sake of completeness. With the abbreviation

$$\alpha = \frac{1 - \left(\frac{p_{2a}}{p_{1a}}\right)^2}{\ln\frac{r_{2a}}{r_{1a}}} \qquad (10.5a)$$

and the substitution

$$u^2 = 1 - \alpha \ln\frac{r}{r_{1a}} \qquad\qquad r = r_{1a} \quad u = 1$$

$$r = r_{1a}\cdot e^{\frac{1-u^2}{\alpha}} \qquad\qquad r = r_{2a} \quad u = \frac{p_{2a}}{p_{1a}}$$

$$dr = -\frac{2}{\alpha}\, r_{1a}\cdot e^{\frac{1-u^2}{\alpha}}\cdot u \qquad (10.5b)$$

$u = \sqrt{1 - \alpha \ln\dfrac{r}{r_{1a}}}$	$r.dr = -\dfrac{2}{\alpha} r_{1a}^2\, e^{\frac{2(1-u^2)}{\alpha}}\cdot u\, du$

the equation No. 10.4 becomes:

$$K_{Ia} = -\frac{4}{\alpha}\, p_{1a}\, r_{1a}^2\, e^{\frac{2}{\alpha}} \int_{1}^{\frac{p_{2a}}{p_{1a}}} u\cdot u\, e^{-\frac{2}{\alpha}u^2}\, du \qquad . \quad (10.5c)$$

The above form can be simplified by partial integration, and the result is:

$$K_{Ia} = -\frac{4}{\alpha}\, p_{1a}\, r_{1a}^2\, e^{\frac{2}{\alpha}} \left\{ \left. -\frac{\alpha}{4} u\, e^{-\frac{2}{\alpha}u^2} \right|_{1}^{\frac{p_{2a}}{p_{1a}}} + \frac{\alpha}{4} \int_{1}^{\frac{p_{2a}}{p_{1a}}} e^{-\frac{2}{\alpha}u^2}\, du \right\} \qquad (10.5d)$$

If the remaining integral is transformed by further substitution, namely

$$t^2 = \frac{2}{\alpha} u^2 \qquad\qquad du = \sqrt{\frac{\alpha}{2}}\, dt$$

$$u = 1 \qquad\qquad t = \sqrt{\frac{2}{\alpha}} \qquad\qquad (10.5e)$$

$$u = \frac{p_{2a}}{p_{1a}} \qquad\qquad t = \frac{p_{2a}}{p_{1a}}\sqrt{\frac{2}{\alpha}}$$

the following is obtained

$$K_{Ia} = \pi\, p_{1a}\, r_{1a}^2 \left\{ \frac{p_{2a}}{p_{1a}}\left(\frac{r_{2a}}{r_{1a}}\right)^2 - 1 - \sqrt{\frac{\alpha}{2}}\; e^{\frac{2}{\alpha}} \int_{\sqrt{\frac{2}{\alpha}}}^{\frac{p_{2a}}{p_{1a}}\sqrt{\frac{2}{\alpha}}} e^{-t^2} dt \right\} \qquad (10.5f)$$

The integral still remaining is the error integral

$$\int_1^2 e^{-t^2}\, dt = \frac{\sqrt{\pi}}{2}\,(\phi_2 - \phi_1), \qquad\qquad (10.5g)$$

which is shown in reference (XI) for given limits in table form.

Thus the following transformation is obtained:

$$K_{Ia} = \pi\, p_{1a}\, r_{1a}^2 \;\frac{r_{2a}^2}{r_{1a}^2} \left\{ \frac{p_{2a}}{p_{1a}}\left(\frac{r_{2a}}{r_{1a}}\right)^2 - 1 - \sqrt{\frac{\pi\alpha}{8}}\; e^{\frac{2}{\alpha}} \left[\phi\left(\frac{p_{2a}}{p_{1a}}\sqrt{\frac{2}{\alpha}}\right) - \phi\left(\sqrt{\frac{2}{\alpha}}\right) \right] \right\} \quad (10.5h)$$

or

$$K_{Ia} = \pi\, p_{1a}\, r_{2a}^2\, C_{\kappa a}, \qquad\qquad (10,6)$$

where

$$C_{\kappa a} = \left(\frac{r_{1a}}{r_{2a}}\right)^2 \left\{ \frac{p_{2a}}{p_{1a}}\left(\frac{r_{2a}}{r_{1a}}\right)^2 - 1 - \sqrt{\frac{\pi\alpha}{8}}\; e^{\frac{2}{\alpha}} \left[\phi\left(\frac{p_{2a}}{p_{1a}}\right)\sqrt{\frac{2}{\alpha}} - \phi\left(\sqrt{\frac{2}{\alpha}}\right) \right] \right\} \qquad (10.6a)$$

is a dimension-less load factor which depends only on the pressure ratio p_{2a}/p_{1a} and the ratio of the radii r_{2a}/r_{1a}. In the following Table, the $C_{\kappa a}$ values are listed which were calculated as functions of the two parameters.

		p_{2a}/p_{1a}					
		0,00	0,20	0,40	0,60	0,80	1,00
	∞	0,000	0,200	0,400	0,600	0,800	1,000
	100,000	—	0,216	0,420	0,626	0,834	0,999
	10,000	0,403	0,453	0,559	0,689	0,825	0,990
	5,000	0,451	0,491	0,581	0,694	0,815	0,960
	3,333	0,465	0,499	0,575	0,675	0,773	0,910
$\dfrac{r_{2a}}{r_{1a}}$	2,500	0,459	0,486	0,552	0,638	0,728	0,840
	2,000	0,431	0,453	0,508	0,579	0,661	0,750
	1,666	0,382	0,402	0,445	0,502	0,568	0,640
	1,428	0,317	0,313	0,362	0,405	0,455	0,510
	1,250	0,230	0,240	0,260	0,289	0,321	0,359
	1,111	0,124	0,126	0,140	0,154	0,172	0,189

(10.6b)

Diagram 5 (p. 60) shows the graphical plotting of the load capacity factors for the flow in outward direction.

Inward flow

By means of the abbreviation

$$b = \frac{1 - \left(\frac{p_{2i}}{p_{1i}}\right)^2}{\ln \frac{r_{ai}}{r_{ii}}} \qquad (10.6c)$$

and the substitution

$$v^2 = 1 - b \ln \frac{r_{ai}}{r} \qquad\qquad r = r_{ai} \quad v = 1$$

$$r = r_{ai} \, e^{\frac{v^2-1}{b}} \qquad\qquad r = r_{ii} \quad v = \frac{p_{2i}}{p_{1i}} \qquad (10.6d)$$

$$dr = r_{ai} \, \frac{2}{b} \, e^{\frac{v^2-1}{b}} \cdot v$$

$$\boxed{v = \sqrt{1 - b \ln \frac{r_{ai}}{r}}} \qquad \boxed{r\,dr = \frac{2}{b} \, r_{ai}^2 \, e^{\frac{2(v^2-1)}{b}} \, v \, dv}$$

the axial force deduced from equation No. 10.5 is

$$K_{Ii} = \frac{4}{b} \, \pi \, p_{1i} \, r_{ai}^2 \int_{\frac{p_{2i}}{p_{1i}}}^{1} v^2 \, e^{\frac{2(v^2-1)}{b}} \, dv \qquad (10.6e)$$

or

$$K_{Ii} = \frac{4}{b} \, \pi \, p_{1i} \, r_{ai}^2 \, e^{-\frac{2}{b}} \int_{\frac{p_{2i}}{p_{1i}}}^{1} v \cdot v \cdot e^{\frac{2v^2}{b}} \, dv \quad , \qquad (10.6f)$$

which gives, after partial integration,

$$K_{Ii} = \pi \, p_{1i} \, r_{ai}^2 \, e^{-\frac{2}{b}} \left\{ \left| v \, e^{\frac{2v^2}{b}} \right|_{\frac{p_{2i}}{p_{1i}}}^{1} - \int_{\frac{p_{2i}}{p_{1i}}}^{1} e^{\frac{2v^2}{b}} \, dv \right\} \qquad (10.6g)$$

By further substitution, namely

$$\boxed{s^2 = \frac{2v^2}{b}} \qquad \boxed{dv = \sqrt{\frac{b}{2}} \, ds}$$

$$v = 1 \qquad\qquad s = \sqrt{\frac{2}{b}}$$

$$v = \frac{p_{2i}}{p_{1i}} \qquad\qquad s = \frac{p_{2i}}{p_{1i}} \sqrt{\frac{2}{b}}$$

(10.6h)

the integral is simplified and, with the limits introduced, it reads:

$$K_{Ii} = \pi \, p_{1i} \, r_{ai}^2 \left\{ 1 - \frac{p_{2i}}{p_{1i}} \left(\frac{r_{ii}}{r_{ai}}\right)^2 - \sqrt{\frac{b}{2}} \, e^{-\frac{2}{b}} \int_{\frac{p_{2i}}{p_{1i}}\sqrt{\frac{2}{b}}}^{\sqrt{\frac{2}{b}}} e^{s^2} \, ds \right\} \, . \qquad (10.6i)$$

The remaining integral represents, according to reference (XII), the progression:

$$\int e^{s^2} ds = S + \frac{s^3}{3 \cdot 1!} + \frac{s^5}{5 \cdot 2!} + \frac{s^7}{7 \cdot 3!} + \cdots = \psi(s) \qquad (10.6j)$$

For the boundary conditions between 0 and 2, the ψ values can be obtained from a Table given in reference (XI). For limiting values larger than 2, the series was discontinued, for the present calculations, after the 10th member. Thus the force K_{Ii} becomes

$$K_{Ii} = \pi p_{1i} r_{1i}^2 \left\{ 1 - \frac{p_{2i}}{p_{1i}} \left(\frac{r_{1i}}{r_{1i}}\right)^2 - \sqrt{\frac{b}{2}} \; e^{-\frac{2}{b}} \left[\psi\left(\sqrt{\frac{2}{b}}\right) - \psi\left(\frac{p_{2i}}{p_{1i}}\sqrt{\frac{2}{b}}\right) \right] \right\} \qquad (10.6k)$$

or

$$K_{Ii} = \pi p_{1i} r_{1i}^2 \, C_{ki} , \qquad (10,7)$$

where

$$C_{ki} = 1 - \frac{p_{2i}}{p_{1i}} \left(\frac{r_{1i}}{r_{1i}}\right)^2 - \sqrt{\frac{b}{2}} \; e^{-\frac{2}{b}} \left[\psi\left(\sqrt{\frac{2}{b}}\right) - \psi\left(\frac{p_{2i}}{p_{1i}}\sqrt{\frac{2}{b}}\right) \right] \qquad (10.7a)$$

represents again a dimension-less factor which depends only on the ratio of the pressures and radii. The C_{ki} values were calculated as functions of the two parameters; they are compiled in the Table which follows and plotted graphically in Diagram 6 (p. 62)

		p_{2i}/p_{1i}					
		0,00	0,20	0,40	0,60	0,80	1,00
	∞	1,000	1,000	1,000	1,000	1,000	1,000
	10,000	0,881	0,895	0,911	0,936	0,962	0,990
	5,000	0,806	0,816	0,835	0,864	0,908	0,960
$\dfrac{r_{1i}}{r_{2i}}$	3,333	0,733	0,744	0,769	0,808	0,856	0,910
	2,500	0,653	0,664	0,693	0,736	0,784	0,840
	2,000	0,565	0,576	0,605	0,645	0,695	0,750
	1,666	0,468	0,478	0,506	0,543	0,589	0,640
	1,428	0,366	0,373	0,396	0,428	0,466	0,510
	1,250	0,253	0,258	0,275	0,299	0,327	0,360
	1,111	0,129	0,134	0,143	0,156	0,172	0,190

(10.7b)

10.2 Isothermal turbulent radial flow.

If the equations No. 9.7 and 9.11, respectively, for the course of pressure, derived for simplified conditions (w.dw = 0, Ω = 0), are introduced into equation No. 10.3, again an analytical solution of the integral is possible.

Outward flow

The equation

$$K_{Ia} = 2\pi p_{1a} \int_{r_{1a}}^{r_{2a}} r \sqrt{1 - \frac{1 - \left(\frac{p_{2a}}{p_{1a}}\right)^2}{\frac{1}{r_{1a}} - \frac{1}{r_{2a}}} \left(\frac{1}{r_{1a}} - \frac{1}{r}\right)} \; dr \qquad (10.8)$$

using the following abbreviations

$$m = \frac{1 - \left(\frac{p_{2a}}{p_{1a}}\right)^2}{1 - \frac{r_{1a}}{r_{2a}}} \qquad \text{and} \qquad n = 1 - m \qquad (10.8a)$$

becomes

$$K_{Ia} = 2\pi p_{1a} \int_{r_{1a}}^{r_{2a}} \sqrt{nr^2 + r_{1a} m r} \; dr \; . \qquad (10.9)$$

According to reference (XII), the solutions depend on the magnitude of coefficients.

a) for $n < 0$, i.e. if $\left(\frac{p_{2a}}{p_{1a}}\right)^2 < \frac{r_{1a}}{r_{2a}}$ \qquad (10.9a)

the result is

$$K_{Ia} = \pi r_{2a}^2 p_{1a} \left\{ \left(1 + \frac{r_{1a}}{r_{2a}} \frac{m}{2n}\right) \frac{p_{2a}}{p_{1a}} - \left(\frac{r_{1a}}{r_{2a}}\right)^2 \left(1 + \frac{m}{2n}\right) + \right.$$

$$\left. + \left(\frac{r_{1a}}{r_{2a}}\right)^2 \frac{m^2}{4n\sqrt{-n}} \left[\arcsin\left(\frac{2n}{m}\frac{r_{2a}}{r_{1a}} + 1\right) - \arcsin\left(\frac{2n}{m} + 1\right)\right] \right\} \qquad (10.10)$$

or $\qquad K_{Ia} = \pi r_{2a}^2 p_{1a} C'_{Ka_1} \; . \qquad (10.11)$

b) for $n > 0$, i.e. if $\left(\frac{p_{2a}}{p_{1a}}\right)^2 > \frac{r_{1a}}{r_{2a}}$ \qquad (10.11a)

the following applies

$$K_{Ia} = \pi r_{2a}^2 p_{1a} \left\{ \left(1 + \frac{r_{1a}}{r_{2a}} \frac{m}{2n}\right) \frac{p_{2a}}{p_{1a}} - \left(\frac{r_{1a}}{r_{2a}}\right)^2 \left(1 + \frac{m}{2n}\right) - \right.$$

$$\left. - \left(\frac{r_{1a}}{r_{2a}}\right)^2 \frac{m^2}{4n\sqrt{n}} \left[\text{Arc}\cos\left(\frac{2n}{m}\frac{r_{2a}}{r_{1a}} + 1\right) - \text{Arc}\cos\left(\frac{2n}{m} + 1\right)\right] \right\} \qquad (10,12)$$

or $\qquad K_{Ia} = \pi r_{2a}^2 p_{1a} C'_{Ka_2}. \qquad (10,13)$

Depending on the sign of n, the first or the second term must be used for the determination of the load capacity. The factors C_{ka} are dimension-less values which depend on the ratios of the pressure and the radii. They are compiled in the following Table, and in Diagram 5a.

				p_{2a}/p_{1a}			
		0,00	0,20	0,40	0,60	0,80	1,00
	100,000	0,075	0,220	0,410	0,605	0,801	0,999
	10,000	0,248	0,329	0,473	0,638	0,811	0,990
	5,000	0,337	0,396	0,515	0,651	0,802	0,960
	3,333	0,385	0,448	0,525	0,645	0,771	0,910
	2,500	0,404	0,446	0,515	0,620	0,722	0,840
$\dfrac{r_{2a}}{r_{1a}}$	2,000	0,392	0,425	0,482	0,564	0,651	0,750
	1,666	0,359	0,380	0,428	0,491	0,576	0,640
	1,428	0,305	0,321	0,354	0,405	0,459	0,510
	1,250	0,223	0,230	0,254	0,289	0,322	0,359
	1,111	0,120	0,130	0,146	0,157	0,172	0,189

(10.13a)

Inward flow.

The integral

$$K_{Ii} = 2\pi\,p_{1i}\int_{r_{2i}}^{r_{1i}} r\,\sqrt{1 - \frac{1 - \left(\frac{p_{2i}}{p_{1i}}\right)^2}{\frac{1}{r_{2i}} - \frac{1}{r_{1i}}}\left(\frac{1}{r} - \frac{1}{r_{1i}}\right)}\; dr \tag{10.14}$$

using the following abbreviations

$$k = \frac{1 - \left(\frac{p_{2i}}{p_{1i}}\right)^2}{\frac{r_{1i}}{r_{2i}} - 1} \qquad \text{and} \qquad \ell = 1 + k \tag{10.14a}$$

becomes

$$K_{Ii} = 2\pi\,p_{1i}\int^{r_{1i}} \sqrt{\ell\,r^2 - r_{1i}\,k\,r}\; dr . \tag{10.15}$$

Since the coefficient ℓ is always greater than zero, there is only one solution:

$$K_{Ii} = \pi\,r_{1i}^2\,p_{1i}\left\{\left(1 - \frac{k}{2\ell}\right) - \left(\frac{r_{2i}}{r_{1i}} - \frac{k}{2\ell}\right)\frac{r_{2i}}{r_{1i}}\frac{p_{2i}}{p_{1i}} - \right. \tag{10.16}$$
$$\left. - \frac{k^2}{4\ell\sqrt{\ell}}\left[\text{ArcCos}\left(\frac{2\ell}{k} - 1\right) - \text{ArcCos}\left(\frac{2\ell}{k}\frac{r_{2i}}{r_{1i}} - 1\right)\right]\right\} .$$

The following is obtained if a load capacity factor, C_{ki}, is introduced:

$$K_{Ii} = \pi r_{1i}^2 p_{1i} C_{ki} \quad .$$
(10.17)

The following Table and Diagram 6a shows the relationship of these C_{ki} values:

		p_{2i}/p_{1i}					
		0,00	0,20	0,40	0,60	0,80	1,00
$\dfrac{r_{1i}}{r_{2i}}$	10,000	0,941	0,942	0,949	0,960	0,973	0,990
	5,000	0,868	0,872	0,885	0,905	0,930	0,960
	3,333	0,785	0,791	0,809	0,836	0,871	0,910
	2,500	0,693	0,702	0,723	0,755	0,794	0,840
	2,000	0,594	0,603	0,629	0,661	0,702	0,750
	1,666	0,488	0,498	0,520	0,554	0,594	0,640
	1,428	0,374	0,386	0,406	0,434	0,469	0,510
	1,250	0,256	0,258	0,282	0,302	0,329	0,359
	1,111	0,130	0,131	0,149	0,158	0,168	0,189

(10.17a)

11. Optimization and economy

11.1 Optimum geometry for bearings without compensating space.

If the bearing gas is fed into the clearance of the bearing at the site $r_{1a} = r_{1i} = r_0$ - this can be done by a circular clearance as feeding organ, or by individual nozzles which open into a compensating channel of close to zero width - and if the flow is always in radial direction, r_0 can assume any value between r_{2i} and r_{2a}. Therefore, criteria must be found for which r_0 has the most economical or favorable value, respectively.

A) Bearing for the smallest flow volume

If a bearing shall have a gas consumption which is small as possible, i.e. the output of the bearing gas compressor shall be at a minimum at given pressures, namely:

p_B pressure of the bearing gas in front of the throttling devices,

$p_{1a} = p_{1i} = p_1$ highest pressure in the clearance

$p_{2a} = p_{2i} = p_2$ pressure surrounding the bearing

and if the radii r_{2i} and r_{2a} are given, the following must apply:

$$\dot{G}_I = \dot{G}_a + \dot{G}_i = \text{Min !}$$
(11.0a)

or
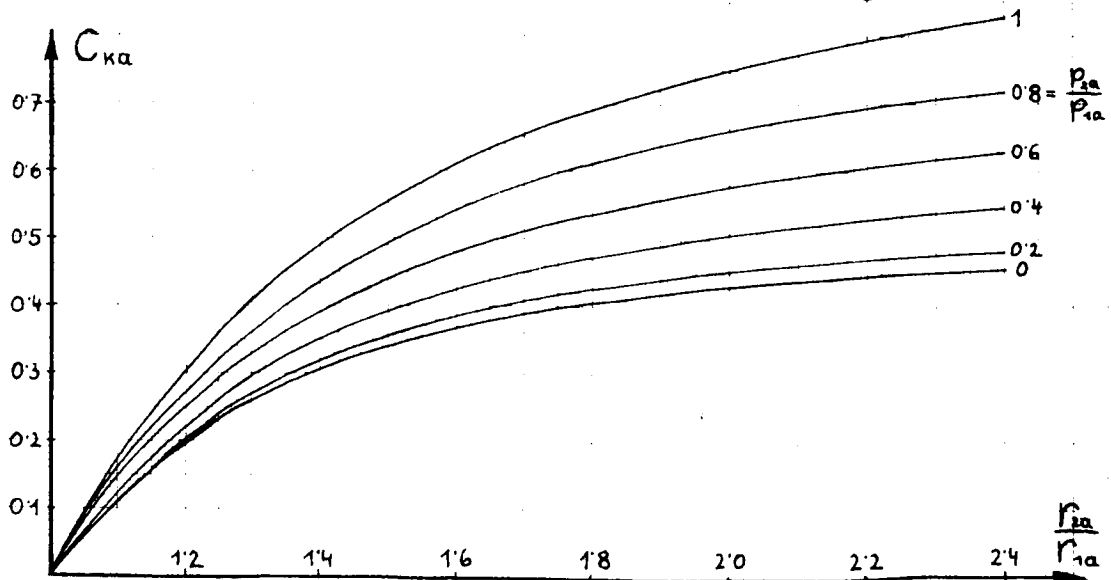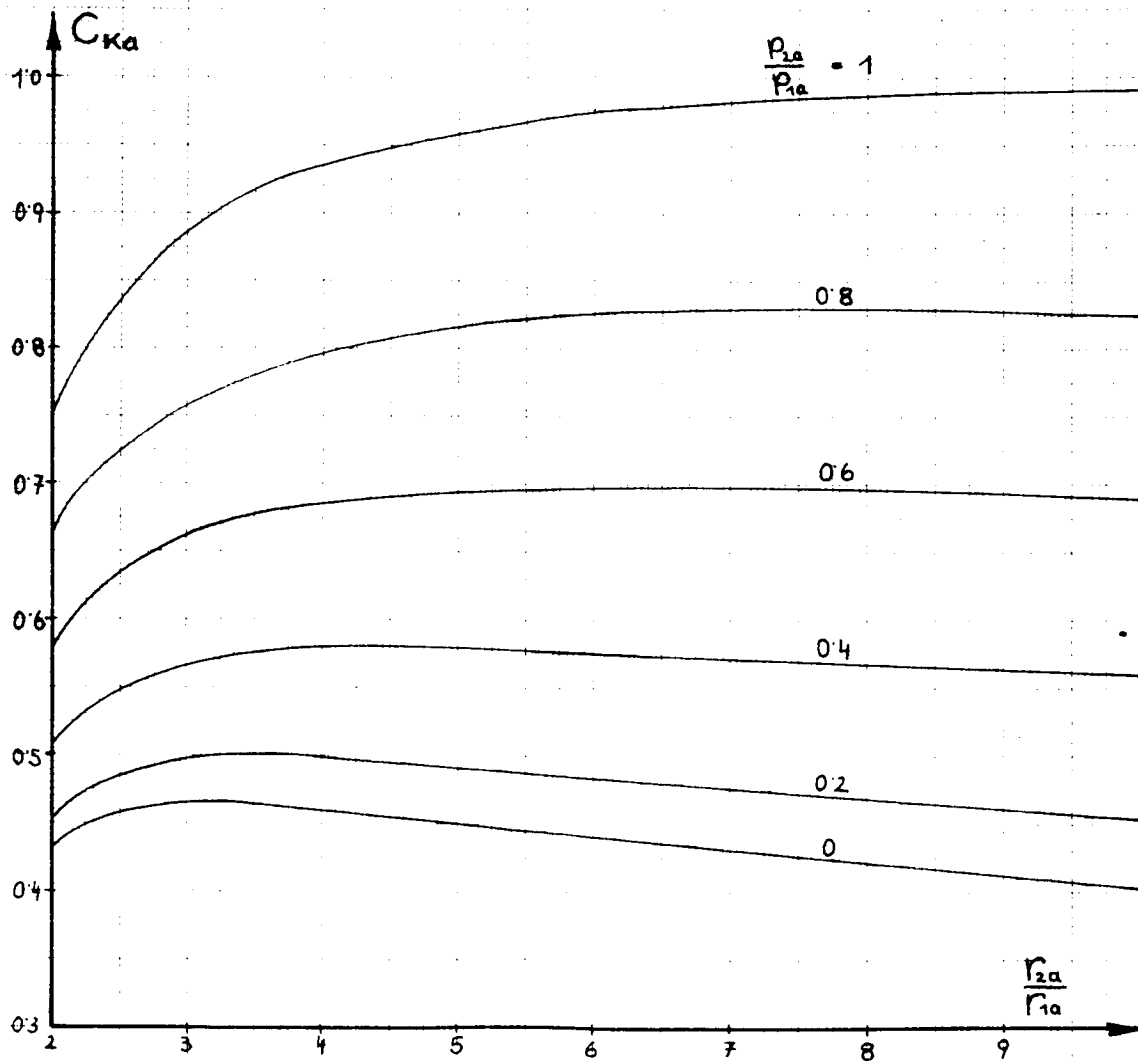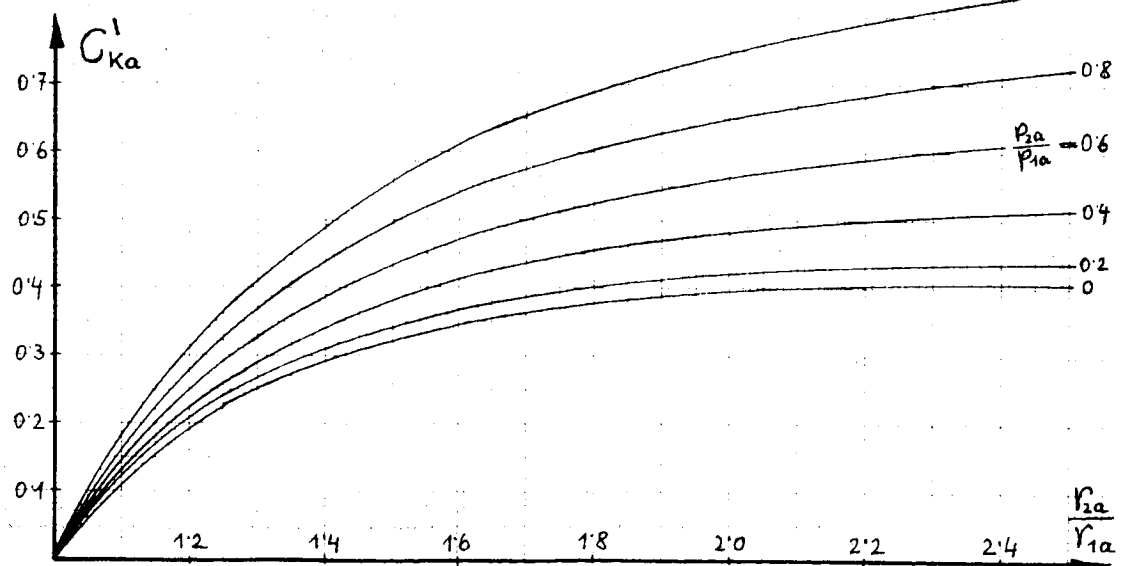$$\frac{\partial(\dot{G}_a + \dot{G}_i)}{\partial r_0} = 0$$
(11.1)

Diagramm 5a
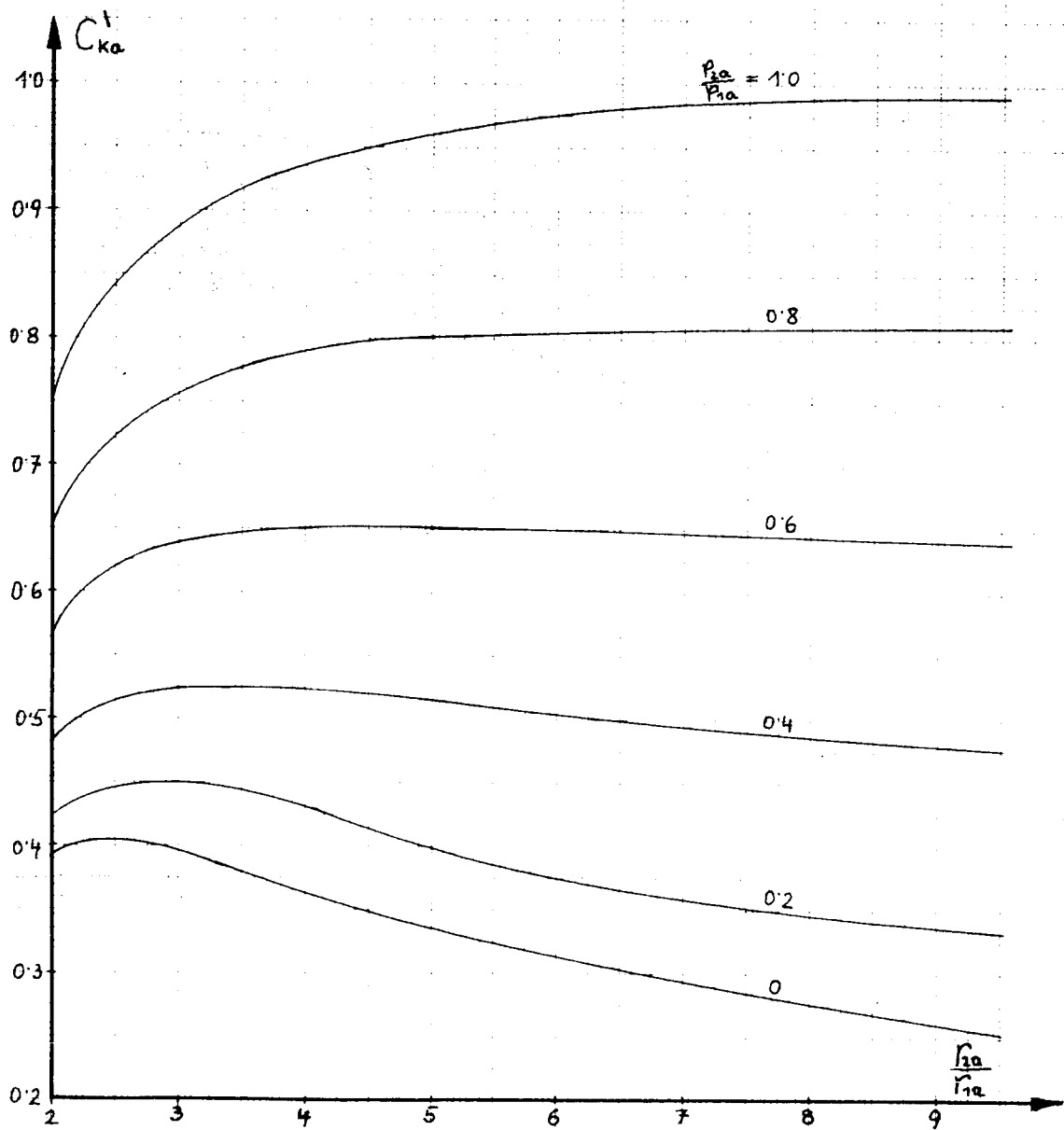
Diagramm 6

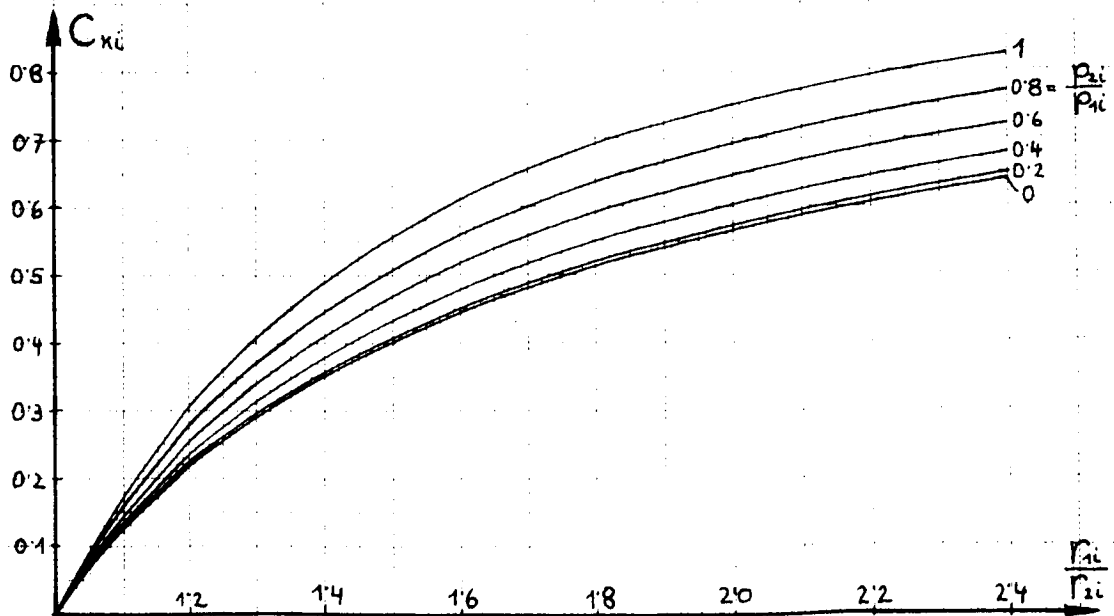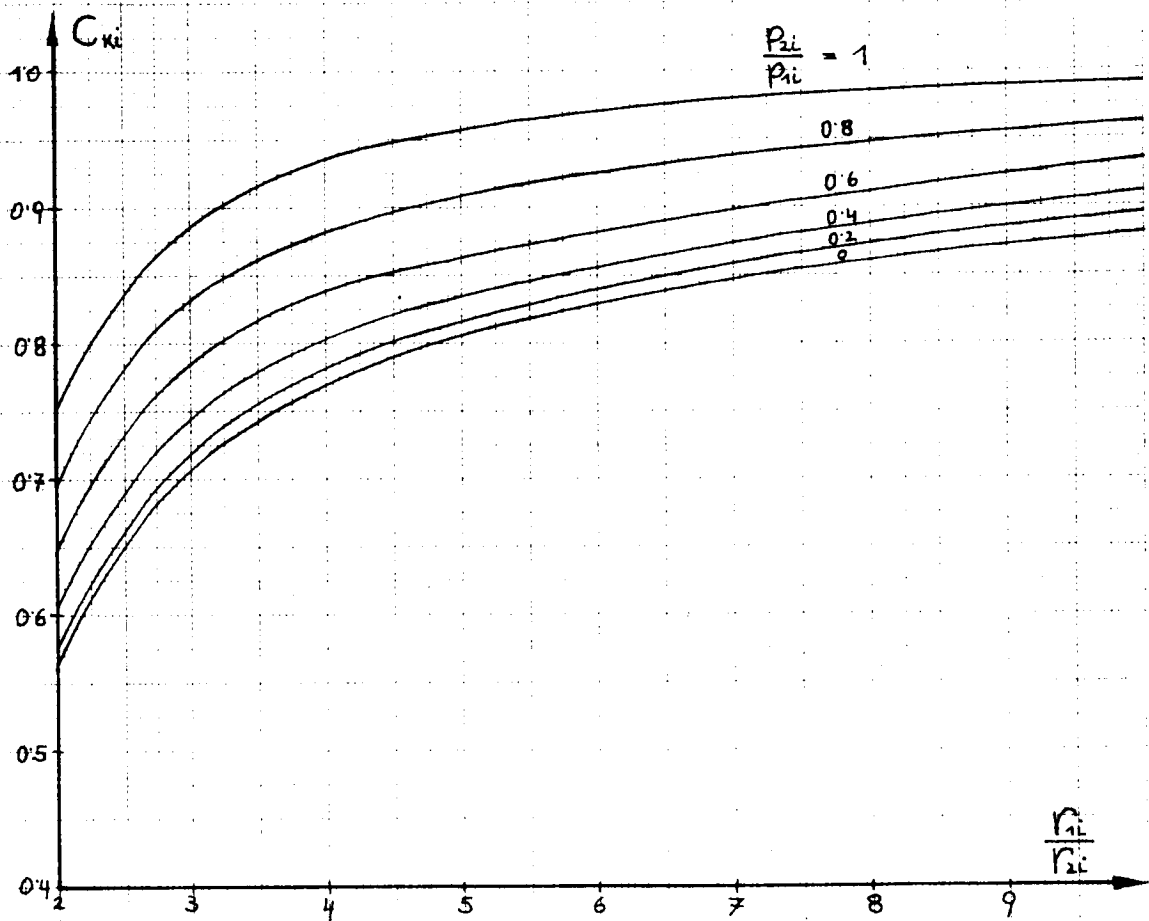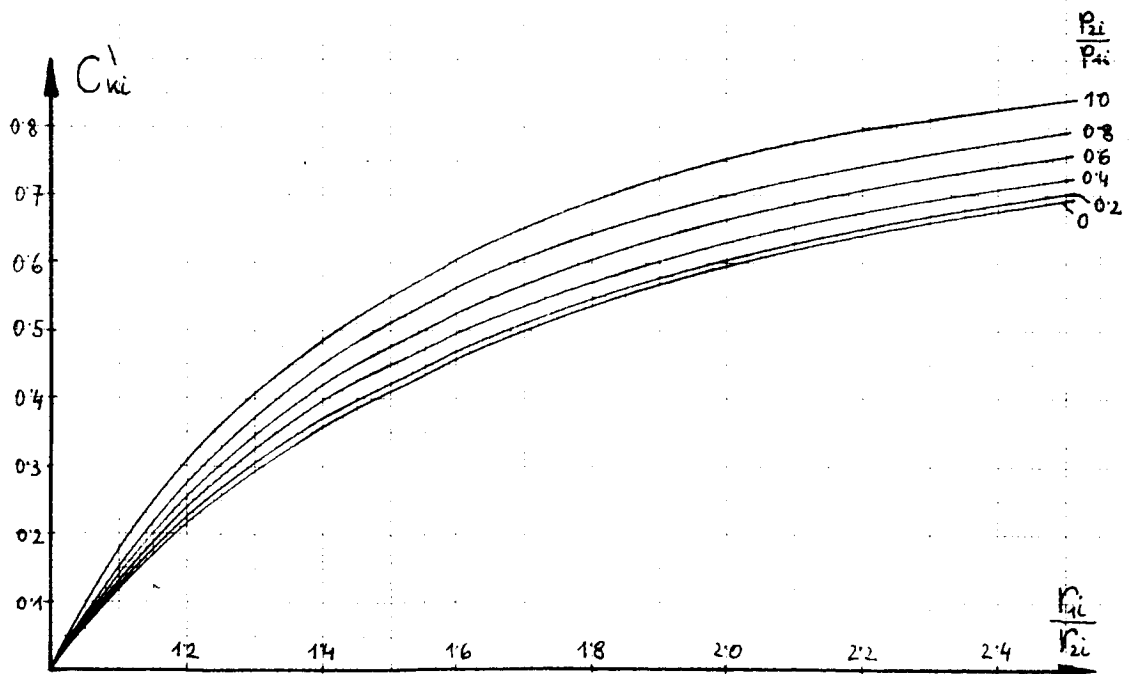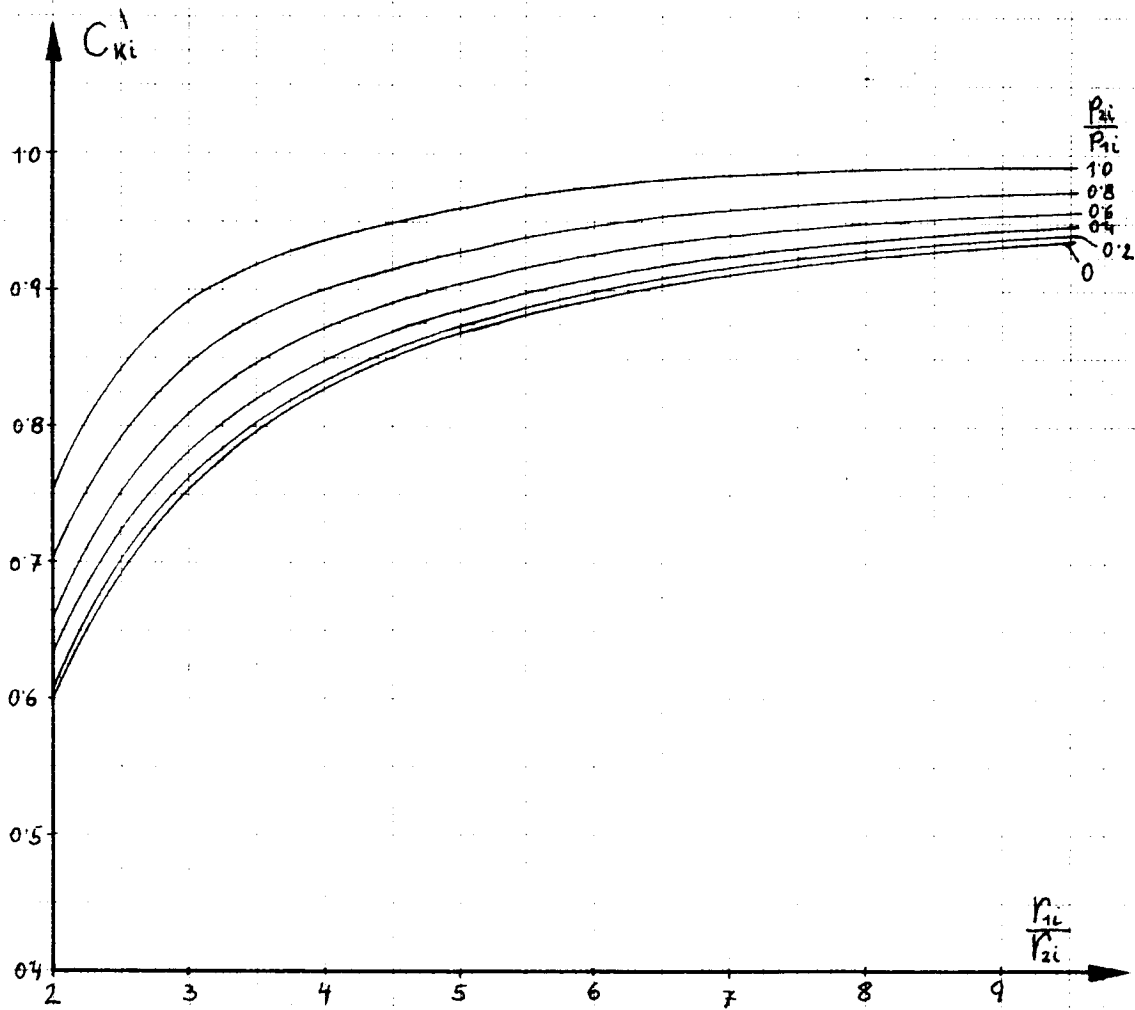Diagramm 6a

Laminar flow.

If the equations No. 7.19 and 7.20 are introduced into equation No. 11.1, the following will occur:

$$\frac{\partial}{\partial r_o}\left(\frac{\pi h^3 (p_1^2 - p_2^2)}{12 \eta RT \ln\frac{r_{2a}}{r_o}} + \frac{\pi h^3 (p_1^2 - p_2^2)}{12 \eta RT \ln\frac{r_o}{r_{2i}}}\right) = 0 \quad . \tag{11.1a}$$

If the constant factors are omitted and the equation is further transformed, the result is

$$\frac{\partial}{\partial r_o}\left(\frac{\ln\frac{r_o}{r_{2i}} + \ln\frac{r_{2a}}{r_o}}{\ln\frac{r_{2a}}{r_o}\ln\frac{r_o}{r_{2i}}}\right) = 0 \tag{11.1b}$$

and

$$\frac{\partial}{\partial r_o}\left(\ln\frac{r_{2a}}{r_o}\ \ln\frac{r_o}{r_{2i}}\right) = 0 \quad . \tag{11.1c}$$

The differentiation with respect to r_o thus gives:

$$-\frac{1}{r_o}\ln\frac{r_o}{r_{2i}} + \frac{1}{r_o}\ln\frac{r_{2a}}{r_o} = 0 \ , \tag{11.1d}$$

for which the following results:

$$\frac{r_o}{r_{2i}} = \frac{r_{2a}}{r_o} \qquad \text{or} \qquad r_o = \sqrt{r_{2a}\ r_{2i}} \tag{11.2}$$

In a bearing with laminar flow and lowest gas consumption, the radius of the inlet site r_o must equal the geometrical average of largest and smallest bearing diameter. This formula (No. 11.2) is illustrated, by way of comparison, in Diagram 7. It can be easily seen, besides, that the amount of throughput is a minimum when both partial flows are of equal size.

$$\dot{G}_a = \dot{G}_i.$$

On p. 68, the course of pressure in the bearing clearance, the volumes of throughput and the load capacity for constant initial and terminal pressures and given main dimensions of the bearing are shown diagrammatically for variations of r_o between r_{2i} and r_{2a}. whereas $\dot{G}_I$ is infinitely large at the sites r_{2i} and r_{2a}, and has the smallest value at $r_o = \sqrt{r_{2a} \cdot r_{2i}}$, the load capacity K_I increases continuously from r_{2i} to r_{2a}.

Turbulent flow.

If the equations No. 9.13 and No. 9.14 are introduced into the equation No. 11.1, the consequence is:

$$\frac{\partial}{\partial r_o}\left[\sqrt{\frac{8\pi^2 h^3 g (p_1^2 - p_2^2)}{\lambda_{Ta} RT \left(\frac{1}{r_o} - \frac{1}{r_{2a}}\right)}} + \sqrt{\frac{8\pi^2 h^3 g (p_1^2 - p_2^2)}{\lambda_{Ti} RT \left(\frac{1}{r_{2i}} - \frac{1}{r_o}\right)}}\right] = 0 \quad . \tag{11.2a}$$

If the constant magnitudes are omitted and it is, furthermore, assumed that $\lambda_{Ta} \approx \lambda_{Ti}$, the following remains:

$$\frac{\partial}{\partial r_o}\left[\frac{1}{\sqrt{\frac{1}{r_o} - \frac{1}{r_{2a}}}} + \frac{1}{\sqrt{\frac{1}{r_{2i}} - \frac{1}{r_o}}}\right] = 0 \quad . \tag{11.2b}$$

Partial differentiation with respect to r_o and further simplification gives:

$$1 - \frac{r_o}{r_{2a}} = \frac{r_o}{r_{2i}} - 1 \tag{11.2c}$$

and thus for the radius in question:

$$r_o = \frac{2\, r_{2a}\, r_{2i}}{r_{2a} + r_{2i}} \tag{11.2d}$$

or the following equations:

$$\frac{r_o}{r_{2a}} = \frac{2}{1 + \frac{r_{2a}}{r_{2i}}} \qquad \text{and} \qquad \frac{r_o}{r_{2i}} = \frac{2}{1 + \frac{r_{2i}}{r_{2a}}} \quad . \tag{11.3}$$

The amount of throughput of the bearing with turbulent flow has, likewise, a minimum at $\dot{G}_a = \dot{G}_i$. By equating No. 9.13 and No. 9.14 directly, the same result is obtained. In Diagram 7, equation No. 11.3 is illustrated in the form of a curve. It can be seen, as a striking feature, that radius r_o is appreciably closer to r_{2i} in turbulent flow than it is in laminar flow.

B) Bearing for load capacity/flow volume = maximum.

In the following discussions. again p_B, $p_{1a} = p_{1i} = p_1$, $p_{2a} = p_{2i} = p_2$, as well as the radii r_{2i} and r_{2a} are constant and given. The diagrams on p. 68 show G_I and K_I as a function of the gas inlet radius r_o. The inclusion of the absolute load capacity K_I in the discussions on optimization makes only sense if the equivalent comparative value of K_I versus G_I has been clarified. In addition to the frequent cases where G_I is to be kept as small as possible, there are applications of aerostatic bearings where the amount of throughput is rather unimportant. In these cases, however, the bearing must have the highest possible load capacity at increased gas consumption. Thus, if one arrives at a comparison between optimum load capacity and minimum throughput and if the criterion

$$\frac{K_I}{G_I} = \text{Max} ! \quad , \tag{11.4}$$

is selected for the determination of r_o, an optimization can be performed in a relatively simple way. If the equations No. 10.6, 10.7, 7.19 and 7.20 of the isothermal laminar flow are introduced into formula No. 11.4, the following result is obtained:

$$\frac{K_I}{G_I} = \frac{\pi p_1 \left(r_{2a}^2 C_{ka} + r_o^2 C_{ki} \right)}{\frac{\pi h^3 (p_1^2 - p_2^2)}{12 \eta RT} \left[\frac{1}{\ln \frac{r_{2a}}{r_o}} + \frac{1}{\ln \frac{r_o}{r_{2i}}} \right]} = Max \ ! \quad (11.4a)$$

If the magnitudes which are kept constant are eliminated, the following remains:

$$\left[\left(\frac{r_{2a}}{r_{2i}} \right)^2 C_{ka} + \left(\frac{r_o}{r_{2i}} \right)^2 C_{ki} \right] \ln \frac{r_{2a}}{r_o} \ln \frac{r_o}{r_{2i}} = Max \ ! \ , \quad (11.4b)$$

where C_{ka} and C_{ki} are functions of the ratios r_{2a}/r_o, r_o/r_{2i} and, respectively, $r_{2a} \cdot r_o/r_{2i} \cdot r_{2a}$. The maximum of this function could be obtained by equating the partial differentiation with respect to r_o to zero. Since, however, this cannot be performed analytically, the function for various ratios r_{2a}/r_{2i} over r_o/r_{2a} was plotted graphically and the optimum values obtained for the individual curves

$$\frac{r_o}{r_{2i}} = f\left(\frac{r_{2a}}{r_{2i}} \right) \quad (11.4c)$$

were recorded in Diagram 7. For the determination of the C_k values, a pressure ratio $p_2/p_1 = 0.20$ which remains constant was assumed. Since the C_k curves (cf. pp. 60 and 62) show similar courses for various pressure ratios, it can be assumed that the present result depends on pressure to a limited extent only.

11.2 Optimum geometry for a bearing with compensation space.

The annular compensation space which is the fundamental principle of these studies serves for the uniform distribution of the gas prior to the clearance flow and for increasing the load capacity. The feeding nozzles open into this space. If the depth of the compensationspace s $\gg$ h is designed much larger than the bearing clearance, p_1 is constant over the area of the recess. Besides, the effective throttling length of the bearing clearance is shortened by the compensating space in such a way that the throughput is increased; on the other hand, it reduces also the friction in the bearing when the shaft is rotating.

As far as the interrelationship of the limiting radii of the compensation space, r_{1i} and r_{1a} is concerned, a law similar to equation No. 11.2 has been established:

$$r_{1a} \cdot r_{1i} = r_{2a} \cdot r_{2i} \quad (11.5)$$

This selection was made in such a way that, with isothermal laminar flow which is presumed to occur in the discussions below, the two partial amounts $\dot{G}_a$ and $\dot{G}_i$ are equal.

The following question arises now: How large should the compensating space be in a bearing the limiting dimensions of which are given, and which pressure of the bearing gas is required in order to reduce the total power input which is composed of the effect of the bearing gas compressor N_1 and of the friction due to the rotation N_2 of the shaft, to a minimum, if the load capacity K_I has been established?
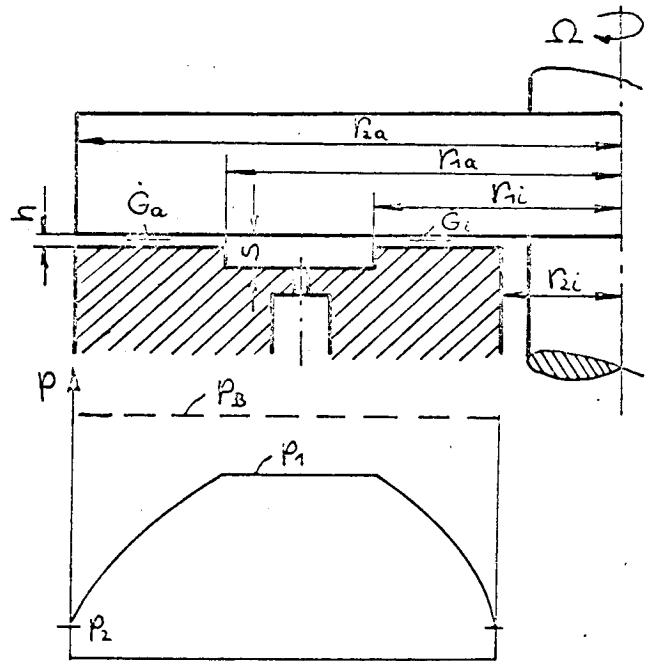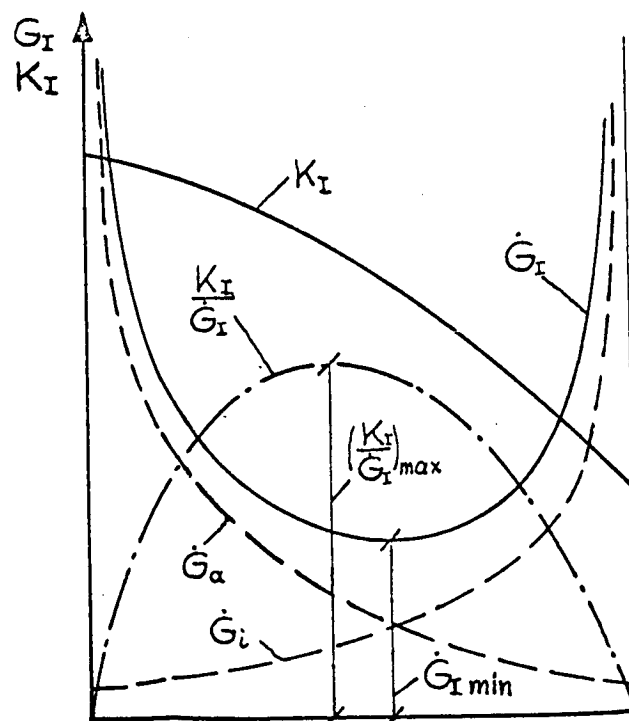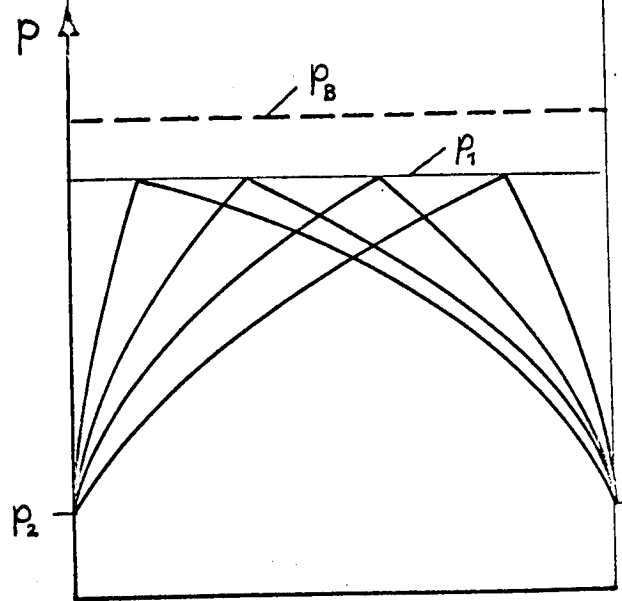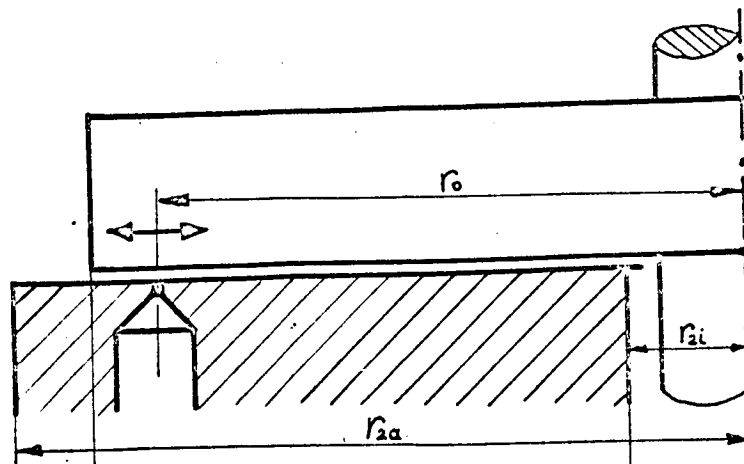

Diagramm 7
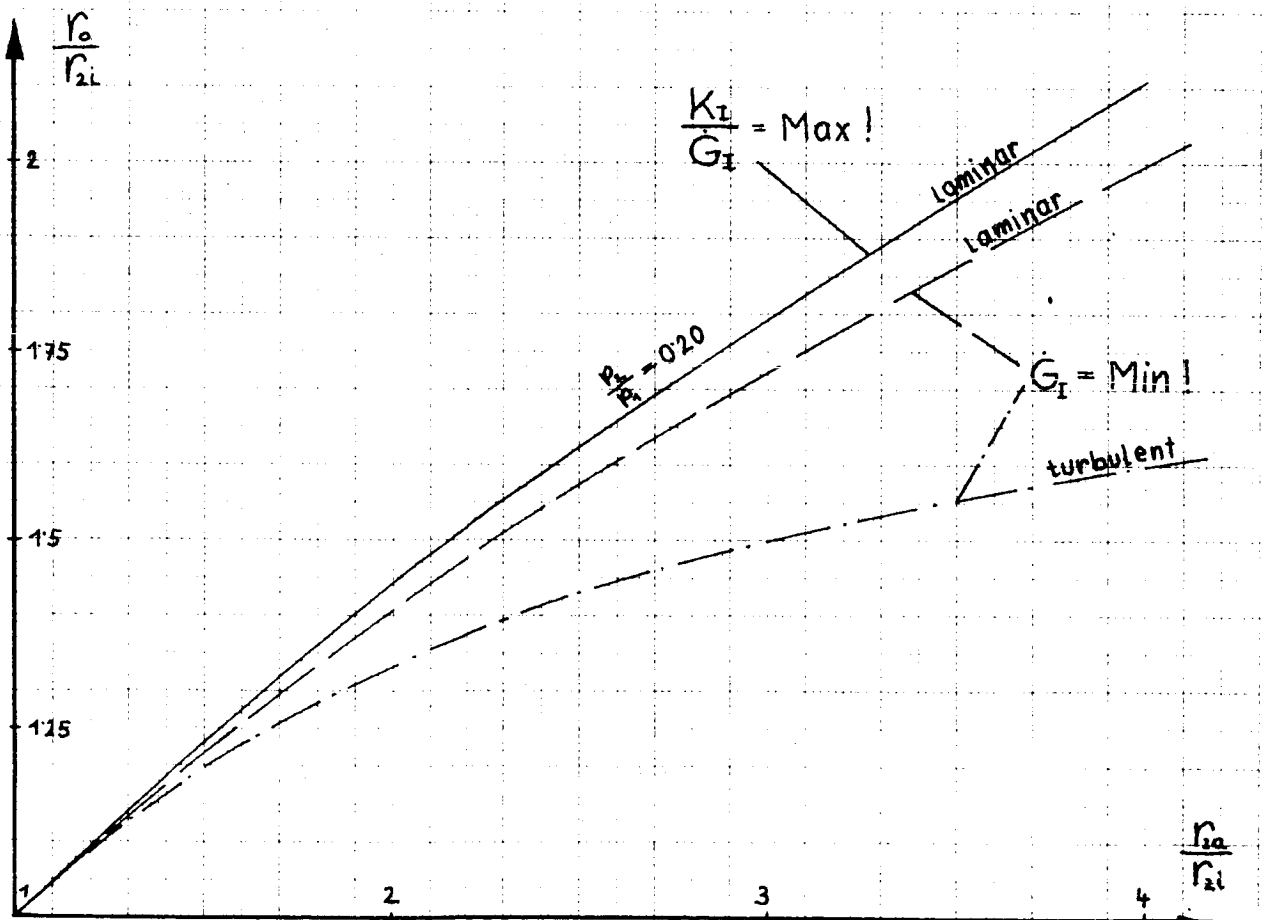
Gas consumption and load capacity as function of the gas inlet radius r_o

Let us suppose that in a bearing which can be loaded unilaterally the following is given:

$$r_{2a} \; , \; r_{2i} \; , \; K_I \; , \; p_1/p_B \; , \; p_2 \; , \; \varkappa \; , \; \eta \; , \; h, \; \Omega \; , \; \eta_{Ko} \tag{11.5b}$$

and that the following should be determined:

$$p_1 \; , \; p_B \; , \qquad N_1 \; + \; N_2 \; = \; f(\; r_{2a} / r_{2i} \;) \tag{11.5c}$$

and that the energy of the compressor of the bearing gas N_1 be given by:

$$N_1 = \eta_{Ko} \, H_{ad} \, \dot{G}_I \; , \tag{11.6}$$

where η_{ko} is the adiabatic efficiency of the bearing gas compressor, H_{ad} is the adiabatic delivery head of the compressor and $\dot{G}_I$ is the throughput volum. of the bearing per second. Then the delivery head can be calculated from

$$H_{ad} = RT_2 \frac{\varkappa}{\varkappa-1} \left[\left(\frac{p_B}{p_2}\right)^{\frac{\varkappa-1}{\varkappa}} - 1 \right] \tag{11.7}$$

It is presumed that the compressor aspirates from the surroundings of the bearing and then furnishes a final pressure of p_B. The amount of throughput $\dot{G}_I$ is determined with the aid of equations No. 7.19 and No. 7.20 for the laminar isothermal clearance flow.

$$\dot{G}_I = \dot{G}_a + \dot{G}_i = \frac{\pi h^3 (p_1^2 - p_2^2)}{12 \, \eta \, R \, T_2} \left(\frac{1}{\ln \frac{r_{2a}}{r_{2a}}} + \frac{1}{\ln \frac{r_{2i}}{r_{2i}}} \right) \cdot \tag{11.8}$$

In the following it is assumed that the aspiration temperature T_2 of the compressor is equal to the gas temperature of the clearance flow. If the equations No. 11.7 and No. 11.8 are introduced into equation No. 11.6, the result is:

$$N_1 = \frac{\pi}{12} \frac{\varkappa}{\varkappa-1} \frac{\eta_{Ko} h^3 p_2^2}{\eta} \left(\frac{1}{\ln \frac{r_{2a}}{r_{2a}}} + \frac{1}{\ln \frac{r_{2i}}{r_{2i}}} \right) \left[\left(\frac{p_1}{p_2}\right)^2 - 1 \right] \left[\left(\frac{p_B}{p_2}\right)^{\frac{\varkappa-1}{\varkappa}} - 1 \right] \tag{11.8a}$$

or using the condition No. 11.5 and the resolution

$$\frac{p_B}{p_2} = \frac{p_B}{p_1} \cdot \frac{p_1}{p_2} \tag{11.8b}$$

the following is obtained:

$$N_1 = \frac{\pi}{6} \frac{\varkappa}{\varkappa-1} \frac{\eta_{uo} h^3 p_2^2}{\eta} \frac{1}{\ln \frac{r_{2a}}{r_{1a}}} \left[\left(\frac{p_1}{p_2}\right)^2 - 1 \right] \left[\left(\frac{p_3}{p_1} \frac{p_1}{p_2}\right)^{\frac{\varkappa-1}{\varkappa}} - 1 \right] \; . \qquad (11.9)$$

The ratio p_1/p_2 must be determined, in compensating spaces of different size, from the stipulation of a constant load capacity K_I. Considering the equations No. 10.6 and 10.7, the absolute load capacity of the whole bearing area is:

$$K_I = \pi p_1 \left[(r_{1a}^2 - r_{1i}^2) + r_{2a}^2 C_{ka} + r_{1i}^2 C_{ki} \right] \qquad (11.10)$$

and, according to equation No. 11.5, the following applies:

$$K_I = \pi p_1 r_{2i}^2 \left\{ \left(\frac{r_{1a}}{r_{2i}}\right)^2 \left[\left(\frac{r_{1a}}{r_{2a}}\right)^2 + C_{ka} \right] - \frac{r_{2a}}{r_{1a}} \left(1 - C_{ki} \right) \right\} \; . \qquad (11.11)$$

the pressure ratio

$$\frac{p_1}{p_2} = \frac{K_I}{\pi r_{2i}^2 p_2 \left\{ \left(\frac{r_{1a}}{r_{2i}}\right)^2 \left[\left(\frac{r_{1a}}{r_{2a}}\right)^2 + C_{ka} \right] - \frac{r_{2a}}{r_{1a}} \left(1 - C_{ki} \right) \right\}} \qquad (11.12)$$

for a certain size of the compensation space can be obtained by iteration: select p_1/p_2 and determine C_{ka} and C_{ki} from the diagrams 5 and 6 (p. 60 and 62)
calculate p_1/p_2 according to equation No. 11.12.

If the assumed and the calculated pressure ratio p_1/p_2 are in good agreement, N_1 can be determined from equation No. 11.9.

The friction effect N_2 of the bearing can be derived, if equation No.5.1 applies, from the equation No. 7.21. It is for s h:

$$N_2 = M_d \cdot \Omega = 2\pi \eta \frac{\Omega^2}{h} \left\{ \int_{r_{1a}}^{r_{2a}} r^3 dr + \int_{r_{2i}}^{r_{1i}} r^3 dr \right\} \qquad (11.12a)$$

or, after integration

$$N_2 = \frac{\pi \eta \Omega^2}{2h} \left(r_{2a}^4 - r_{1a}^4 + r_{1i}^4 - r_{2i}^4 \right) \; . \qquad (11.13)$$

Considering equation No. 11.5, the following can be concluded:

$$N_2 = \frac{\pi \eta \Omega^2 r_{2i}^2}{2h} \left\{ \left(\frac{r_{1a}}{r_{2i}}\right)^4 \left[1 - \left(\frac{r_{1a}}{r_{2a}}\right) \right] + \left(\frac{r_{2a}}{r_{1a}}\right)^4 - 1 \right\} \; . \qquad (11.14)$$

Since a general optimization according to the stipulation

$$\frac{\partial(N_1 + N_2)}{\partial\left(\frac{r_{2a}}{r_{1a}}\right)} = 0 \qquad (11.14a)$$

cannot be performed analytically, it is useful to form the sum of N_1+N_2 for the different sizes of the compensating space and to determine the optimum graphically. For an actual case with the following values:

$$
\begin{array}{llll}
r_{2a} = 0,133 \text{ m} & \varkappa = 1,4 \\
r_{2i} = 0,055 \text{ m} & \eta = 1,9 \cdot 10^{-6} \text{ kp s/m}^2 \\
K_I = 1579 \text{ kp} & h = 30 \cdot 10^{-6} \text{ m} \\
p_1/p_B = 0,80 & \eta_{uo} = 0,80 \\
p_2 = 1 \cdot 10^4 \text{ kp/m}^2
\end{array}
\qquad (11.14b)
$$

the effects N_1 and N_2 were calculated as function of r_{2a}/r_{1a}, the r.p.m. were determined and both represented in Diagram 8.

Result: (11.14c)

r_{2a}/r_{1a}	p_1/p_2	p_B/p_2	N_1 (m kp/s)	N_2 (m kp/s)		
				$\Omega = 1000$	$\Omega = 1750$	$\Omega = 2000$
1,556	5,00	6,25	77,65	30,18	84,2	181,5
1,480	4,83	6,05	79,13	26,04	78,2	168,6
1,330	4,39	5,49	87,85	23,09	64,4	138,8
1,210	4,01	5,02	106,80	17,62	49,2	105,9
1,110	3,72	4,65	139,50	11,15	31,0	67,1
1,000	3,43	4,30	∞	0,00	0,00	0,0

Although a general conclusion referring to the most economical bearing as far as the compensation space is concerned cannot be reached, it is, nevertheless, evident from the example that, if the number of rotations is zero or small, a bearing without compensating space requires, at constant load capacity, the smallest power input. This can be explained the following way: If a compensating space is present, a lower pressure may suffice, but the volume of through-put becomes appreciably larger on account of the reduced throttling in the shortened bearing clearance. From this it can be concluded that the load capacity in bearings with a low number of rotations or large heights of the clearance should not be obtained by large compensating spaces but rather by high pressure of the bearing gas. If the machine works at very high r.p.m., the effect of friction plays a larger role and, in this case, a larger compensating space is justified.

11.3 Optimum height of the bearing clearance.

Another possibility of determining the smallest power input of a bearing with given dimensions (including compensating space) and pressures can be derived from the formula:

$$\frac{\partial(N_1 + N_2)}{\partial h} = 0 \qquad (11.15)$$

An optimum value for the bearing clearance can be calculated this way.

If the equations No. 11.9 and 11.13 are written in abbreviated form, one obtains

$$N_1 = A h^3 \qquad (11.15a)$$

$$N_2 = \frac{B}{h} \quad ,$$

where "A" and "B" have the following meaning:

$$A = \frac{\pi}{6} \cdot \frac{\varkappa}{\varkappa - 1} \frac{\eta_{\kappa o} \, p_1^2}{\eta} \frac{1}{\ln \frac{r_{2a}}{r_{1a}}} \left[\left(\frac{p_1}{p_2} \right)^2 - 1 \right] \left[\left(\frac{p_3}{p_2} \right)^{\frac{\varkappa - 1}{\varkappa}} - 1 \right] \qquad (11.15b)$$

$$B = \frac{\pi \, \eta \, \Omega^2}{2} \left(r_{2a}^4 - r_{1a}^4 + r_{1i}^4 - r_{2i}^4 \right)$$

and, from the following equation:

$$\frac{\partial (N_1 + N_2)}{\partial h} = \frac{\partial}{\partial h} \left(A h^3 + \frac{B}{h} \right) = 0 \qquad (11.15c)$$

the optimum height of the clearance is obtained:

$$h_{opt} = \sqrt[4]{\frac{B}{3A}} \quad . \qquad (11.16)$$

For an example with the same data as compiled on p.71, the optimum height of the clearance, h_{opt}, was calculated as function of the compensating space. The following values resulted:

r_{2a}/r_{1a}	p_1/p_2	h_{opt}		
1,556	5,00	$24,63.10^{-6}$ m		I
1,480	4,83	$24,21.10^{-6}$		
1,330	4,39	$23,02.10^{-6}$		
1,210	4,01	$20,90.10^{-6}$	}	II
1,110	3,72	$17,04.10^{-6}$		
1,C00	3,43	0		III

(11.16a)
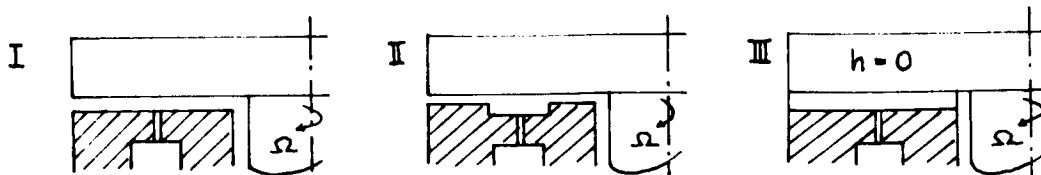
11.4 Power input for different gases.

In the following, the influence of different gases on the power input required for the operation of an aerostatic thrust bearing is illustrated by a fundamental comparison. In this comparison, one and the same bearing is examined in different gases, but with constant axial thrust. The nozzle

pressure ratio p_1/p_B = 0.80 is, likewise, constant with all gases. The total theoretical power input is composed of N_1 and N_2, where the compressor energy N_1 for adiabatic conditions is determined from equation No. 11.9 and the bearing friction effect from equation No. 11.13. The examples with the values:

$$r_{2i} = 0,055 \text{ m} \qquad h = 20.10^{-6} \text{ m}$$
$$r_{1i} = 0,087 \text{ m} \qquad p_{1a} = p_{1i} = 4,80.10^4 \text{ kp/m}^2$$
$$r_{1a} = 0,089 \text{ m} \qquad p_{2a} = p_{2i} = 1,00.10^4$$
$$r_{2a} = 0,133 \text{ m} \qquad p_B = 6,00.10^4$$
$$\Omega = 1570 \text{ 1/s} \qquad T = 293 \text{ °K}$$
$$\qquad \qquad \zeta_{ko} = 1$$
(11.16b)

gives the following table with various gases:

Gas	$\mathrm{æ}$	$10^6 \eta$ $kp\,s/m^2$	$\dfrac{10^{-6}\mathrm{æ}}{\eta(\mathrm{æ}-1)}$	$\left(\dfrac{p_B}{p_2}\right)^{\frac{\mathrm{æ}-1}{\mathrm{æ}}}-1$	N_1 $m\,kp/s$	N_2 $m\,kp/s$	N_1+N_2 $m\,kp/s$
Luft	1,40	1,85	1,890	0,670	27,5	106	133,5
N_2	1,40	1,78	1,968	0,670	28,6	102	130,6
He	1,66	1,90	1,327	1,040	30,0	109	139,0
CO_2	1,30	1,50	2,890	0,510	32,0	86	118,0
Sattdampf	1,33	1,30	3,100	0,560	37,6	74,5	112,1
Freon 11	1,12	1,09	8,322	0,219	39,5	62,5	102,0
NH_3	1,31	0,950	4,450	0,529	51,0	54,5	105,5
H_2	1,41	0,896	3,840	0,685	57,1	51,3	108,4

(11.16c)

Air - nitrogen - helium - carbon dioxide - saturated steam - Freon 11 - ammonia - hydrogen.


It can be concluded from this table that the power input for the compressor of the bearing gas N_1 (or the total effect at Ω = 0) depends, practically, only on the viscosity of the gas. The smaller viscosity η is, the larger an amount excapes through the bearing clearance and the larger is N_1. The influence of $\mathrm{æ}$ is only minor. The order of the gases examined corresponds to the power input for Ω = 0.

If, however, the bearing friction which is generated by rotation is also taken into consideration, the order is changed, since N_2 increases with increasing viscosity. What importance the friction effect has compared to the compressor effect does not only depend on η but also on the size of the compensating space and the angular velocity Ω. In the example considered here, the order of the gases with respect to minimum total power input is almost reversed.

11.5 Optimum nozzle pressure ratio in double-acting bearings.

The studies of optimum conditions made so far referred to bearings which are supplied only unilaterally with bearing gas and, therefore, can take up the required axial thrust in only one direction.

It happens, however, frequently in practice that the thrust of machines which are subject to non-stationary conditions (starting and arresting period, fluctuating level of pressure, pumps, compressors, etc.) works temporarily in both directions. The following discussions are based on a bilateral bearing of entirely symmetrical design which has, at the same height of the clearance, the same load capacity in both directions. A bearing designed according to this principle has the disadvantage of a high gas consumption. On the side I of the bearing which is loaded by K_{ges}, a small clearance h_I is formed, while, on the unloaded side, a much larger clearance, h_{II} in correspondence with the total axial clearance, is present. Since the unloaded side must be continuously prepared for a possible take-up of thrust, an unused quantity of gas G_{II} escapes here steadily.
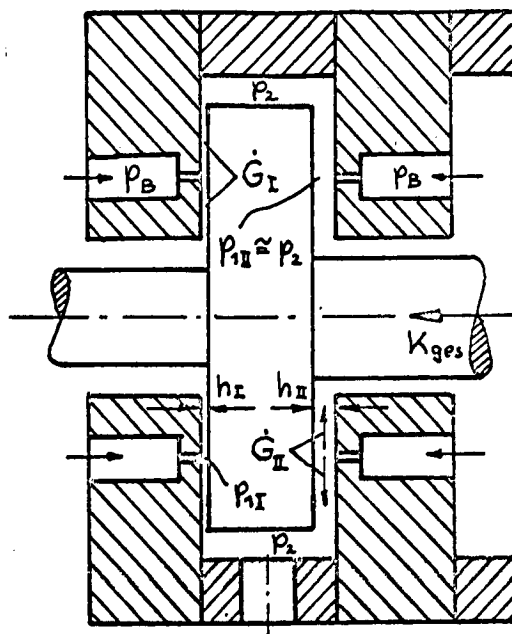
Optimation consist here in the following: To find the nozzle pressure ratio p_B/p_{1I} or, respectively, the required pressure p_B at which the compressor output N_1 for a given bearing pressure ratio p_{1I}/p_2 becomes a minimum for the preparation of the total bearing gas.

In this connection, the following abbreviations are used: $\dot{G}_I$ is the amount of throughput per second through the carrying clearance h_I, (Kg/sec); $\dot{G}_{II}$ is the amount of throughput per second through the non-carrying clearance h_{II} (kg/sec); p_{1I} is the highest pressure in the carrying clearance h_I (kp/m^2), which is determined by the magnitude of the axial thrust; $p_{1II} \cong p_2$, since $h_{II} \gg h_I$, is the counter-pressure of the nozzles on the non-carrying side of the bearing, approximately equal to the pressure surrounding the bearing, p_2 (kp/m^2); p_B is the pressure of the bearing gas in front of the inlet nozzles $\cong$ final pressure of the bearing gas compressor (kp/m^2); m is the number of stages of the compressor; H_{ad} is the adiabatic delivery head of a compressor stage (m).

For the derivation, the following values are considered as given: K_{ges}, K_I, K_{II}, p_2, p_{1I}, $\dot{G}_I$.

Assumptions: The nozzles are designed as cylindrical throttles or apertures. The outflow from the nozzles is considered as adiabatic change of state. On the non-carrying side of the bearing, the outflow from the nozzles is critical, provided that

$$\frac{p_B}{p_2} > \left(\frac{2}{\varkappa+1}\right)^{\frac{\varkappa}{\varkappa-1}} . \qquad (11.16d)$$

In a similar way as in equation No. 11.6, the compressor output, free of losses, for m stages becomes:

$$N_{1m} = (\dot{G}_I + \dot{G}_{II})\, m\, H_{ad} \quad . \qquad (11.17)$$

The amount of throughput, in adiabatic change of state, through cylindrical nozzles or aperatures for the carrying bearing clearance is:

$$\dot{G}_I = \mu\, F_D\, p_B \sqrt{\frac{2g\,\varkappa}{RT_B(\varkappa-1)}\left[\left(\frac{p_{1I}}{p_B}\right)^{\frac{2}{\varkappa}} - \left(\frac{p_{1I}}{p_B}\right)^{\frac{\varkappa+1}{\varkappa}}\right]} \qquad (11.18)$$

and, considering the assumption mentioned above, for the non-carrying clearance:

$$\dot{G}_{II} = \mu\, F_D\, p_B \sqrt{\frac{2g\,\varkappa}{RT_B(\varkappa-1)}\left[\left(\frac{2}{\varkappa+1}\right)^{\frac{2}{\varkappa-1}} - \left(\frac{2}{\varkappa+1}\right)^{\frac{\varkappa+1}{\varkappa-1}}\right]} \quad . \qquad (11.19)$$

The partial delivery head of the m-stage compressor is, with adiabatic compression:

$$H_{ad} = RT\frac{\varkappa}{\varkappa-1}\left[\left(\frac{p_B}{p_2}\right)^{\frac{\varkappa-1}{m\varkappa}} - 1\right] \quad , \qquad (11.20)$$

where $(\frac{p_B}{p_2})^{\frac{1}{m}}$ is the ratio of the stage pressures.

If equations No. 11.18, No. 11.19 and No. 11.20 are introduced into equation No. 11.17, the following result is obtained:

$$N_{1m} = mRT\frac{\varkappa}{\varkappa-1}\dot{G}_I\left\{1 + \sqrt{\frac{\left[\left(\frac{2}{\varkappa+1}\right)^{\frac{2}{\varkappa-1}} - \left(\frac{2}{\varkappa+1}\right)^{\frac{\varkappa+1}{\varkappa-1}}\right]}{\left[\left(\frac{p_{1I}}{p_B}\right)^{\frac{2}{\varkappa}} - \left(\frac{p_{1I}}{p_B}\right)^{\frac{\varkappa+1}{\varkappa}}\right]}}\right\}\left[\left(\frac{p_B}{p_2}\right)^{\frac{\varkappa-1}{m\varkappa}} - 1\right] \quad . \qquad (11.21)$$
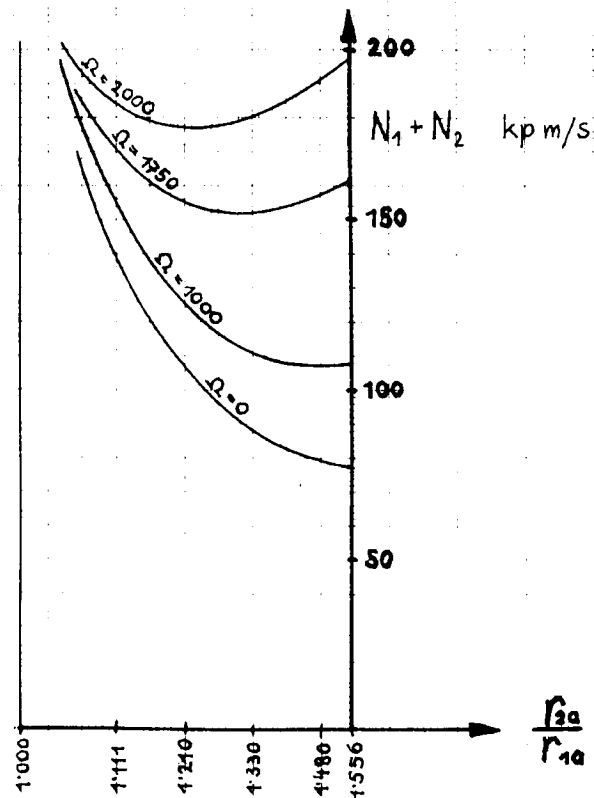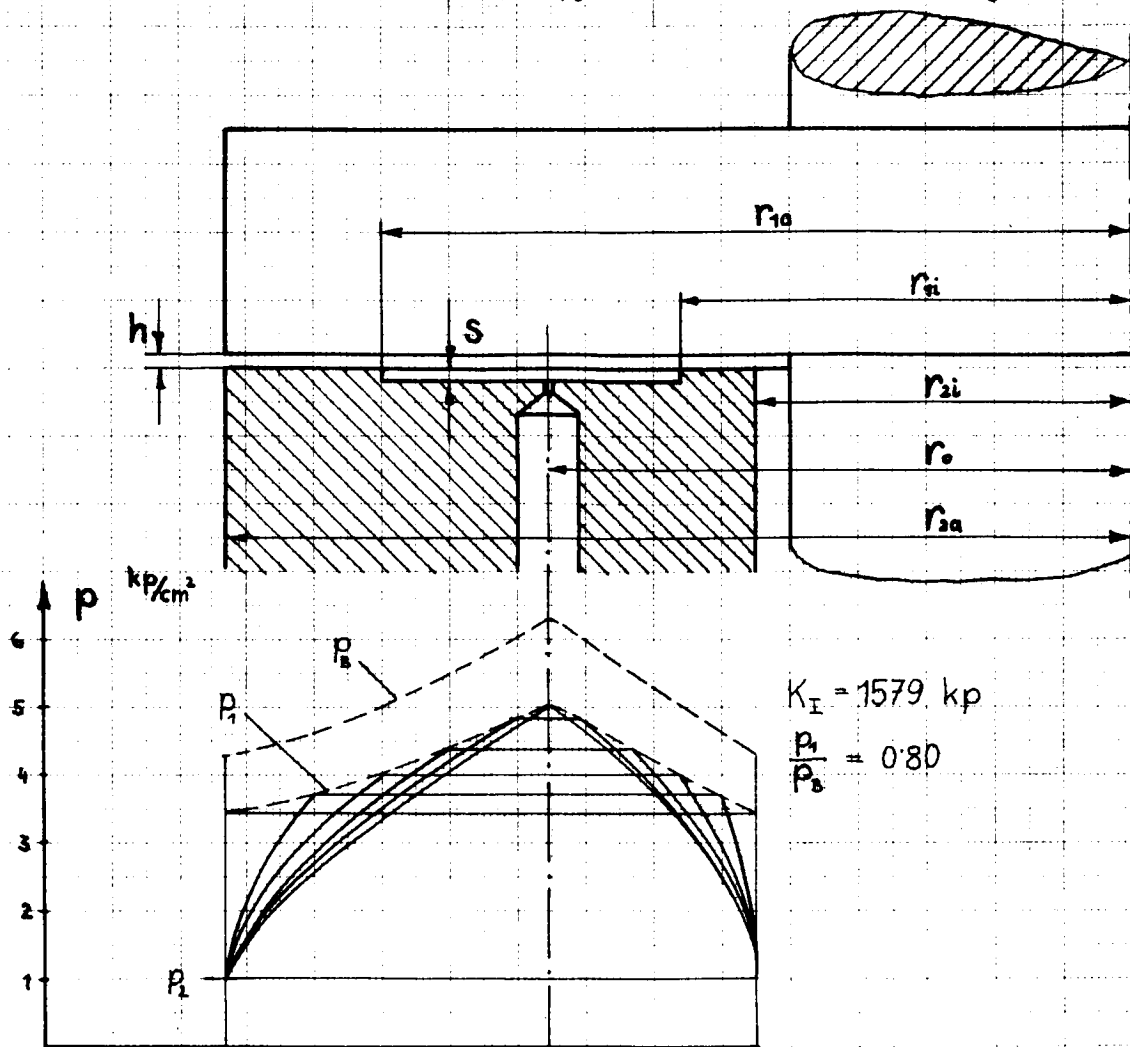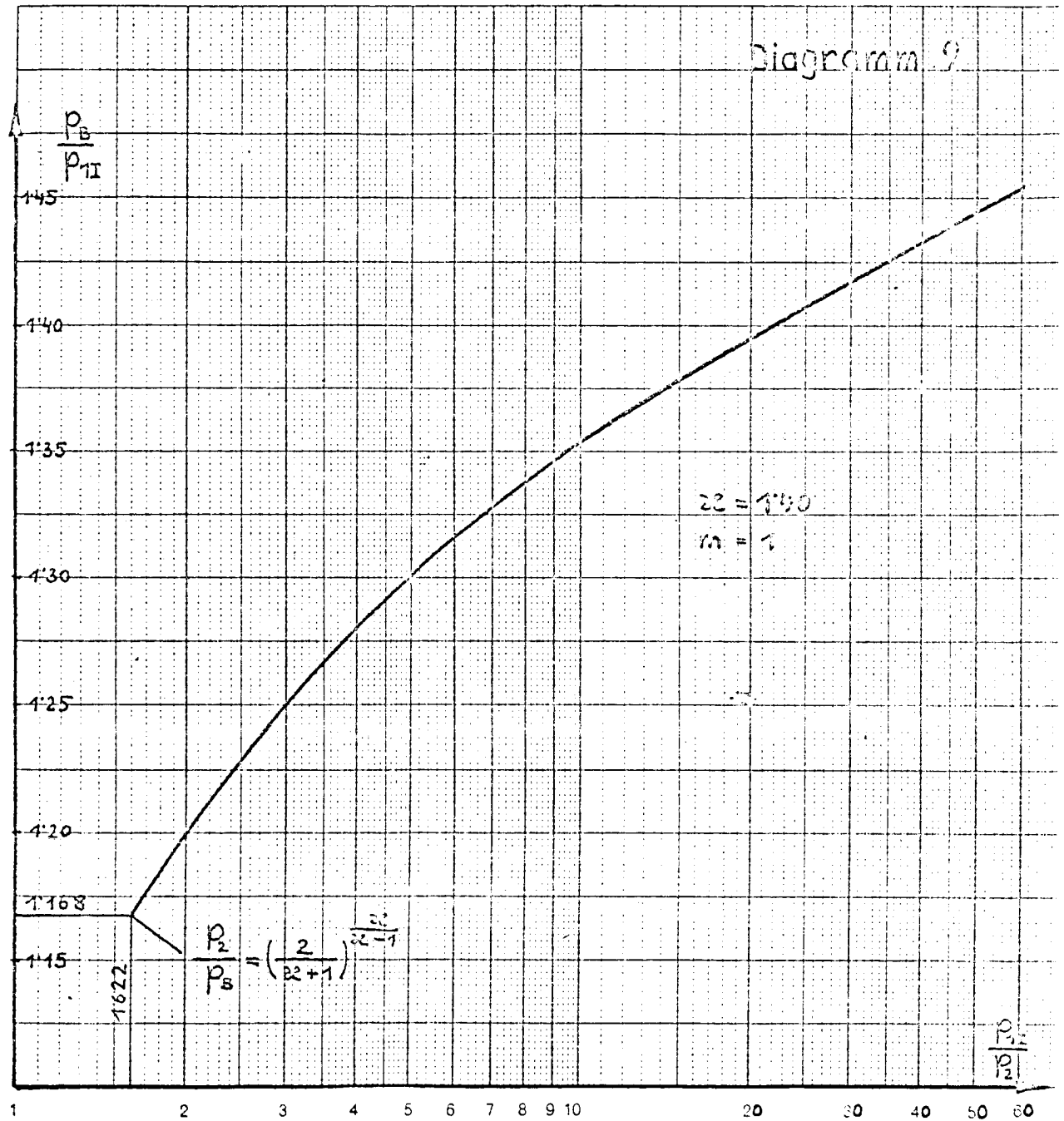
If the following condition is met:

$$\frac{p_B}{p_2} = \frac{p_B}{p_{1I}} \cdot \frac{p_{1I}}{p_2} \quad . \qquad (11.21a)$$

the power input N_{1m} is now only a function of the desired pressure ratio p_{1I}/p_B and the optimization

$$\frac{\partial N_{1m}}{\partial\left(\frac{p_{1I}}{p_B}\right)} = 0 \qquad (11.22)$$

can be performed. For m = 1 and $\varkappa$ = 1.40 the minimum effects at various pressure ratios p_{1I}/p_2 by variation of p_{1I}/p_B were determined by graphical plotting. The result is represented in Diagram 9.

Diagramm 8

r_{1a}

r_{ai}

r_{2i}

r_o

r_{2a}

h

S

$p \quad ^{kp/cm^2}$

p_a

p_1

p_2

$K_I = 1579 \ kp$

$\dfrac{p_1}{p_a} = 0.80$

6

5

4

3

2

1

200

$\Omega = 2000$

$\Omega = 1750$

$N_1 + N_2 \quad kp \ m/s$

150

$\Omega = 1000$

$\Omega = 0$

100

50

$\dfrac{r_{2a}}{r_{1a}}$

1'000

1'111

1'210

1'330

1'480

1'556

Diagramm 9

Determination of the optimum p_B/p_{1I} and p_B:

From the given load capacity K_I the pressure ratio p_{1I}/p_2 is determined (For example, $p_{1I}/p_2 = 6.00$). From Diagram 9 it can be seen that, for $m = 1$, p_B/p_{1I} equals 1.316. This allows the design of the required nozzle area. The corresponding pressure p_B is in this case:

$$p_B = p_2 \frac{\dfrac{p_B}{p_{1I}}}{\dfrac{p_2}{p_{1I}}} \qquad (11.22a)$$

For example, $p_B = 7.90 \, p_2$.

12. Properties and design of the throttle elements.

In order to impart to the bearing the property of increasing its load capacity with decreasing height of the clearance, the bearing gas must be ad-mitted to the clearance by means of throttle elements. (cf. the explanations on pp. 10-14). These throttle elements may consist of individual nozzles which open directly into the bearing clearance or into a compensating space, or gap-shaped throttles (e. g. annular gap) or inserts of porous material.

If, in a bearing of geometrically fixed magnitudes, also h_I and K_I are given, then also p_{II} is determined. Since the amount of throughput through the bearing clearance must be equal to the quantity of feeding gas, $\dot{G}_{clearance} = \dot{G}_{throttle}$, the operating point P_I of the bearing is the intersection of the characteristic of the throttle elements and the characteristic of the bearing clearance.
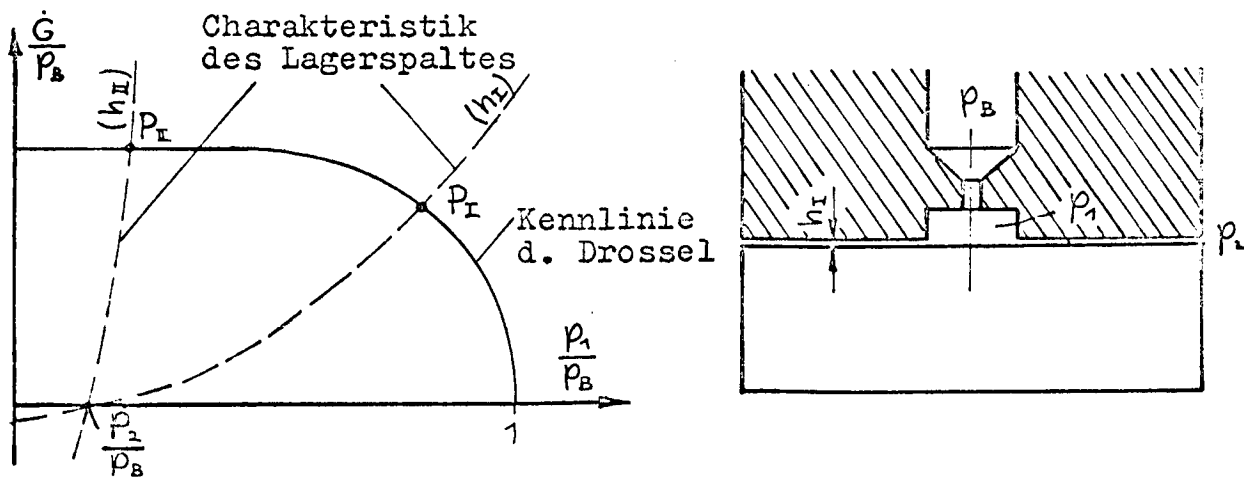
(top) characteristic of the bearing clearance -
(bottom) characteristic of the throttle

In bilateral thrust bearings, the curve h_I indicates the carrying, the characteristic h_{II} the non-carrying bearing clearance.

The characteristics of the throttle elements, which will be investigated more in detail later for various cases, depend, above all, on the kind of throttles and on their effective cross section area. The characteristic of the bearing clearance is mainly determined by the height of the clearance, geometry of the bearing, and the viscosity of the gas (in laminar flow), and, respectively, by the friction conditions in the clearance (in turbulent flow).

The characteristic of the bearing clearance is determined for the radial isothermal laminar flow. The amount of throughput through the bearing clearance is given by the equations No. 7.19 and 7.20:

$$\dot{G}_I = \dot{G}_a + \dot{G}_i = \frac{\pi h^3 (p_1^2 - p_2^2)}{12 \eta RT} \left(\frac{1}{\ln \frac{r_{2a}}{r_{1a}}} + \frac{1}{\ln \frac{r_{1i}}{r_{2i}}} \right) \quad (12.0a)$$

Thus the characteristic is:

$$\frac{\dot{G}}{p_B} = a \left(\frac{p_1}{p_B} \right)^2 - b \qquad (12.1)$$

The constants are here:

$$a = \frac{\pi h^3 p_B}{12 \eta RT} \left(\frac{1}{\ln \frac{r_{2a}}{r_{1a}}} + \frac{1}{\ln \frac{r_{1i}}{r_{2i}}} \right) \qquad (12.1a)$$

and

$$b = a \left(\frac{p_2}{p_B} \right)^2 . \qquad (12.1b)$$

The equation No. 12.1 is here a parabola of second order which is shifted downwards from the origin in the direction of the ordinate by the magnitude b.

12.1 Short cylindrical nozzles and apertures ($1 \lesseqgtr d$).

The figures at right show satisfactory designs of nozzle (left) and aperture, $1 \ll d$ (right). The aperture, though prepared with somewhat greater efforts, has, however, no fundamental advantages over the short cylindrical nozzle.

Düse $L \lessgtr d$ Blende $L \ll d$
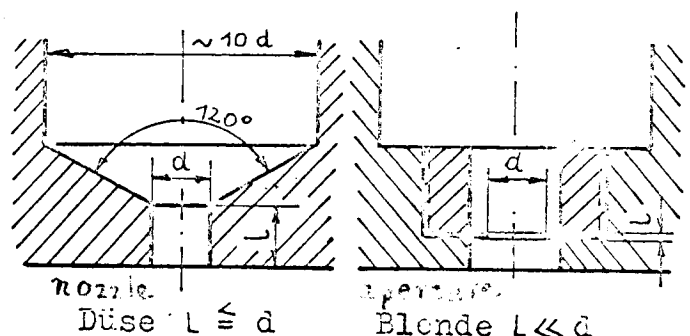
The area F_D of the required throttle cross section of the nozzles can be determined for a bearing with given values p_{1I}, p_2 and $\dot{G}_I$ from the nozzle characteristic which, assuming an adiabatic change of state, of the flow, gives the following result:

$$\dot{G}_I = \dot{G}_a + \dot{G}_i = \mu F_D \, p_B \sqrt{\frac{2g\,\varkappa}{RT_B(\varkappa-1)}\left[\left(\frac{p_1}{p_B}\right)^{\frac{2}{\varkappa}} - \left(\frac{p_1}{p_B}\right)^{\frac{\varkappa+1}{\varkappa}}\right]} \qquad (12.2)$$

The effective throttle area F_D depends not only on the diameter of the bore-holes of the nozzles, but also on the arrangement of the nozzles in the bearing. The coefficient μ is a flow factor depending on the shape of the nozzles (sharp or rounded-off edges) and on the Renumber of the nozzle flow. Another way of writing equation No. 12.2 is

$$\frac{\dot{G}\sqrt{T_B}}{\mu F_D \, p_B} = f\left(\frac{p_1}{p_B}, \varkappa, R\right) \qquad (12.2a)$$

It is represented in Diagram 10 for some frequently used gases, assuming ideal gas properties. At a given effective throttle area F_D and constant pressure p_B, the amount of throughput $\dot{G}$ increases with decreasing pressure p_1 until the value

$$\left(\frac{p_1}{p_B}\right)_{krit} = \left(\frac{2}{\varkappa+1}\right)^{\frac{\varkappa}{\varkappa-1}} \qquad (12.2b)$$

is attained where, since velocity of sound has been reached in the throttle cross section, the amount of discharge reaches a constant value which does no longer change with further decrease of p_1.

A) Opening of nozzles into a compensating space.

If a uniform radial flow shall occur in the bearing, the individual nozzles which are evenly distributed along the circumference of the diameter $2r_0$ must open into a compensating channel which is recessed in a bearing disc. This compensating space is preferably designed as continuous annular channel.

In order to guarantee as great a stability as possible in the bearing relative to self-induced vibrations (cf. Chapter 16), the volume of the compensating space should be small. The lower limit for the cross section of the compensating space is established by the requirement that the highest velocity of the gas in the channel be not greater than the velocity at the inlet into the bearing clearance.
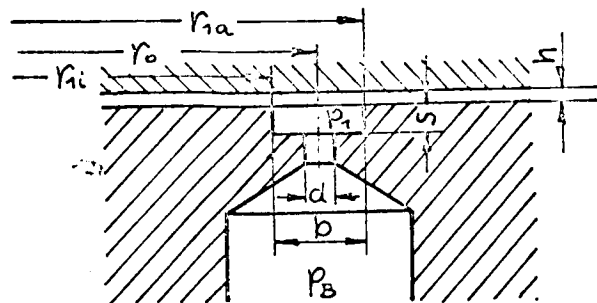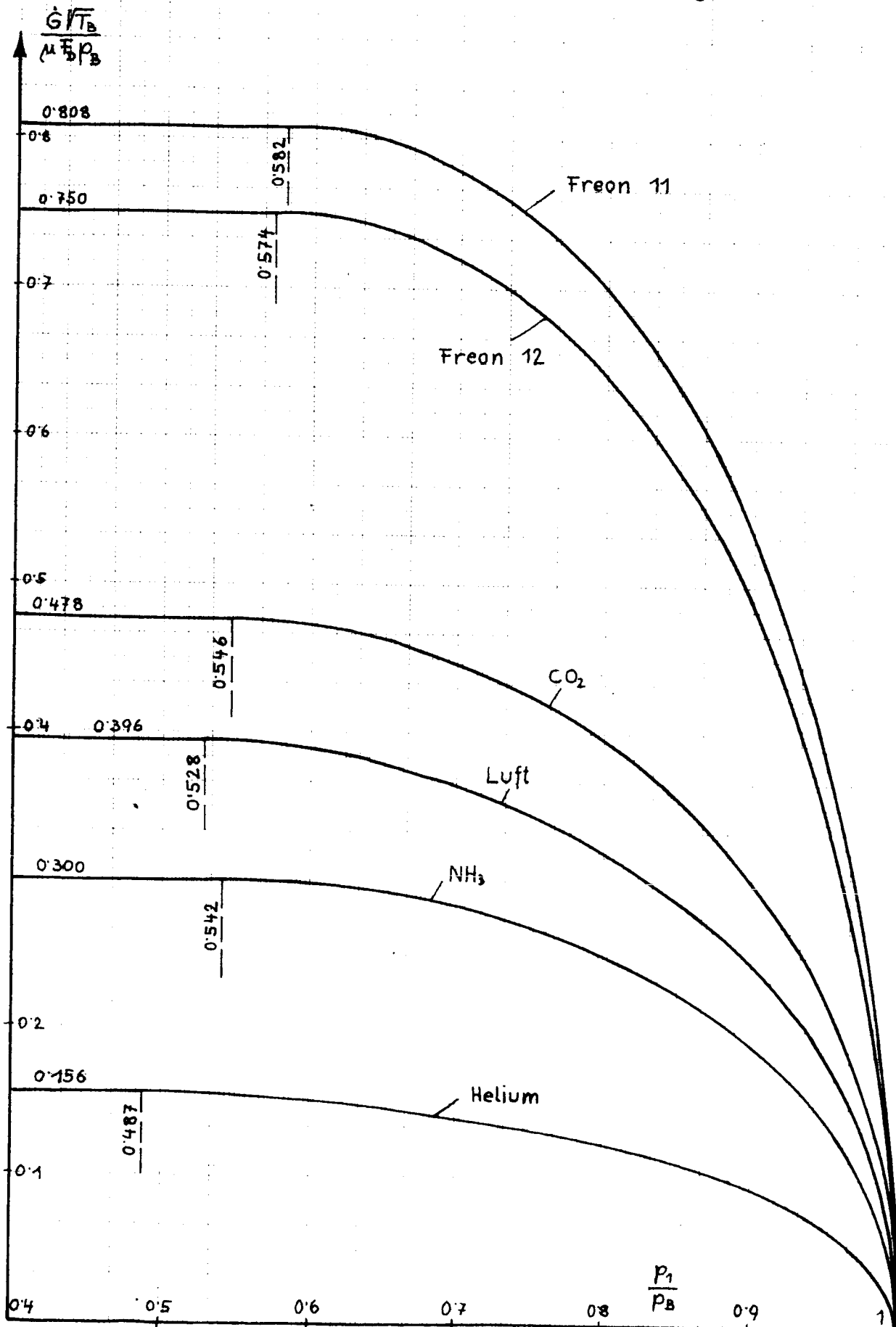
Diagramm 10

In the following, b is the width of the compensating channel; s is the depth of the compensating channel; h_I is the height of the clearance at normal operating conditions; and n the numbers of nozzles.

If it is assumed that the entry velocities into the outer and inner bearing clearance are approximately equal and if the width of the channel,

$$2\,r_o \simeq r_{1a} + r_{1i}$$

is small, the requirement stated above is met by equating the cross section of the channel and the cross sections at the entry into the bearing clearance. Thus the following is obtained:

$$b \cdot s = \frac{2\,r_o\,\pi\,h_I}{n} \,. \qquad (12.3)$$

It can be concluded from equation No. 12.3 that an increase in the number of nozzles has the advantage of a reduction of the channel cross section and thus of an improvement of the stability of the bearing.

The effective throttling area F_D of nozzles or apertures which open into an compensating space can be figured to be the whole amount of the cross section.

$$F_D \simeq n\,\frac{d^2\,\pi}{4} \qquad (12.4)$$

B. Opening of the nozzles directly into the bearing clearance.

(Nozzles with variable throttle cross section, depending on the clearance).

If the nozzles are arranged in such a way that their cylindrical borehole opens directly into the clearance, the effective throttle area is not equal to the cross section of the nozzle, $d^2/4$, but is formed by the edge of the nozzle and the height of the clearance. When the following applies
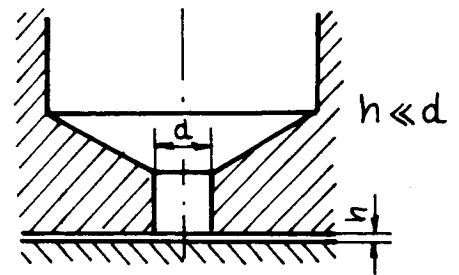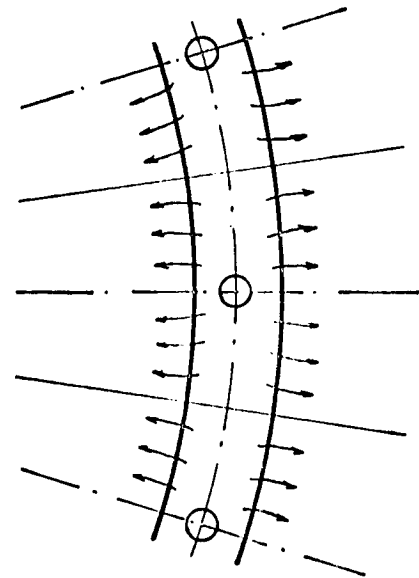
$$d\,\pi\,h < \frac{d^2\,\pi}{4} \qquad (12.4a)$$

the effective throttle area is

$$F_D = n \, d \pi \, h. \qquad (12.5)$$

For reasons of design, $d_{min} \simeq 10 \, h$. For nozzles which open directly into the bearing clearance, the characteristic

$$\frac{\dot{G}}{p_B} = f\left(h, \frac{p_1}{p_B}\right) \qquad (12.5a)$$

depends also on the height of the clearance. The consequence is that, upon reduction of the clearance by an additional load on the bearing, the load capacity can only be raised insignificantly on account of the stronger throttling effect. In order to impart good load capacity to such a bearing in the region of low clearance widths, the nozzle must have an appropriately larger borehole diameter d on account of its small effective throttling area. In such a case, however, the amount of throughput would increase in an undesirable degree if the clearance were enlarged by reducing the load of the bearing.

C. Nozzles with boreholes on the side of the clearance.

In order to avoid the danger of self-induced vibrations (cf. Chapter 16) which appear when a compensating space is present, and the disadvantages mentioned sub B), individual nozzles with a borehole at the side of the clearance were successfully installed in various experimental devices and machines. The largest diameter D of the borehole is, in this case, selected in such a way that, for the smallest height of the clearance h_{min} occuring during operation, the requirement

$$\frac{d^2 \pi}{4} = D \pi \, h_{min} \qquad (12.6)$$

is fulfilled. The effective throttling area F_D is, for $h > h_{min}$, identical with the cross section area of the nozzle. Thus equation No. 12.4 applies also here.
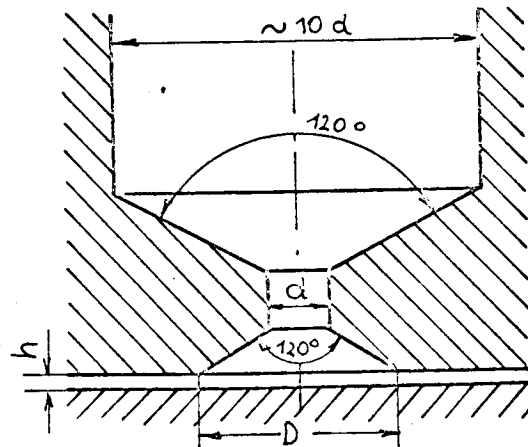
The effect of the borehole on the side of the clearance in cylindrical nozzles, compared to nozzles which open directly into the bearing clearance, on the load capacity and amount of throughput was ascertained clearly by an experiment. Diagram 27 shows measurements of the load capacity K_{ges} and the amount of throughput $\dot{G}_I$ in a bearing which can be loaded unilaterally, without compensating space. In the first experiment, the four cylindrical nozzles opened directly into the bearing clearance, whereas, in the second test, the nozzles had a borehole on the side of the clearance. It was found that, with constant nozzle cross sections, the load capacity characteristic $K_{ges} = f(h)$ of the bearing with counterbored nozzles was shifted into a region of greater clearance heights while the course of the curve was similar. The load capacity at equal heights of the clearance is markedly greater than in a bearing with nozzles without counterbore. The amounts of throughput show a similar behaviour. The bearing with counterbored nozzles, has, the clearance being

equal, (at least in the region of small h) an increased gas comsumption corresponding to the larger effective throttling area,

$$\frac{\dot{G}_{anges.}}{\dot{G}_{nicht\ anges.}} \cong \frac{D}{d} \quad \left(= \frac{2\cdot0}{0\cdot7} = 2\cdot85 \right) \quad . \qquad (12.5b)$$

(anges) with borehole
(nicht anges) without borehole.

The values obtained in the experiments verify this ratio satisfactorily, at least for small heights of the clearance.

In a synopsis of the three cases A), B) and C), let me add a comparison of the dependence of the effective throttle area F_D on the bearing clearance h.

The design according to C) is quite similar to the case A), whereas the direct opening of cylindrical nozzles into the clearance according to B) is unfavorable.
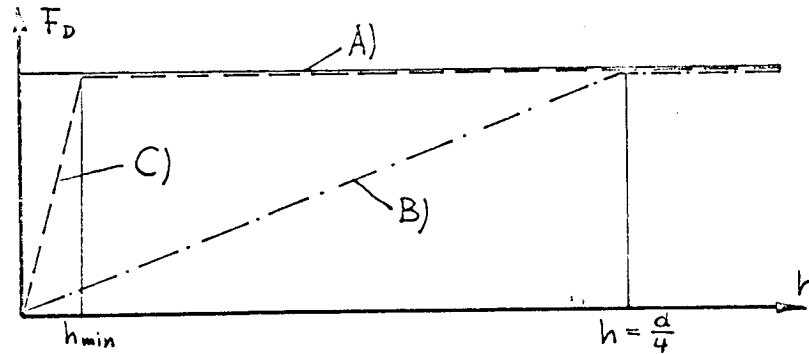

12.2 Capillary nozzles $1 \gg d$.

The friction of the gas entering through a capillary and the resulting great reduction of the pressure p_1 cause an appreciably flatter pattern of the throttle characteristic, i.e. below the nozzle characteristic, compared to the short nozzle, at an equal effective throttle area F_D. The consequence is that, at equal throttling area and equal height of the clearance, the load capacity of the bearing with short cylindrical nozzles is markedly higher than that of the bearing with capillary nozzles.

On account of the flat throttle characteristic, the use of capillary nozzles is also disadvantageous as far as stability at self-induced vibrations is concerned (cf. Chapter 16).

Short nozzle

Capillary
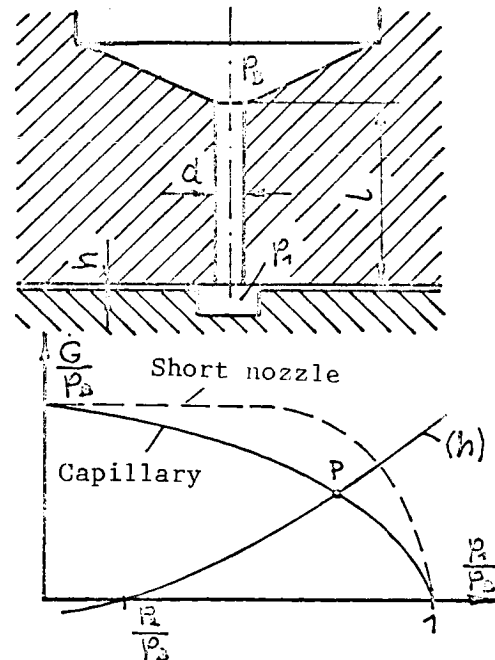
12.3 Venturi nozzles.

In most aerostatic bearings, the inlet nozzles were designed as cylindrical boreholes. A disadvantage of these nozzles is, however, that, at a given feeding pressure p_B, the amount of flow decreases comparatively fast, if the counter-pressure p_1 increases above the critical value, p_{crit}, where the velocity in the nozzle is still that of sound. In order to obtain a high load capacity, it is desirable to select the inlet pressure p_1 of the bearing clearance which corresponds to the counterpressure of the nozzle as close as possible to the available feeding pressure. At a given bearing clearance, the amount of flow is also given and, on account of the decrease of the amount at increasing counterpressure p_1, it is necessary to select comparatively large feeding nozzle cross sections. This involves not only the disadvantage that a large amount of gas escapes in bilaterally loadable and symmetrically built thrust bearings in the wide clearance on the non-carrying side, but it interferes also with the rigidity and the stability of the bearing. In order to avoid these disadvantages, venturi nozzles for the admission of gas were installed in one of the experimental devices. (Figs. 1 and 2). In contrast to the cylindrical nozzle with the narrowest cross section area F_{Da}, the counterpressure p_1 in the venturi nozzle with an equal narrowest cross section can be increased considerably without an appreciable reduction of the quantity on account of the subsequent diffuser. The use of venturi nozzles is, of course, only justified if they open into a compensating channel or if the diffuser is counterbored at the side of the clearance in such a way that the effective throttling area is formed by the narrowest nozzle cross section and the effect of the diffuser can be fully exploited.
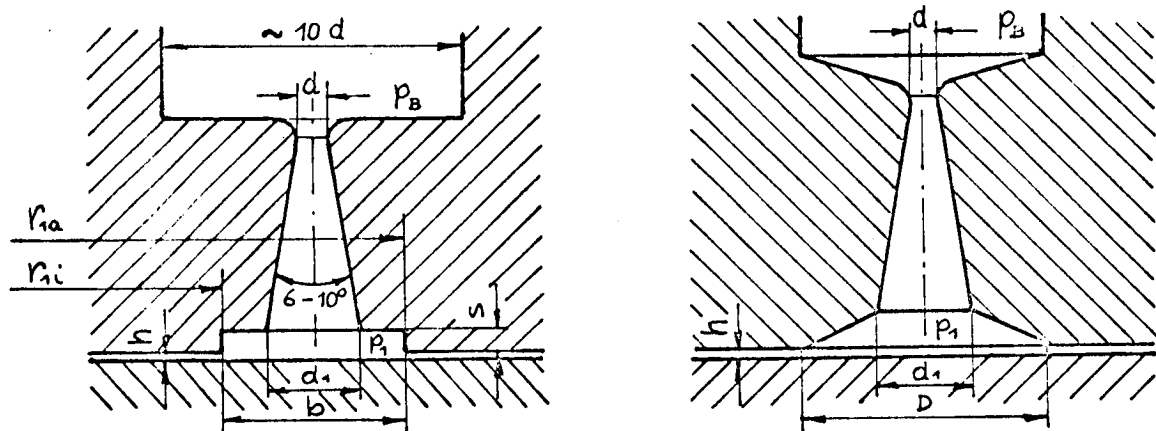
The following diagram illustrated schematically a comparison of the throttle characteristics (volumes of throughput as a function of the nozzle pressure ratio p_1/p_B) for regular nozzles and venturi nozzles.

The meaning of the curves is the following: Curve a) is the characteristic of venturi nozzles in a flow involving a loss (η_D = 0.65; narrowest cross section area F_{Da}). Curve b) is the characteristic for cylindrical nozzles (with a larger narrowest cross section area F_{Db}). Curve c) is the characteristic of cylindrical nozzles without diffuser (narrowest cross section area F_{Da}). Curve d) is the characteristic of the carrying bearing clearance (cf. p. 78).

It can be concluded from this comparison that the operating point P cannot be reached by cylindrical nozzles (charactertistic "c) of the same cross section F_{Da} as the venturi nozzles. Using cylindrical nozzles of larger cross section area F_{Db} (characteristic "b") the operating point could be reached, but the volume of throughput increases considerably with an enlargement of the clearance by reducing the load of the bearing. In symmetrically designed bearings with bilateral load capacity an amount which is larger by ΔG_{ab} than in the case of venturi nozzles with the cross section F_{Da} would continuously escape on the non-carrying side in the presence of nozzles with the cross section area F_{Db}.
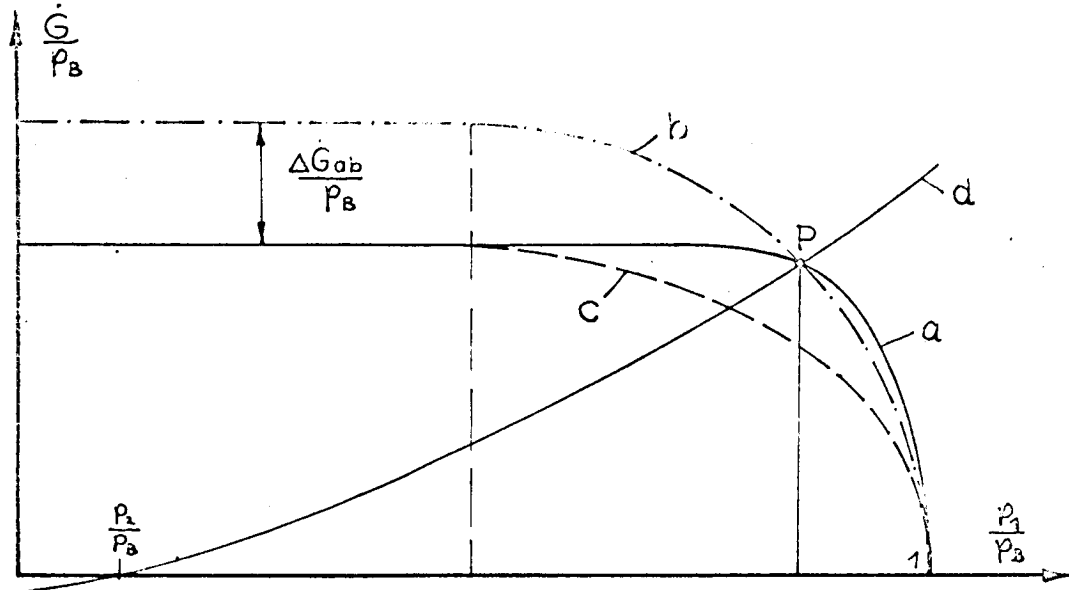
Determination of the characteristic for venturi nozzles.

The velocity occurring in the smallest cross section of the venturi nozzle is retarded again in the adjoining diffuser. It is assumed in the calculation that the change of state in the narrowed part of the nozzle and thus also the course of velocity is adiabatic and free of losses. Otherwise, the calculation would be more complicated. In a nozzle which is not loss-free and widens subsequently, the maximum velocity is not in the narrowest cross section. At least in Laval nozzles with supersonic flow, sound velocity appears only after the narrowest cross section.
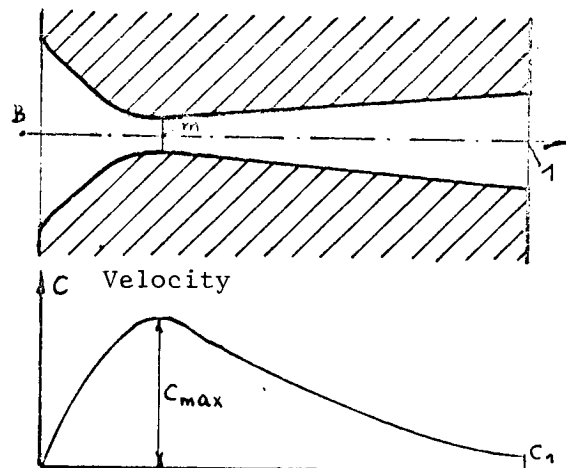
The throttling characteris-
tic of the venturi nozzle should
have an almost rectangular course
with a flow free of losses and a
very small cross section ratio

$$\beta = \frac{F_m}{F_1} \qquad (\beta^2 \ll 1)$$ (12.6a)

(cf. the curve marked "with diffuser η_D = 1" in the sketch which follows).
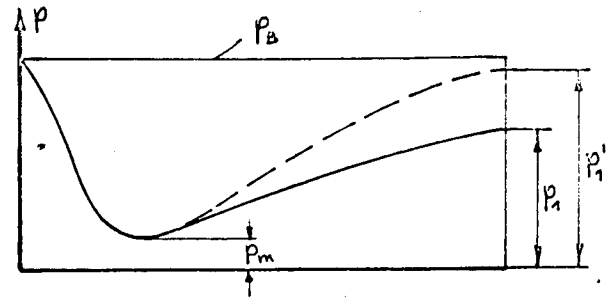
The two curves without and with diffuser show the pressure recovery in the loss-less diffuser $p_1' - P_m$. At an efficiency factor of the diffuser of $\eta_d < 1$, the pressure recovery would be only $\eta_D(p_1' - p_m)$. Thus one can obtain, without difficulties, the whole course of pressure for $\eta_D < 1$ from the characteristic of nozzles without diffuser, where the compressibility has already been taken into consideration.
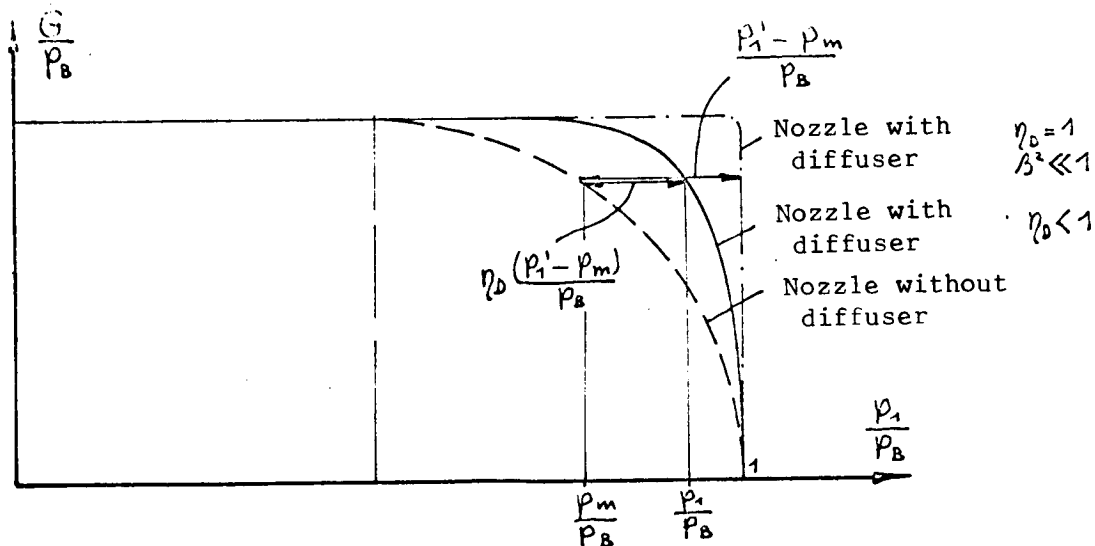
In an experimental example (cf. diagram 11) with 4 venturi nozzles with an aperture angle of 10°, an area ratio β = 0.145 ($\beta^2 \approx 0.021$), and an diffuser length of 7.5 mm, an efficiency factor of η_D = 0.65 was measured. This value appears to be correct, considering the large widening angle, the poor rounding-off of the narrowest part of the nozzle and the high Mach numbers, compared to the results measured in reference (XIII). The outflow coefficient μ was determined from the quotient of maximum volume of throughput, calculated theoretically from the nozzle area present, by the largest measured throughput volume.

$$\mu = \frac{G_{max} \text{ gemessen}}{G_{max} \text{ gerechnet m. } F_D} = 0.96$$ (12.6b) (gemessen) measured –

(gerechnet) calculated.

The efficiency factor of the diffuser is defined by:

$$\eta_D = \frac{p_1 - p_m}{p_1' - p_m} \quad (12.6c)$$

where p_1 is the pressure actually measured in the back of the nozzles; p_m is the pressure in the narrowest cross section; p_1' is the pressure in the back of the venturi nozzles in a loss-free flow.

For $\beta^2 \ll 1$, $p_1' \cong p_B$, and thus the pressure ratio is:

$$\frac{p_m}{p_B} \simeq \frac{\frac{p_1}{p_B} - \eta_D}{1 - \eta_D} \quad (12.7)$$

The throttle characteristic of the venturi nozzle for a very large area ratio can be obtained from the characteristic of nozzles without widening, equation No. 12.2, by introduction of the formula No. 12.7 into the nozzle pressure ratio of equation No. 12.2. The result is:

$$\frac{\dot{G}}{p_B} = \mu F_D \sqrt{\frac{2g\varkappa}{RT_B(\varkappa-1)}\left[\left(\frac{\frac{p_1}{p_B} - \eta_D}{1 - \eta_D}\right)^{\frac{2}{\varkappa}} - \left(\frac{\frac{p_1}{p_B} - \eta_D}{1 - \eta_D}\right)^{\frac{\varkappa+1}{\varkappa}}\right]} \quad . \quad (12.8)$$

The general conclusion is: Bearings equipped with venturi nozzles afford either, at a given amount of throughput, a higher load capacity or, at a given load capacity, a saving of consumed bearing gas. In diagram 12, measurements of the pressure p_1 as a function of the height of the bearing clearance h in the same bearing are compared for venturi nozzles and cylindrical nozzles of identical narrowest cross section. The following can be seen: In those regions where the pressure ratio p_1/p_B is higher than the critical, the pressure p_1 is higher in the venturi nozzles, at equal height of the clearance, i.e. the load capacity is improved; with large bearing clearances, however, where the flow through the venturi nozzles is over-critical, the load capacity is lower than in a bearing with short cylindrical nozzles without expansion on account of higher losses by supersonic flow, and formations of shocks and eddies. Another advantage of the venturi nozzles can, likewise, be seen in Diagram 12. In the region which is most important for bearings, i.e. at heights of the clearance which are neither too small nor too high, the curve $p_1 = f(h)$ runs steeper than that in bearings with regular cylindrical nozzles.

This results in a greater rigidity of the bearing, i.e. the height of the clearance does not change as much with increase or decrease of the load as in the bearing with regular nozzles. The higher rigidity has an advantageous effect on the stability connected with self-induced vibrations (cf. Chapter 16).

12.4 Throttle elements with variable pressure-dependent cross section.

Still better characteristics than those of regular cylindrical and venturi nozzles can be obtained by throttle elements where the effective

throttling area F_D increases with increasing nozzle pressure ratio p_1/p_B. The design and construction of such throttles involves, however, certain difficulties.

In reference (XIV), the use of individual nozzles of elastic raw material (plastics, silicone rubber) is described where the cross section area changes as a function of the difference between the feeding pressure p_B and the pressure in the back of the nozzle p_1. In the region of large nozzle pressure ratios p_1/p_B the elastic material is compressed in such a way that a constriction of the cross section is produced. If, on the other hand, p_1/p_B is small, no deformation of the nozzle occurs and the whole cross section initially provided is available for the flow through it.
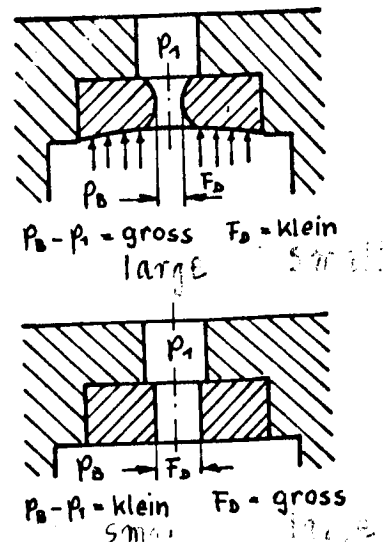
Two more designs of nozzles with variable, pressure-dependent cross section are sketched in the drawings on the right side. In the first picture, a needle body N is supported by a spiral spring Fe. The greater the difference of pressures $p_B - p_1$ is, the smaller is the effective throttling area F_D between needle body and seat i.e. at a small nozzle pressure ratio less bearing gas escapes through the nozzle. In the second figure, a leaf spring fulfills this task. At an increasing pressure difference $p_B - p_1$, the spring is bent to a greater extent, reducing, at the same time, the effective throttle cross section.

An exact analytical determination of the characteristic for such throttling elements is not feasible in most cases. It is, therefore, advantageous to obtain the throttle characteristic by experimental methods. The design of a bearing or the determination of the operating point, and the entire course of the load capacity over the height of the clearance h, respectively, can than be performed readily. The advantages of such throttling elements appear immediately by studying the diagram drawn below. The volume of throughput of the nozzles described above either remain constant over p_1/p_B or even increase somewhat (curve e), while the throttle characteristic for a cylindrical nozzle (curve f) with constant cross section drops sharply in the region of large p_1/p_B. The characteristic of the bearing clearance (curve g) intersects the throttle characteristic in the operating point P of the bearing.
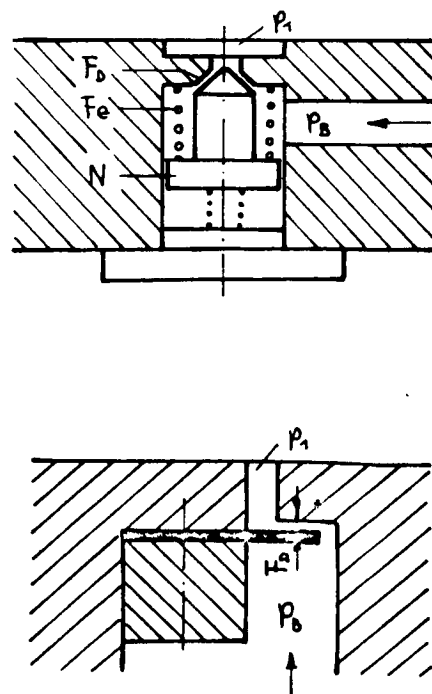
Diagramm 11

Result of the Measurements: 4 Venturi Nozzles
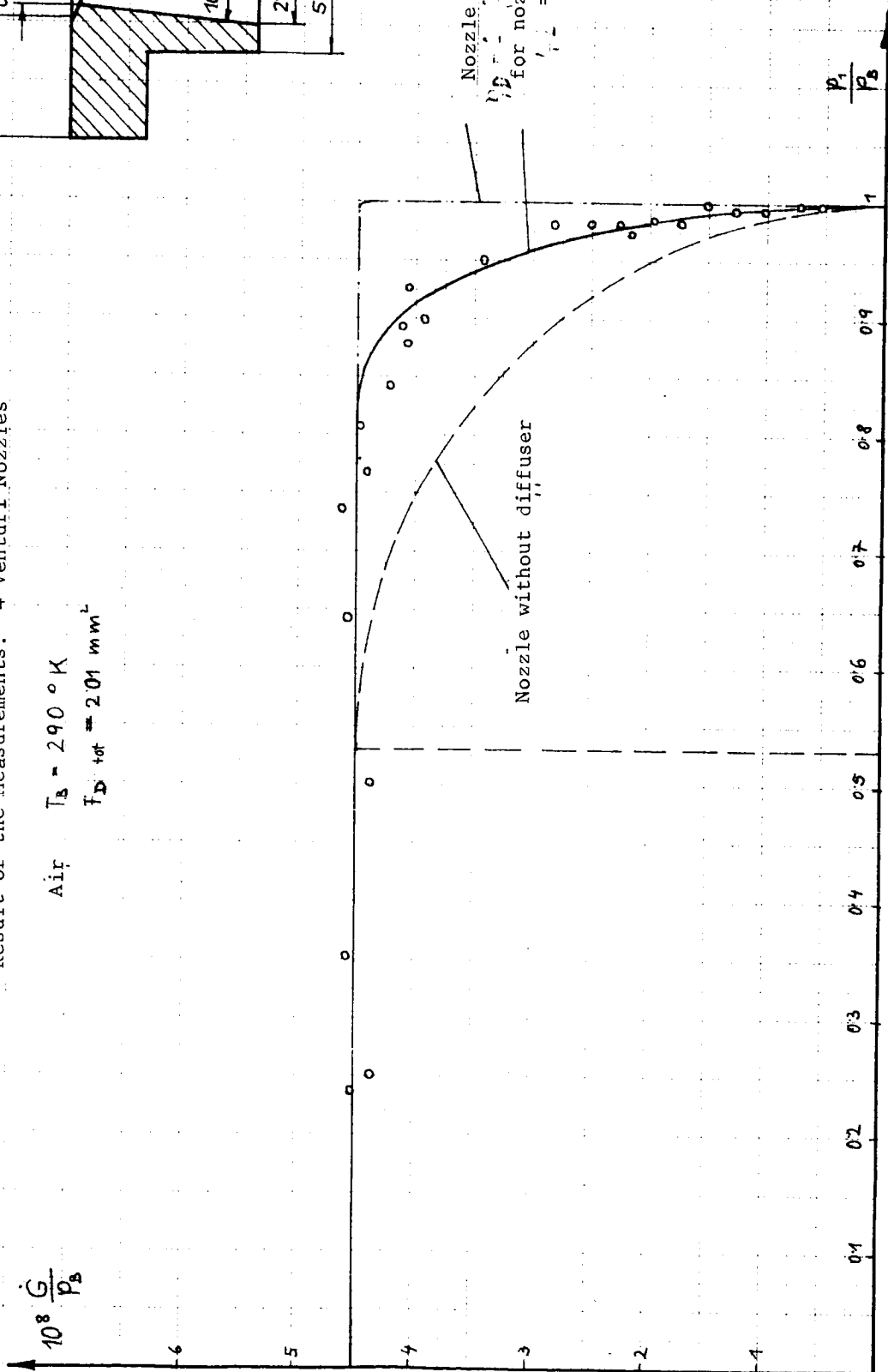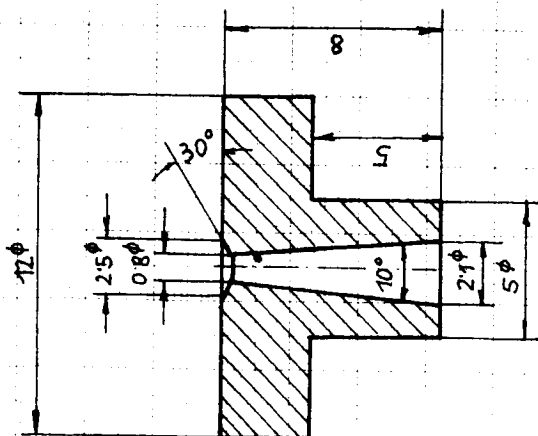
Air $T_B = 290\ ^\circ K$

$T_{D\ tot} = 201\ mm^L$

$10^8\ \dfrac{\dot{G}}{p_B}$

Nozzle with diffuser

$\nu_D = \langle\ \rangle$, calculated
for nozzle with diffusor
$\nu_i = 0.65$

Nozzle without diffuser

$\dfrac{p_1}{p_B}$

Diagramm 12

Measurement with air $T_B = 290°K$ in the bearing

4 Venturi nozzles   " $F_D = 2·01mm^2$

4 cylindrical nozzles   " $F_D = 2·01mm^2$

$r_{2i} = 50mm$

$r_{1i} = 77mm$

$r_{1a} = 83mm$

$r_{2a} = 120mm$

$s = 1mm$

$b = 0·5mm$

$h \cdot (10^6 m)$

$P_1 \left[\frac{kp}{m^2}\right]$

$p_B = 21·10^4$

$p_B = 16·10^4$

$22·10^4$
20
18
16
14
12
$10·10^4$
8
6
4
2
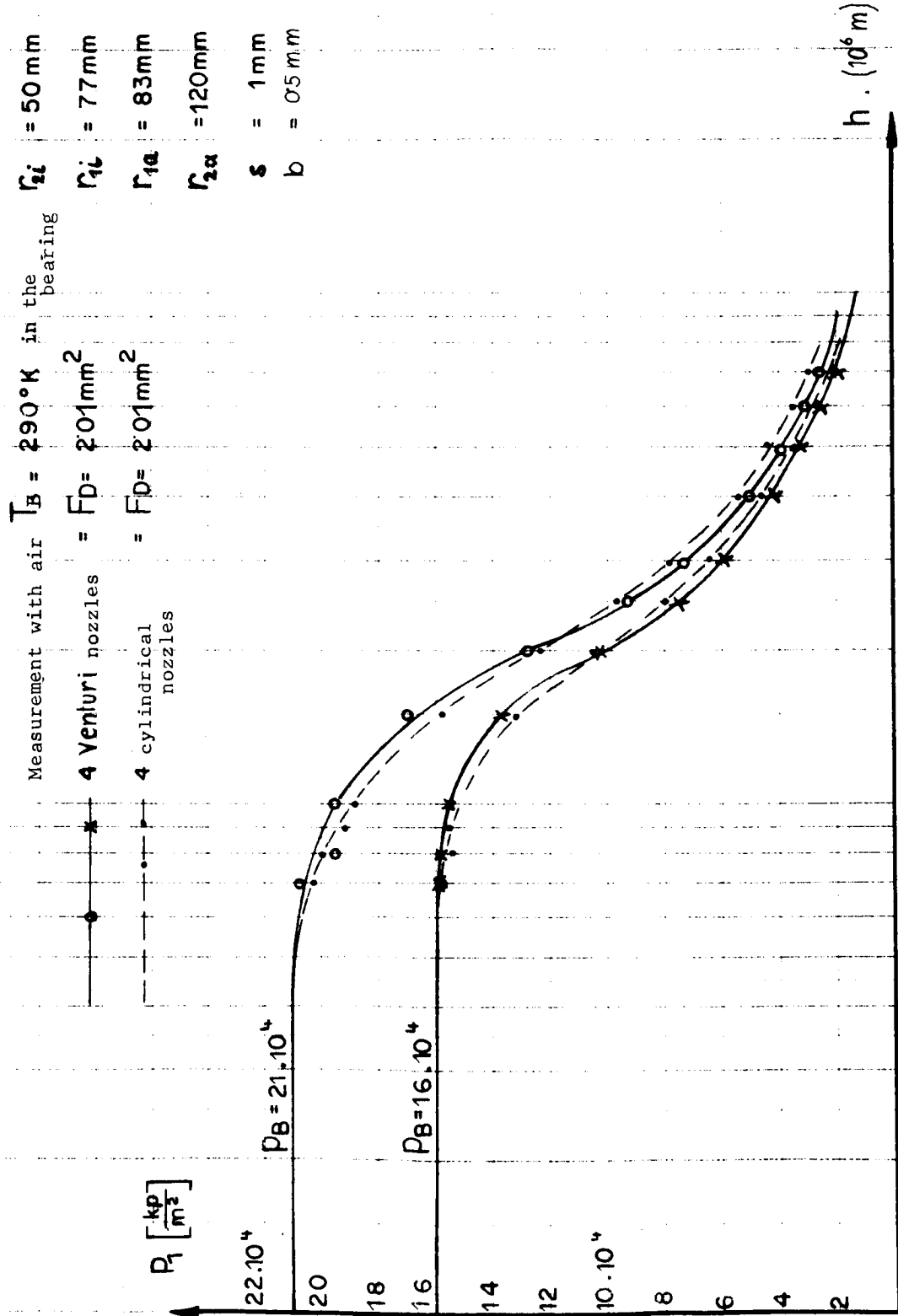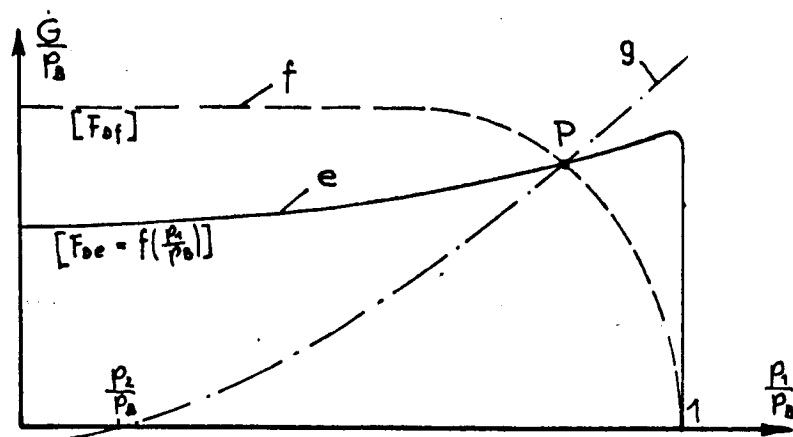
A bearing with regular nozzles (F_D = const) consumes appreciably more gas at increasing clearance, on account of reduction of the load, than a bearing with the throttle elements described above. As a consequence, the rigidity, i.e. the increase of the load capacity K_{ges} at a certain decrease of the bearing clearance h, is considerably greater in the latter case. In this comparison, the bearing geometry, the operating point P and the feeding pressure p_B are assumed to be constant.
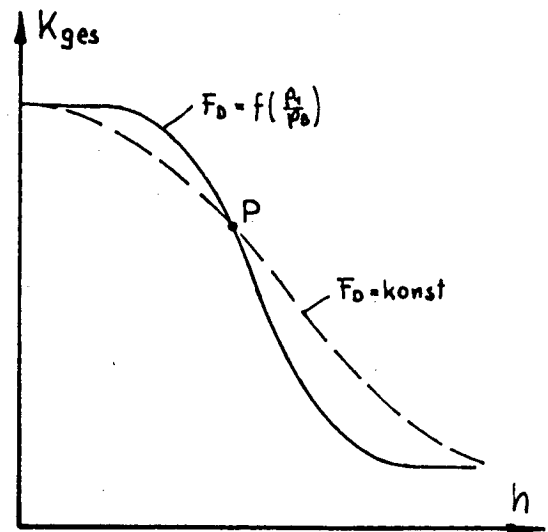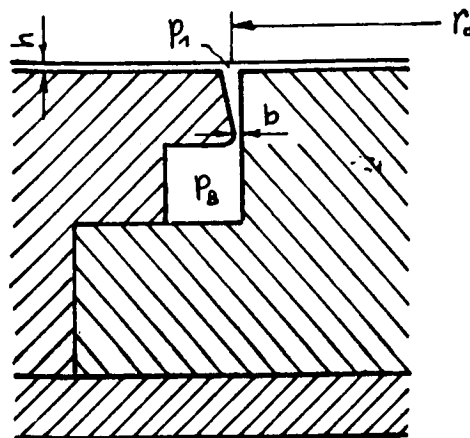

12.5 Annular inlet clearance.

The compensating channel for equalizing the gas (cf. page 67) can be eliminated when the bearing gas is fed through a ring-shaped inlet clearance which extends over the whole circumference of the diameter 2 r_o. The sketch at right suggests a design for such a feeding through an annular clearance. Such bearings without compensating space are stable as far as self-induced vibrations are concerned. (cf. Chapter 16). The boundary walls of the throttle clearance may consist either of parallel planes (corresponding to the cylindrical nozzle) or of widening planes (corresponding to the venturi nozzle). Since the
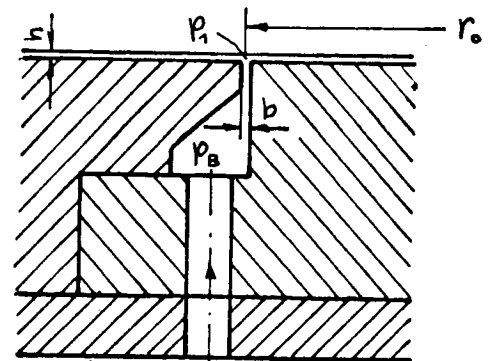
required throttle cross section area F_D is very small compared to the area of the bearing - in most cases $F_L/F_D \approxeq 5000 \div 7000$ - and the circumference $2r_o \pi$ is comparatively long, the width b of the annular clearance is of the same order of magnitude as the carrying bearing clearance. The precise adjustment of such a fine clearance which remains uniform over the entire circumference involves difficulties in most cases. Besides, special constructions such as composite bearing discs are required which can provoke a distortion of the bearing surface.

The throttle characteristic of the annular inlet clearance with parallel walls is identical with the nozzle characteristic (equation No. 12.2), whereas the characteristic for the venturi annular clearance can be calculated from equation No. 12.8.

12.6 Gas feed through porous inserts.

An intrinsically different way of feeding gas into the bearing clearance consists in introducing the gas through individual cylindrical or annular inserts which are arranged in the fixed bearing disc and are made of porous material. The properties and possibilities of use of a porous metal (bronze, stainless steel) sintered together from minute balls is described in reference (XV). The distribution of the gas can be done in such a way that a radial flow occurs over the entire bearing, whereby the compensating space which can provoke self-induced vibrations is eliminated. In certain cases, an increase of load capacity or a reduction of the volume of throughput can be achieved in bearings with feeding elements of porous surfaces, compared to a bearing with conventional throttle elements. The throttle characteristic of a porous material is similar to that of a capillary nozzle (cf. p. 83) and depends above all on the porosity and the thickness of the material.
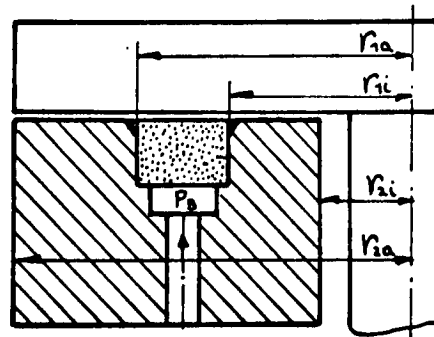
13. Non-radial clearance flow.

In order to avoid the danger of the appearance of self-induced vibrations, (cf. Chapter 16) it is advisable to allow the inlet nozzles to open directly into the bearing clearance without increase of the clearance volume (annular or compensating spaces). Thus each inlet nozzle must feed a certain

sector of the bearing area; the clearance flow is, therefore, no longer uniform and radial to the axis of the bearing. Since only local pressure peaks form around the nozzles, relative to their number, the load capacity is reduced compared to a bearing with an annular channel.

13.1 Potential flow.

In the following, the mathematical interrelationships will be studied and compared which apply to the incompressible and the compressible isothermal flow with any distribution whatsoever in narrow clearances. In this connection, it is assumed that the influence of inertia of the flowing medium is negligible in comparison with that of friction. This prerequisite is not completely applicable, however, to the immediate vicinity of the inlet nozzle, since the influence of acceleration outweighs that of friction there. The following studies are performed in cylindrical coordinates. The symbols have the following meanings:

r = radius; φ = angle of the coordinates; $\bar{v}_r$, $\bar{v}_\varphi$ = the radial velocity or tangential velocity, respectively, averaged over the height of the clearance; ϱ = density of the flowing medium; p = absolute pressure; ϕ = potential function; ψ = flow function; $C_1 - C_4$ = constants calculated from the boundary conditions.

Incompressible clearance flow   Compressible clearance flow

Formulation from equation No. 7.6

$$\bar{V}_r = - \frac{h^2}{12\varrho} \frac{\partial p}{\partial r} \qquad (13.1)$$

$$\bar{V}_\varphi = - \frac{h^2}{12\varrho} \frac{\partial p}{r\partial\varphi} \qquad (13.2)$$

Continuity

$$\frac{\partial\bar{V}_r}{\partial r} + \frac{\bar{V}_r}{r} + \frac{\partial\bar{V}_\varphi}{r\partial\varphi} = 0 \qquad\qquad \left| \qquad \frac{\partial(\varrho\bar{V}_r)}{\partial r} + \frac{\varrho\bar{V}_r}{r} + \frac{\partial(\varrho\bar{V}_\varphi)}{r\partial\varphi} = 0 \right. \qquad (13.2a)$$

Density function

$$\varrho = konst \qquad\qquad \left| \qquad \varrho = \frac{p}{gRT} \right. \qquad (13.2b)$$

By introduction of the equations No. 13.1 and No. 13.2 into the continuity equation, the following is obtained if the density function is taken into consideration:

Incompressible clearance flow   Compressible clearance flow

$$\Delta p = \frac{\partial^2 p}{\partial r^2} + \frac{\partial p}{r \partial r} + \frac{\partial^2 p}{r^2 \partial \varphi^2} = 0 \quad \left| \quad \frac{\partial\left(p\frac{\partial p}{\partial r}\right)}{\partial r} + \frac{p}{r}\frac{\partial p}{\partial r} + \frac{\partial\left(p\frac{\partial p}{r\partial \varphi}\right)}{r\partial \varphi} = 0 \right. \quad (13.2c)$$

Correlation

$$p = C_1 \phi + C_2 \qquad \qquad \qquad p^2 = C_3 \phi + C_4 \qquad (13.3)$$

Potential equation

$$\frac{\partial^2 \phi}{\partial r^2} + \frac{\partial \phi}{r \partial r} + \frac{\partial^2 \phi}{r^2 \partial \varphi^2} = 0 \qquad (13.4)$$

Solution of the potential equation

$$\Phi(z) = \Phi(r.e^{i\varphi}) = \phi + i\psi \qquad (13.4a)$$

Velocity components   Flow density components

$$\bar{V}_r = \frac{\partial \phi}{\partial r} = \frac{\partial \psi}{r\partial \varphi} \qquad \qquad p\bar{V}_r = \frac{\partial \phi}{\partial r} = \frac{\partial \psi}{r\partial \varphi}$$

$$\bar{V}_\varphi = \frac{\partial \phi}{r\partial \varphi} = -\frac{\partial \psi}{\partial r} \qquad \qquad p\bar{V}_\varphi = \frac{\partial \phi}{r\partial \varphi} = -\frac{\partial \psi}{\partial r} \qquad (13.4b)$$

Field of flow

ϕ = const   potentials lines or isobars, respectively

ψ = const   flow lines

This leads to the following conclusion: Every laminar flow in narrow clearances can be considered as potential flow if the influence of acceleration is disregarded, and the potential lines are assumed to be isobars, both in incompressible and in compressible media. The flow lines and the isobars form an orthogonal network. The difference between incompressible and compressible flow is only the correlation between p, $\bar{v}$, ϕ and ψ . Whereas, in incompressible flow, the pressure is a linear function of the potential value, this relationship is expressed by a quadratic function in compressible flow. An analogous connection between velocity and flow density is obtained by differentiation of the potential function.

13.2 Load capacity.

If the boundary values p_1 and p_2 are given and the magnitudes of ϕ_1 and ϕ_2 are determined from the bearing geometry, the constants C_3 and C_4 can be calculated from equation No. 13.3; the result is:

$$C_3 = \frac{p_1^2 - p_2^2}{\phi_1 - \phi_2} \qquad (13.5)$$

$$C_4 = p_1^2 - \phi_1 \frac{p_1^2 - p_2^2}{\phi_1 - \phi_2} \; , \qquad (13.6)$$

From this the pressure distribution in the clearance is found to be:

$$p = \sqrt{p_1^2 - \frac{p_1^2 - p_2^2}{\phi_2 - \phi_1}(\phi - \phi_1)} \qquad (13.7)$$

If equation No.13.7 is introduced into the integral for the load capacity, equation No. 10.3, the following result is obtained:

$$K_I = \iint\limits_{(F_k)} \sqrt{p_1^2 - \frac{p_1^2 - p_2^2}{\phi_2 - \phi_1}(\phi - \phi_1)} \; r.dr.d\varphi \; . \qquad (13.8)$$

13.3 Amount of flow.

The volume flowing between two flow lines very close to each other is:

$$dV = h\left(\overline{V}_r.r.d\varphi - \overline{V}_\varphi \, dr\right) \qquad (13.8a)$$

The corresponding weight/second is, if the gas equation No.7.9 is used:

$$d\dot{G} = \frac{h}{RT}\left(\overline{V}_r.p.r.d\varphi - \overline{V}_\varphi.p.dr\right) . \qquad (13.8b)$$

If the velocity components are eliminated by means of the equation No. 13.1 and No. 13.2 the consequence is as follows:

$$d\dot{G} = -\frac{h^3}{12\eta RT}\left(p\frac{\partial p}{\partial r} r.d\varphi - p\frac{\partial p}{r.\partial\varphi} dr\right) . \qquad (13.9)$$

The partial differentiations of equation No. 13.3 with respect to r and , respectively, have the following results

$$2p\frac{\partial p}{\partial r} = C_3\frac{\partial \phi}{\partial r} \qquad \text{and} \qquad 2p\frac{\partial p}{r.\partial\varphi} = C_3\frac{\partial \phi}{r.\partial\varphi} \; , \qquad (13.9a)$$
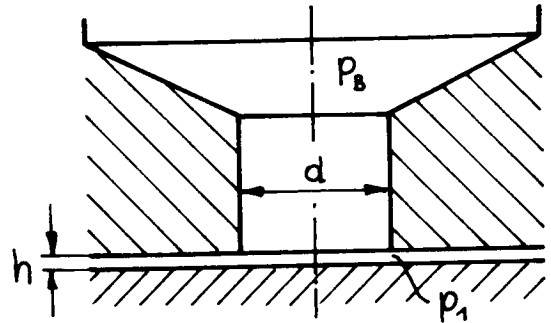
Introduction into equation No. 13.9 yields:

$$d\dot{G} = -\frac{h^3 C_3}{24 \eta RT}\left(\frac{\partial \phi}{\partial r} r \cdot d\varphi - \frac{\partial \phi}{r \partial \varphi} dr\right) \qquad (13.9b)$$

Integration affords the amount of gas escaping along a potential line:

$$\dot{G} = \frac{h^3 (p_1^2 - p_2^2)}{24 \eta RT(\phi_2 - \phi_1)}\left[\int_{\varphi_1}^{\varphi_2}\frac{\partial \phi}{\partial r} r \cdot d\varphi - \int_{r_1}^{r_2}\frac{\partial \phi}{r \partial \varphi} dr\right] \quad . \qquad (13.10)$$

In a bearing which is fed by individual nozzles which open directly into the clearance, the volume of be easily determined in another way if the counter-pressure p_1 in back of the nozzles is known. On account of the small heights of the clearance and the relatively much larger nozzle diameters, the area formed by the boundary of the nozzle and the height of clearance should be considered as site of throttling, rather than the nozzle cross section. (cf. Chapter 12.1B). For small nozzle cross sections, in comparison with the bearing area, the potential lines in the immediate vicinity of the nozzle are circles, and the nozzle orifice itself is potential line ϕ_1 corresponding to p_1. Therefore, the pressure gradient next to the nozzle orifice is uniform, and the same amount of gas per unit of boundary flows into the clearance over the whole circumference. The amount of gas flowing through a nozzle can, therefore, be calculated in a similar way as equation No. 12.2, from:

$$\Delta \dot{G}_0 = \mu\, d\, \pi\, h\, p_B \sqrt{\frac{2g\varkappa}{(\varkappa-1)RT}\left[\left(\frac{p_1}{p_B}\right)^{\frac{2}{\varkappa}} - \left(\frac{p_1}{p_B}\right)^{\frac{\varkappa+1}{\varkappa}}\right]} \quad . \qquad (13.11)$$

where p_B is the absolute pressure in front of the nozzle; p_1 is the absolute pressure in back of the nozzle; h is the height of the clearance; μ is the outflow coefficient; d is the diameter of the nozzle; $\Delta \dot{G}_D$ is the weight of throughput per second through a nozzle.

In a bearing where the drawing at the right represents a sector, a summation of $\Delta \dot{G}_D$ had to be done according to separate counter-pressures p_1. In the following equation, n is the number of the nozzle groups.
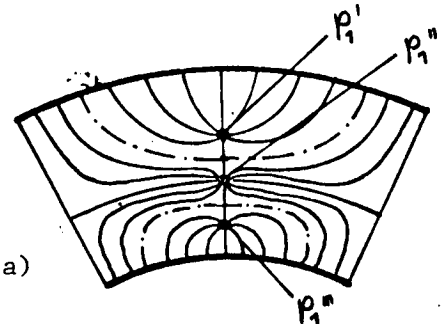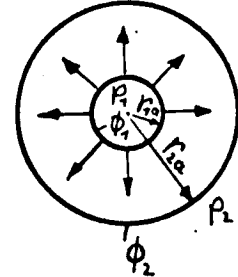
$$\dot{G} = n\left[\Delta \dot{G}_0(p_1') + \Delta \dot{G}(p_1'') + \Delta \dot{G}(p_1''')\right] \qquad (13.11a)$$

13.4 Application of the potential theory.

A) Analytical method.

A complete integration of the load capacity of the bearing and the amount of throughput can only be performed for simple flow patterns. For example, in the case of radial source flow from one single nozzle in the center of a circular thrust bearing, where the following applies:

$$\Phi(z) = \ln(r.e^{i\varphi}) = \phi + i\psi \qquad (13.11b)$$

the potential function and the flow function are given by

$$\phi = \ln r \quad , \quad \psi = \varphi \quad . \qquad (13.11c)$$

With the boundary conditions

$$
\begin{array}{ll}
\phi = \phi_1 & \phi = \phi_2 \\
p = p_1 & p = p_2 \\
r = r_{1a} & r = r_{2a}
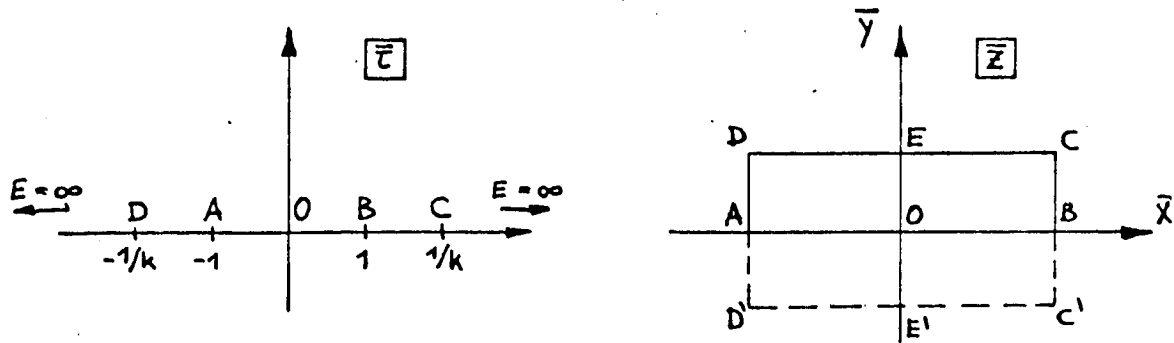\end{array} \qquad (13.11d)
$$

the already known equations No. 10.4 and No. 7.19 which can be solved, are obtained for the load capacity and the amount of throughput, respectively.

B) Numerical investigation of bearings with individual nozzles uniformly distributed on the circumference 2 r_o.

The symbols used have the following meaning: r_a is the outside radius of the bearing; r_i is the inside radius of the bearing; r_o is the radius of the bearing, on the circumference of which the nozzles are arranged: n is the number of nozzles on the circumference $2r_o\pi$; d is the diameter of the nozzle, or the largest diameter of the counterbore of the nozzle (cf. Chapter 12.1.C); k is the modulus of the elliptic functions; K is the half period in direction of the circumference; K' is the half period in radial direction; ϕ_1 is the potential value at the nozzle boundary; ϕ_2 are the potential values at the boundaries of the bearing; V is the adjustment factor.

The mathematical formulation of the problem can be done by a ray-like arrangement of alternate sources and sinks at a specified distance, originating from a center. The number of the rays must correspond to the number of nozzles distributed over the circumference. Thus two adjoining boundary potential lines which contain n sources and form circles, surround a bearing with annular support surface.

As can be seen in the drawing above, a boundary flow line runs from the source 1 to the trough 4 across two points 2 and 3 where the flow line has to change its angle suddenly by 90° in the same direction in each case. This fact suggests that a flow field with two periods is involved, where the period in radial direction is given by the alternate arrangement of sources and troughs; whereas the period in the direction of circumference is given by the continuously recurrent image which is formed by reflection by the walls which are impermeable to the flow (connecting lines 2 -3, 2' - 3').

For greater clarity, the most essential features of fields with two periods will be pointed out briefly. If $\bar{z}$, $\bar{\tau}$, $\bar{u}$, $\bar{w}$, $\bar{\zeta}$ are different planes between which conformal representations are performed, it can be concluded according to reference (XXIV) that the upper half-plane of the $\bar{\tau}$ - plane is transferred into the interior of a rectangle of the $\bar{z}$ - plane by the transformation

$$\bar{z} = \int_0^{\bar{\tau}} \frac{d\bar{\tau}}{\sqrt{(1 - \bar{\tau}^2)(1 - k^2\bar{\tau}^2)}} \, , \qquad (13.11e)$$

where the term on the right side represents an elliptical integral of first kind.

By the simplifcation, $\bar{\tau} = \sin \bar{u}$, the integral is transformed into:

$$\bar{z} = \int_0^{\bar{u}} \frac{d\bar{u}}{\sqrt{1 - k^2 \sin^2 \bar{u}}} \qquad (13.11f)$$

The inversion function of this elliptical integral, i.e. the corresponding elliptical function of first kind reads

$$\bar{u} = am \ (\ \bar{z}, \ k \ ) \quad (\text{amplitudinis } \bar{z} \ ) \ . \qquad (13.11g)$$

This function which was introduced and calculated by Jacobi represents a transformation which transfers the interior of a rectangle of the $\bar{u}$ - plane onto a half-plane of the $\bar{z}$ - plane. It can be concluded, furthermore, from reference (XXIV) that the function "sinus amplitudinis $\bar{z}$"

$$\bar{w} = \sin \ am \ (\bar{z}, k) = sn \ (\bar{z}, k)$$

$$= \left[\bar{z} - (1 + k^2) \frac{\bar{z}^3}{3!} + (1 + 14 k^2 + k^4) \frac{\bar{z}^5}{5!} + \ldots \right]^{(13.12)}$$

represents a simple source flow of the $\bar{w}$ - plane into the two-period (source and sink) flow of the $\bar{z}$ - plane, which is illustrated on p. 100 (left).

A source with the complex potential $\Phi = \ln \bar{w}$ in the $\bar{w}$ - plane is transformed, by the function No. 13.12 into:
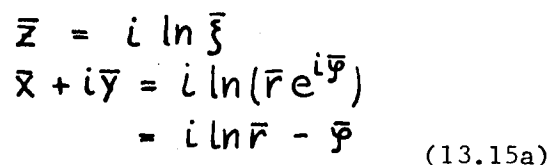
$$\Phi (\bar{z}) = \ln \ sn \ (\bar{z}, k) \ . \qquad (13.13)$$

Thus this function represents the two-period source and sink field which is illustrated on p. 100 (left). In order to arrive at the potential flow which is looked for, another transformation is required:

$$\bar{z} = i \ \ln \bar{\zeta} \qquad (13.14)$$

by which all straight lines of the $\bar{z}$ -plane which are parallel to the $\bar{x}$ -axis are conformally mapped in concentric circles of the $\bar{\zeta}$ -plane, and all straight lines parallel to the $\bar{y}$ -axis in radial rays of the $\bar{\zeta}$ - plane which pass through the center. If equation No. 13.14 is introduced into equation No. 13.13, the following result is obtained:

$$\Phi(\bar{\xi}) = \ln\left[sn\left\{i\ln(\bar{\xi},k)\right\}\right] = \phi + i\psi \quad . \qquad (13.15)$$

This complex function represents in its real portion the potential lines ϕ and in its imaginary portion the flow lines ψ . The last transformation (No. 13.14) attains not only a transition of parallel strips into closed circular bands, but also a logarithmic distortion of the periods which are equal in the $\bar{y}$ - direction in such a way that, with increasing radius, the periods increase steadily.

$$\bar{z} = i \ln \bar{\xi}$$
$$\bar{x} + i\bar{y} = i \ln(\bar{r} e^{i\bar{\varphi}})$$
$$= i \ln \bar{r} - \bar{\varphi} \qquad (13.15a)$$
$$\bar{x} = -\bar{\varphi}$$
$$\bar{y} = \ln \bar{r}$$
$$\Delta\bar{y} = \ln\frac{r_o}{r_i} = \ln\frac{r_a}{r_o}$$

A circle of the radius $\bar{r} = e^0 = 1$ is coordinated to the line $\bar{y} = 0$ of the $\bar{z}$ - plane by the projection $\bar{z} = i \ln \bar{\xi}$ in the $\bar{\xi}$ - plane. The straight line in infinite distance parallel to the $\bar{x}$ - axis of the $\bar{z}$ - plane corresponds to the zero point of the $\bar{\xi}$ - plane through $\bar{z} = i \ln \bar{\xi} = -i \infty$. The entire lower half-plane of the $\bar{z}$ - plane would be projected to the interior of the circle $r = 1$ of the $\bar{\xi}$ - plane, while the upper half plane of the $\bar{z}$ - plane is projected on the exterior of the circle $\bar{r} = 1$. Since the circle S - S (figure at the lower right) corresponds to the straight line e (in the left figure below), this circle is the flow line for the bearing flow.
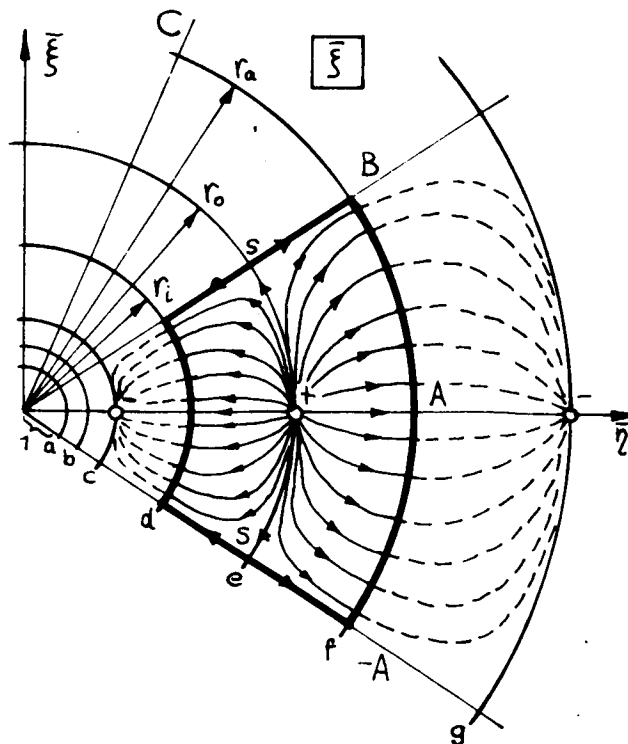
The constant k is designated as modulus of the elliptical function and depends on the elementary periods K and K' or their ratio K/K'.

In order to have the boundary conditions, selected for the bearing, fulfilled by the transformation function No. 13.15, the following coordinations between the figures above must be observed.

$\bar{y}$ - period		$\bar{r}$ - period
a . . . 0		a . . . $r_0\left(\sqrt{r_i/r_a}\right)^4\left(\sqrt{r_a/r_i}\right)^0$
b . . . K'/2		b . . . $r_0\left(\sqrt{r_i/r_a}\right)^4\left(\sqrt{r_a/r_i}\right)^1$
c . . . 2K'/2		c . . . $r_0\left(\sqrt{r_i/r_a}\right)^4\left(\sqrt{r_a/r_i}\right)^2$
d . . . 3K'/2	logarithmic	d . . . $r_0\left(\sqrt{r_i/r_a}\right)^4\left(\sqrt{r_a/r_i}\right)^3 = r_i$
e . . . 4K'/2	coordination	e . . . $r_0\left(\sqrt{r_i/r_a}\right)^4\left(\sqrt{r_a/r_i}\right)^4 = r_0$
f . . . 5K'/2		f . . . $r_0\left(\sqrt{r_i/r_a}\right)^4\left(\sqrt{r_a/r_i}\right)^5 = r_a$
g . . . 6K'/2		g . . . $r_0\left(\sqrt{r_i/r_a}\right)^4\left(\sqrt{r_a/r_i}\right)^6$

arithmetical progression   geometrical progression

If, on the outset, the site of the gas feed r_0 is chosen in such a way that the following applies:

$$r_0^2 = r_a \cdot r_i \qquad (13.16)$$

(cf. equation No. 11.2), it is feasible to insert the $\bar{r}$ -periods of the plane into a geometrical progression with the quotient $\sqrt{r_a/r_i}$.

$\bar{x}$ - period		- period	
A . . . 0		A . . . 0	
B . . . K		B . . . π/n	
C . . . 2K	linear coordination	C . . . $2\pi/n$	
D . . . 3K		D . . . $3\pi/n$	(13.16a)
E . . . 4K		E . . . $4\pi/n$	
.		.	
.		.	
.		.	
Λ' . . . 2nK		Λ' . . . 2π	

Thus an angle of 360° corresponds to the distance 2nK. If this value is exceeded in the $\bar{x}$ - direction, the cycle is resumed in the $\bar{\xi}$ - plane (2nd leaf according to Riemann).

By comparison of the corresponding periods, the constants for the Jacobi function

$$K' = \ln r_o \left(\sqrt{r_i/r_a}\right)^4 \left(\sqrt{r_a/r_i}\right)^5 - \ln r_o \left(\sqrt{r_i/r_a}\right)^4 \left(\sqrt{r_a/r_i}\right)^3 - \ln \frac{r_a}{r_i} = 2 \ln \frac{r_a}{r_o} \qquad (13.16b)$$

and $k = \dfrac{\pi}{n}$ are obtained. For the ratio

$$\frac{K}{K'} = \frac{\pi}{n \ln \frac{r_a}{r_i}} = f(k) \qquad (13.16c)$$

the modulus k^2 for the transformation function can be obtained from one of the references (XXIV) or (XXV). The comodulus k' which will play a role in later studies is determined by the equation:

$$k^2 + k'^2 = 1.$$

Since the coordination between K and k and, respectively, between K' and k' is unequivocally defined by integrals (XXIV) and the magnitudes of the K and K' values calculated from the given bearing conditions are not in agreement, in their absolute values, with the values of the basic progressions given in the function tables (XXV), another transformation must be made in such a way that the arguments and periods in the direction of the coordinates are enlarged or reduced. This conversion factor will be designated as adjustment factor V. Thus the following applies:

$$V = \frac{K_T}{K} = \frac{K'_T}{K'} , \qquad (13.16d)$$

where T is an index indicating the relationship to the Table. The arguments for this coordinate directions are found, in analogy to the periods, as:

$$r - \text{direction} \ldots V \ln r/r_o \quad (K'_T = V \ln r_a/r_i)$$

$$\varphi - \text{direction} \ldots V \widehat{\varphi} \quad (K_T = V \pi/n)$$

By introduction of this last transformation into equation No. 13.15

$$\bar{\zeta} = \zeta^V = \left(\frac{r}{r_o} e^{i\varphi}\right)^V \qquad (13.16e)$$

The final adjusted function of representation results:

$$\phi(\zeta) = \ln\left[\text{sn}\left\{i \ln \zeta^V\right\}\right] . \qquad (13.17)$$

The solution, or separation of equation No. 13.17 into real and imaginary portions, is done the following way: If the inner logarithmic function is resolved, one obtains:

$$\phi(\zeta) = \ln\left[\text{sn}\left(-V\varphi + iV \ln\frac{r}{r_o} , k\right)\right] = \phi + i\psi . \qquad (13.17a)$$

Then the "sinus amplitudinis" is solved according to the addition theorem described in reference (XI), and the result is:

(13.18)

$$\phi(\xi) = \ln \frac{sn(-V\varphi, k)\, dn(V\ln\frac{r}{r_0}, k') + i\, cn(-V\varphi, k)\, dn(-V\varphi, k)\, sn(V\ln\frac{r}{r_0}, k')\, cn(V\ln\frac{r}{r_0}, k')}{cn^2(V\ln\frac{r}{r_0}, k') + k^2 sn^2(-V\varphi, k)\, sn^2(V\ln\frac{r}{r_0}, k')},$$

where cn and dn represent the cosinus (cosine) and delta amplitudinis functions, respectively. Since, however, the following applies:

$$sn(-V\varphi, k) = -sn(V\varphi, k)$$
$$cn(-V\varphi, k) = cn(V\varphi, k) \qquad (13.18a)$$
$$dn(-V\varphi, k) = dn(V\varphi, k)$$

and equation No. 13.18 is resolved according to the following principle

$$\ln(a + ib) = \ln\sqrt{a^2 + b^2} + i\, \arctg \frac{b}{a} \qquad (13.18b)$$

the results are as follows:

$$\phi = \ln\frac{\sqrt{sn^2(V\varphi, k)\, dn^2(V\ln\frac{r}{r_0}, k') + cn^2(V\varphi, k)\, dn^2(V\varphi, k)\, sn^2(V\ln\frac{r}{r_0}, k')\, cn^2(V\ln\frac{r}{r_0}, k')}}{cn^2(V\ln\frac{r}{r_0}, k') + k^2 sn^2(V\varphi, k)\, sn^2(V\ln\frac{r}{r_0}, k')} \qquad (13.19)$$

and

$$\psi = \arctg\frac{cn(V\varphi, k)\, dn(V\varphi, k)\, sn(V\ln\frac{r}{r_0}, k')\, cn(V\ln\frac{r}{r_0}, k')}{-sn(V\varphi, k)\, dn(V\ln\frac{r}{r_0}, k')} \qquad (13.20)$$

Boundary conditions: The boundary values of the potential ϕ as a function of the bearing geometry can be easily found.

1) If the nozzle diameter or the largest diameter of the counterbore of the nozzle (cf. Chapter 12.1 C) d $\ll$ r_0, one obtains for small arguments $V\varphi$
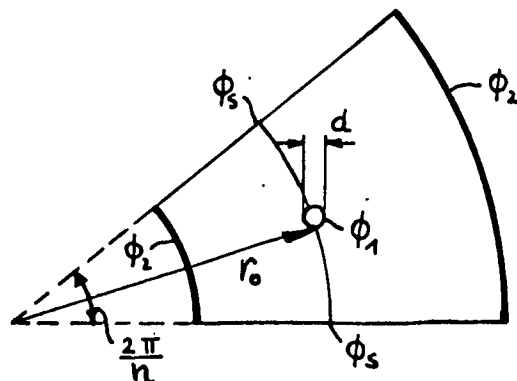
$$sn\, V\varphi \cong V\varphi \qquad (13.20a)$$
$$cn\, V\varphi = dn\, V\varphi \cong 1$$

and for $r = r_o$ the result is:

sn (0) $\cong$ 0,   cn (0) = dn (0) $\cong$ 1.

From this one obtains, by introduction into equation No. 13.19:

$$\phi_1 = \ln \frac{V \cdot d}{2 r_o} \qquad (13.20b)$$

2) The following can be given as potential value of all circular potential lines (limiting potential lines)

$$\phi_2 = \ln \frac{1}{\sqrt{k}} \qquad (13.20c)$$

whereas the potential for the stagnation point S situated between two adjacent flow fields is ($r = r_o$, $\varphi = \pi/n$)

$$\phi_s = 0$$

The coordination of pressure and potential was given already before by equation No. 13.3.

Example of calculation.

In a bearing of the following given dimensions and operating values:

flow medium: air

n = number of nozzles which open directly into the clearance.

r_a	=	60,0 mm	Strömungsmedium Luft			
r_o	=	38,75 mm	p_1	=	˙8.10⁴	kp/m²
r_i	=	25,0 mm	p_2	=	1.10⁴	kp/m²
d	=	0,7 mm	η	=	1,85.10⁻⁶	kp.s/m²
F_L	=	93,4 cm²	h	=	20.10⁻⁶	m
n	..	Anzahl der direkt in den Spalt mündenden Düsen	T	=	293	°K
			R	=	29,3	m/°K

$(13.20d)$

the load capacity and the flow volume were determined at a varying number of nozzles, n. Since the integrals No. 13.8 and No. 13.10 cannot be solved mathematically, only a numerical procedure could be applied, using the potential function found, No. 13.19. By subdivision of the half-sector of the carrying surface in the r- and φ -direction into many small parts Δ r and $\Delta \varphi$,   the load capacity is obtained as:

$$K_I = 2n \sum_{r_i}^{r_a} \sum_0^{\pi/n} p \cdot r \cdot \Delta r \, \Delta\varphi \qquad (13.21)$$

and the amount of flow as:

$$\dot{G} = \frac{2n\,h^3\,(p_1^2 - p_2^2)}{24\,\eta\,RT\,(\phi_2 - \phi_1)}\left[r_a \sum_0^{\pi/n} \frac{\phi_2 - \phi_{\Delta r_a}}{\Delta r_a}\Delta\varphi + r_i \sum_0^{\pi/n} \frac{\phi_2 - \phi_{\Delta r_i}}{\Delta r_i}\Delta\varphi\right], \qquad (13.22)$$

where $\phi_{\Delta r_a}$ and $\phi_{\Delta r_i}$ represent potentials dependent on φ at a distance of Δr_a and Δr_i from the outer and inner boundary, respectively.

Results

n	K	K'	k²	k'²	V	K_T	K'_T	φ₁	φ₂
4	0,785	0,875	0,390	0,610	2,25	1,770	1,960	-3,897	0,236
6	0,524	0,875	0,080	0,920	3,06	1,604	2,684	-3,550	0,631
10	0,314	0,875	0,004	0,996	5,01	1,574	4,385	-3,010	1,382
20	0,157	0,875	0,000	1,000	10,00	1,570	8,750	-2,405	3,697

n	K_I^{kp}	C	$\dot{G}_a$ gr/s	$\dot{G}_i$ gr/s	$\dot{G}$ gr/s	$\dot{G}_a/\dot{G}_{(n=\infty)a}$	$\dot{G}_i/\dot{G}_{(n=\infty)i}$
4	233	0,312	0,394	0,363	0,757	0,2075	0,1911
6	284	0,380	0,625	0,576	1,202	0,3295	0,3035
10	348	0,465	0,942	0,870	1,812	0,4970	0,4590
20	422	0,564	1,482	1,365	2,847	0,7805	0,7190
∞	486	0,650	1,899	1,899	3,798	1	1

$$(13.22a)$$

On page 106, the isobars calculated for the data given are illustrated for n = 4, 6, and 20 nozzles at a magnification of 2 : 1.
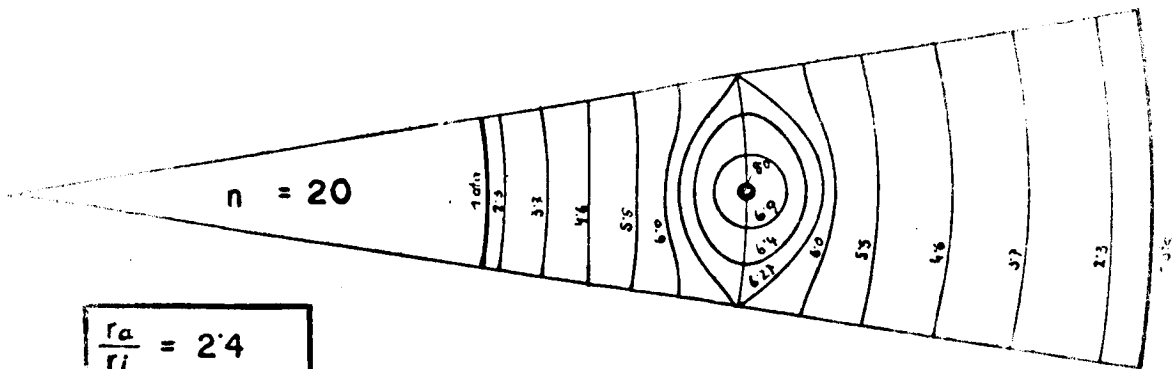
Load capacity.

The results of the calculated example are plotted in the Diagrams 13 and 15 as functions of the number of nozzles. The load capacity of the bearing was represented there with the aid of a dimension-less load factor

$$C = \frac{K_I}{F_L \cdot p_1}, \qquad (13.23)$$

where K_I is the absolute carrying capacity of the bearing; F_L is the area of the bearing $\pi \cdot (r_a^2 - r_i^2)$; p_1 is the absolute pressure directly in back of the nozzles. The factor C is, of course, not applicable everywhere but is again a function of the ratios p_1/p_2 and r_a/r_i. In order to allow a comparison to a bearing with radial flow only (annular clearance feed n = ∞) with respect to load capacity, the load factor $C_{n=\infty}$ is
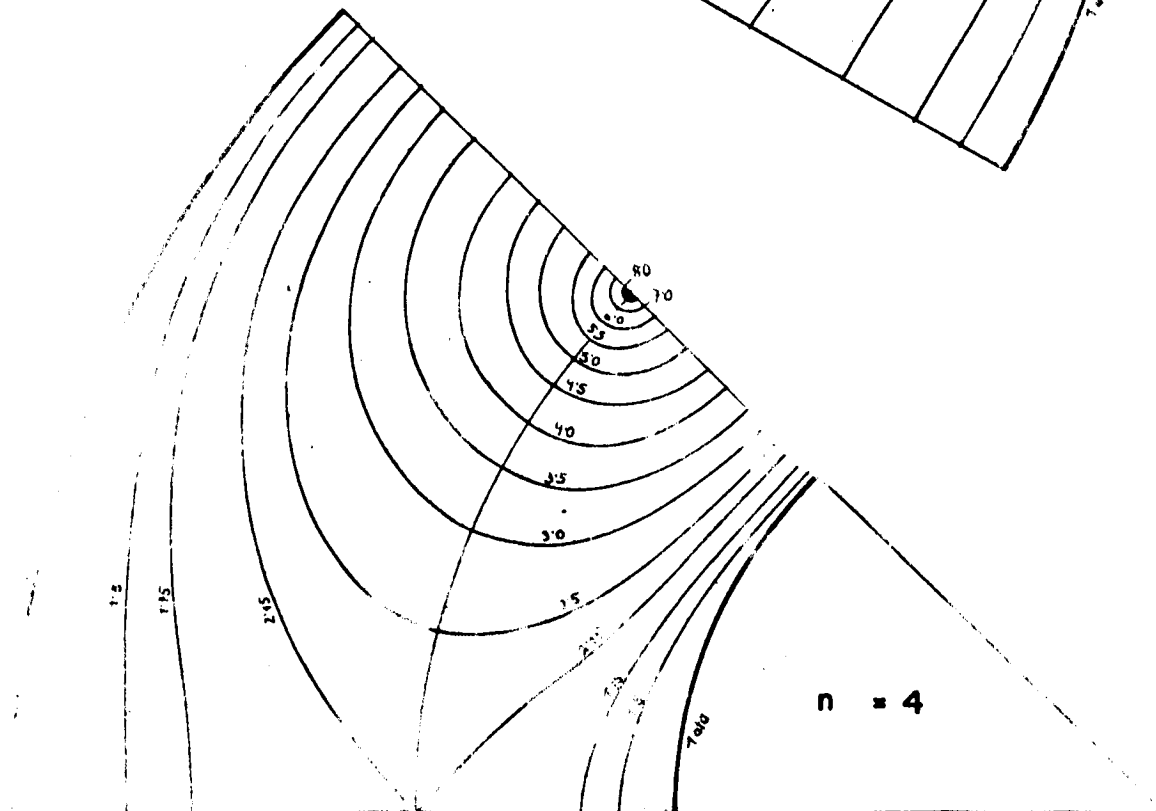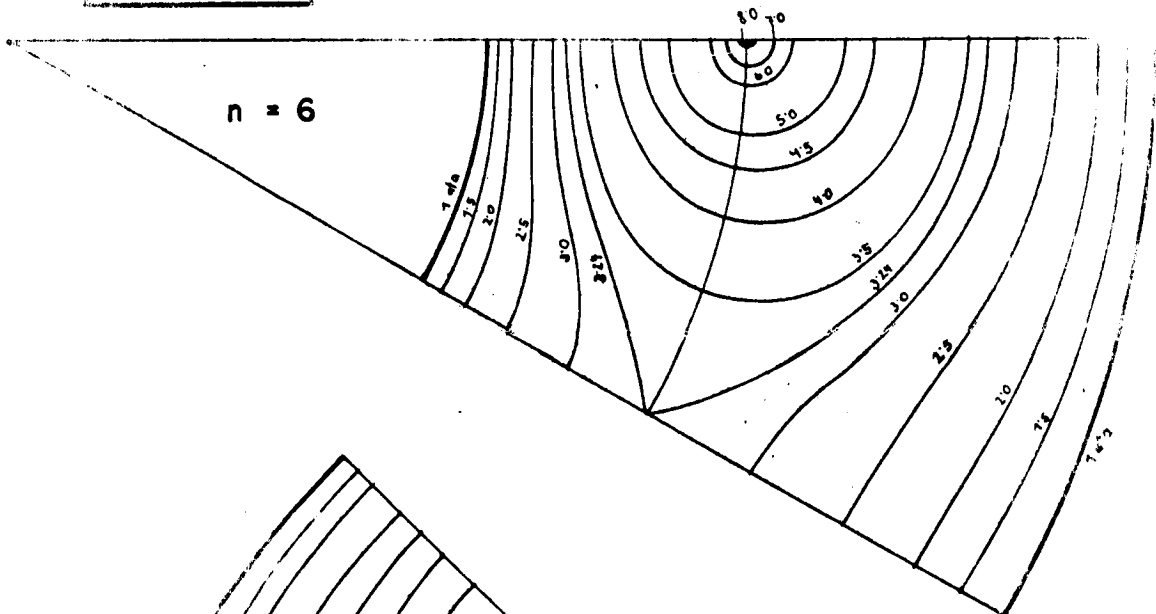
Calculated Isobars

calculated. From the equations No. 10.6 and 10.7 it can be deduced that the absolute load capacity for such a bearing is:

$$K_I = \pi \, p_1 \left(r_a^2 \, C_{ka} + r_0^2 \, C_{ki} \right) . \qquad (13.23a)$$

By the equation No. 13.23 and consideration of equation No. 13.16, this is transformed into

$$C_{n=\infty} = \frac{C_{ka} + C_{ki} \frac{r_i}{r_a}}{1 - \left(\frac{r_i}{r_a} \right)^2} . \qquad (13.24)$$

In the comparison of individual bearings to each other, not the absolute number of the feeding nozzles is decisive, but rather a proportionality factor obtained from the distribution of the nozzles and width of the ring; this factor gives approximately similar potential distributions for the individual bearing sectors. In order to be able to arrive at a more generally applicable result from the calculated examples given above, a sector ratio τ is introduced which can be determined from the quotient
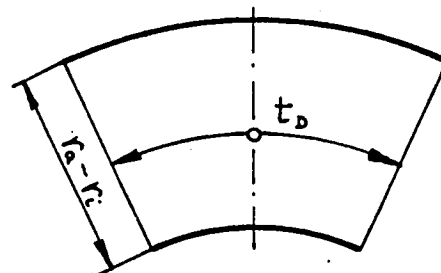
$$\tau = \frac{t_D}{r_a - r_i} = \frac{2 \pi r_0}{n (r_a - r_i)} \qquad (13.24a)$$

Using the equation No. 13.16, the following is obtained:

$$\tau = \frac{2 \pi}{n \sqrt{\frac{r_a}{r_i}} \left(1 - \frac{r_i}{r_a} \right)} . \qquad (13.25)$$

In Diagram 15, the ratio of the load capacity factors $C/C_{n=\infty}$ in the calculated example is plotted as a function of τ . In order to answer the question how many nozzles should be arranged on the circumference $2 \, r_0$ - this question will come up when a bearing is being designed - the fact that the load capacity increases steadily with an increasing number of nozzles, must be remembered. As can be seen in Diagram 13, however, the course of C shows first a steep rise with an increasing number of nozzles, but increases only slightly beyond a point which is established to a greater or lesser degree; Thus in that region, an enlargement of the number of nozzles does not bring about a considerable increase in load capacity. In the calculated example (r_a/r_i = 2.4) this critical number of nozzles would be n = 20 - 24. The loss in the calculated load capacity compared to a bearing with annular clearance feed would be about 11% (if it is based on the measured values, only about 5%). Corresponding to this number of nozzles, the following is obtained:

τ = 0.25 - 0.35, and, for the design of new bearings:

$$n = \frac{18 - 25}{\sqrt{\frac{r_a}{r_i}}\left(1 - \frac{r_i}{r_a}\right)} \qquad (13.26)$$

is the optimum number of nozzles.

Amount of flow.

The results of the calculations of the flow weights of bearing air are represented in the Diagrams 14 and 16. The outward and inward flowing portions are divided by the amount of throughput $\dot{G}_n = \infty$ which is required at a strictly radial flow (cf. equations No. 7.19 and 7.20). The fact is worth mentioning that, in spite of conformance a with equation No. 13.16, the values for $\dot{G}_a$ and $\dot{G}_i$ are different in the presence of individual nozzles. In order to make this fact more clearly visible, a nozzle with the boundary flow line (circle $2 r_o \pi$) is drawn in a magnified scale. Since the boundary of the nozzle is formed by potential line ϕ_1 and a uniform mass flow perpendicular to ϕ_1 prevails, a larger portion of the circumference of the nozzle is available for the flow outwards.
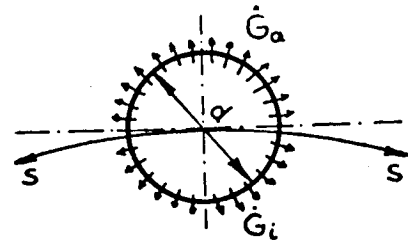
Measuring results.

In the Figures 1 and 2, in which the experimental equipment is illustrated, the course of the flow lines and the pressure distribution in a bearing with four individual nozzles which open directly into the clearance, could be measured. The actual sites of the pressure taps where the measurements were taken, and those reduced to a quarter sector, respectively, are shown on p.112. The picture of the flow lines could be taken by means of small amounts of oil and water of condensation which entered the bearing, at the beginning of the measurements, on account of the absence of a satisfactory separator, together with the compressed air and left behind yellowish colored traces on the bearing surfaces. One half of a bearing with the detected course of the flow lines is illustrated on the top of p.113. Since the radius of the feeding nozzles r_o is only slightly different from the conditions according to equation No. 13.16, the line which separates the mass flows outwards from those inwards is, as expected, a circle. Likewise, the stagnation point S is clearly visible. The isobars measured for two different bearing gas pressures P_B are also plotted on p. 113 (middle and bottom). A comparison by superimposition of the flow lines and isobars shows a very satisfactory orthogonality of the two groups of curves.

In Diagram 13, measuring points for the load capacity factor C are plotted as a function of n. The points at n = 4 and n= 30 were measured by means of the experimental equipment which is illustrated in Figures 1 and 2. The point at n = 8 could be ascertained on the thrust bearing of the experimental compressor (cf. Fig. 12). This shows clearly that the measured values are always higher than the theoretical results. This deviation can be traced

back, in part, to the fact that, in the theoretical studies, the retarding portion w.dw of the flowing medium which occurs at high entrance velocities into the clearance, was disregarded. The total energy which is introduced into the bearing consists not only of the static pressure p_1 which was measured and was the base for the comparisons of the calculations, but also of the velocity component which is transformed into pressure energy and friction energy in the course of the clearance flow.

The area of the nozzle cross sections has no influence on the absolute load capacity of the bearing, unless the character of the flow is significantly changed, but it has an influence on the correlation between height of the clearance and load capacity. If, for example, cylindrical feeding nozzles which open directly into the clearance are counterbored at the side of the clearance (cf. Chapter 12.1 C), a shift of the load capacity characteristic into the region of larger clearance widths is obtained. The advantage of achieving a larger clearance and thus increased safety of operation at equal bearing load is counterbalanced by an increased volume of throughput. Measurements in a bearing with and without counterbored nozzle on the side of the clearance are shown in Chapter 15. Summarizing, it can be stated that the number of individual nozzles has an influence on the absolute load capacity; and that, on the other hand, the effective area of the feeding nozzles has an influence on the correlation between K_I and h.

14. Bearing characteristics.

In the present chapter, the characteristic magnitudes are represented dimension-less for various arrangements of the bearings and flow patterns by means of the continuity requirement between the amount of gas flowing into the bearing through the nozzles and that escaping from the clearance.

The functions designated as bearing characteristics in the following were derived under these conditions: 1) The change of kinetic energy of the flowing gas was disregarded; 2) The rotation of the disc was disregarded; 3) Short cylindrical nozzles, throttling clearances of apertures as feeding elements were present.

The characteristics

$$ f\left(\varkappa, \frac{p_1}{p_2}, \frac{p_2}{p_B}\right) = \Lambda \qquad (14.0a) $$

represent there pressure dependent functions the values of which are determined by a dimensionless number which characterizes the kind of bearing and nozzles. The bearing characteristics are very useful for the determination of the total course of K_{ges} or $\overset{*}{G}$ over h. By this method proposed for representation of the bearing, furthermore, not only the condition of the bearing at any time can be shown, but also the influence of change of the size of the bearing, of the area of the feeding nozzles, of the kind and temperature of the gas and of the height of the clearance appear immediately.
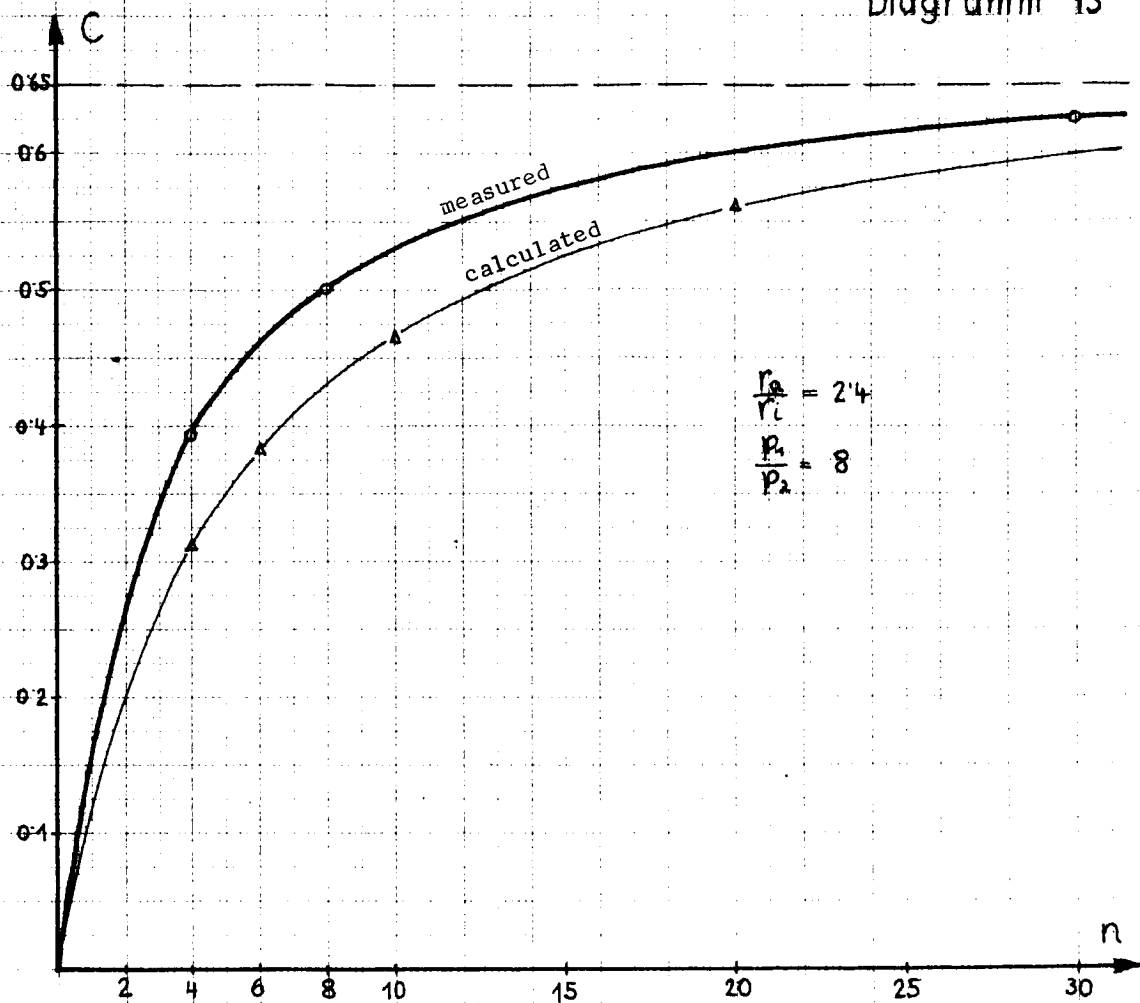
Diagramm 13

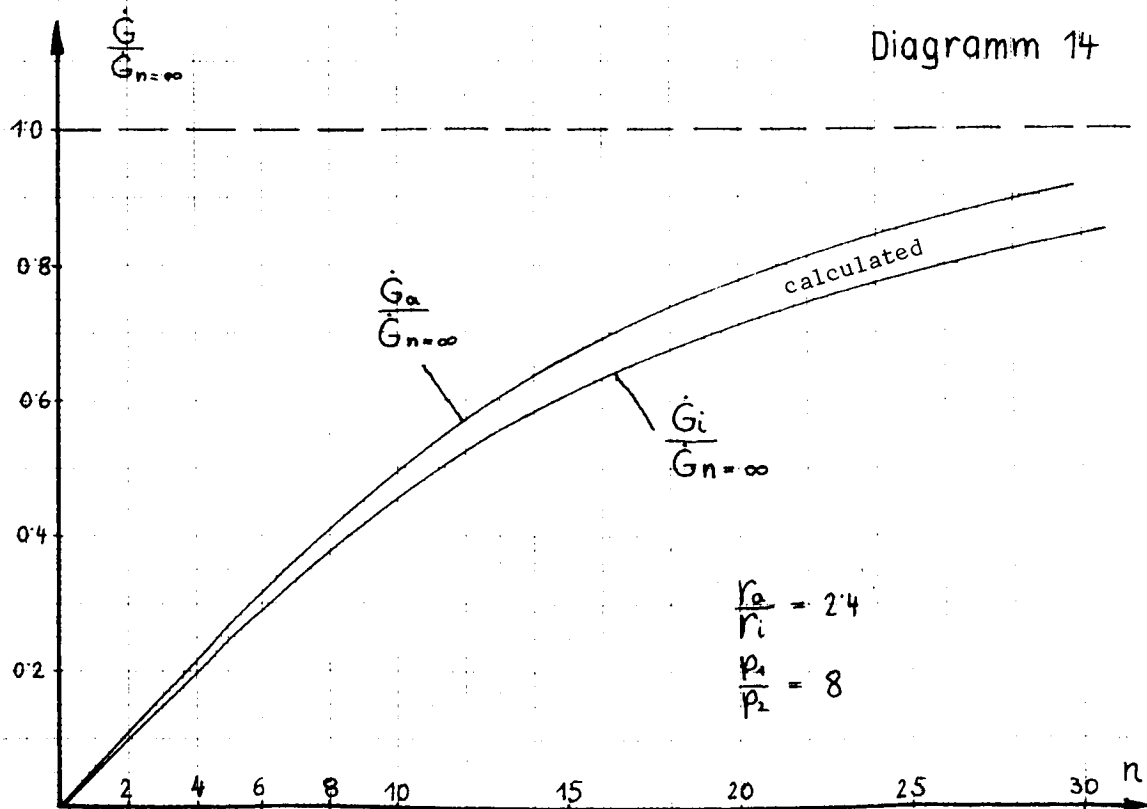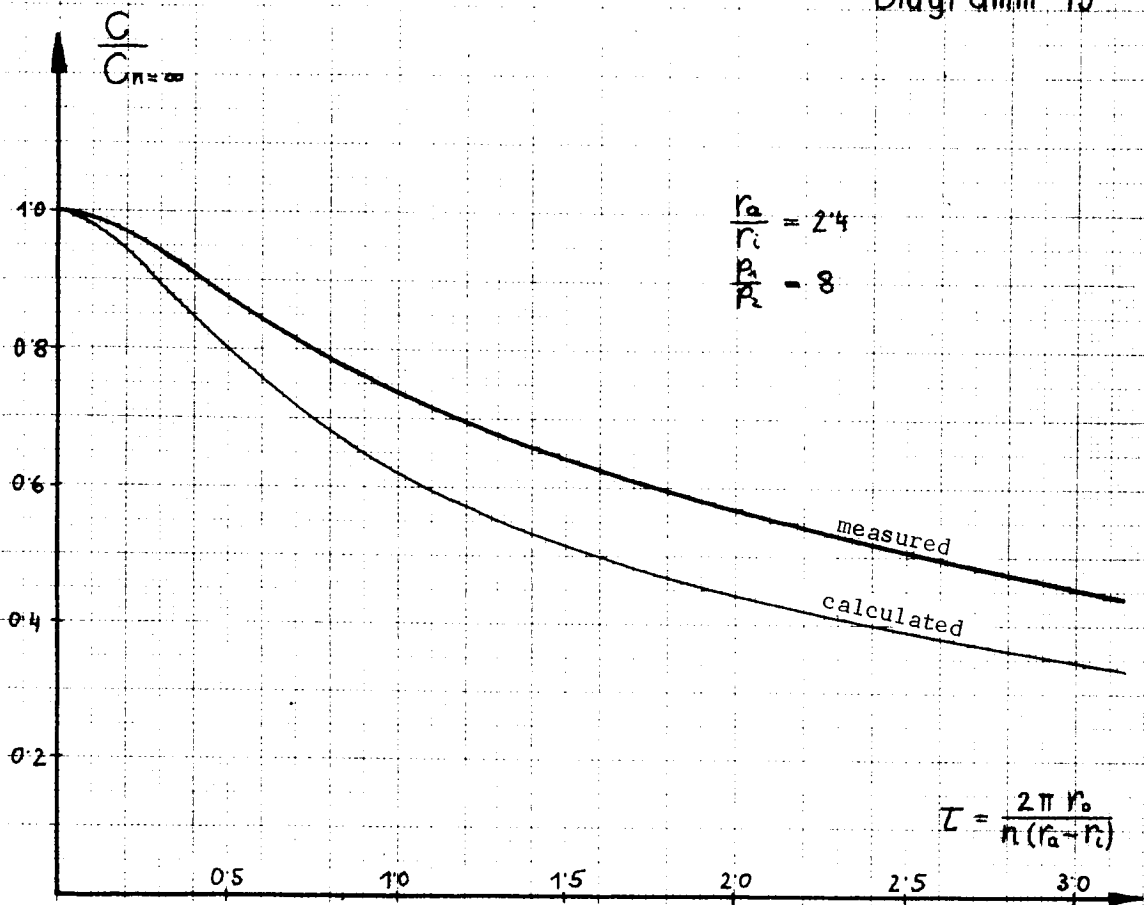$\frac{r_a}{r_i} = 2\cdot 4$
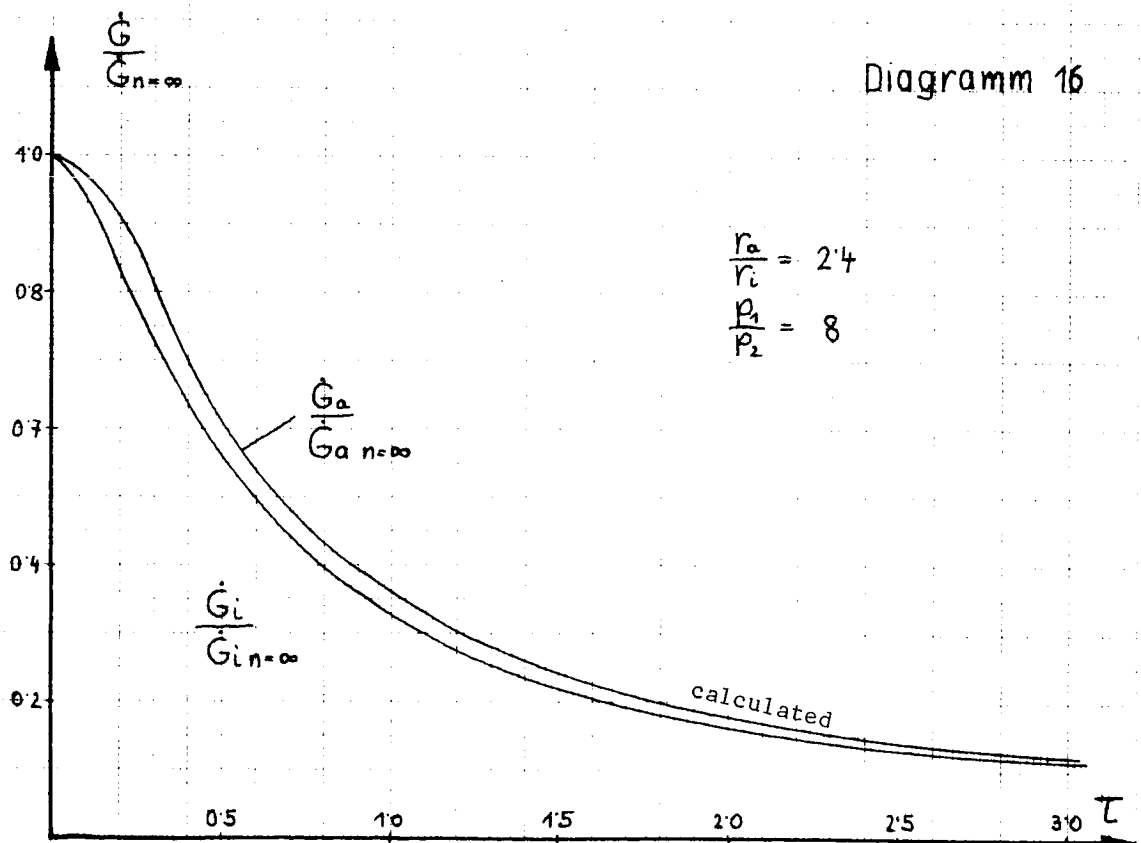
$\frac{p_1}{p_2} = 8$

Diagramm 14

$\frac{r_a}{r_i} = 2\cdot 4$

$\frac{p_1}{p_2} = 8$

Diagramm 15

$$\frac{r_a}{r_i} = 2\cdot4$$

$$\frac{p_1}{p_2} = 8$$

measured

calculated

$$\mathcal{L} = \frac{2\pi\, r_o}{n\,(r_a - r_i)}$$

Diagramm 16

$$\frac{r_a}{r_i} = 2\cdot4$$

$$\frac{p_1}{p_2} = 8$$

$$\frac{\dot{G}_a}{\dot{G}_{a\,n=\infty}}$$

$$\frac{\dot{G}_i}{\dot{G}_{i\,n=\infty}}$$

calculated

Actual distribution of boreholes in which the
pressure was measured
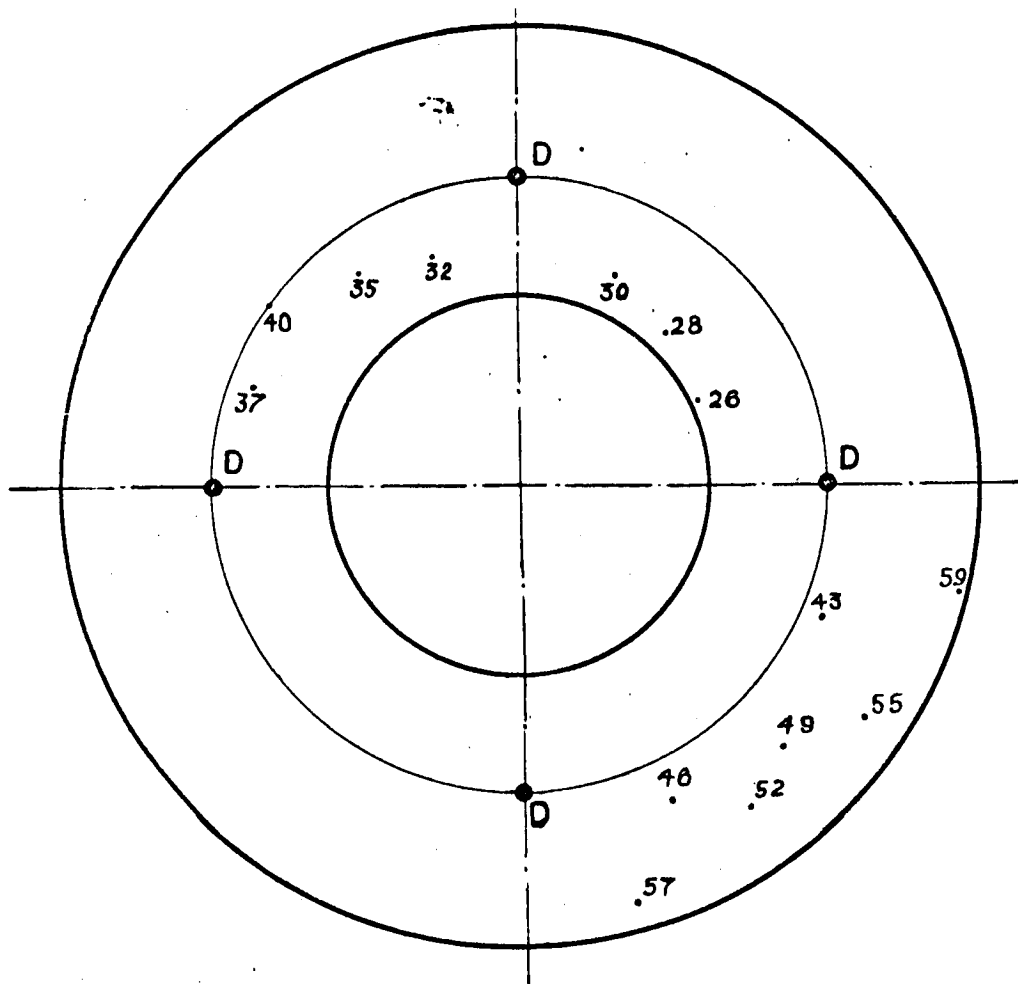
Boreholes reduced to one sector
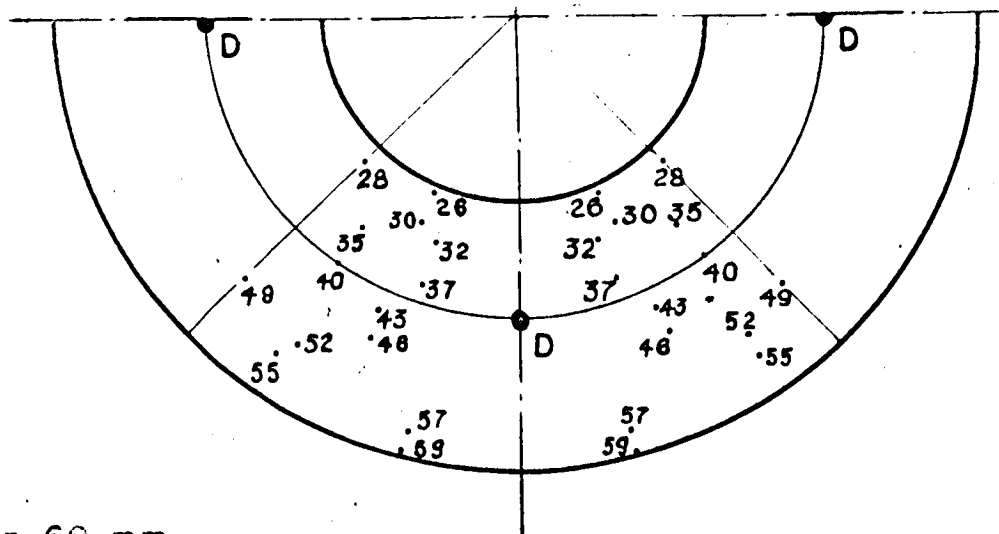
r_a = 60 mm

r_o = 40 mm

r_i = 25 mm

D = nozzle
Number = Radius of the
borehole

Measurements

Flow Lines

ra = 60 mm
ro = 40 mm
ri = 25 mm
d = 0'7 mm
n = 4

Isobars

(Atmospheres)

p_1 = 8 ata

p_2 = 1 ata

K_I = 293 kp

ϕ_2

Isobars

p_1 = 10 ata

p_2 = 1 ata

K_I = 373 kp

ϕ_2

14.1 Radial flow.

A) Laminar.

In order to have equilibrium in the bearing, the amount of gas which enters through the feeding nozzles must be equal to the amount which flows out through the clearance. Thus, if the equation No. 12.2 is equated to the sum of the two equations No. 7.19 and 7.20, the following is obtained after contraction of the individual members to dimension-less terms:

$$\frac{\pi}{12}\left[\frac{h^3 p_2}{\mu F_0 \eta \sqrt{2gRT}}\right]\left\{\frac{1}{\ln\frac{r_{1a}}{r_{1a}}} + \frac{1}{\ln\frac{r_{1i}}{r_{2i}}}\right\} = \frac{p_B}{p_2}\frac{\sqrt{\frac{\varkappa}{\varkappa-1}\left[\left(\frac{p_1}{p_2}\frac{p_2}{p_B}\right)^{\frac{2}{\varkappa}} - \left(\frac{p_1}{p_2}\frac{p_2}{p_B}\right)^{\frac{\varkappa+1}{\varkappa}}\right]}}{\left[\frac{p_1}{p_2}\right]^2 - 1},$$

(14.1)

where the following equation was applied

$$\frac{p_1}{p_B} = \frac{p_1}{p_2}\frac{p_2}{p_B} \qquad\qquad (14.1a)$$

For constant pressure ratios p_B/p_2 and adiabatic exponents $\varkappa$, variation of p_1/p_2 yields different values for the term on the right side of equation No. 14.1; they must always be equal to the bearing characteristic Λ . Thus the following applies to the characteristic for the laminar radial clearance flow inwards and outwards:

$$\Lambda_L = \frac{\pi}{12}\left[\frac{h^3 p_2}{\mu F_0 \eta \sqrt{2gRT}}\right]\left\{\frac{1}{\ln\frac{r_{1a}}{r_{1a}}} + \frac{1}{\ln\frac{r_{1i}}{r_{2i}}}\right\} . \qquad (14.2)$$

It should be considered in this connection that the term of the square root in equation No. 14.1 for

$$\frac{p_1}{p_B} \geqq \left(\frac{2}{\varkappa+1}\right)^{\frac{\varkappa}{\varkappa-1}} \qquad (14.2a)$$

has the following limiting value on account of the critical outflow from the nozzles (velocity of sound):

$$\sqrt{\frac{\varkappa}{\varkappa-1}}\left(\frac{2}{\varkappa+1}\right)^{\frac{1}{\varkappa-1}} \qquad (14.2b)$$

Diagrams 17 and 18 show the Λ_L values as a function of the pressure ratios for $\varkappa = 1.4$ (air) and $\varkappa = 1.66$ (helium). It can be seen that the influence of $\varkappa$ is very slight.

The same characteristics apply, of course, also to bearings where the flow is only in one direction. The Λ_L values, modified accordingly, are, for the outward flow:

$$\Lambda_L = \frac{\pi h^3 p_2}{12\mu F_0 \eta \sqrt{2gRT}} \cdot \frac{1}{\ln\frac{r_{1a}}{r_{1a}}} \qquad (14.3)$$

and for inward flow, exclusively, in a bearing

$$\Lambda_L = \frac{\pi h^3 p_2}{12 \mu F_D \eta \sqrt{2gRT}} \cdot \frac{1}{\ln \frac{r_{1i}}{r_{2i}}} \quad . \quad (14.4)$$

B) **Turbulent.**

In a similar way as in the laminar flow, the amount of gas which enters through the throttle elements (cf. equation No. 12.2) is equated to the amount flowing through the bearing (cf. equations No. 9.13 and 9.14). Thus the dimension-less characteristics are obtained from:

$$\frac{\sqrt{4\pi^2 h^3}}{\mu F_D}\left[\frac{1}{\sqrt{\lambda_{Ta}\left(\frac{1}{r_{1a}} - \frac{1}{r_{2i}}\right)}} - \frac{1}{\sqrt{\lambda_{Ti}\left(\frac{1}{r_{2i}} - \frac{1}{r_{1i}}\right)}}\right] =$$

$$= \frac{p_B}{p_2}\sqrt{\frac{\frac{\varkappa}{\varkappa-1}\left[\left(\frac{p_1}{p_B}\frac{p_2}{p_B}\right)^{2/\varkappa} - \left(\frac{p_1}{p_2}\frac{p_2}{p_B}\right)^{\frac{\varkappa+1}{\varkappa}}\right]}{\left(\frac{p_1}{p_2}\right)^2 - 1}} \quad . \quad (14.5)$$

For the term

$$\sqrt{\frac{\varkappa}{\varkappa-1}\left[\left(\frac{p_1}{p_B}\right)^{\frac{2}{\varkappa}} - \left(\frac{p_1}{p_B}\right)^{\frac{\varkappa+1}{\varkappa}}\right]} \quad (14.5a)$$

the same limitation applies as in the case of laminar flow. The function of the different pressure ratios on the right side of equation No. 14.5 varies somewhat from the conditions at laminar flow. For $\varkappa$ = 1.4 and 1.66, the charactertics for several pressure ratios of the bearing gas, p_B/p_2, were represented in Diagrams 19 and 20. The following bearing characteristics result for the **bearing** with flow in both directions

$$\Lambda_T = \frac{\sqrt{4\pi^2 h^3}}{\mu F_D}\left[\frac{1}{\sqrt{\lambda_{Ta}\left(\frac{1}{r_{1a}} - \frac{1}{r_{2a}}\right)}} + \frac{1}{\sqrt{\lambda_{Ti}\left(\frac{1}{r_{2i}} - \frac{1}{r_{1i}}\right)}}\right], \quad (14.6)$$

for the bearing with outward flow only

$$\Lambda_T = \frac{\sqrt{4\pi^2 h^3}}{\mu F_D} \frac{1}{\sqrt{\lambda_{Ta}\left(\frac{1}{r_{1a}} - \frac{1}{r_{2a}}\right)}} \quad (14.7)$$

and for the bearing with inward flow only

$$\Lambda_T = \frac{\sqrt{4\pi^2 h^3}}{\mu F_D} \frac{1}{\sqrt{\lambda_{Ti}\left(\frac{1}{r_{2i}} - \frac{1}{r_{1i}}\right)}} \quad . \quad (14.8)$$

14.2 Parallel flow.

A) Laminar

The amount of throughput through a parallel clearance of constant height and the length 1 is, when the change of the state of gas is isothermal:

$$\dot{G} = \frac{h^3 b p_2^2 \left[\left(\frac{p_1}{p_2} \right)^2 - 1 \right]}{24 \eta RT L} \qquad (14.9)$$

If, therefore the equation No. 14.9 is equated to the equation No. 12.2, the dimensionless characteristics are after a transformation:
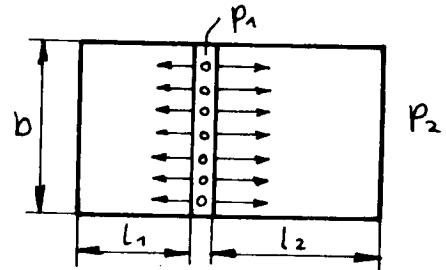
$$\frac{h^3 b p_2}{24 \mu F_D \eta \sqrt{2g RT} L} = \frac{p_B}{p_2} \frac{\sqrt{\frac{\varkappa}{\varkappa - 1} \left[\left(\frac{p_1}{p_2} \frac{p_2}{p_B} \right)^{\frac{2}{\varkappa}} - \left(\frac{p_1}{p_2} \frac{p_2}{p_B} \right)^{\frac{\varkappa+1}{\varkappa}} \right]}}{\left(\frac{p_1}{p_2} \right)^2 - 1} \qquad (14.10)$$

The right side corresponds again to the pressure function which has been derived in radial flow; The Diagrams 17 and 18 apply here, too. Thus the bearing characteristic for parallel flow in one direction is

$$\Lambda_L = \frac{h^3 b p_2}{24 \mu F_D \eta \sqrt{2g RT} L} \, , \qquad (14.11)$$

and, if it occurs in both directions

$$\Lambda_L = \frac{h^3 b p_2}{24 \mu F_D \eta \sqrt{2g RT}} \left(\frac{1}{L_1} + \frac{1}{L_2} \right) \qquad (14.12)$$

B. Turbulent

The amount of throughput for the compressible, isothermal flow throughh a parallel clearance is

$$\dot{G} = \sqrt{\frac{2g h^3 b^2}{\lambda_T RT L} (p_1^2 - p_2^2)} \, , \qquad (14.13)$$

Thus, by equating to equation No. 12.2, the characteristics represented in Diagrams 19 and 20 can be applied in an analogous way. The bearing characteristic for the parallel flow in one direction only is, therefore:

$$\Lambda_T = \frac{b}{\mu F_D} \sqrt{\frac{2gh^3}{RT \lambda_T L}} \qquad (14.14)$$

For the flow in two directions from a central channel, the characteristic is as follows:

$$\Lambda_T = \frac{b}{\mu F_D} \sqrt{\frac{2gh^3}{RT}} \left[\frac{1}{\sqrt{\lambda_{T_1} L_1}} + \frac{1}{\sqrt{\lambda_{T_2} L_L}} \right] . \qquad (14.15)$$

14.3 Potential flow.

The bearing characteristics calculated before for the laminar clearance flow apply also to a bearing equipped with nozzles which open directly into the clearance where the flow pattern is given by a potential function (cf. Chapter 13).

A) Annular shape

If the amounts of throughput through n nozzles (cf. equation No. 12.2) and through the bearing clearance (cf. equation No. 13.10) are equated, the consequence is:

$$-\frac{c_3 h^3 n}{24 \eta RT} \left[\int_0^{\frac{2\pi}{n}} \left(\frac{\partial \phi}{\partial r}\right)_{r_a} r\, d\varphi + \int_0^{\frac{2\pi}{n}} \left(\frac{\partial \phi}{\partial r}\right)_{r_i} r\, d\varphi \right] =$$

$$= \mu F_D p_B \sqrt{\frac{2g\varkappa}{(\varkappa-1)RT}\left[\left(\frac{p_1}{p_B}\right)^{2/\varkappa} - \left(\frac{p_1}{p_B}\right)^{\frac{\varkappa+1}{\varkappa}}\right]} \qquad (14,16)$$
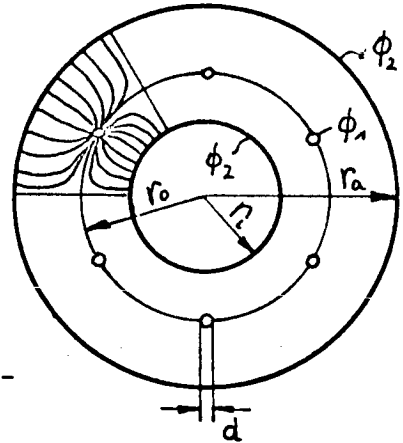
If equation No. 13.5 is also taken into consideration, the result for the characteristics is:

$$\frac{h^3 n\, p_2}{24 \eta \mu F_D \sqrt{2gRT}} \cdot \frac{\left[\int_0^{\frac{2\pi}{n}}\left(\frac{\partial \phi}{\partial r}\right)_{r_a} r\, d\varphi + \int_0^{\frac{2\pi}{n}}\left(\frac{\partial \phi}{\partial r}\right)_{r_i} r\, d\varphi\right]}{(\phi_1 - \phi_2)} =$$

$$= \frac{p_B}{p_2}\, \frac{\sqrt{\dfrac{\varkappa}{\varkappa-1}\left[\left(\dfrac{p_1}{p_2}\dfrac{p_2}{p_B}\right)^{2/\varkappa} - \left(\dfrac{p_1}{p_2}\dfrac{p_2}{p_B}\right)^{\frac{\varkappa+1}{\varkappa}}\right]}}{\left(\dfrac{p_1}{p_2}\right)^2 - 1} \qquad (14.17)$$

The bearing characteristic can also be written in abbreviated form:

$$\Lambda_L = \frac{h^3 n \, p_2}{24 \, \eta \, \mu \, F_D \sqrt{2gRT}} \, \varphi_\phi \qquad (14.18)$$

where φ_ϕ represents a value which depends on n, p_1/p_2 and r_a/r_i. In an experiment with n = 4, r_a/r_i = 2.4, d = 0.7 and μ = 0.78, for example, the following results were obtained:

$$p_1/p_2 \quad = \; 3, \qquad\qquad 8$$
$$\varphi_\phi \quad = 14,85 \qquad 9,96 \qquad (14.18a)$$

B) Rectangular shape.

The laminar isothermal flow through a clearance with an arrangement according to the drawing at the right, requires an amount of through-put of

$$\dot{G} = \frac{h^3 (p_1^2 - p_2^2)}{12 \, \eta \, RT} \frac{\int_0^b \left(\frac{\partial \phi}{\partial y}\right)_{\frac{L}{2}} dx}{(\phi_1 - \phi_2)} \qquad (14.19)$$

By equating this formula to equation No. 12.2, the bearing characteristic results as:
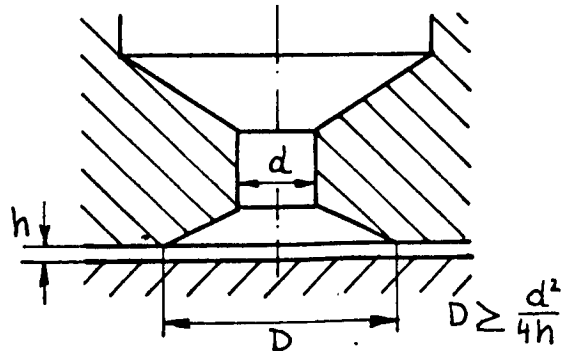
$$\Lambda_L = \frac{h^3 \, p_2}{12 \eta \, \mu \, F_D \sqrt{2gRT}} \frac{\int_0^b \left(\frac{\partial \phi}{\partial y}\right)_{\frac{L}{2}} dx}{(\phi_1 - \phi_2)} , $$
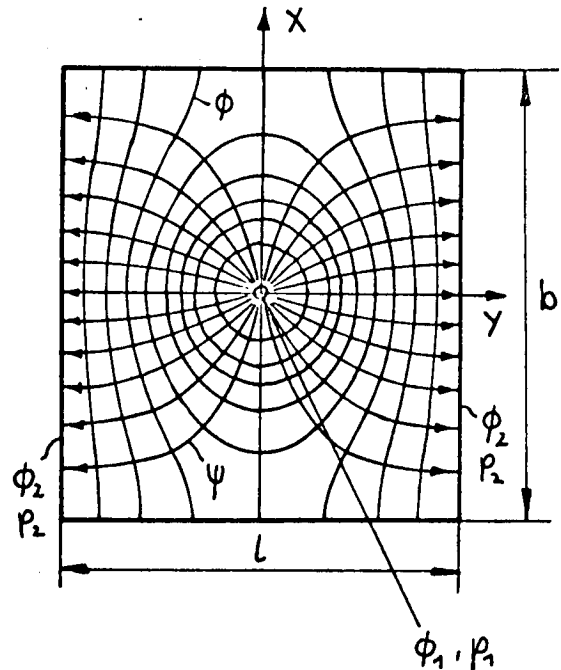
$$(14.20)$$

Its dependence on the pressure ratios is again shown in Diagrams 17 and 18. For the effective throttle area F_D the following applies both to annular (A) and rectangular (B) bearing surfaces but depending on the design of the nozzle:

$$D \geq \frac{d^2}{4h}$$
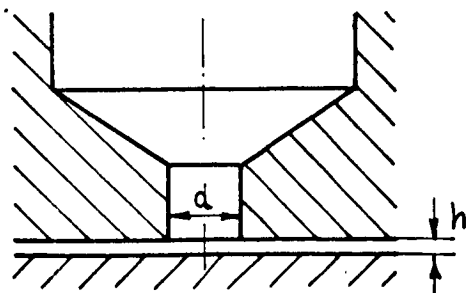
$$\boxed{F_D = d \pi h} \qquad\qquad \boxed{F_D = d^2 \frac{\pi}{4}} \qquad (14.20a)$$

Synopsis of the bearing characteristics
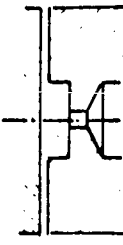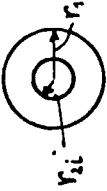
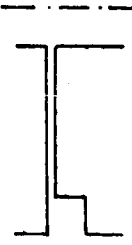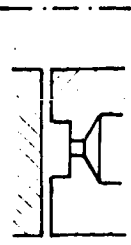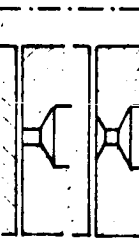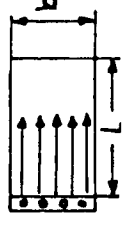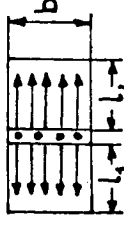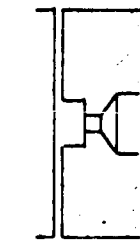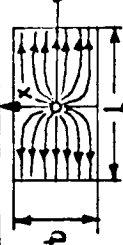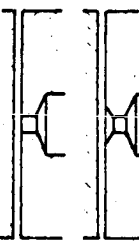| Type of flow	throttling area	type of feed	Λ_L (laminar)	Λ_T (turbulent)
r_{1a} — radial outwards	$F_D = n d^2 \dfrac{\pi}{4}$		$\dfrac{\pi h^3 p_2}{12\,\mu F_D\,\eta\sqrt{2gRT}} \cdot \ln \dfrac{r_{2a}}{r_{1a}}$	$\dfrac{2\pi\sqrt{h^3}}{\mu F_D\,\sqrt{\lambda_{Ta}}\sqrt{\left(\frac{1}{r_{1a}}-\frac{1}{r_{2a}}\right)}}$
r_{2i} — radial inwards	$F_D = 2 r_i \pi h$ oder $F_D = n d^2 \dfrac{\pi}{4}$		$\dfrac{\pi h^3 p_2}{12\,\mu F_D\,\eta\sqrt{2gRT}} \ln \dfrac{r_{2i}}{r_{1i}}$	$\dfrac{2\pi\sqrt{h^3}}{\mu F_D\,\sqrt{\lambda_{Ti}}\sqrt{\left(\frac{1}{r_{1i}}-\frac{1}{r_{2i}}\right)}}$
r_{1a}; r_{1a},r_{1i} — radial outwards and inwards	$F_D = n d^2 \dfrac{\pi}{4}$		$\dfrac{\pi h^3 p_2}{12\,\mu F_D\,\eta\sqrt{2gRT}} \left[\dfrac{1}{\ln \frac{r_{2a}}{r_{1a}}} + \dfrac{1}{\ln \frac{r_{2i}}{r_{1i}}} \right]$	$\dfrac{2\pi\sqrt{h^3}}{\mu F_D}\left[\dfrac{1}{\sqrt{\lambda_{Ta}\left(\frac{1}{r_{1a}}-\frac{1}{r_{2a}}\right)}} + \dfrac{1}{\sqrt{\lambda_{Ti}\left(\frac{1}{r_{1i}}-\frac{1}{r_{2i}}\right)}} \right]$
r_0; r_0 — potential flow	$F_D = n d \pi h$; $F_D = n d^2 \dfrac{\pi}{4}$		$\dfrac{n h^3 p_2 \left(\int_0^{2\pi/n}\left(\frac{\partial\phi}{\partial r}\right)_{r_a}\! r\,d\varphi + \int_0^{2\pi/n}\left(\frac{\partial\phi}{\partial r}\right)_{r_i}\! r\,d\varphi \right)}{24\,\eta\,\mu F_D\sqrt{2gRT}\,(\phi_1-\phi_2)}$	—
b, L — parallel flow	$F_D = b h$ oder $F_D = n d^2 \dfrac{\pi}{4}$		$\dfrac{h^3 b p_2}{24\,\mu F_D\,\eta\sqrt{2gRT}} \cdot L$	$\dfrac{b}{\mu F_D}\sqrt{\dfrac{2 g h^3}{\lambda_T RT L}}$
b, L_1, l_2, L — parallel flow	$F_D = n d^2 \dfrac{\pi}{4}$		$\dfrac{h^3 b p_2}{24\,\mu F_D\,\eta\sqrt{2gRT}} \left(\dfrac{1}{L_1} + \dfrac{1}{L_2} \right)$	$\dfrac{b}{\mu F_D}\sqrt{\dfrac{2 g h^3}{\lambda_T RT}}\left[\dfrac{1}{\sqrt{L_1}} + \dfrac{1}{\sqrt{L_2}} \right]$
y, x, b, L — potential flow	$F_D = d \pi h$; $F_D = d^2 \dfrac{\pi}{4}$		$\dfrac{h^3 p_2 \int_0^{b}\left(\frac{\partial\phi}{\partial y}\right)_{\frac{L}{2}} dx}{12\,\eta\,\mu F_D\sqrt{2gRT}\,(\phi_1-\phi_2)}$	—

Diagramm 17

Laminar clearance flow

$\varkappa = 1\cdot40$

$\dfrac{p_1}{p_B} > \left(\dfrac{p_1}{p_B}\right)_{krit.}$

$p_B/p_2 = 10$

8

6

4

$p_B/p_2 = 2$

$\dfrac{p_1}{p_2}$

Diagramm 18

Laminar clearance flow

Helium

$\varkappa = 1.66$

$\frac{p_1}{p_B} > \left(\frac{p_1}{p_B}\right)_{krit.}$

$\frac{p_B}{p_2} = 10$

8

6

4

$\frac{p_B}{p_2} = 2$

$\frac{p_1}{p_2}$

−121

Diagramm 19

Turbulent clearance flow

$\varkappa = 1{,}40$

$\frac{p_1}{p_B} > \left(\frac{p_1}{p_B}\right)_{krit.}$
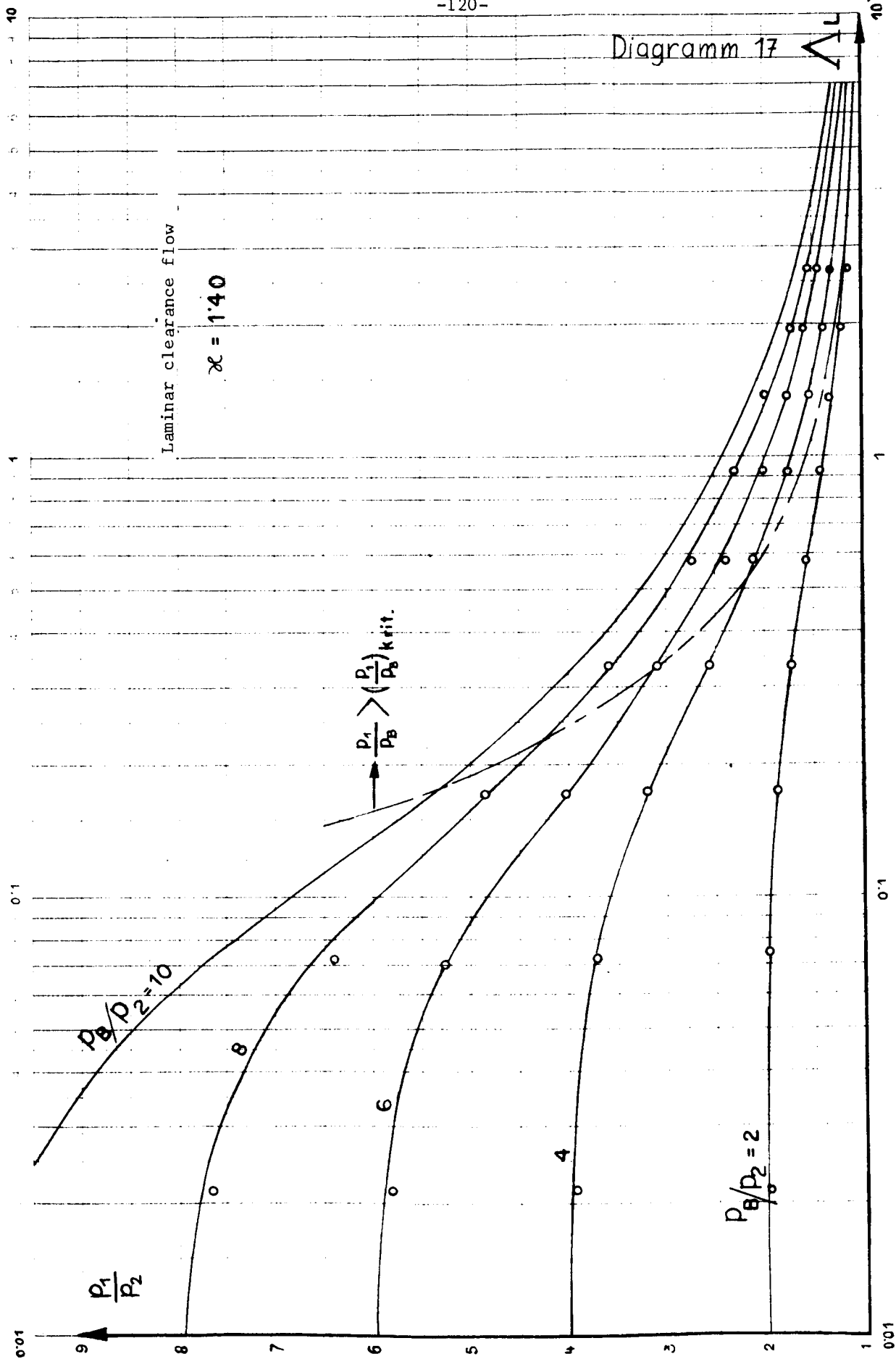
$\frac{p_B}{p_2} = 10$

8

6

4

$\frac{p_B}{p_2} = 2$

Λ_T

$\frac{p_1}{p_2}$
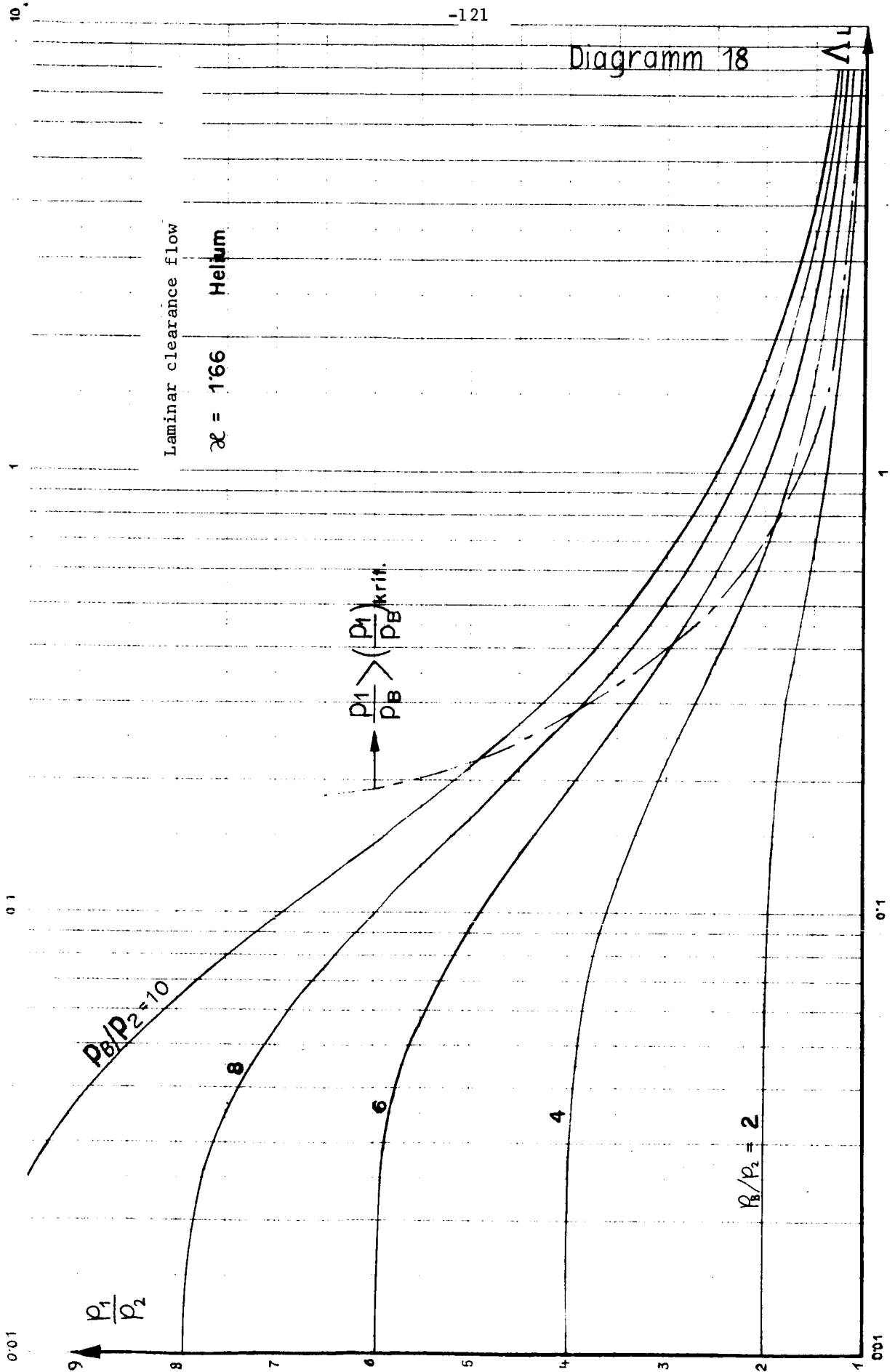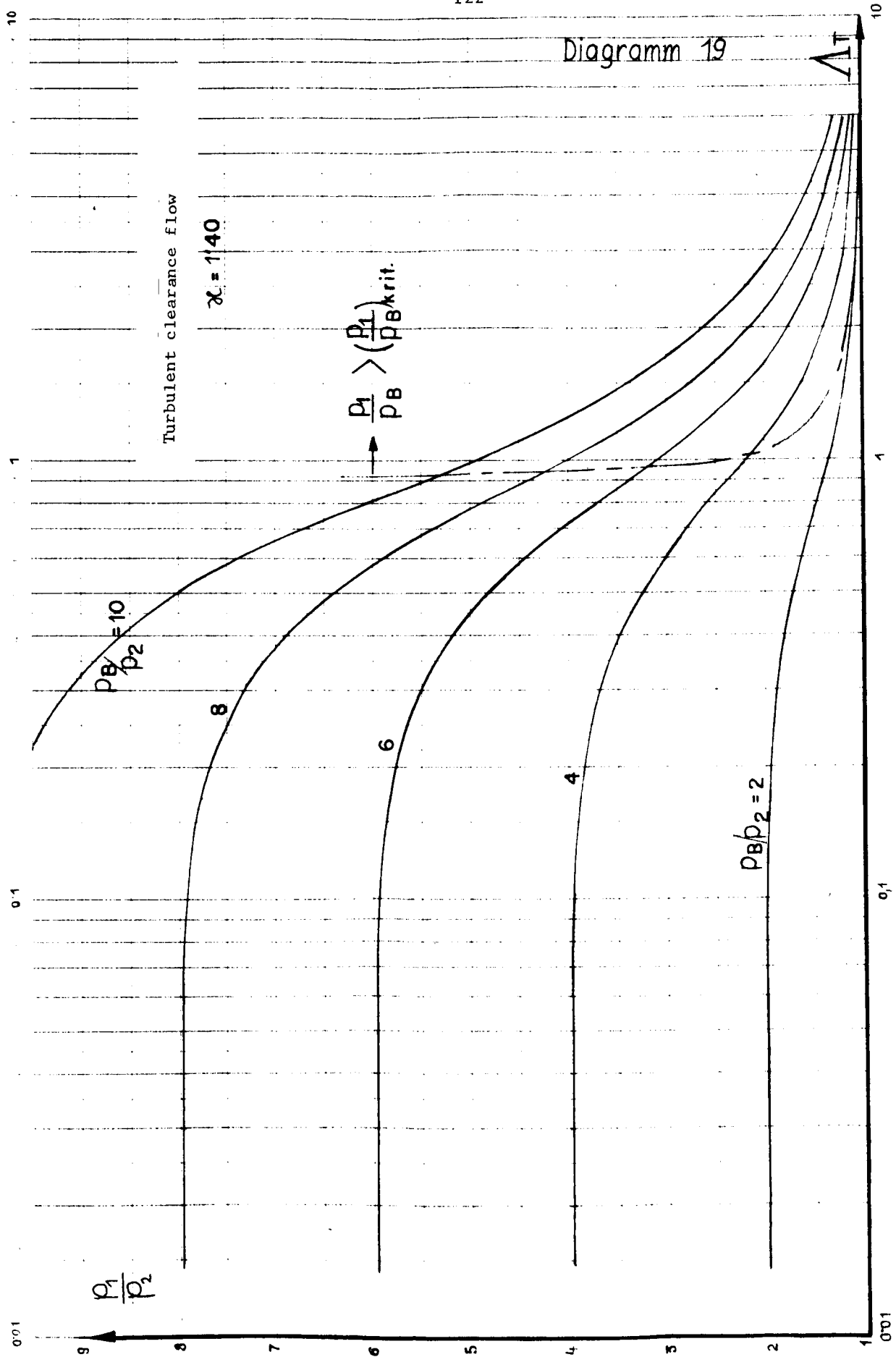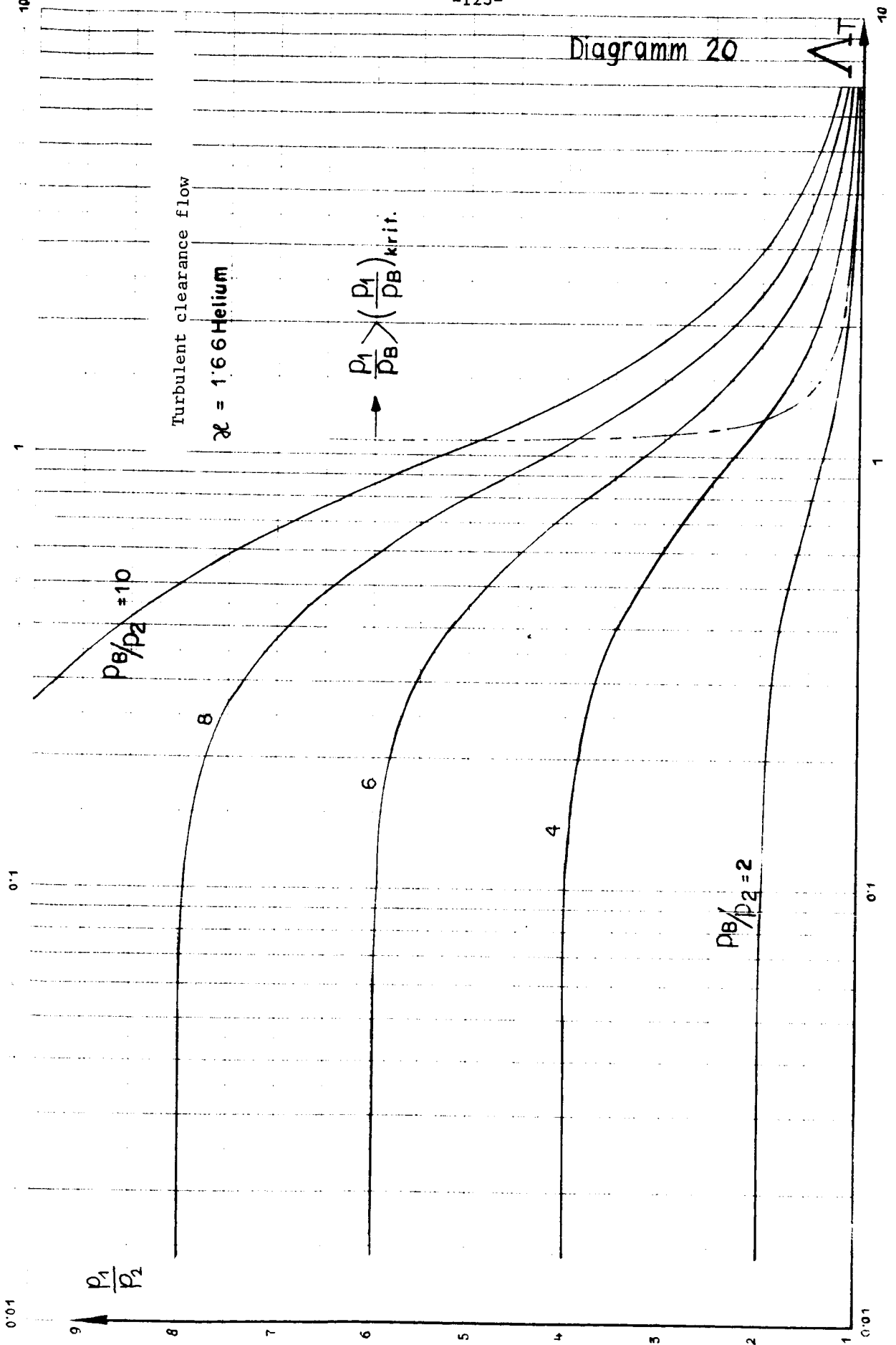
Diagramm 20

15. Results of the experiments.

All the experiments were performed in air at regular ambient tempera-ture. The required compressed air was tapped partly from the factory pipe system (7 atmospheres) and partly from a special valve testing station (40 at.) which was fed by a two-stage "Rotasko" compressor system. The air was puri-fied by a filter with layers of cotton, silica gel and activated carbon. At the outlet of the filter, a sintered porous steel plate was inserted in order to prevent the penetration of solid materials into the bearing.

15.1 Heating.

In the following, it will be shown in an experimental bearing how the average temperature of the fixed axial disc I changes from the initial value as a function of time and what the stationary final temperature of the disc will be if the removal of heat is taken into consideration. The experiments were performed with the gas bearing testing apparatus which is shown, as a section, on p. 137(cf. also Figs. 3 - 11). The double-acting thrust bearing was loaded by means of a pressurized air cushion on the front side of the right end of the shaft. On the left, carrying side of the thrust bearing, a clear-ance h_I which was large enough for operation was adjusted by the admission of the bearing air. On the right, load-free side II of the bearing no air was fed. In the initial stage (n = 0), the temperature of all parts of the bear-ing was equal to the temperature of the bearing gas at the inlet; it was kept constant during the experiment. At the start of the measurements, the rotation of the shaft was very quickly adjusted to the desired r.p.m. value which remained constant during the test. On account of the heat of friction in the carrying bearing clearance, the parts of the bearing underwent a slow heating.

Calculation model and assumptions:

Since the heat transfer in the clearance (cf. Chapter 6) is very good, it is assumed, at any time, the tempera-tures of the gas at the outlet from the bearing and those of the parts I and III are equal. The heat which is generated in the clearance h_I causes heating of the discs I and III and, besides, com-pensates the different losses of heat to the outside. Between the fixed disc I and the spacing ring K, several cali-brated shim-discs B (of 3 mm thickness) were inserted in order to increase the total free axial space and to reduce heat conduction between disc I and the casing. Since the ratio $h_{II}/h_I \cong$ 3000/20 = 150, the amount of heat generated in the clearance h_{II} by rotation is smaller by the same factor and can thus be disregarded.
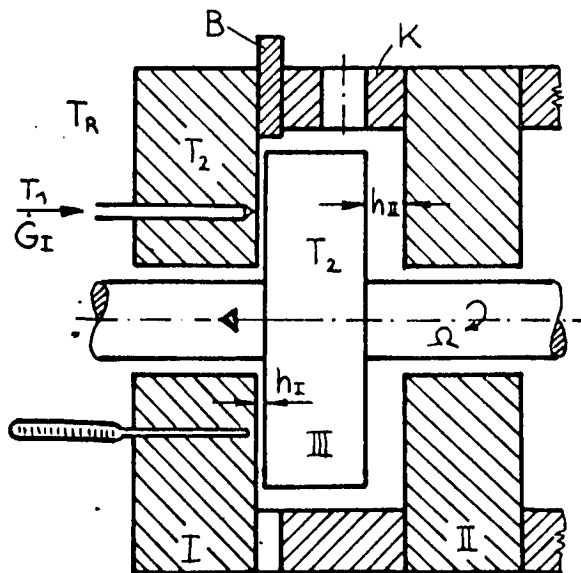
The meaning of the symbols used in the following is:

$\overset{'}{G} = \overset{\bullet}{G}_a + \overset{\bullet}{G}_i$ (kg/sec)   is the total amount of gas flowing through the bearing;

c_p (kcal/kg °C)   is the specific heat of the bearing gas;

$\overline{G}$ (kg)   is the weight of the discs I and III;

$\overline{c}_p$ (kcal/kg °C)   is the specific heat of the bearing discs;

t (sec)   is the time;

T_1 (° C)   is the temperature of the bearing gas at the inlet;

$T_2 = f(t)$ (° C)   is the temperature of the bearing gas at the outlet = temperature of the discs I and III;

$T_R = T_1$ (° C)   is the temperature in the surroundings of the test equipment;

T_2^x (° C)   is the stationary final temperature of the discs I and III;

η (kp sec/m^2)   is the dynamic viscosity of the gas;

R (m/° C)   is the gas constant;

h_I (m)   is the height of the clearance on the loaded side of the bearing;

Ω (1/sec)   is the angular velocity;

A (kcal/m kp)   is the energy equivalent;

r (m)   is the radius of the bearing;

δ (kcal/sec °C)   is the factor of the portion of heat removed by shaft and casing.

Heat balance

1) The heat generated in the clearance h_I by rotation can be determined from equation No. 6.8

$$dQ_{zvz} = \dot{G}\, dq_{zvz} = \pm \frac{2\pi \eta \Omega^2 A}{h_I} r^3 dr \; , \qquad (15.1)$$

(a, + : flow outwards   i, -: flow inwards)

Integration of this equation using the limits $r_{1a} - r_{2a}$ and $r_{2i} - r_{1i}$ gives: (NB. The bearing has a continuous ring channel; cf. Fig. 8)

$$Q_{zvz} = A\dot{G}_a \int_{r_{1a}}^{r_{2a}} dq_{zvz} + A\dot{G}_i \int_{r_{2i}}^{r_{1i}} dq_{zvz} = \frac{\pi \eta \Omega^2 A}{2 h_I}\left[r_{2a}^4 - r_{1a}^4 + r_{1i}^4 - r_{2i}^4 \right] \qquad (15.2)$$

2) The heat removed by heat conduction across shaft and casing, and by convection (ventilation, air currents) is almost proportional to $T_2 - T_1$;

on the other hand, the portion of heat removed by natural convection is proportional to $(T_2 - T_1)^{5/4}$. Since the exponent of the second item does not deviate very much from 1 and, besides, its value is low, it can be assumed that the total heat removed $\sum Q_v$ can be defined by the following term:

$$\sum Q_v \cong \delta (T_2 - T_1) \qquad (15.2a)$$

The factor δ represents a constant whose value depends on the cooling conditions in the bearing.

    3) The heat removal per second by the flow of the bearing as is:

$$Q_{\dot{G}} = \dot{G} c_p (T_2 - T_1) . \qquad (15.2b)$$

    4) A portion of the heat produced is accumulated in the bearing discs I and III.

$$Q_{sp} = \bar{G} \bar{c}_p \frac{dT_2}{dt} \qquad (15.2c)$$

Thus the heat balance can be derived from:

$$Q_{zu2} = \left[\dot{G} c_p + \delta \right](T_2 - T_1) + \bar{G} \bar{c}_p \frac{dT_2}{dt} . \qquad (15.3)$$

Written in another way, it is

$$\frac{dT_2}{b - a T_2} = dt , \qquad (15.4)$$

where a and b have the following meaning

$$a = \frac{\dot{G} c_p + \delta}{\bar{G} \bar{c}_p} \qquad \text{and} \qquad b = a T_1 + \frac{Q_{zu2}}{\bar{G} \bar{c}_p} \qquad (15.4a)$$

Integration of equation No. 15.4 yields the dependence of the bearing temperature T_2 on time

$$- \frac{1}{a} \ln(a T_2 - b) = t + C . \qquad (15.4b)$$

The integration constant C becomes, if the limiting conditions are t = 0, $T_2 = T_1$:

$$C = - \frac{1}{a} \ln(a T_1 - b) , \qquad (15.4c)$$

This gives, for the course of the temperature:

$$T_2 = T_1 + \frac{Q_{zu2}}{G c_p + \delta} \left(1 - e^{-at} \right). \qquad (15.5)$$

After a sufficiently long period of time ($t \rightarrow \infty$), the following applies:

$$0 \leftarrow e^{-at} \ll 1 \qquad (15.5a)$$

and the final temperature is:

$$T_2^x = T_1 + \frac{Q_{zu2}}{\dot{G}c_p + \delta} \qquad . \qquad (15.6)$$

The linear rise of temperature at the beginning of the measurement can be found from equation No. 15.4 assuming t = 0, δ = 0, $T_2 = T_1$.

$$\left(\frac{dT_2}{dt}\right)_{t=0} = \frac{Q_{zu2}}{\bar{G}\bar{c}_p} \qquad (15.7)$$

The measurements reported in the following are to show the order of magnitude of the heating and of the starting period in aerostatic thrust bearings. In the different series of experiments, only the r.p.m. were changed, while the other operating conditions, namely load capacity and amount of throughput remained constant. The dimensions and operating conditions of the experimental bearing were as follows:

r_{2i}	= 0,055	m	$\bar{G}$	=	69,75	kg
r_{4i}	= 0,087	m	$\bar{c}_p$	=	0,11	kcal/kg °C
r_{4a}	= 0,089	m	$\dot{G}$	=	$1,26.10^{-3}$	kg/sec
r_{2a}	= 0,133	m	c_p	=	0,24	kcal/kg °C
s	= 0,7	mm	R	=	29,3	m/°C
(Ringkanaltiefe s)			$T_1 = T_R$	=	17,0	°C
h_I	= 20.10^{-6}	m	η	=	$1,90.10^{-6}$	kp sec/m²
h_{II}	= 3.10^{-3}	m				

Ringkanaltiefe = depth of the annular channel.   (15.7a)

Diagram 21 shows the measured temperature of dics I. during the preheating period as a function of the r.p.m. The results of the partly measured and calculated values are: (t^x = length of starting period)

u/min = r.p.m.   -   gerechnet = calculated   -   gemessen = measured.

n	Q_{zu2}	$(dT_2/dt)_{t=0}$	T_2^x	δ	t^x Anlaufzeit	
u/min	gerechnet	gerechnet	gemessen	gerechnet	gemessen	
10 000	0,1149	0,898	41,2	0,04720	130	
12 300	0,1731	1,355	53,3	0,04745	140	(15.7b)
15 000	0,2560	2,000	67,4	0,05050	135	
	kcal/sec	°C/min	°C	kcal/s °C	min	

The measured temperature gradients at the beginning of the experimental series are in complete agreement with the calculated values. The factor δ was calculated from equation No. 15.6 by means of the measured final temperatures T_2^x. The measurements show that the starting period t^x is almost the same at different numbers of rotation. The equation No. 15.6 can be written in another way:

$$\underbrace{\frac{\delta(T_2^x - T_1)}{Q_{zu2}}}_{A} + \underbrace{\frac{\dot{G}c_p(T_2^x - T_1)}{Q_{zu2}}}_{B} = 1 \qquad (15.7c)$$

in order to illustrate the portions of heat which are removed, on the one
hand, by the bearing discs and, on the other hand, by the bearing gas itself.

n u/min $r.p.m.$	A %	B %	(15.7d)
10 000	93,64	6,37	
12 300	93,67	6,33	
15 000	93,06	5,95	

Summary: The experiments show that heating of aerostatic bearings must be
taken into consideration because the heat removed by the bearing gas, in con-
trast to fast running hydrostatic oil bearings, is only a small portion of
the amount of heat generated. The components of the bearing and of the adja-
cent casing must, therefore, be designed in such a way that satisfactory re-
moval of heat is possible.(if necessary fins or a cooling system should be
provided). On account of the relatively small heat of friction, preheating to
the thermally stationary state takes a very long time.

The problem of heating of the bearing becomes, however, less important
at a higher pressure level of the gas surrounding the bearing (e.g. in encased
machines or those operating under higher pressure). The amount of heat intro-
duced by bearing friction (cf. equation No. 15.2) depends only on the viscosity
of the gas when the dimensions of the bearing, the height of the clearance and
the r.p.m. remain constant. But since η is independent of the pressure level,
the amount of heat introduced is the same at low and high ambient pressure.
But the effect of the amount of bearing gas through $\dot{G}$ is quite different.
According to equations No. 7.19 and 7.20, $\dot{G}$ increased, at constant height of
the clearance, significantly with pressure p_1 and p_2, respectively, i.e. the
heat removed by the bearing gas

$$Q_{\dot{G}} = \dot{G}\, c_p\, \Delta T \qquad (15.7e)$$

increases with the pressure level while Q_{zu2} remains constant. From this it
can be concluded that the excess temperature of the bearing

$$\Delta T \sim \frac{\eta}{\dot{G}\, c_p} \qquad (15.7f)$$

is substantially lower at a higher pressure level than at normal surrounding
pressure.

15.2 Pressure patterns.

The pattern of the radial pressure was measured, with the shaft in
fixed position, in the thrust bearing of the testing setup (cf. Figs, 3 - 11
and the longitudinal section of the testing apparatus on p. 137). The fixed
bearing disc (cf. Fig. 8) was equipped with a circular annular groove into
which, in order to render the gas feed more uniform, 20 cylindrical inlet
nozzles of 0.7 mm hole diameter opened. On account of the high absolute
pressures, 7 mercury high-pressure differential manometers, which are illus-
trated in Fig. 5, were connected in series. Fig. 6 shows the connections of
the instrument leads from the fixed bearing disc. The measuring pressure taps
4 mm diameter which open into the carrying bearing clearance can be clearly

seen in Fig. 10. In order to avoid mutual interference of the pressure taps. their arrangement in the direction of the circumference was somewhat staggered. (cf. Fig. 8). In Diagram 22, the measuring results for different initial pressures p_1 at constant surrounding pressure p_2 are plotted for a height of the clearance h = 20 x 10^{-6}m. The fully drawn curve represents the theoretical course of pressure as it can be deduced from the approximation equations No. 7.14 and No. 7.18.

15.3 Bearing characteristics.

By means of the large gas bearing testing apparatus (Figs. 3- 11), the bearing characteristics Λ_L were measured for laminar air flow in the clearance as a function of p_1/p_2 and plotted in Diagram 17. A preliminary experiment was performed in order to determine of the nozzle outflow coefficient μ . From the amount of flow in critical flow, through the nozzles, μF_D could be obtained. In order to adhere to the desired dimensions of the clearance, several spacing foils of equal thickness were inserted into the carrying bearing clearance at equal distances; besides, the whole shaft or the movable bearing disc, respectively (cf. Fig. 7) was subjected to a strong pressure during the measurement by means of a heavy thrust which was produced by the application of a pressurized air cushion on the front side of the shaft (cf. the longitudianal section on p.137 , on the far right). The pressure p_1 could be determined very accurately - in a similar way as in the measurement of the distribution of pressure - by means of the differential monometers in series. As can be seen in Diagram 17, the concordance between calculation and experiment is rather good. No experiments were performed in the turbulent region of the flow.

15.4 Amount of throughput.

A) Bearing with annular compensating space

In an experimental bearing with the following dimensions

$$
\begin{array}{llll}
r_{2i} & = 0,055 \text{ m} & F_D & = 7,70 \cdot 10^{-6} \text{ m}^2 \quad (15.7g) \\
r_{1i} & = 0,087 \text{ m} & n & = 20 \\
r_{1a} & = 0,089 \text{ m} & s & = 0,70 \quad \text{mm} , \\
r_{2a} & = 0,133 \text{ m}
\end{array}
$$

where r is the radius of the bearing, F_D is the area of the nozzle, n is the number of nozzles and s is the depth of the annular compensating channel, the amount of throughput was measured for laminar air flow at a temperature of T = 291° K, a dynamic viscosity η = 1.85 x 10^{-6} kp sec/m^2 and an ambient pressure of p_2 = 1 x 10^4 kp/m^2 and compared with the values calculated according to equations No. 7.19 and 7.20. Diagram 23 shows the results of these experiments, i.e. the amount of throughput as a function of the height of the clearance. From the preliminary experiment, the average value of the nozzle outflow coefficient μ was found to be 0.78. The twenty cylindrical nozzles distributed on the circumference of the compensating channel have a total area of F_D = 7.70 x 10^{-6} m^2. For the comparative calculation, the
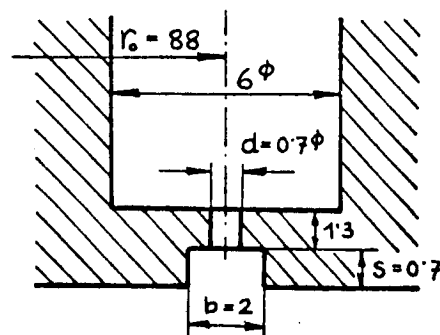
connection between h and p_1 was obtained by the bearing characteristics in Diagram 17 (p. 105). The result for the given values is:

$$\Lambda_L = 2.685 \times 10^{12} \times h^3.$$

Thus the calculation of $\dot{G}$ over h is most advantageously done the following way: h is chosen, Λ_L is calculated, the corresponding pressure ratio p_1/p_2 is determined from Diagram 17 and, finally, the amount of throughput $\dot{G}$ is calculated from equations No. 7.19 and 7.20.

The measurement of the volume of throughput was done by means of a DIN (=German Industry Standards) orifice of 6 or 9 mm, respectively, diameter which was inserted in a measuring section. The pressure difference of the orifice was indicated by the high-pressure differential manometer which is illustrated in Fig. 6 (left front).

B) Bearing without compensating space.

In a later design, the annular channel of the bearing described sub A) was filled with a hardening plastic, then the surface of the bearing was leveled again and the nozzles were bored again through the plastic layer. Thus the nozzles opened directly into the bearing clearance through the cylindrical borehole. As expected, the measurements showed that the amount of throughput (cf. Diagram 24) has now a considerably flatter slope with increasing bearing clearance. This fact can be traced back to the throttling effect between boundary of the nozzle and bearing clearance. A comparison of the two measurements A) (Diagram 23) and B) Diagram 24) shows that the maximum amount of throughput is larger in the second case. The reason for this is that, after filling the annular channel with plastic, the nozzles were drilled for a second time and thus got a somewhat larger diameter.
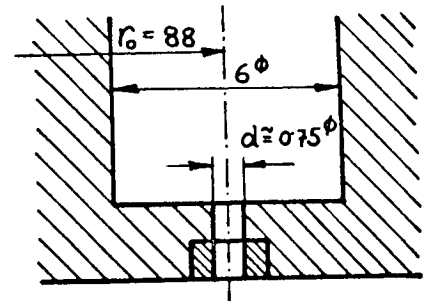
15.5 Load capacity.

A) Bearing with annular compensating space.

In Diagram 25, the effective load capacity of the bearing described in Chapter 15.4A is shown for the same gas states as a function of the height of the clearance. The calculated load capacity, which is represented in said Diagram as fully drawn line, is, as can be deduced from equations No. 10.6 and 10.7:

$$K_{ges} = p_1 \pi \left[r_{1a}^2 + r_{2a}^2 C_{Ka} + r_{1i}^2 (C_{Ki} - 1) \right] - p_2 \pi (r_{2a}^2 - r_{2i}^2), \quad (15.8)$$

where the area of the bearing is:

$$F_L = \pi (r_{2a}^2 - r_{2i}^2) = 461 \ cm^2 \quad (15.8a)$$

Diagramm 21

Diagramm 22

calculated according to equations 7.13 and 7.17.

Diagramm 23

$\dot{G}$ (gr/s)

$r_{2a} = 133$ mm
$r_{1a} = 89$ mm
$r_{1i} = 87$ mm
$r_{2i} = 55$ mm

$n = 20$
$d = 0.7$ mm
$b = 2$ mm
$t = 0.7$ mm

$\left(\dfrac{p_1}{p_5}\right) < 0.528$

$p_5/p_2 = 8$

6

4

Calculated according
to equation
No. 7.19 and 7.20.

2

h (μm)

10   20   30   40   50   60   70   80

Diagramm 24

Diagramm 25

r_{2a} = 133 mm n = 20
r_{1a} = 89 mm d = 0·7 mm
r_{1i} = 87 mm b = 2 mm
r_{2i} = 55 mm t = 0·7 mm

Calculated according to equations No. 10.6 and 10.7.

K_{ges} (kp)

p_8/p_1 = 8
6
4
2

h (µm)

Diagramm 26

$r_{2a} = 133$ mm
$r_{2i} = 55$ mm
$r_o = 88$ mm
$n = 20$
$d = 0.75$ mm

K_{ges} (kp)

h (µm)

$p_a/p_i = 8$
6
4
3
2

TESTING APPARATUS FOR GAS BEARINGS

Top: Flexible Suspension
Bottom: Fixed Support

For the mathematical determination of K_{ges} over h, one chooses advantageously again the height of the clearance h, whereby the corresponding pressure ratio p_1/p_2 for the given bearing gas pressure p_B is obtained by means of the bearing characteristic from Diagram 17. The two load capacity factors C_{ka} and C_{ki} can subsequently be determined by interpolation from the Diagrams 5 and 6 (p. 60 and 62). It can be seen in Diagram 25 that the measured points obtained are in every case lower than the calculated values. This deviation can probabl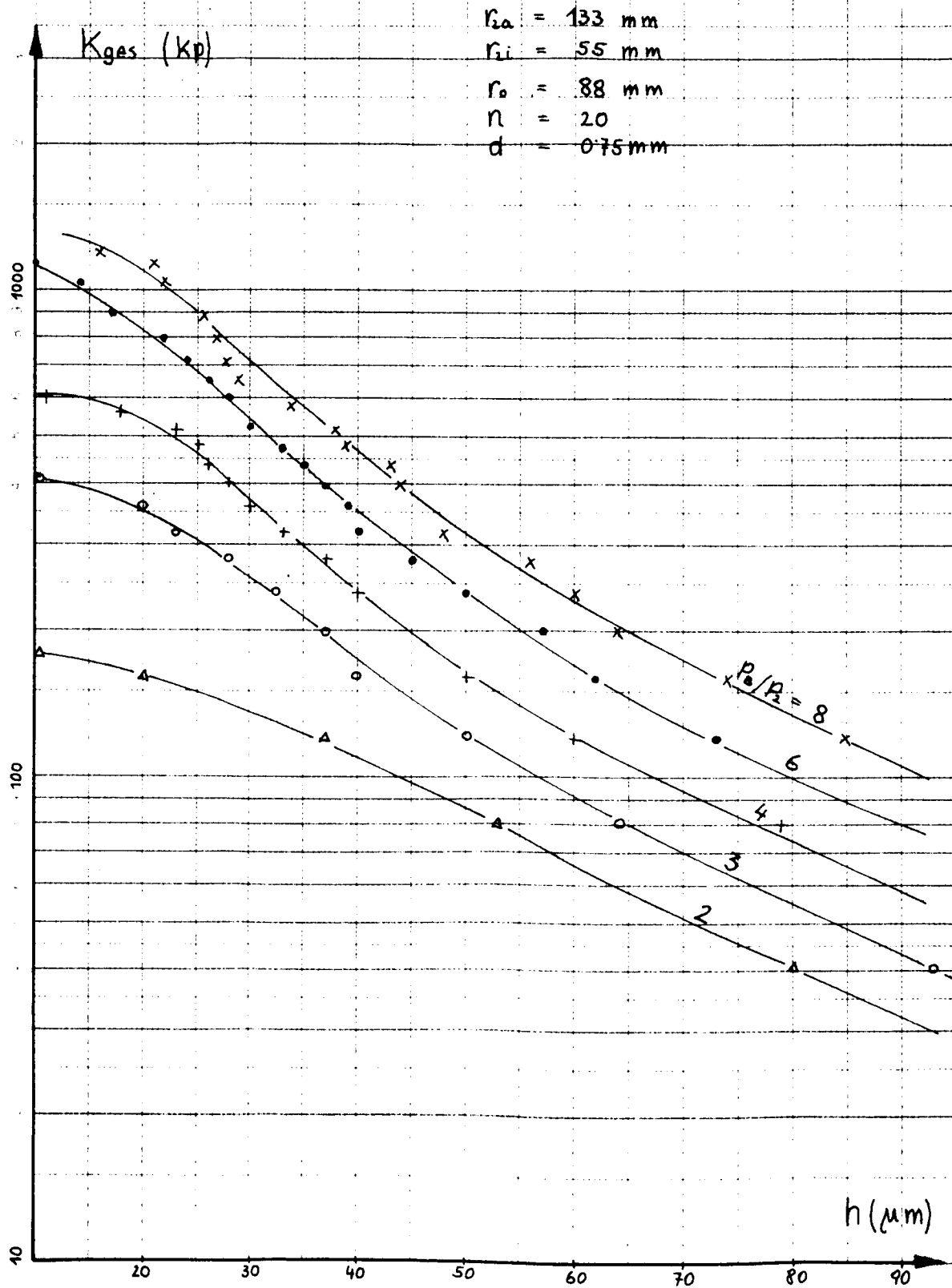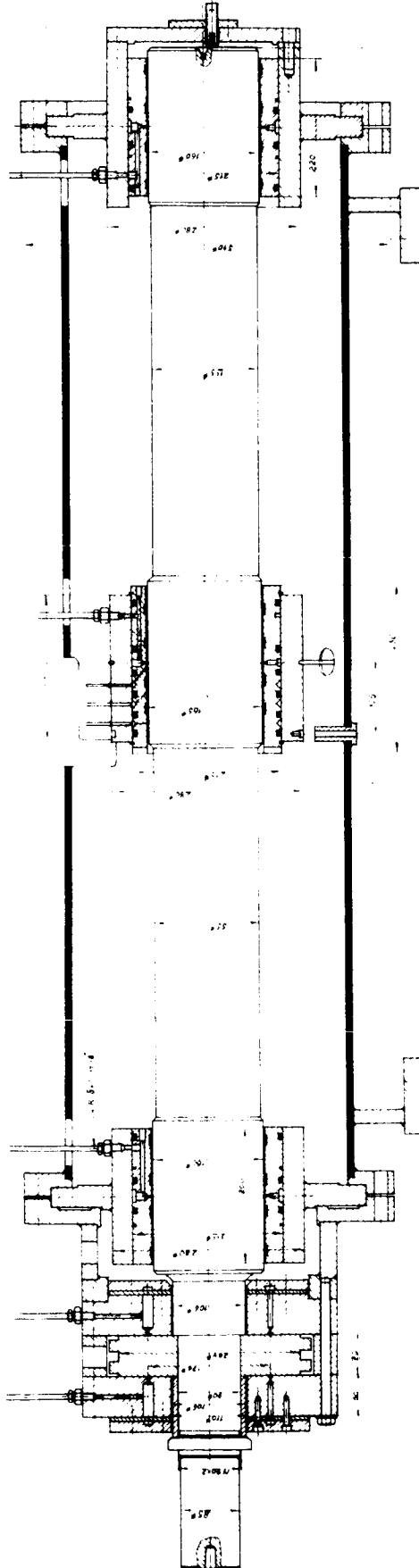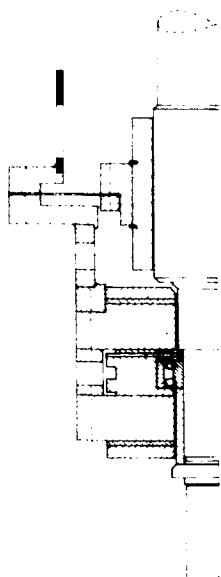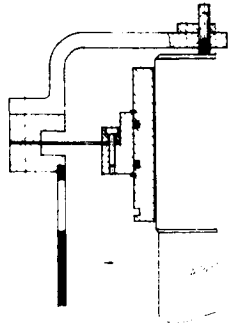y be traced back to insufficient precision of the manometer used for measuring the pressure acting upon the free end of the shaft.

B) Bearing without compensating space.

The measuring results for the load capacity of the changed bearing (cf. Chapter 15.4B) are plotted in Diagram 26 as a function of the height of the clearance. It can be seen, in this connection that K_{ges} is substantially smaller than in the bearing with annular channel. The load was again applied by means of a pressurized air cushion on the front side of the free end of the shaft.

15.6 Nozzles with a counterbore at the side of the clearance.

By means of the testing device which is illustrated in Figs. 1 and 2, a comparative measurement was made in one and the same bearing with different nozzle designs. In the first experiment, the four cylindrical nozzles opened directly into the bearing clearance, whereas, in the second experiment, they were slightly chamfered on the side of the clearance. Diagram 27 shows the load capacity K_{ges} and the amount of throughput $\dot{G}$ for both designs as a function of the height of the clearance h. By the counterbore on the side of the clearance and the enlargement of the effective throttling area connected therewith ($d \pi h \rightarrow d^2 \pi /4$) the load capacity characteristic was shifted into a region of larger widths of the clearance, the flow characteristic, on the other hand, into a region a smaller clearance widths. This design has the advantage that a bearing can be operated, at the same load, with a larger clearance and thus guarantees a safer operation. This improved load effect is, however, counterbalanced by an increased flow of bearing gas.

It could be shown in this experimental device, and also in other ones, that the counterbore on the side of the clearance (enlargement of the clearance volume) of the magnitude $D \geq \dfrac{d^2}{4 h}$ does not cause an unstable operation as far as self-induced vibrations are concerned.

15.7 Measurement of the axial shift in a machine.

The determination of the effective axial shift in a machine during operation can be performed in aerostatic axial bearings according to a very simple method. If, firstly, it is assumed that the feeding pressure p_B for the bearing gas remains constant and that the bearing discs do not perform any rotatory motion, there develops, in the presence of an axial shift in the bearing clearance, a pressure peak whose total value corresponds to the shift prevailing at that time over entire area of the bearing. Thus, the

greater the axial shift is, the greater
pressures must be present in the bearing
clearance. If a bore for pressure
measurement is made in the fixed bear-
ing disc at any place whatsoever (pre-
ferably in a region with high pres-
sure), exterior application of a
known pressure (either mechanically
e.g. by a stretching device and
spring balance, or pneumatically by
a pressurized air cushion) allows
to measure the corresponding refer-
ence pressure p_R and to plot it in
the form of a calibration curve as a
function of this axial shift K_{ges}:
It is immaterial, in this connection,
whether the bearing disc has a con-
tinuous annular channel for gas con-
pensation on the side of the clearance
or only individual nozzles which open
directly into the clearance. This
method can also be applied in double-
acting bearings (cf.the testing device
on p. 137) where the carrying side is
influenced by the non-carrying side.
The only precaution to be taken is
that the calibration curve be drawn
under the same conditions (equal bear-
ing gas pressure also on the non-
carrying side of the bearing) as they
will occur later during operation.
If the calibration curve is drawn for
a bearing, the axial shift produced by the machine can now be determined, con-
versely, by measurement of the reference pressure p_R.
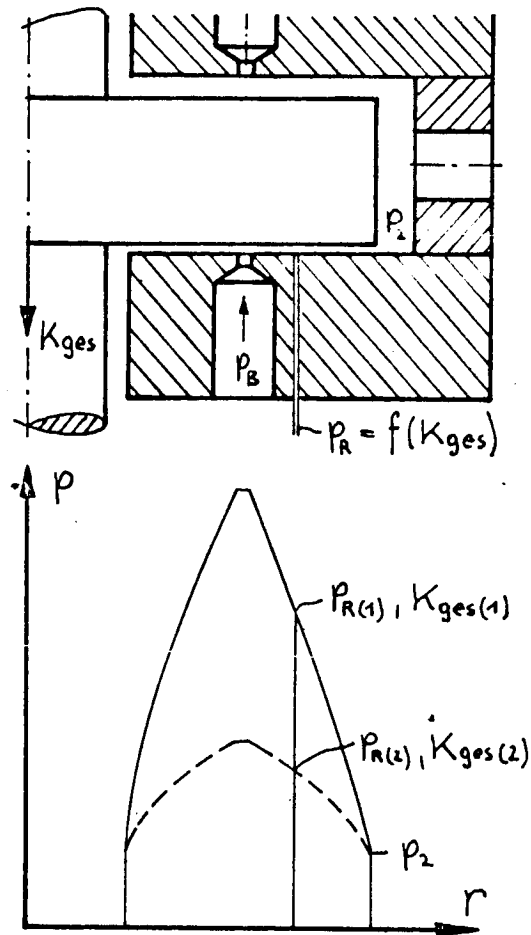
In practical cases, however,
the presumptions described above are
not satisfied. The bearing gas pres-
sure p_B fluctuates always in a higher
or lesser degree, while the components
of the bearing perform a motion relative
to one another. As can be seen, however,
in Chapters 8.1 and 8.2, the influence
of the kinetic energy of the gas flowing
in the clearance - this energy being sub-
ject to changes on account of pressure
fluctuations - and the influence of the
rotation of the disc are very slight and can be disregarded, especially for
small pressure levels (p_2 = 1 atmosphere). At increasing pressure p_B and
constant axial shift only the volume of flow and the bearing clearance
are enlarged, whereas the pressure peak and the reference pressure must remain
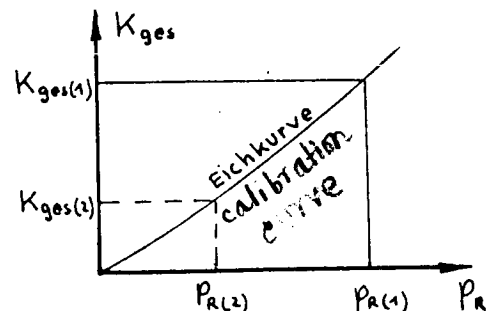
the same, corresponding to the shift. The influence of rotation becomes only noticeable at a high pressure level p_2; it can, however, be expressed arithmetically and corrected in the calibration curve. By means of this reference pressure measurement, an inclined position which might occur in the rotating bearing disc can be detected (fluctuation of p_R at slow rotation of the shaft) and can be corrected.
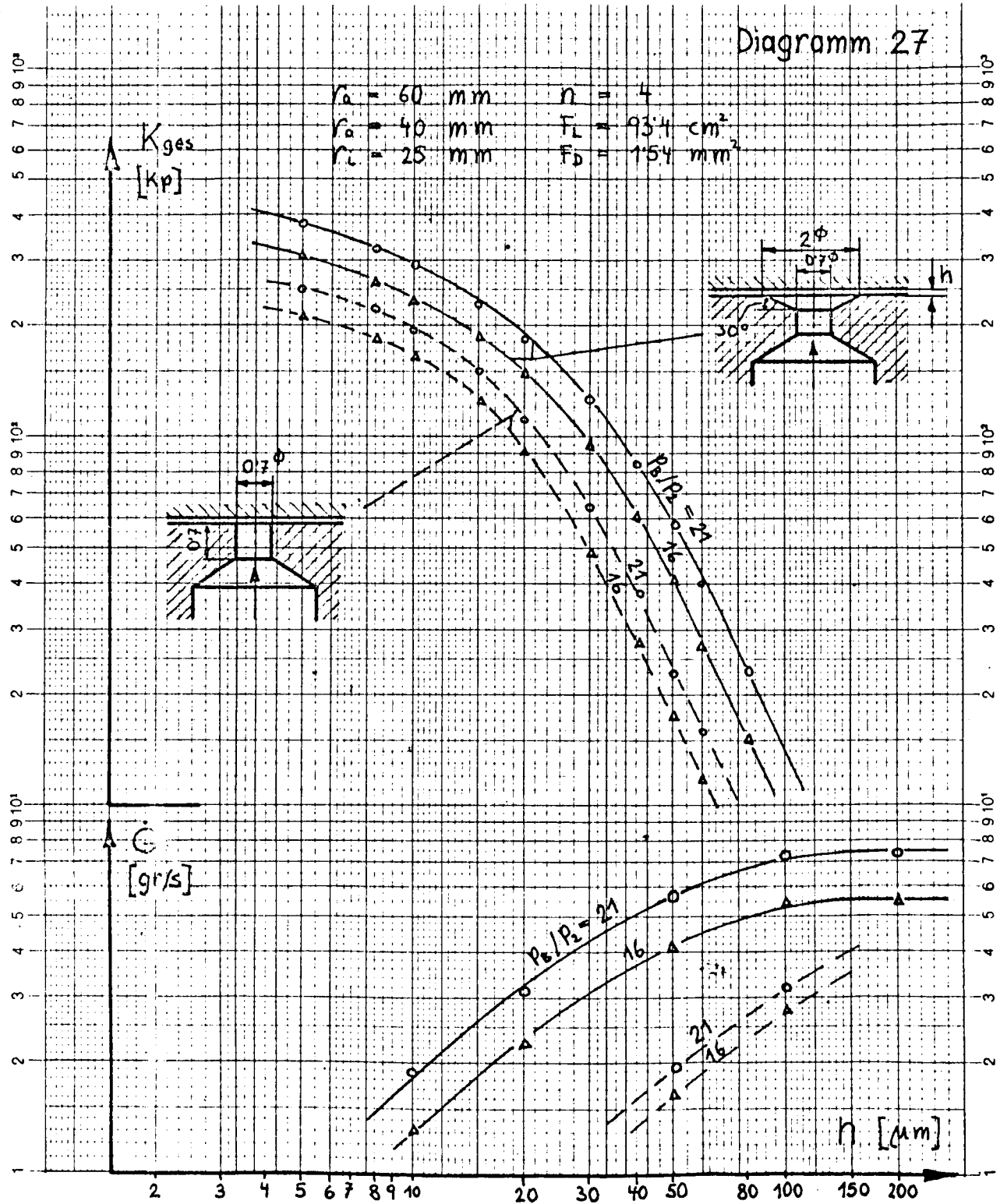

Diagramm 27

Diagram 28 shows the calibration curve for axial shift measurement in the four-stage radial compressor "Zurich 52" which is illustrated in Fig. 12. The borehole for reference pressure measurement is located between two of the eight nozzles which open directly into the clearance. The pressure p_B of the bearing air introduced fluctuated during the measurement between 7.2 and 7.8 at. The load was applied to the resting shaft by means of a cable line and was measured with a spring balance. The pressure p_R was determined with a tube spring manometer. In Diagram 29, the axial shift which had been determined with the aid of the calibration curve (Diagram 28) and the measured pressure p_R, is plotted as it occurs in actual operation at different r.p.m.

16. Self-excited vibrations.

A self-excited vibration is defined as a free vibration with negative damping. Every vibration with negative damping is dynamically unstable, i.e. the amplitude become larger with time. The changing force which maintains the vibration is generated by the mutual movement of the bearing components themselves and is controlled by them.

In aerostatic bearings, self-induced vibrations occur especially in those cases where additional spaces are provided in one of the bearing discs on the side of the clearance, in back of the throttling elements. The installation of compensating channels or pockets serves mainly for the improvement of the gas distribution in the clearance and affords thus a considerable increase of the load capacity compared to a bearing with punctiform gas feed. This instability causes an undersirable very noisy vibration of the movable bearing disc and of the adjoining free masses (rotor).
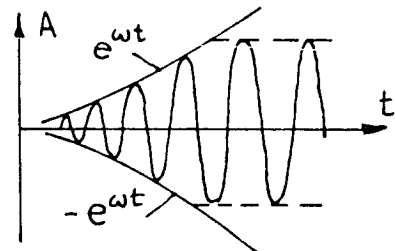
The reason for the appearance of such a vibration can be traced back to the discontinuity between the amount of gas which flows into the compensating space through the feeding elements and that which escapes from the bearing through the clearance, and also to the fact that the compensating volume can be accumulated on account of the compressibility of the gas. From this fluctuation of quantity, a corresponding pressure fluctuation results which is decisive for the exciting force.

In the bibliography listed in p. 8, a linear differential equation of third degree is shown which relates to the height h of the clearance as a function of time. This vibration equation was derived from the change of the amount of gas in the bearing with time.

16.1 Equation of vibration.

In the following, the equation of vibration is established first in a similar way as in paper (XVII), but for the case of a thrust bearing which consists of annular supporting surfaces and with consideration of the actual conditions relative to pressure distribution and amount of flow. In this connection, it is assumed that the vibration of the bearing interferes with the characteristic parameters to a small extent only. Besides, the simplified equations for the clearance flow are used which were determined with the assumptions: $w \cdot dw = 0$, $\Omega = 0$, $T = $ const. In order to simplify the calculation, the

temperature T_B of the entering gas is equated to the temperature of the carrying gas flowing in the bearing clearance. The symbols used have the following meaning:

p_B	bearing gas pressure in front of the feeding nozzles (absolute)
p	static pressure in the bearing clearance (absolute)
p_1	pressure in the compensating space (absolute)
p_2	ambient pressure (absolute)
h	bearing clearance
m	vibrating mass
$\dot{G}_{aus}$	weight of gas escaping from the bearing through the clearance per second
$\dot{G}_{ein}$	weight of gas entering the bearing through the feeding elements per second
G_L	total weight of gas in the bearing
T_B	temperature of the entering gas = temperature of the gas during clearance flow
r	radius of the bearing
F_D	effective throttling area of all feeding nozzles
s	depth of the annular compensating space
b	width of the annular compensating space
V_A	volume of the compensating space
Δ	sign for a small deviation from the equilibrium position
$-$	terms containing this crossbar denote the state in equilibrium position

----

The following drawing shows the arrangement of the bearing and the course of pressure in the radial clearance as basis for the determination of the self-induced vibrations. The inclusion of the resonator chambers described below, which are connected to the compensation channel, in the vibration equation would be necessary for the exact study, but is too complicated for an analytical treatment. The calculations are, therefore, limited initially to the determination of the properties of a bearing (influences of the different parameters on the stability, frequency of the bearing vibration) without any precautions for removing the vibrations.

In formulating the basic equations, it is assumed that the pressure at the start of the clearance flow (i.e. at r_{la} and r_{li}) is equal to the pressure
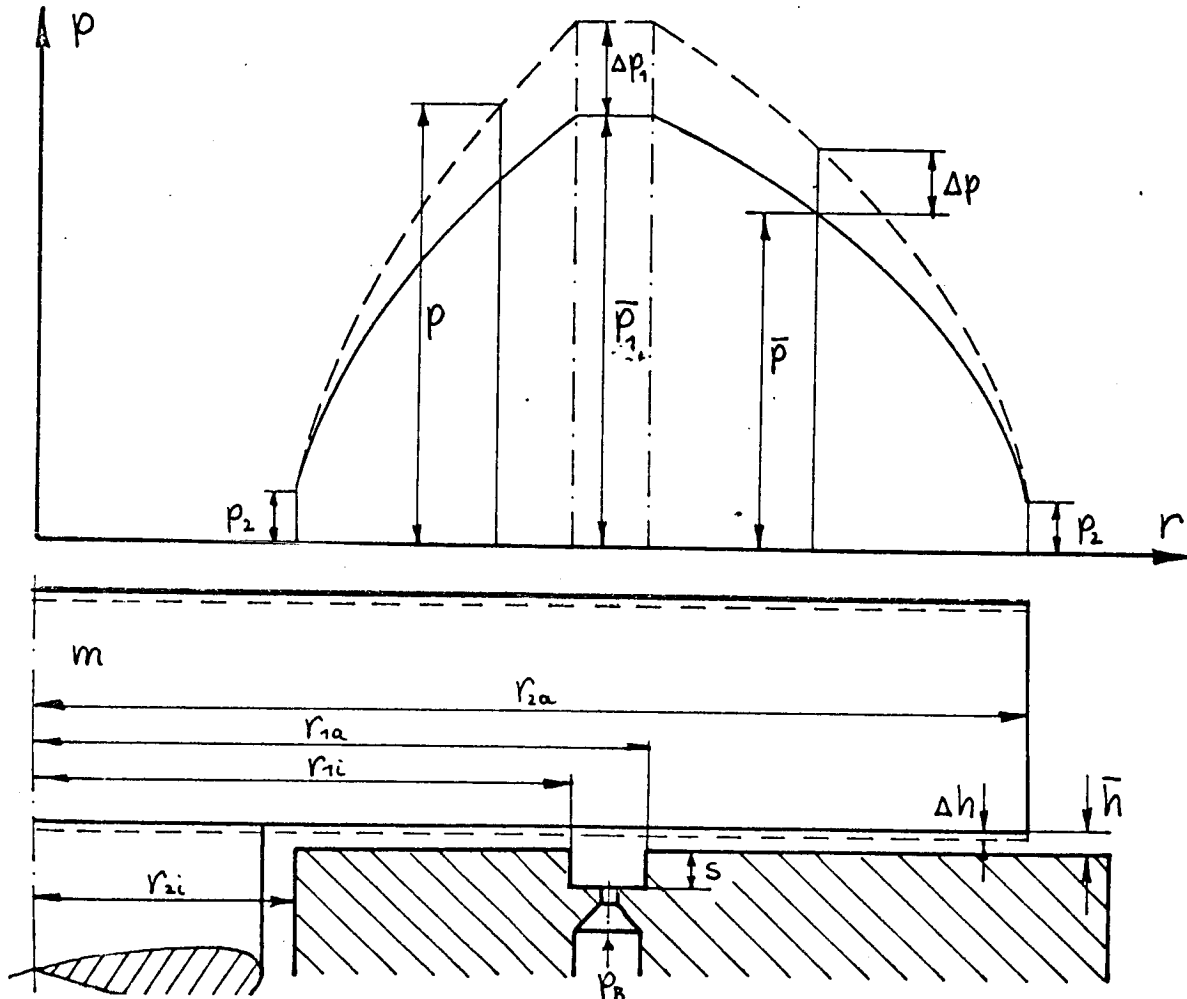
in the compensating space. Furthermore, the differentials are replaced by finite differences on account of the small changes of the magnitudes p_1, G_{ein}, G_{aus} and h during the vibration. Thus we obtain the following:

$$P_1(t) = \overline{P_1} + \Delta P_1(t) \qquad \dot{G}_{ein}(t) = \overline{\dot{G}}_{ein} + \Delta \dot{G}_{ein}(t)$$

$$p(r,t) = \overline{p}(r) + \Delta p(r,t) \qquad \dot{G}_{aus}(t) = \overline{\dot{G}}_{aus} + \Delta \dot{G}_{aus}(t) \qquad (16.0a)$$

$$h(t) = \overline{h} + \Delta h(t) \qquad \overline{\dot{G}}_{ein} = \overline{\dot{G}}_{aus}.$$

The first basic equation is a consequence of the fact that the difference between the amount of gas flowing in and out per unit of time must be equal to the change of the weight of the gas in the whole bearing with time.

$$\Delta \dot{G}_{ein}(t) - \Delta \dot{G}_{aus}(t) = \frac{dG_L}{dt} \qquad (16.1)$$

In the case of short cylindrical feeding nozzles or orifices, the amount entering, at constant pressure p_B, depends only on $p_1(t)$ and is, according to equation No. 12.2:

$$\dot{G}_{ein}(t) = \mu\, F_D\, p_B \sqrt{\frac{2g\varkappa}{(\varkappa-1)RT_B}} \sqrt{\left(\frac{p_1(t)}{p_B}\right)^{2/\varkappa} - \left(\frac{p_1(t)}{p_B}\right)^{\frac{\varkappa+1}{\varkappa}}} \;, \qquad (16.2)$$

From this the following can be derived:

$$\Delta\dot{G}_{ein}(t) = \left(\overline{\frac{\partial\dot{G}_{ein}}{\partial p_1}}\right)\Delta p_1(t) = \alpha\cdot\Delta p_1(t) \qquad (16.3)$$

and the time-independent constant is:

$$\left(\overline{\frac{\partial\dot{G}_{ein}}{\partial p_1}}\right) = \alpha = \frac{\mu\, F_D}{2\varkappa}\sqrt{\frac{2g\varkappa}{(\varkappa-1)RT_B}}\; \frac{2\left(\frac{\bar{p}_1}{p_B}\right)^{\frac{2-\varkappa}{\varkappa}} - (\varkappa+1)\left(\frac{\bar{p}_1}{p_B}\right)^{\frac{1}{\varkappa}}}{\sqrt{\left(\frac{\bar{p}_1}{p_B}\right)^{2/\varkappa} - \left(\frac{\bar{p}_1}{p_B}\right)^{\frac{\varkappa+1}{\varkappa}}}} \qquad (16.4)$$

The amount of gas excaping from the bearing through the clearance depends, however, on the pressure $p_1(t)$ and the height of the clearance $h(t)$. For isothermal laminar radial flow, $\dot{G}_{aus}$ can be determined by means of the equations No. 7.19 and 7.20:

$$\dot{G}_{aus}(t) = \dot{G}_a + \dot{G}_i = \frac{\pi h^3(t)\left(p_1^2(t)-p_2^2\right)}{12\,\eta\,RT_B}\left[\frac{1}{\ln\frac{r_{1a}}{r_{1a}}} + \frac{1}{\ln\frac{r_{1i}}{r_{2i}}}\right] . \qquad (16.5)$$

Thus a small difference $\Delta\dot{G}_{aus}$ becomes:

$$\Delta\dot{G}_{aus}(t) = \left(\overline{\frac{\partial\dot{G}_{aus}}{\partial h}}\right)\Delta h(t) + \left(\overline{\frac{\partial\dot{G}_{aus}}{\partial p_1}}\right)\Delta p_1(t) \qquad (16.6)$$

or

$$\Delta\dot{G}_{aus}(t) = \beta\cdot\Delta h(t) + \gamma\cdot\Delta p_1(t) , \qquad (16.7)$$

where the constants have the following meaning:

$$\beta = \frac{\pi\bar{h}^2\left(\bar{p}_1^2 - p_2^2\right)}{4\,\eta\,RT_B}\left[\frac{1}{\ln\frac{r_{1a}}{r.}} + \frac{1}{\ln\frac{r_{1i}}{r.}}\right] \qquad (16.8)$$

$$\gamma = \frac{\pi\bar{h}^3\bar{p}_1}{6\,\eta\,RT_B}\left[\frac{1}{\ln\frac{r_{1a}}{r_{1a}}} + \frac{1}{\ln\frac{r_{1i}}{r_{2i}}}\right] \qquad (16.9)$$

The amount of gas between the two bearing discs results from:

$$G_L = \frac{2\pi h(t)}{RT_B}\left[\int_{r_{1a}}^{r_{1a}} p\cdot r\cdot dr + \int_{r_{1i}}^{r_{1i}} p\cdot r\cdot dr + \frac{r_{1a}^2 - r_{1i}^2}{2}\left(1 + \frac{s}{h(t)}\right)p_1(t)\right]. \qquad (16.10)$$

If the equations No. 7.13 and 7.17 which apply to laminar isothermal clearance flow are introduced for the course of pressure, the integrals give the following solutions according to Chapter 10.1:

$$\int_{r_{ia}}^{r_{1a}} p \cdot r \, dr = \frac{C_{ka}}{2} r_{1a}^2 \, p_1(t) = \xi_1 \cdot p_1(t) \qquad (16.10a)$$

$$\int_{r_{1i}}^{r_{1i}} p \cdot r \, dr = \frac{C_{ki}}{2} r_{1i}^2 \, p_1(t) = \xi_2 \cdot p_1(t)$$

Besides, the following applies:

$$\xi_3 = \frac{r_{1a}^2 - r_{1i}^2}{2} \quad . \qquad (16.10b)$$

Since the factors C_{ka} and C_{ki} which depend on the ratios of pressure and radii do not vary too much for small pressure fluctuations (cf. Diagrams 5 and 6) the values ξ_1 and ξ_2 which can be obtained from the equilibrium data, were assumed to be independent of the fluctuations with time. The compilation of the constants gives:

$$\xi = \frac{2\pi}{R \, T_B} \left(\xi_1 + \xi_2 + \xi_3 \right) = \frac{C \, F_L}{R \, T_B} \quad , \qquad (16.10c)$$

where C is a load capacity factor referred to the whole bearing. Thus equation No. 16.10 can be written in a simpler way:

$$G_L = \xi \cdot h(t) \cdot p_1(t) + \vartheta \cdot p_1(t) = \xi (\overline{h} + \Delta h)(\overline{p_1} + \Delta p_1) + \vartheta (\overline{p_1} + \Delta p_1) , \quad (16.11)$$

where ϑ has the following meaning:

$$\vartheta = \frac{\pi s (r_{1a}^2 - r_{1i}^2)}{R \, T_B} = \frac{V_A}{R \, T_B} \qquad (16.11a)$$

According to equation No. 16.11, the amount of gas in the bearing depends both on the pressure and on the height of the clearance. The differentiation with respect to the time t gives: (NB. In the following all terms marked with a period sign on top mean differentiation with respect to time).

$$\frac{d G_L}{d t} = \left(\overline{\frac{\partial G_L}{\partial p_1}} \right) \Delta \dot{p_1} + \left(\overline{\frac{\partial G_L}{\partial h}} \right) \Delta \dot{h} = \delta \, \Delta \dot{p_1} + \varepsilon \, \Delta \dot{h} \quad . \qquad (16.12)$$

where the coefficients are:

$$\delta = \xi \cdot \overline{h} + \vartheta \quad \text{and} \quad \varepsilon = \xi \cdot \overline{p_1} \quad . \qquad (16.12a)$$

If the individual equations derived, No. 16.3, No. 16.7 and No. 16.12, are introduced into equation No. 16.1, it follows that:

$$(\alpha - \gamma) \Delta p_1(t) - \beta \, \Delta h(t) = \delta \, \Delta \dot{p_1}(t) + \varepsilon \, \Delta \dot{h}(t) \quad . \qquad (16.13)$$

For the calculation of the height of the clearance h as function of the time t, another equation is required whereby the pressure in equation No. 16.13 can be eliminated.

The equilibrium of forces between acceleration of the mass (free bearing components and shaft) and the spring action of the bearing can be expressed, without outside damping or friction, by the following equation:

$$m \cdot \Delta \ddot{h}(t) = 2\pi \int_{r_{2i}}^{r_{2a}} (p(t) - \bar{p}) r \, dr = 2\pi \int_{r_{2i}}^{r_{2a}} \Delta p(t) \, r \, dr \qquad (16.14)$$

Considering the data given above, the following can be concluded:

$$m \, \Delta \ddot{h}(t) = 2\pi (\zeta_1 + \zeta_2 + \zeta_3) \, \Delta p_1(t) \qquad (16.14a)$$

which can also be written in another way:

$$\Delta p_1 = \frac{m}{2\pi(\zeta_1 + \zeta_2 + \zeta_3)} \Delta \ddot{h} \quad . \qquad (16.15)$$

The desired vibration equation is obtained by introduction of this equation into equation No. 16.13

$$\Delta \dddot{h} + a \cdot \Delta \ddot{h} + b \cdot \Delta \dot{h} + c \cdot \Delta h = 0 \quad . \qquad (16.16)$$

where a, b, and c have the following meaning:

$$a = \frac{\gamma - \alpha}{\delta}$$

$$b = \frac{2\pi(\zeta_1 + \zeta_2 + \zeta_3)\varepsilon}{m\delta} = \frac{CF_L\varepsilon}{m\delta} \qquad (16.16a)$$

$$c = \frac{2\pi(\zeta_1 + \zeta_2 + \zeta_3)\beta}{m\delta} = \frac{CF_L\beta}{m\delta}$$

16.2 Influences on the stability.

The stability criterion for the vibration equation of third degree, given by Routh (cf. reference XXVI) is based on the condition of positive damping. The bearing drawn diagrammatically on p. 143 is stable, as far as self-excited vibrations are concerned, if the following applies:

$$a \cdot b > c \qquad (16.17)$$

A) Feeding nozzles.

In order to get a high value for "a", α must be as small as possible. But since α can only assume negative values between 0 and $-\infty$, the requirement stated above is satisfied if the tangent to the characteristic of the throttling elements has as steep a slope as possible in the

operating point. In order to amplify the comparison of short cylindrical nozzles (characteristic D) and capillaries (characteristics K), which is given in reference (XVII), the venturi nozzle (characteristic V) has been included. For the comparison, the effective throttling area F_D and the pressure p_1 in the point of interpretation towards the feeding nozzles is maintained constant. (Equal $\dot{G}_{max}$ and equal load capacity in the point of interpretation).
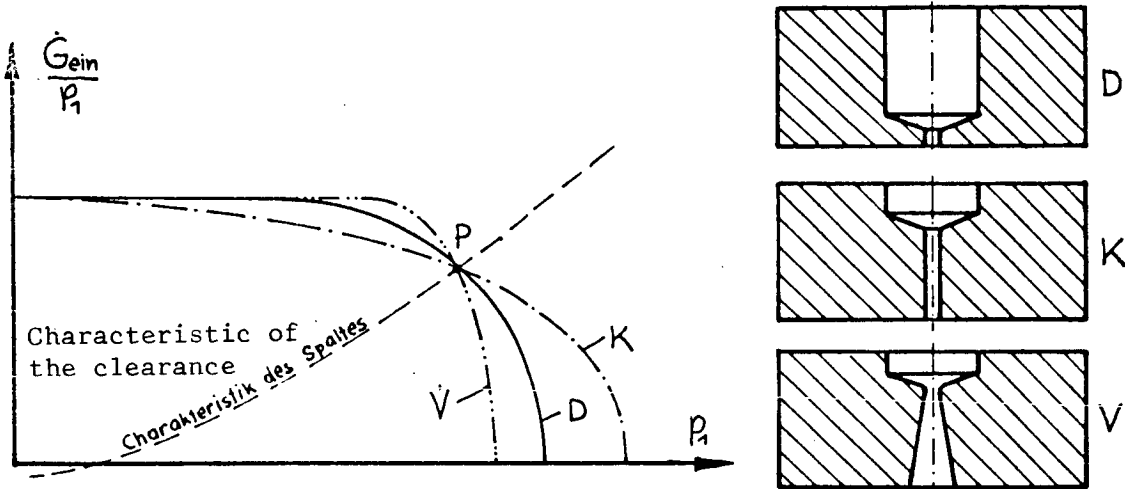
As can be concluded from the above comparison, the capillary nozzle has the tangent with the lowest slope in P. The venturi nozzle, which has a strongly bulging characteristic on account of the diffuser adjacent to the lowest cross section, at high pressure ratios p_1/p_B, (cf. Diagram 11) has, in certain regions, a better stabilizing effect on the bearing than the short cylindrical nozzle.

B) Volume of the compensating space.

If all the individual terms are introduced into the Routh stabilization equation No. 16.17, the following applies:

$$(\gamma - \alpha)\varepsilon \geq d\beta , \qquad \text{(16.17a)}$$

This is transformed, by introduction of the abbreviations and consideration of the volume between the bearing discs, V_L :

$$V_L = F_L \bar{h} = (r_{2a}^2 - r_{2i}^2)\,\pi\,\bar{h} \qquad \text{(16.17b)}$$

into

$$\frac{\dot{V}_A}{C V_L} \leq \frac{(\gamma - \alpha)\bar{p}_1}{\bar{h}\,\beta} - 1 \qquad \text{(16.17c)}$$

Thus the following result is obtained

$$\frac{V_A}{CV_L} \leq \frac{\bar{p}_1\left[\frac{\pi \bar{h}^3 \bar{p}_1}{6\eta RT_B}\left(\frac{1}{\ln\frac{r_{2a}}{r_{1a}}} + \frac{1}{\ln\frac{r_{2i}}{r_{1i}}}\right) + \frac{F_D \mu}{2\varkappa}\sqrt{\frac{2g\varkappa}{(\varkappa-1)RT_B}}\frac{(\varkappa+1)\left(\frac{\bar{p}_1}{p_B}\right)^{\frac{1}{\varkappa}} - 2\left(\frac{\bar{p}_1}{p_B}\right)^{\frac{2-\varkappa}{\varkappa}}}{\sqrt{\left(\frac{\bar{p}_1}{p_B}\right)^{\frac{2}{\varkappa}} - \left(\frac{\bar{p}_1}{p_B}\right)^{\frac{\varkappa+1}{\varkappa}}}}\right]}{\frac{\pi \bar{h}^3(\bar{p}_1^2 - p_2^2)}{4\eta RT_B}\left(\frac{1}{\ln\frac{r_{2a}}{r_{1a}}} + \frac{1}{\ln\frac{r_{2i}}{r_{1i}}}\right)} - 1$$

<div align="right">(16.17d)</div>

The division of the fraction gives:

$$\frac{V_A}{CV_L} \leq \frac{2}{3\left[1-\left(\frac{p_2}{p_1}\right)^2\right]} - 1 +$$
$$+ \frac{2}{\pi}\sqrt{\frac{2g}{\varkappa(\varkappa-1)}}\frac{\mu F_D \eta\sqrt{RT_B}\left[(\varkappa+1)\left(\frac{\bar{p}_1}{p_B}\right)^{\frac{1}{\varkappa}} - 2\left(\frac{\bar{p}_1}{p_B}\right)^{\frac{2-\varkappa}{\varkappa}}\right]}{\bar{h}^3\bar{p}_1\left\{1-\left(\frac{p_2}{p_1}\right)^2\right\}\left[\frac{1}{\ln\frac{r_{2a}}{r_{1a}}} + \frac{1}{\ln\frac{r_{2i}}{r_{1i}}}\right]\sqrt{\left(\frac{\bar{p}_1}{p_B}\right)^{\frac{2}{\varkappa}} - \left(\frac{\bar{p}_1}{p_B}\right)^{\frac{\varkappa+1}{\varkappa}}}}$$

<div align="right">(16.18)</div>

It can be concluded from this equation that the stability increases with decreasing ratio between compensating volume and bearing volume. In the most unfavorable case of bearing operation, $\alpha = 0$, i.e. the mass flow through the feeding nozzles does not change if the pressure p_1 is varied. Thus equation No. 16.18, written in another way, is transformed into:

$$1 + \frac{V_A}{CV_L} \leq \frac{2}{3\left[1-\left(\frac{p_2}{p_1}\right)^2\right]}$$

<div align="right">(16.19)</div>

Another conclusion to be reached is that also bearings without compensating space can be unstable. When V_A is chosen as zero, this can occur at a pressure $p_1 \geq \sqrt{3}\, p_2$.

The introduction of pressures and bearing clearances as they occur practically in static bearings into the stability equation No. 16.18 suggests that the compensating volume should be kept very small. In most cases, the depth s of the annular channel must not be larger than the clearance h itself. By such a limitation, the compensating space loses its original purpose, i.e. improvement of the load capacity by uniform distribution of the carrying gas entering through the nozzles.

With the testing equipment shown in Figs. 1 and 2, experiments relating to the influence of the shape of the compensating spaces were performed, using a bearing with the following principal dimensions: $D_{2a} = 120$ mm, $D_o = 80$ mm, $D_{2i} = 50$ mm, and which was equipped with four short cylindrical nozzles at an angle of $90°$ which were arranged in the fixed bearing disc. The pressure of the carrying gas in front of the bearing was varied between 2 and 20 atmospheres (absolute), whereas the limits of the height of the clearance h were 0 and 100 μm. Some of the cases

investigated are compiled on p. 151 . The experiments showed that the instability of the bearing cannot be eliminated by the shape of the compensating channel. At equal operating conditions, (K_{ges}, p_B, h), the only conclusion that could be reached was that the volume of the compensating space has a great influence on the frequency of the vibration. The larger the volume V_A was designed, the lower was the inherent frequency of the bearing vibration.

C) Other parameters.

The influence of the pressure p_1 upon stability cannot be derived directly from equation No. 16.18. But if the simplified limiting case according to equation No. 16.19 is considered, it appears that, on account of the increase of the load capacity factor C with decreasing pressure ratio p_1/p_2, the influence of the pressure acts in two ways, both working in the same direction. A greater stability is thus achieved by reducing the pressure ratio p_1/p_2. It was found as a result of these experiments that the vibration frequency increases with increasing pressure (at equal width of the clearance).

Summarizing, it can be stated that the stability is improved or increased, respectively, with increasing nozzle F_D, viscosity η of the gas, temperature T_B and gas constant R, and with decreasing height of the clearance.

16.3 Frequency of vibration.

For reasons which will be described later, the calculation of the vibration frequency of the bearing and the components connected with it is required. From the vibration equation No. 16.16 and the formulation of solution

$$\Delta h = e^{\lambda t} \qquad (16.19a)$$

the frequency equation can be obtained:

$$\lambda^3 + a\lambda^2 + b\lambda + c = 0 \quad . \qquad (16.19b)$$

The solutions of these cubic equations are:

$$\lambda_1 = u + v - \frac{a}{3}$$

$$\lambda_2 = -\left(\frac{u+v}{2} + \frac{a}{3}\right) + \frac{i\sqrt{3}}{2}(u-v)$$

$$\lambda_3 = -\left(\frac{u+v}{2} + \frac{a}{3}\right) - \frac{i\sqrt{3}}{2}(u-v)$$

$$(16.19c)$$

where "u" and "v" are

$$u = \sqrt[3]{-q + \sqrt{q^2 + p^3}}$$

$$v = \sqrt[3]{-q - \sqrt{q^2 + p^3}}$$

$$(16.19d)$$

where, again, "q" and "p" mean:

$$q = \frac{a^3}{27} - \frac{ab}{6} + \frac{c}{2} \qquad (16.19e)$$

$$p = \frac{b}{3} - \frac{a^2}{2}$$

Thus the general solution of the vibration equation is:

$$\Delta h = C_1 e^{(u+v-\frac{a}{3})t} + C_2 e^{[-(\frac{u+v}{2} + \frac{a}{3}) + \frac{i\sqrt{3}}{2}(u-v)]t} + C_3 e^{[-(\frac{u+v}{2} + \frac{a}{3}) - \frac{i\sqrt{3}}{2}(u-v)]t} \qquad (16.20)$$

The cyclic frequency of the vibration of the bearing is desired from the imaginary part of the exponents of e (NB: "Hz" = Hertz or cycles)

$$\omega = \frac{\sqrt{3}}{2}(u - \dot{v}) \qquad (16.21)$$

or

$$\nu = \frac{\omega}{2\pi} = \frac{\sqrt{3}}{4\pi}(u - v) \quad [Hz] .$$

As could already be concluded from the experiments described before, this general statement can be made: The larger the pressure p_1, the smaller the compensation volume, the bearing clearance and the vibrating mass are, the greater becomes the frequency.

Example:

For the purpose of comparison, the frequency of the thrust bearing of the large testing device (cf. section on p. 137 and Figs. 3 - 11) are recomputed.

Dimensions of the bearing: (NB. Düsenzahl = number of nozzles)

r_{2a}	=	0,133 m	F_L	=	461.10^{-4} m²	
r_{1a}	=	0,089 m	F_D	=	$6,42.10^{-6}$ m²	(16.21a)
r_{1i}	=	0,087 m	n	=	20 (Düsenzahl)	
r_{2i}	=	0,055 m	h	=	44.10^{-6} m	
b	=	0,002 m	m	=	41,3 kg s²/m	
s	=	$0,7.10^{-3}$ m				

Flow medium: air

T_B	=	291 °K	
R	=	29,3 m/°K	(16.21b)
ⰰ	=	1,4	
η	=	$1,85.10^{-6}$ kp s/m²	

Calculated values:

α	=	0	δ	=	$1,676.10^{-10}$	q	=	$3,042.10^7$	(16.21c)
β	=	17,40	ε	=	0,1006	p	=	$1,483.10^5$	
γ	=	$2,242.10^{-1}$	a	=	134	u	=	$3,245.10^2$	
ζ	=	$3,81.10^{-6}$	b	=	$4,72.10^5$	v	=	$4,570.10^2$	
ϑ	=	$8,775.10^{-11}$	c	=	$8,175.10^7$				

	$d = 0,7$ mm $\ell \cong d$ $V_A = 0$	Section through one of the four feeding nozzles. In the experiment without compensating space, stability of the bearing for all operating conditions.
	$d = 0,7$ mm $D = 2,0$ mm $\ell \cong d$ $V_A = 0,54$ mm³	Chamfering of the nozzles in order to obtain a better distribution of the gas. The bearing vibrates only at pressures p_B above 20 atmospheres (absolute).
	$d = 0,7$ mm $D = 5,0$ mm $s = 0,1$ mm $V_A = 1,96$ mm³	Non-chamfered nozzles with flat central recess. Instability of the bearing within a wide operating range.
	$d = 0,7$ mm $b = 5,0$ mm $s = 0,03$ mm $V_A = 37,7$ mm³ ――――― $b = 1,0$ mm $s = 0,3$ mm $V_A = 67$ mm³ $\gamma \cong 1000$ Hz ――――― $b = 3,0$ mm $s = 1,5$ mm $V_A = 1,12.10^3$ mm³ $\gamma \cong 600$ Hz ――――― $b = 6,0$ mm $s = 12$ mm $V_A = 18,1.10^3$ mm³ $\gamma \cong 80$ Hz	Hz = Hertz = cycles. In these cases, the bearing has an annular channel which connects all nozzles with each other. Strong, self-induced vibrations over almost the whole range of operation
	$d = 0,7$ mm $a = 0,5$ mm $s_1 = 0,2$ mm $V_A = 29$ mm³ $\gamma \cong 1200$ Hz	Five annular channels of equal size, separated from each other. Strong vibrations in the whole range of operation.
	$a = 0,5$ mm $s_1 = 0,2$ mm $s_2 = 0,5$ mm $V_A = 59,6$ mm³ $\gamma \cong 900$ Hz	Five annular channels, seperated from each other; the one in the center has an enlarged volume. Strong vibrations in the whole range of experiments.

From the values given above, a calculated vibration frequency of γ = 108 cycles (Hertz) is obtained, whereas the frequency measured with the audio-frequency generator and cathode-ray oscillograph was 123 cycles (Hz).

16.4 Elimination of self-excited vibrations.

As a rule, the self-induced vibrations occuring in bearings are excited spontaneously without outside influence. The amplitude increases there on account of the negative damping until the energy which is required for a further growth of the amplitude is consumed by interior damping forces. (cf. the Fig. on p. 141). An elimination of the vibration can be achieved if the damping effect can be amplified in the bearing itself or if the vibrating mass can be influenced suitably by external influences.

A) Damping by resonators.

The bearing illustrated on p. 143 (without damping elements) is a system capable of vibrating which, on account of self-excitation at a certain frequency, performs undamped vibrations or even vibrations with negative damping and increasing amplitude. It is irrelevant for the study of the attenuation of such a vibration, which follows, whether self-excited or foreign-excited vibrations are involved. A foreign excited mechanical vibration of a system (principal system M – C in the drawing at right) can be attentuated, as it is known, also in case of resonance ($\omega = \omega_0$) by the attachment of a second spring c and a second mass m, if the inherent frequency ω_m of the system m – c is equal to the inherent frequency of the principal system M – C (cf., e.g. reference XXVI). In an analogous way to the previously described dynamic damping of mechanical vibration , an acoustical element i.e., the Helmholtz resonator, is applied for the elimination of vibrations in aerostatic bearings. Transferred to the case of the bearing, the mass of air in the neck H of the resonator corresponds to the mass m and the volume V_R of the resonator to the spring constant C. In order to damp the principal vibration, the inherent frequency of the resonator must be equal, referring to the mechanical analogy, to the frequency of the self-excited vibration in this case. It is advantageous to branch the resonators off the compensating channel A in order to achieve as good a damping effect as possible in the bearing. For the auxiliary system, the following equation can be formulated if the interior damping forces are disregarded:

$$m\ddot{y} + c_R y = f \cdot p_1(\omega_m t), \quad (16.22)$$

where y is the deflection of the air mass m in the neck of the resonator, c_R is the spring constant of the resonator, f is the cross section area of the neck of the
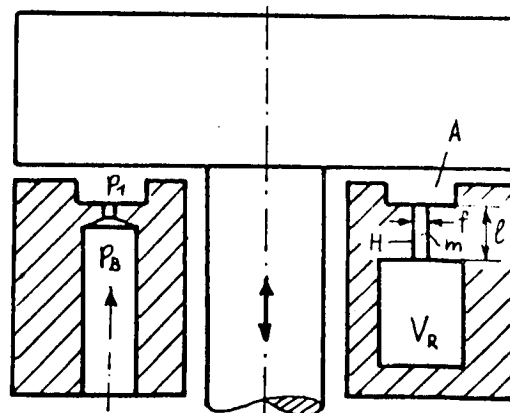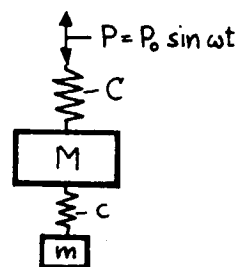
resonator, and $p_1(t)$ the pressure in the compensating space which fluctuates with time. Since the foreign excitation $p_1(t)$ for the auxiliary system vibrates at the frequency ω_M, the inherent frequency of the auxiliary system must be, in order to achieve optimum vibration damping: $\omega_R = \omega_M$. From equation No. 16.22 it can be deduced that the inherent frequency of the resonator is:

$$\omega_R = \sqrt{\frac{C_R}{m}} \qquad (16.23)$$

The spring constant of the resonator becomes:

$$C_R = \frac{f \, dp}{dy} \qquad (16.24)$$

At a displacement dy of the mass m in the neck, the amount G_R in the resonator is increased by the magnitude

$$dG_R = f \cdot \gamma \cdot dy = V_R \, d\gamma \qquad (16.25)$$

If an adiabatic change of state of the gas is assumed in the resonator, where the following applies:

$$\frac{dp}{p} = \varkappa \frac{d\gamma}{\gamma} \qquad (16.26)$$

a combination of equation No. 16.25 and No. 16.26 gives:

$$C_R = \frac{\varkappa f^2 \, p}{V_R} \qquad (16.27)$$

If the mass in the neck of the resonator is

$$m = \frac{f \, \ell^* \, p}{g \, R \, T} \qquad (16.27a)$$

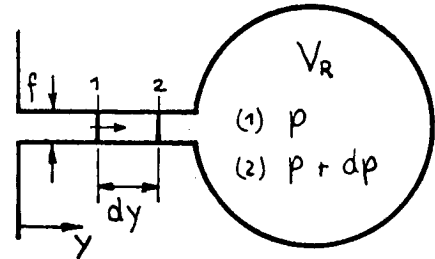the inherent frequency of the resonator will be:

$$\nu_R = \frac{\omega_R}{2\pi} = \frac{1}{2\pi}\sqrt{\frac{f \cdot a_s^2}{V_R \, \ell^*}} \qquad (16.28)$$

where $a_s = \sqrt{\varkappa \, gRT}$ is the sound velocity in the gas, and

$1^* = 1 + \pi/4 \, d$ = the effective length of the neck of the resonator, which is always higher than the actual length, since the gas must also be accelerated in the regions of th mouth; $d(f = d^2 \frac{\pi}{4})$ is the diameter of the neck duct.

Results of the experiments

1) The original design of the bearing discs of the testing apparatus illustrated in Figs. 1 and 2 (D_{2a} = 120 mm, D_{2i} = 50 mm, with an annular compensating channel b = 3 mm, s = 1 mm) did not allow any measurements of load capacity and amount of throughput on account of strong self-excited vibrations with a frequency of 200 to 600 cycles. By the installation of

of 4 equal, symmetrically arranged resonators in one of the bearing discs (stationary disc in Fig. 2) with the following dimensions: d = 1 mm, 1 = 2 mm, V_R = 13.2 cm³, tuned to an inherent frequency of γ_R = 227 cycles (Hertz), all vibrations in all desired ranges of operation could be completely eliminated. The sketch on the right shows diagrammatically the bearing discs used with feeding nozzles and installed resonator chambers.
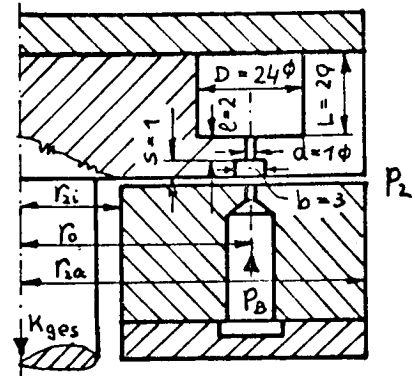
2) According to the design of the large gas bearing testing apparatus (cf. Figs. 3 - 11 and the section on p. 137) the thrust bearing of the dimensions D_{2a} = 266 mm, D_o = 176 mm, D_{2i} = 110 mm, was equipped with an annular compensation channel of the dimensions D_{1a} = 178 mm, D_{1i} = 174 mm, b = 2 mm, s = 0.7 mm, and several differently tuned resonators. In this arrangement, two resonators in pairs with equal dimensions and inherent frequencies were in diametrically opposite positions. On p.158 , the workshop drawing of the fixed axial disc is illustrated without cover. The installed resonators have the following dimensions and calculated inherent frequencies: (NB. Anzahl = number; HZ = cycles (Hertz))

Anzahl	D mm	L mm	$V_R = \frac{D^2\pi}{4}L$ cm³	d mm	f mm²	ℓ mm	e^* mm	γ_R Hz
	6	56	1,58	1	0,785	3,3	4,08	547
2	14	56	8,62	1,5	1,77	3,3	4,5	336
2	14	56	8,62	0,8	0,504	3,3	3,93	192
2	14	51	7,85	0,8	0,504	8,3	8,93	133
1	26	2x51	54,1	0,8	0,504	8,3	8,93	51
1ˣ	(60)	(105)	351	1,5	1,77	8,3	9,5	36,2

(16.28a)

ˣ) with resonator attached outside (cf. Fig. 10) and enlarged neck borehole compared to the drawing on p. 158. The velocity of sound was uniformly assumed to be a_s = 312 m/sec.

The shaft which was, likewise, carried by aerostatic radial bearings could follow, without friction, the vibrations induced by the thrust bearing, since the clutch elements for rotating operation were omitted. The thrust was produced by means of a pressurized air cushion acting upon the front side of the free end of the shaft. The experiments were performed with air at an inlet temperature T_B of about 293°K. In consideration of the annular compensation channel, as described above, and the presence of all the resonators, the thrust bearing proved to be rather unstable. (The channel can be clearly seen in Fig. 8). Diagram 30 shows the individual stable and unstable regions as a

function of the pressure ratio p_1/p_2 and the height of the bearing clearance h. The axial vibration amplitudes of the 410 kp shaft were recorded in a few cases only and amounted to 4 to 10 μm at the high frequencies and up to 50 μm at the low frequencies. As can be seen in Diagram 30, the bearing has two stable and one unstable main regions. It is interesting to note that the unstable region of operation includes two special bands. The first band appears at frequencies between 27 and 47 cycles. The bearing is stable in this region. The second place is, strictly speaking, only a separating line and is characterized by the fact that, upon passing this line, the vibration of the bearing of 52 cycles fades out almost completely and then suddenly increases to 63 cycles. It was not feasible to adjust to a vibration of a frequency between these two values. If the inherent frequencies of the installed resonators are considered (cf. p. 154), an explanation can be given for the behavior just described. The two last-named resonators with ν_R = 51 and 36.2 cycles attentuate the vibrations of the bearing at the respective places more or less satisfactorily. Though, damping is limited here to a very narrow frequency band.

For the next experiment, the neck ducts of all resonators were plugged up in such a way that only the ring channel was responsible for the vibration behavior of the bearing. Some measuring results with this arrangement are included in Diagram 31, using the same way of representation. The inherent frequency of the system was considerably higher in this case and was in the range between ν = 108 and 210 cycles. A comparison of the two series of measurements shows (cf. Diagrams 30 and 31) that the vibration frequency is considerably lowered by the installation of a great number of differently tuned resonators and the lower boundary of stability was further reduced, i.e. shifted into a region of smaller pressure ratios and clearance heights. In this respect, operation without resonators proved to be more advantageous. An arrangement with several resonators of different inherent frequency renders the conditions poorer, since the resonators which are not in resonance have no damping action and contribute only to the enlargement of the compensation volum V_A and thus to the reduction of the vibration frequencies. It may also be assumed that the exciting forces are enhanced by the presence of not accurately tuned resonators and that this overcompensates, in a way, the favorable effect of the resonators.

When, after these experiments and results, those two resonators in the bearing in which the inherent frequency was closest to that of the shaft (the resonators with ν_R = 135 cycles, cf. p. 154) were reopened and thus became operating, no vibrations occurred any longer in the practical working range of the bearing.
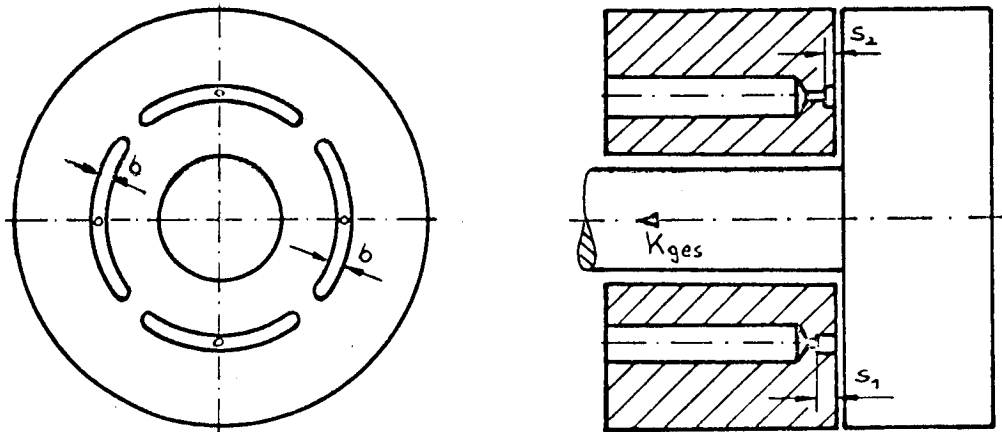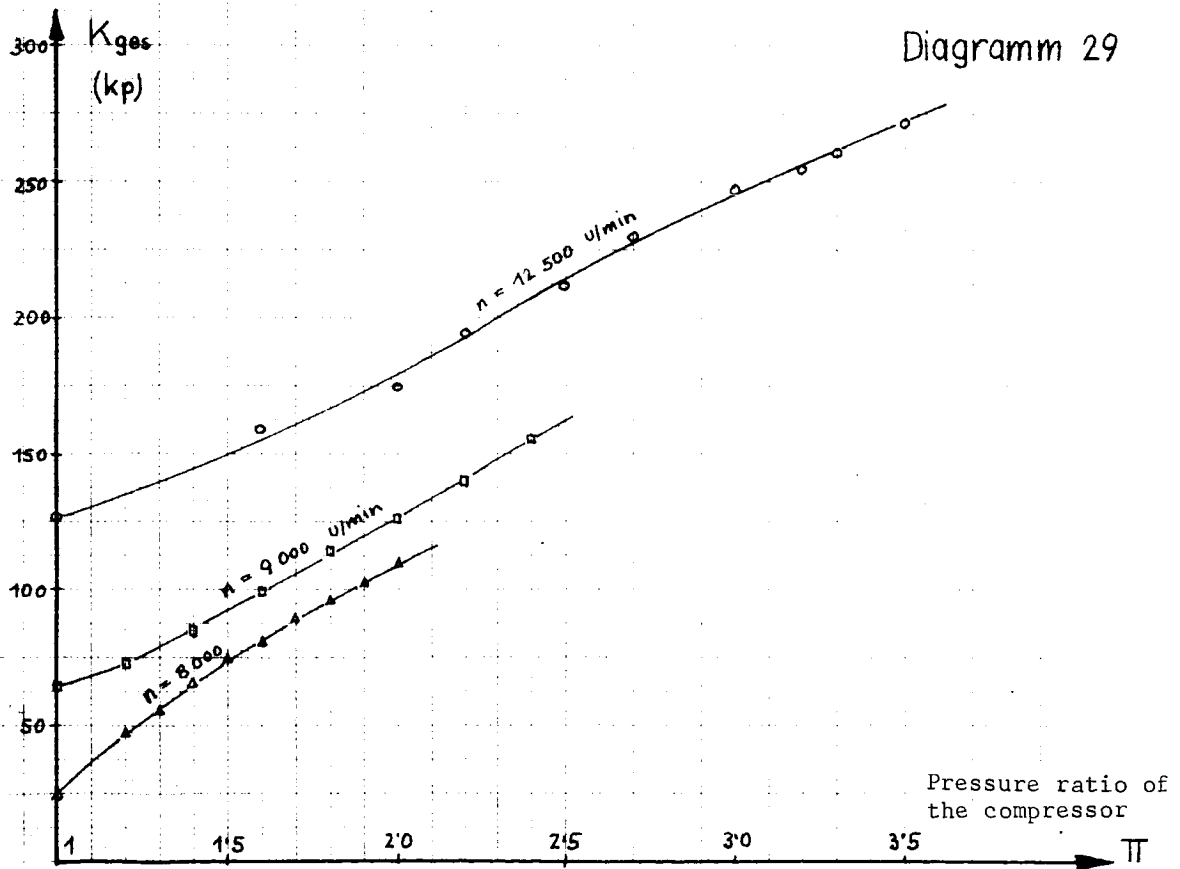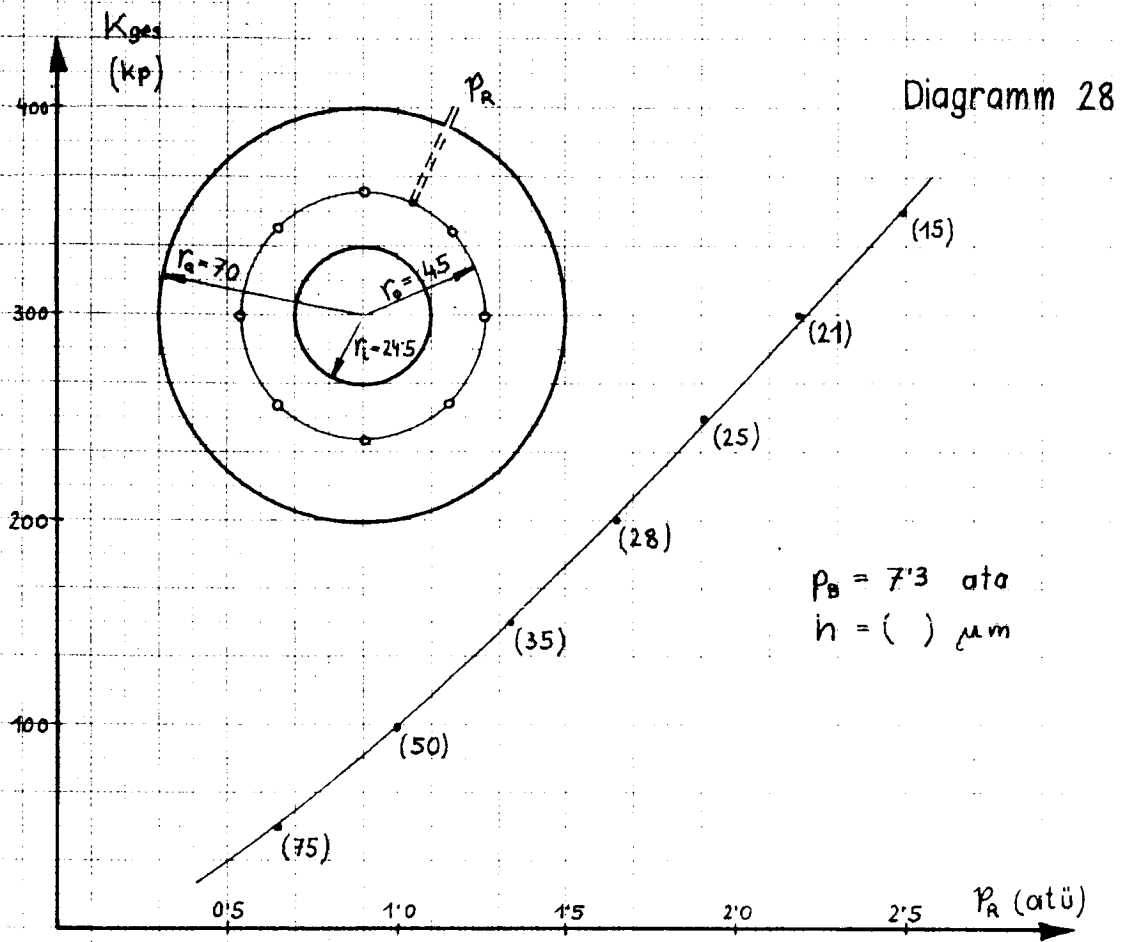
Conclusion.

The preceeding experiment shows that it is not useful to install, at the outset, a great number of resonators of different inherent frequency in the bearing discs. Instead, it is advisable to determine, either by experiment or calculation, the exact inherent frequency of the system and to design and install the resonators in accordance with these results. There is, of course, also the possibility to select such a resonator construction where at least one of the important magnitudes (e.g. V_R) can be tuned to the operating conditions. It could be seen in all experiments performed that high frequency

vibrations could be damped much more easily than very low frequency vibra-
tions. It is, therefore, advantageous to design, first of all, the volume
of the compensating space as small as feasible (cf. also p. 81). Another
reason for tending towards high vibration frequencies is the fact that
large resonator chambers are required for low inherent frequencies, which
involves difficulties in the construction of the components of the bearing.
It is also shown in Experiment 1) that the elimination of vibrations at
higher frequencies is not limited to the frequency for which the resonator
was designed but extends also to adjacent frequencies. It should also be
pointed out that the apertures of the resonators (cross section of the neck
duct) must be sufficiently large. If the opening is too small, the influence
of the viscosity of the gas is felt; this increases the acoustical resistance
of the resonator, decreases the inherent frequency and lowers the attenuating
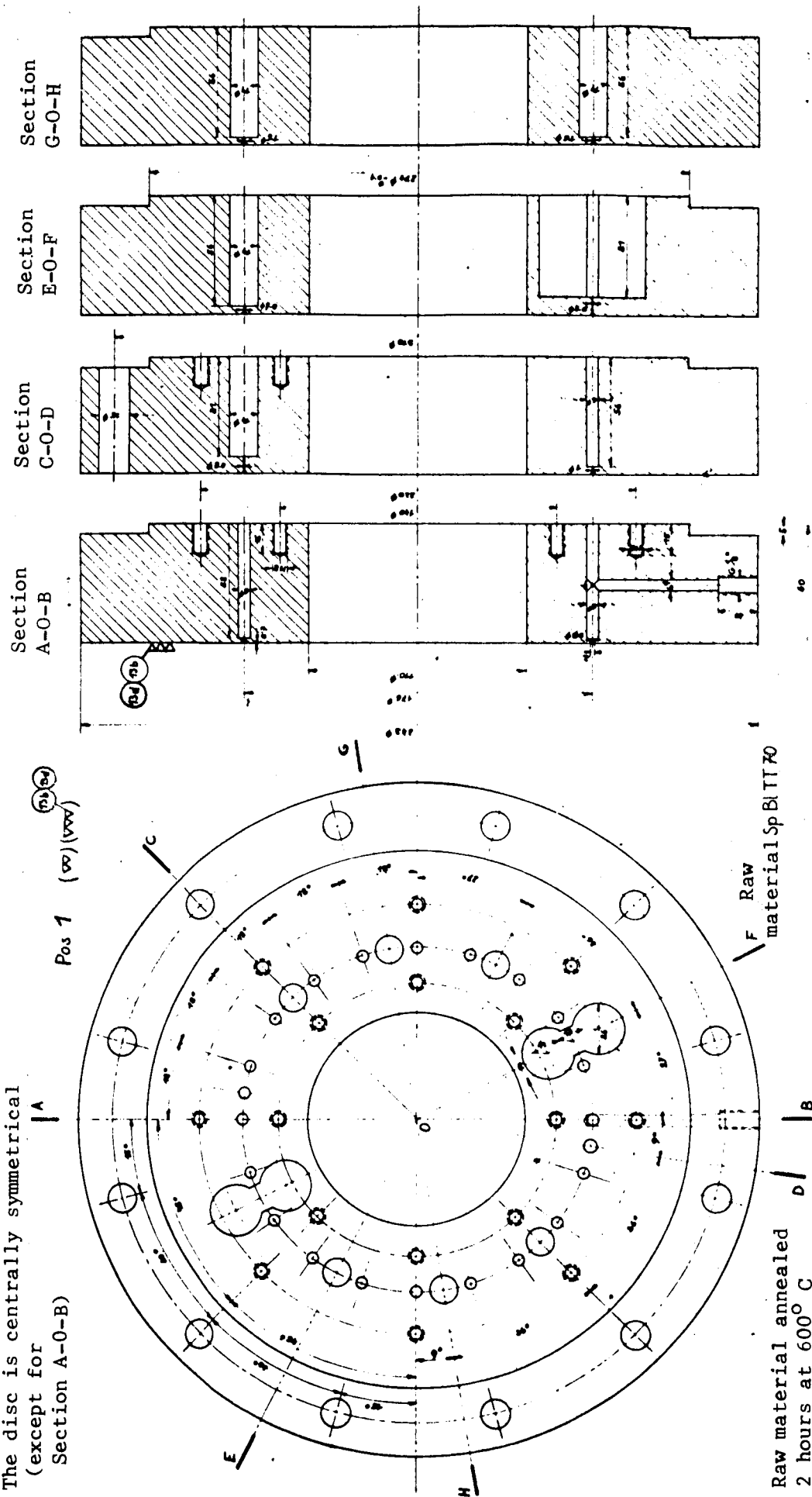effect and the transmission of force, respectively (cf. also reference XXVII).

B) Damping by interference.

The idea of generating several vibrations of different frequencies
in the same bearing in such a way that the vibrations are superimposed and
canceled, was followed up by an experiment with the components of the small
testing apparatus (Figs. 1 and 2). A disc with four feeding nozzles was
used for this purpose, each nozzle opening into a separate compensation space.
(cf. the drawing below).

Diagramm 28

$p_B = 7'3$ ata

$h = (\ )\ \mu m$

Diagramm 29

Pressure ratio of
the compressor

Section
G-O-H

Section
E-O-F

Section
C-O-D

Section
A-O-B

The disc is centrally symmetrical
(except for
Section A-O-B)

Pos 1   (∿)(∿∿)

Raw material annealed
2 hours at 600° C

Raw
material Sp B\TT 70

Fixed bearing disc, with
20 feeding nozzles and
10 resonator chambers.

Diagramm 30

Hz = Hertz (= cycles)

Stable

Stable

Assumed

Unstable

Stable

Sudden Change

65 Hz

70 Hz

52-63 Hz

50 Hz

47 Hz

27 Hz

25 Hz

20 Hz

15 Hz

$\frac{P_1}{P_2}$

5

4

3

2

1

h [μm]

20   30   40   50   60   70   80   90   100   110   120   130   140   150
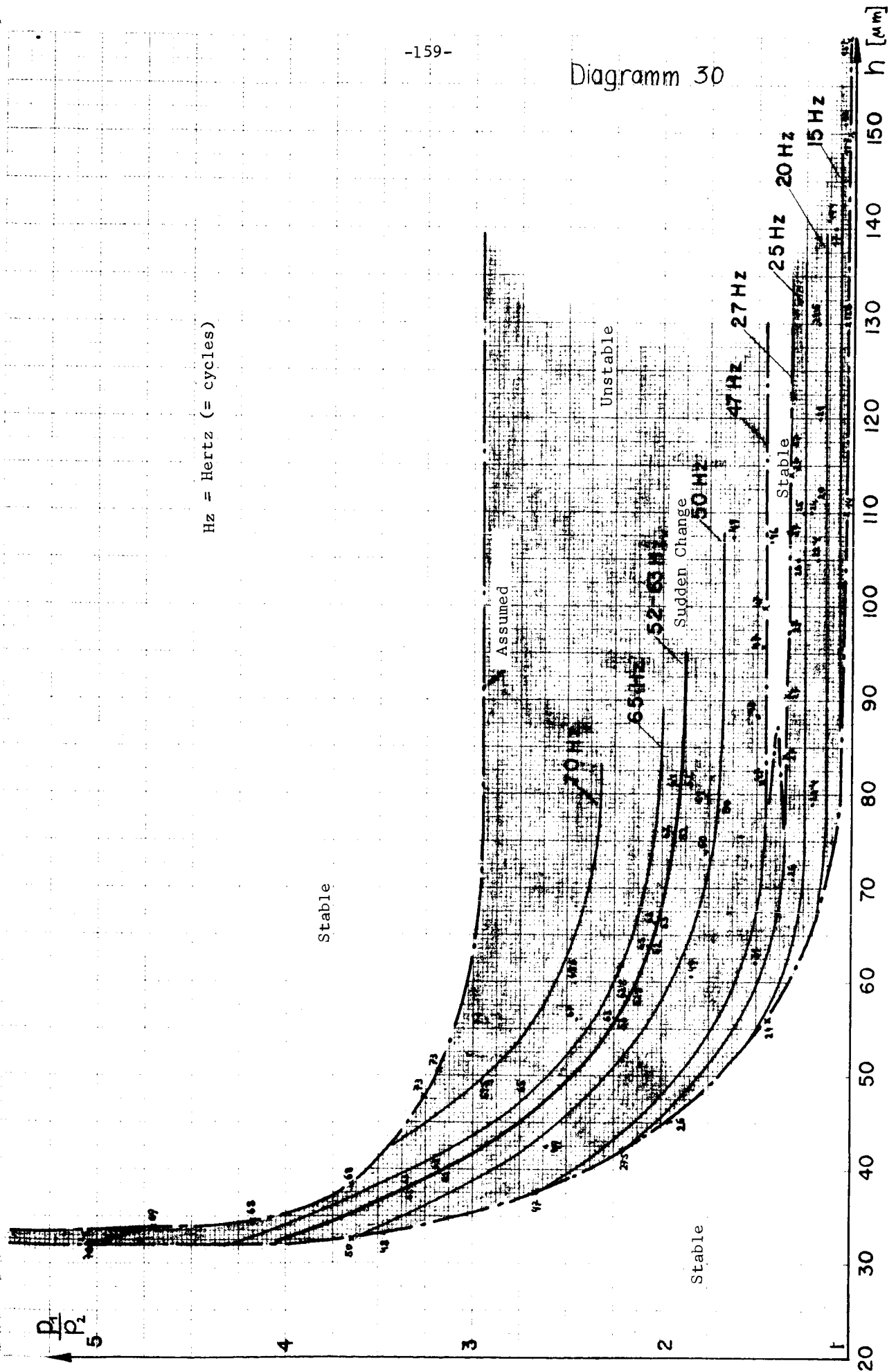
Diagramm 31
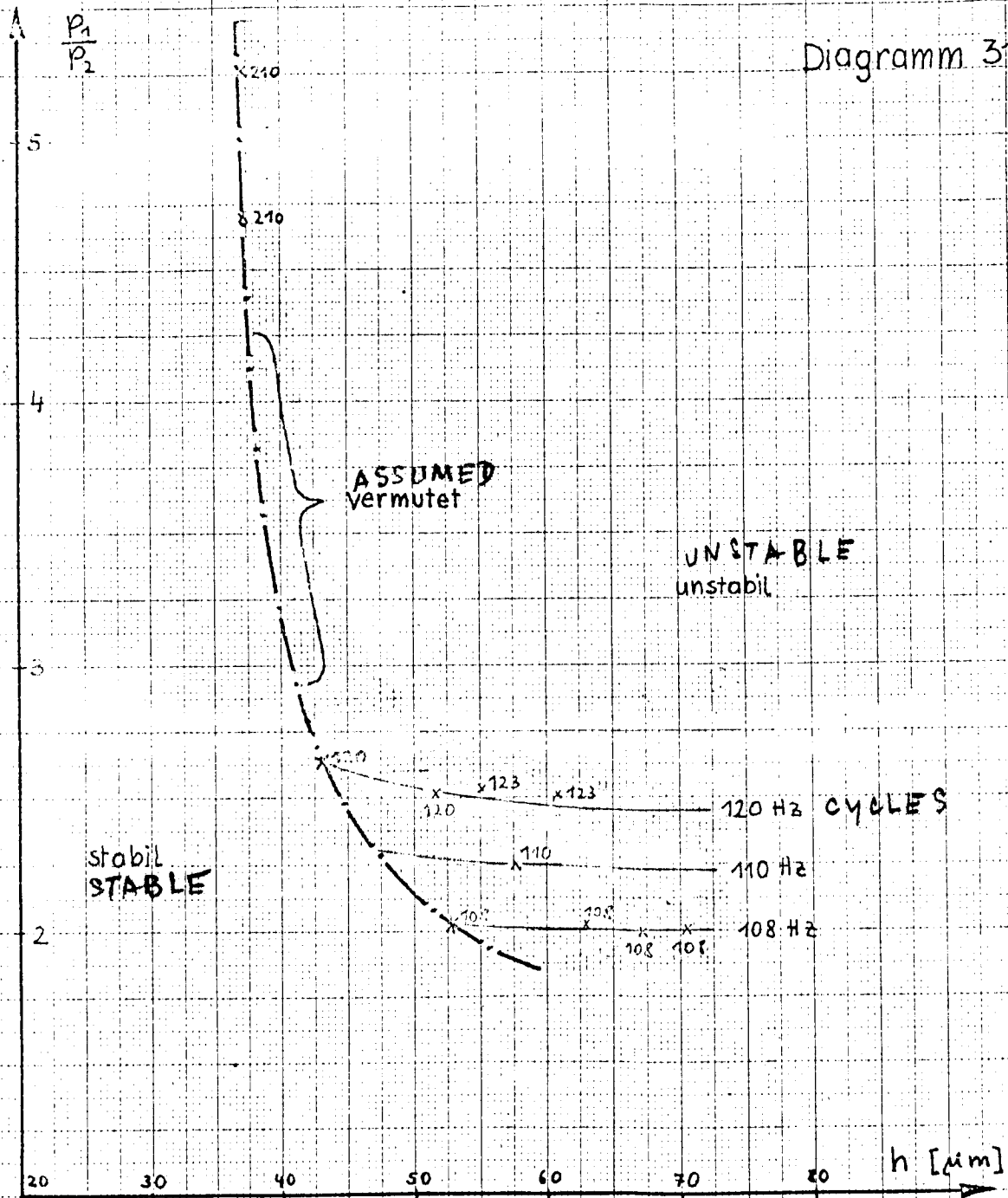
The compensation spaces were first designed in pairs of different size, then all four were constructed at different depths s and arranged in various combinations. The experiments showed that no superimposition of the vibrations, as desired, did occur and that the bearing remained unstable in all cases. The frequency of the vibrations was always that of the largest compensation space; thus the bearing vibrated at the lowest frequency. The predominance of the lowest frequency does not allow any influence by higher frequencies where the energy of vibration is lower. The generation of vibrations of equal frequency, but with a phase shift of 180°, would be desirable but cannot be realized in one and the same bearing.

C) Damping by friction.

The self-excited vibrations generated by the annular compensation channel of the axial bearing in the large testing apparatus (Figs. 3 - 11, or section, p. 137), with simultaneous admission of compressed air into both radial bearings - allowing completely free motion of the shaft - disappeared immediately after the gas feed was cut off to one of the two radial bearings. These experiments were performed while, of course, the shaft did not rotate. Thus the vibration was completely attenuated by friction in the radial bearing as soon as the shaft got into contact with the bearing seat.

When the shaft was entirely free (i.e. pressurized gas was supplied also to the radial bearings), the self-excited vibration of the thrust bearing could be eliminated also by application of a medium heavy lead hammer to the front surface of the shaft. Though, the separation between the friction damping effect proper and the dynamic damping action is not feasible in an accurate way.

In another case, connection of the swinging shaft to the fixed driving aggregate was already sufficient to create a satisfactory attenuation and thus stability of the system. It must be mentioned, however, that the connection was not rigid but allowed, for reasons of measuring technique, shifts in axial directions; thus only the friction in the connecting sleeve was decisive for the attenuation.

16.5 Vibrations of double-acting thrust bearings.

In some machines, the thrust bearing must take up equal or different forces in both directions. The most simple method consists in using in such cases a bilateral symmetrical bearing (cf. left drawing on the next page) where the total axial free space of the shaft $h_I + h_{II}$ is determined by the operating conditions of the machine. As soon as, however, the bearing gas is admitted on both sides of the rotating axial disc, it depends on the absolute axial free space to what extent the two sides of the bearing influence each other in the particular positions as far as load capacity is concerned.
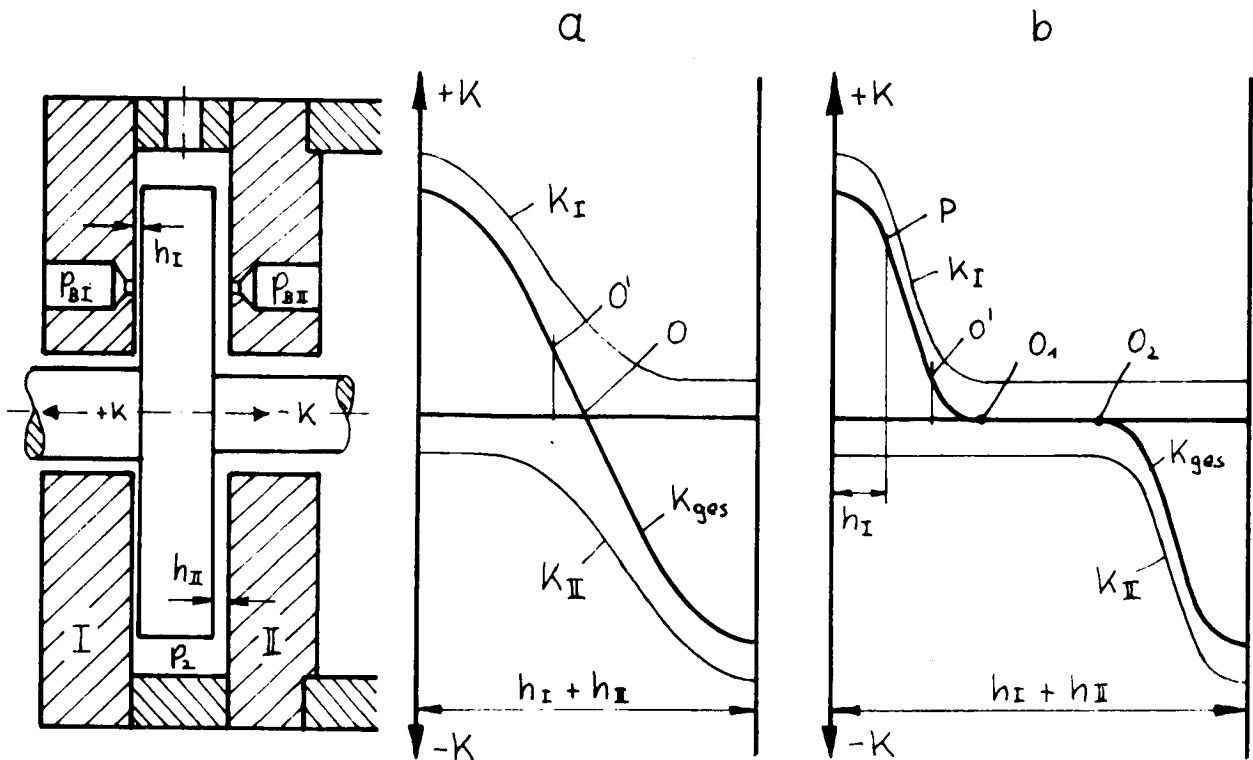
The Drawings A and B above illustrate diagrammatically the bearing characteristics $K_{ges} = f(h)$ at very small (=a) and very large (=b) free axial space. With the small axial free space, there is an appreciable reduction of K_{ges} on account of the counter-thrust. With a large total free space, however, the counteracting force affects the bearing side I only with the portion $K_{II} = F_L \cdot p_2$. In order to maintain the load capacity of the bilateral bearing high, it is advantageous to select the total free space in such a way that the points O_1 and O_2 (cf. Drawing b) just coincide. Without axial thrust of the machine, the widths of the clearances h_I and h_{II} are equal or different in their final adjustment depending on the parameters p_{BI}, p_{BII}, F_{DI} and F_{DII}. In the case of the characteristic a, O is the point of equilibrium, whereas in Drawing b the position of the shaft of the machine between O_1 and O_2 is not defined.

Diagram 32 shows the measuring results of the axial thrust ratios of the bearing in a four-stage radial compressor which is illustrated on p. 166 in section and in Fig. 12 in top view. The section of the thrust bearing illustrated on p. 167 shows the relative sizes of the components as well as the direct opening of the 8 nozzles into the bearing clearance. The rotor of the machine was, likewise, carried by aerostatic radial bearings. In order to avoid damping from outside, the connection to the gear was removed for the vibration experiment. With bilateral gas feed and without

axial thrust, strong axial vibrations of the whole rotor around to 0-position occurred inspite of the absence of a compensation space in back of the nozzles. Vibrations were even found when the free space was enlarged to such an extent that, as shown in Drawing b, there was no longer any mutual influence of the two sides of the bearing. The vibrations did not disappear when one or the other feeding pressure p_B was varied, i.e. at a horizontal shift of the point 0 in the Drawing a. Diagram 32 illustrates clearly how the rigidity of the bearing increases at the site $h_I = h_{II}$ at $p_{BI} = p_{BII}$ with increasing pressure ratio p_B/p_2. This fact became also evident by an increase of the vibration frequency, the vibration amplitude becoming smaller with increasing rigidity. It may be concluded from the considerations which follow that it is not a regular vibrating spring - mass system with the "spring constant" (rigidity of the bearing) $c_L = \Delta K_{ges}/\Delta h$ and the mass of the rotor $m \simeq 16$ which is the reason for this instability, but that a self-excited vibration is involved which is caused by the feeding system and the reversal of the thrust:

1) Although the bearing was stable at unilateral gas feed and a wide range of loads and widths of the clearance, the vibration is excited spontaneously without any external influence at bilateral gas admission for $K_{ges} = 0$.

2) The vibration does not fade out any more, i.e. the interior attenuations which are due to the air cushion between the bearing discs are compensated by the self-excitation.

3) A rough calculation of the vibrating frequency without consideration of damping and self-excitation, from the rigidity values in Diagram 32 gives, e.g. for $p_{BI} = p_{BII} = 6 \times 10^4$ kp/m^2 a spring value of $c_L = 2.46 \times 10^6$ kp/m, from which the following formula can be derived: (NB. Hz = Hertz = cycles)

$$\nu = \frac{1}{2\pi} \sqrt{\frac{c_L}{m}} \quad 62,5 \text{ Hz} \qquad (16.28b)$$

In contrast to this, a frequency of 36 cycles was measured. This discrepancy proves that we are not facing here a simple vibrating spring - mass system.
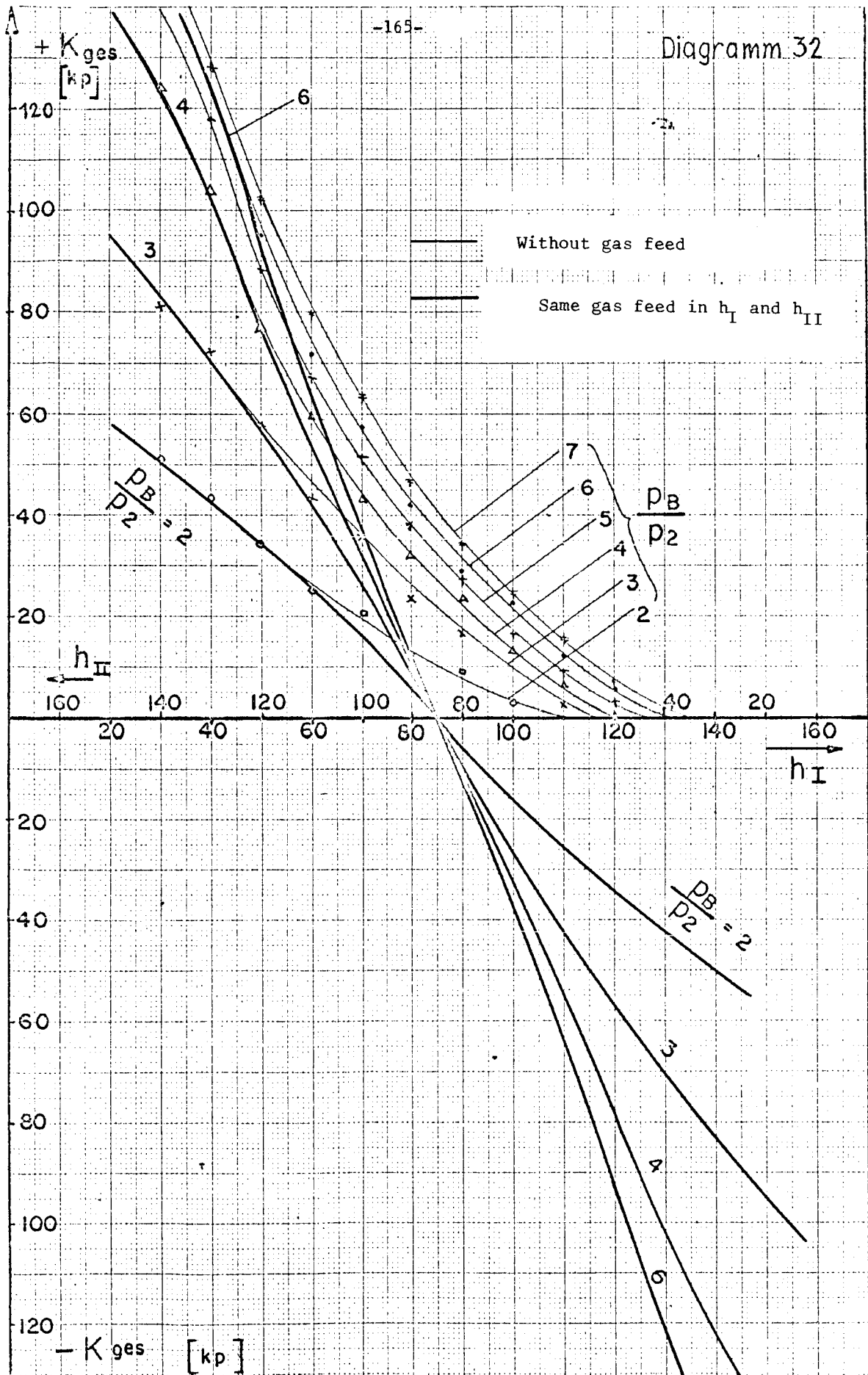
Elimination of vibrations in double-acting bearings.

A) In order to remove the instability which appears at $K_{ges} = 0$, it proved to be effective to apply a relatively low axial thrust into one direction in such a way that 0' (cf. Drawings a and b on p. 162) becomes the new equilibrium point. This could be done pneumatically, in a very simple way, in the case of the bearing of the four-stage radial compressor which is shown as a section on p. 167 , by throttling the exhaust air of the left thrust bearing disc and the adjoining radial bearing slightly by means of a stopcock. In this way, an increased pressure was generated in the collecting chamber, and this pressure exerted a thrust on the front side of the radial bearing journal pin.
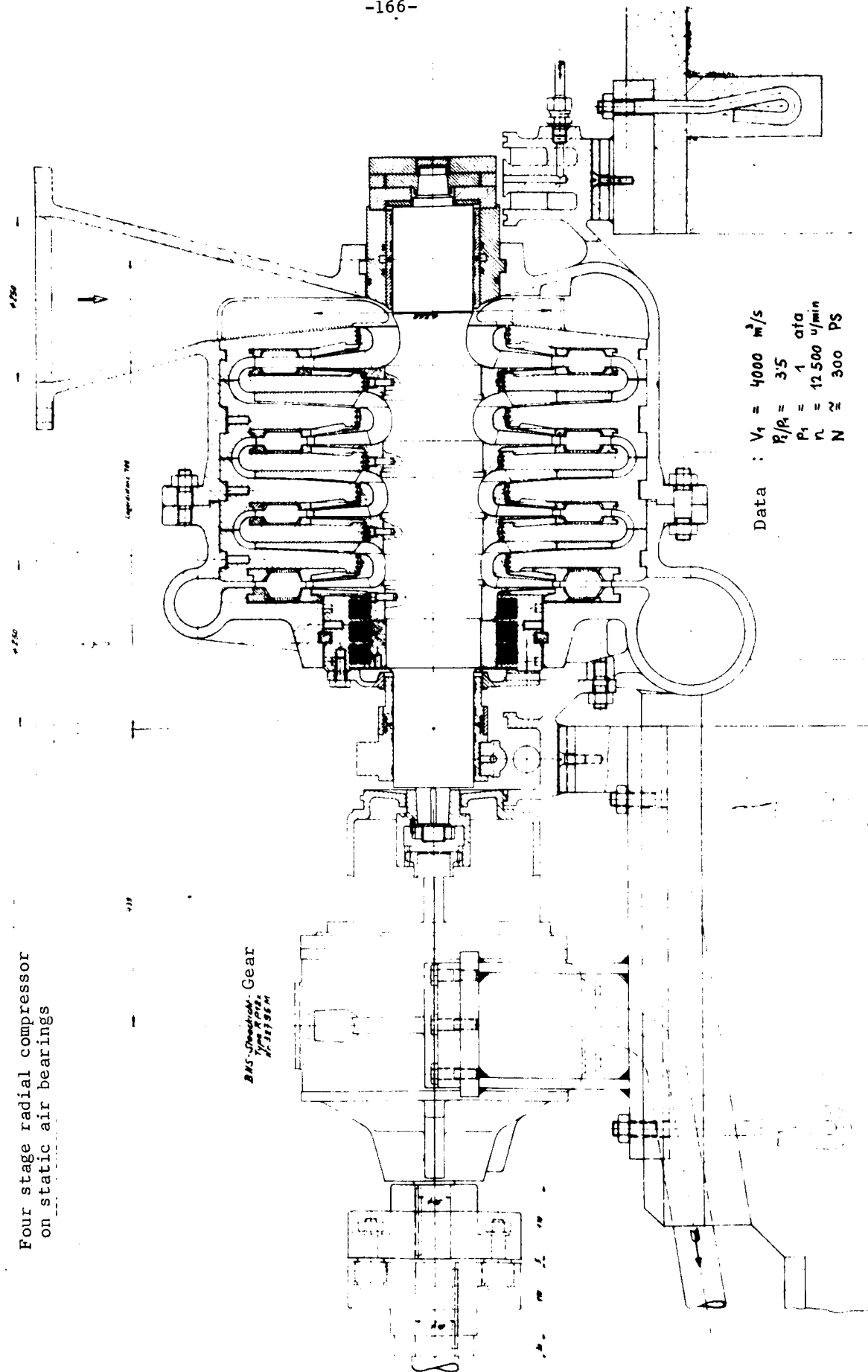
B) An increase of the total free space $h_I + h_{II}$ caused initially a reduc-
tion of the vibration frequency. The reason for this pnenomenon is that
the stroke between O_1 and O_2 (cf. Drawing b on p. 162) which must be
passed by the shaft as an inactive distance, was increased. But if a very
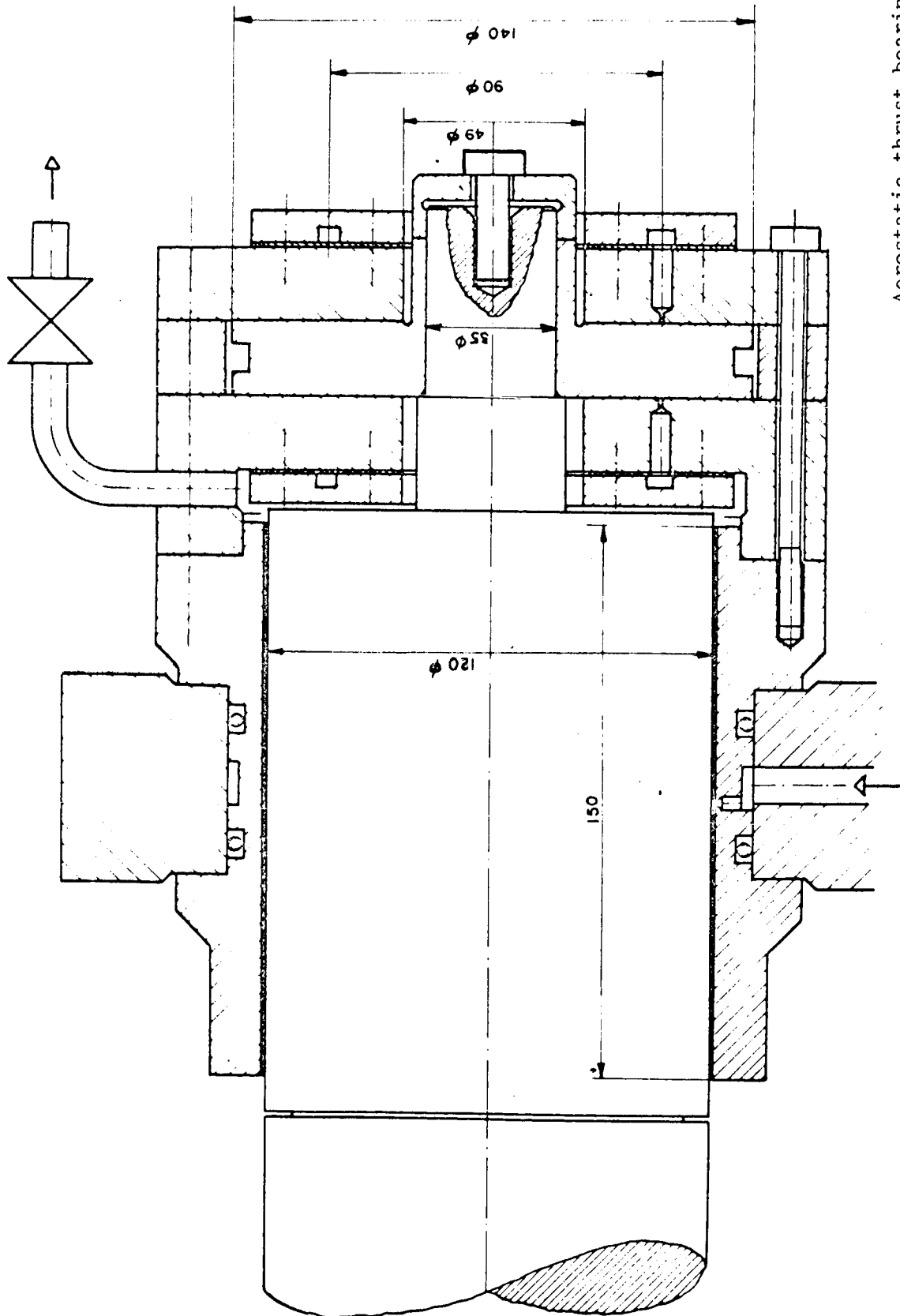large total free bearing space is selected, stability can be achieved.

C) As has already been pointed out in Chapter 16.4 C, only a small exter-
nal damping of friction is necessary in order to eliminate the instability
of the bearing. In the case of the radial compressor illustrated on p. 166
all that was required was a connection of the shaft to the gear by means of
a jaw clutch coupling.

Diagramm 32

Without gas feed

Same gas feed in h_I and h_{II}

Four stage radial compressor
on static air bearings

Data : V_1 = 4000 m³/s
P_2/P_1 = 3·5
P_1 = 1 ata
n = 12.500 u/min
N = 300 PS

BHS-Oberhausen: Gear
Type RP12
Nr 257 95 M

Aerostatic thrust bearing
of the compressor "Zurich 52"
with adjoining radial bearing.

Literature Cited.

| I | SCHLICHTING, H. | Boundary layer theory. Published by Braun, Karlsruhe, 1951. |

I   SCHLICHTING, H.   Boundary layer theory.
Published by Braun, Karlsruhe, 1951.

II   SOO, S.L.   Laminar Flow over an Enclosed
Rotating Disk.
Transactions of the ASME. Febr.1958

III   GRIGULL, U.   Fundamental laws of heat transfer.
Published by Springer, 1961.

IV   LICHT, L. and FULLER, D.D.   A Preliminary Investigation of an Air-Lubricated
Hydrostatic Thrust Bearing.
ASME Paper No 54-Lub-18

V   PIGOTT, J.D. and MACKS, E.F.   Air Bearing Studies
at Normal and Elevated Temperatures.
Lewis Flight Propulsion Laboratory, National Advisory Committee
for Aeronautics, Cleveland, Ohio

VI   OSTERLE, J.F. and HUGHES, W.F.
The Effect of Lubricant Inertia
in Hydrostatic Thrust-Bearing
Lubrication.
Wear, Vol.1 No 6, June 1958

VII   DEUKER, A. et WOJTECH, H.
Radial flow of a viscous liquid
between two discs which are very
close to each other. Theory of
the air bearing.
Revue générale de l'Hydraulique
No 65 Sept.- Oct. 1951

VIII   COMOLET, R.   Flow of a liquid between two
parallel planes. Contribution
to the study of air abutments.
Scientific and technical publications of the French Air
Department, No. 334, 1957.

IX   SHIRES, G.L.   The Viscid Flow of Air in a Narrow
Slot.
Aeronautical Research Council Current Paper No 13 (12329) 1950

X   LAUB, J.H.   Hydrostatic Gas Bearings.
Transactions of the ASME June 1960
Journal of Basic Engineering

XI   JAHNKE und EMDE   Function tables. Third edition.

XII   MEYER zur CAPELLEN   Integral tables.
Published by Springer, 1950

XIII   NAUMANN,   Degree of efficiency of diffusers.
Research report No. 1705, 1942.
Aerodynamic Institute of the Technical
University, Aachen,(West Germany)

XIV   LAUB, J.H.   Elastic Orifices for Gas Bearings.
Transactions of the ASME Dec. 1960
Journal of Ba-sic Engineering

XV   POTET, P.   Filters of sintering metal.
Technische Rundschau Nr. 12, 1960

XVI   HUGHES,W.F. and OSTERLE,J.F.
Heat Transfer Effects in Hydrostatic
Thrust Bearing Lubrication.
Transactions of the ASME No 6 Aug. 1957

XVII   LICHT,L., FULLER,D.D. and STERNLICHT,B.
Self-Exited Vibrations of an Air-
Lubricated Thrust Bearing.
Transactions of the ASME. Febr. 1958

XVIII   ROUDEBUSH, W.H.   An Analysis of the Effect of Several
Parameters on the Stability of an
Air-Lubricated Hydrostatic Thrust
Bearing.
NACA Technical Note 4095

XIX   RICHARDSON,H.H.   Static and Dynamic Characteristics
of Compensated Gas Bearings.
Transactions of the ASME. Oct. 1958

XX   LICHT,L.   Axial, Relative Motion of a Circular
Step Bearing.
Transactions of the ASME. June 1959
Journal of Basic Engineering

XXI   LICHT,L.   Air-Hammer Instability in Pressurized-
Journal Gas Bearings.
ASME Paper No. 60 - WA-10

XXII   LICHT,L. and ELROD,H.
A Study of the Stability of Externally
Pressurized Gas Bearings.
Transactions of the ASME. June 1960
Journal of Applied Mechanics

XXIII   GOTTWALD,F. und VIEWEG,R.
Calculations and model experiments
in water- and air bearings.
Zeitschrift für Angewandte Physik
2.Bd. Heft 11, 1950

XXIV   BETZ, A.   Conformal mapping.
Springer Verlag Berlin, 1948

XXV   MILNE-THOMSON,L.M. The elliptical functions of Jacobi.
Published by Springer, Berlin, 1931.

XXVI   DEN HARTOG,J.P.   Mechanical Vibrations.
Mc.Graw-Hill Publishing Company,Inc.
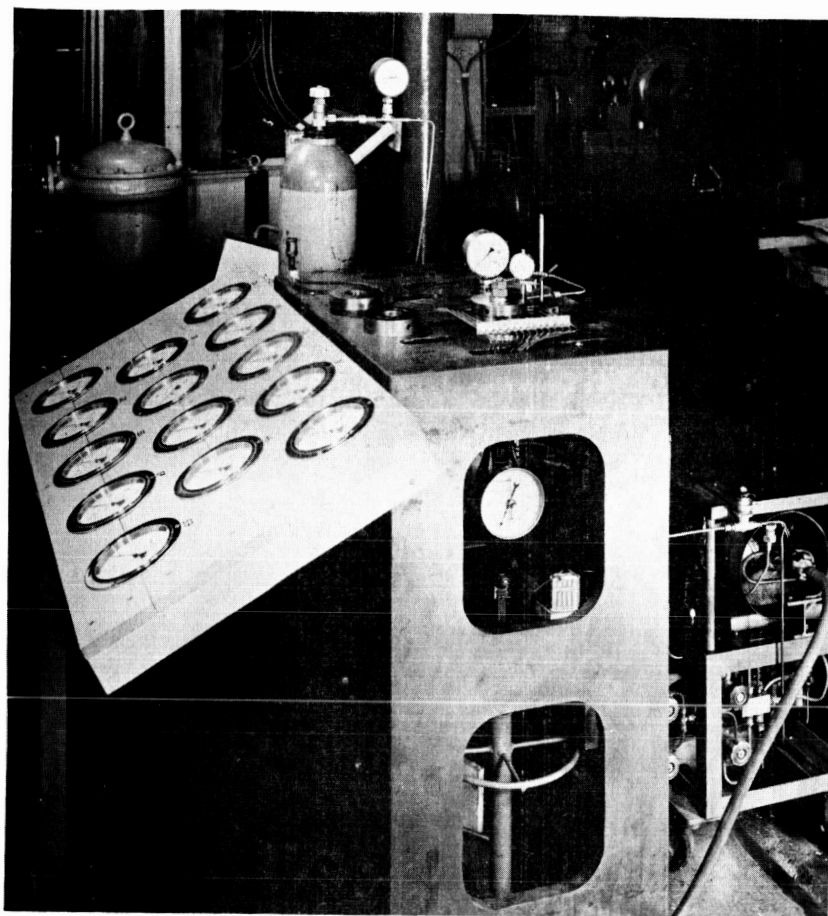New York III. Edition 1947

Fig. 1. Total view of the small testing apparatus for aerostatic thrust bearings. The experiments were performed in non-rotating discs. Loading device and measurement of the clearance are in the center of the picture. On the right: Bearing gas compressor; on the left: Instruments for measuring of the pressure distribution in the bearing clearance.
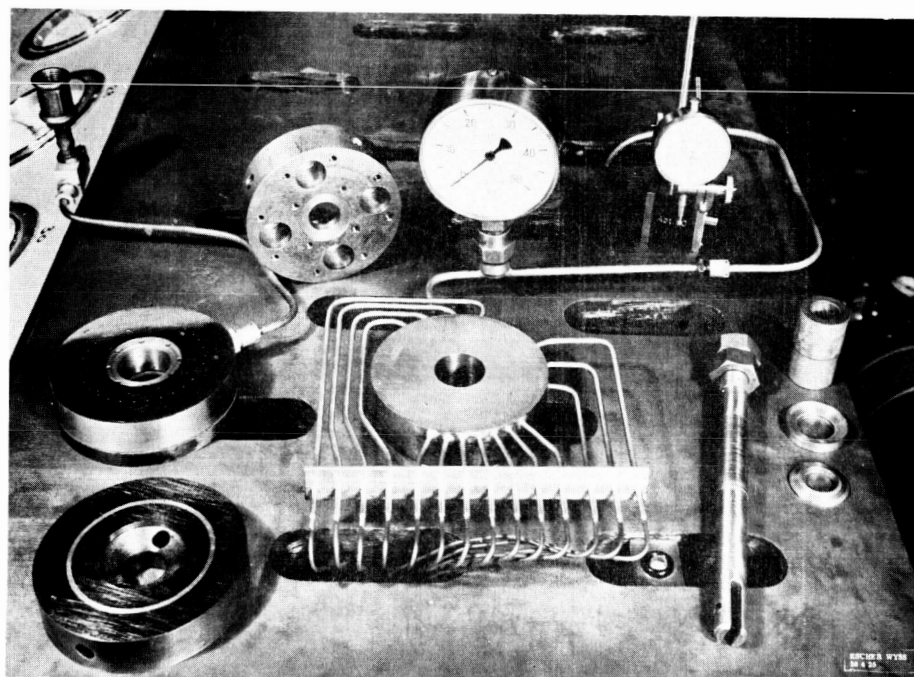

Fig. 2. Different bearing discs and accessories. Left front: Disc with pressure compensation space (annular channel). Center: Discs with 4 and 20, respectively, feeding nozzles. Left back: Stationary disc in back-view with the lid removed and 4 resonator chambers.
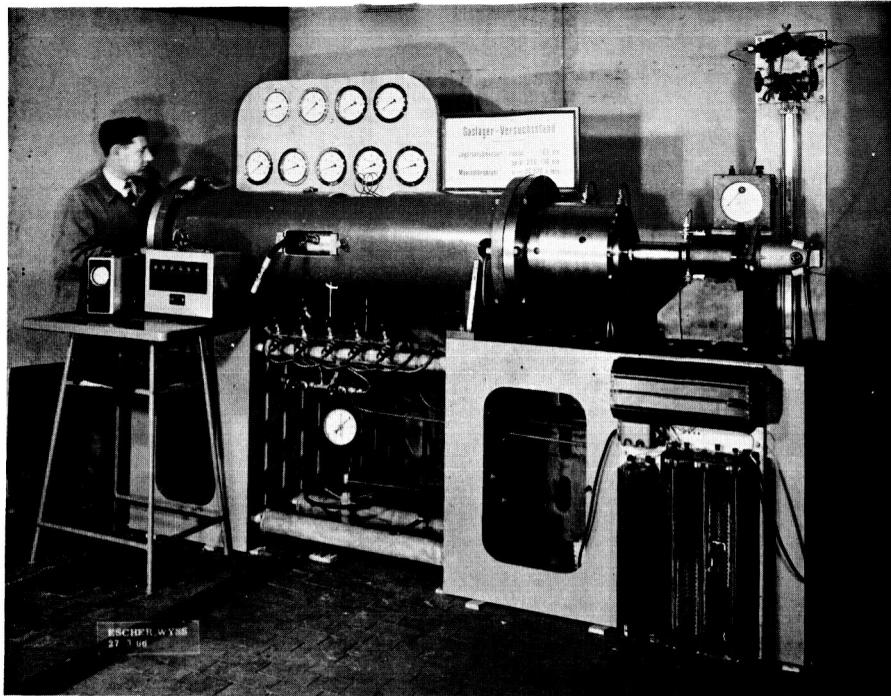
Fig. 3. Large testing apparatus for aerostatic and aerodynamic bearings.
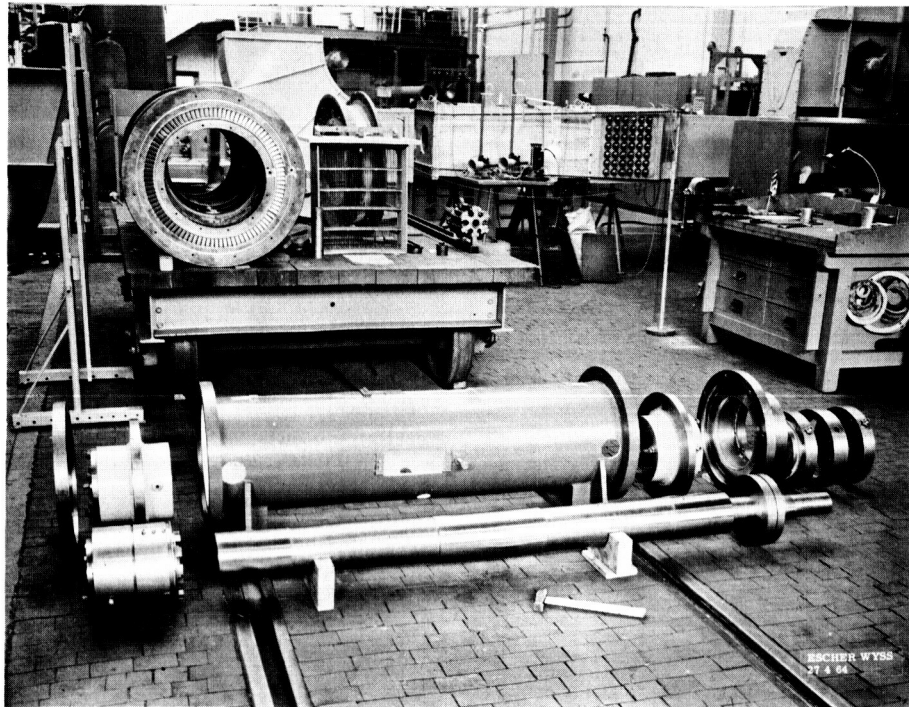
Fig. 4. Individual components of the testing apparatus.
Front: Shaft with thrust bearing disc (weight approx. 400 kp).
Center: Casing of the testing apparatus.
Left: Movable and fixed radial bearing.
Right: Fixed radial bearing and all axial discs.

Fig. 5. View of the side of the thrust bearing and the driving elements. Left back: High pressure Hg manometer for measuring the pressure distribution in the bearing clearance.
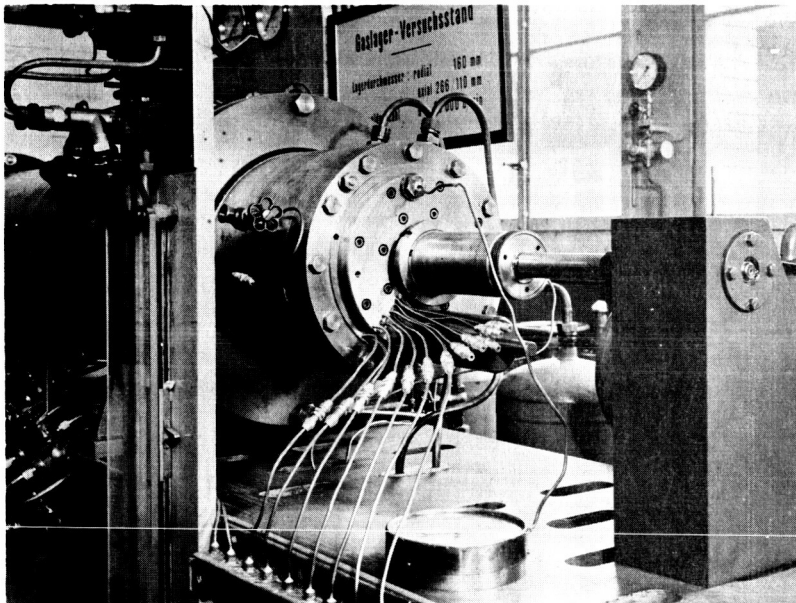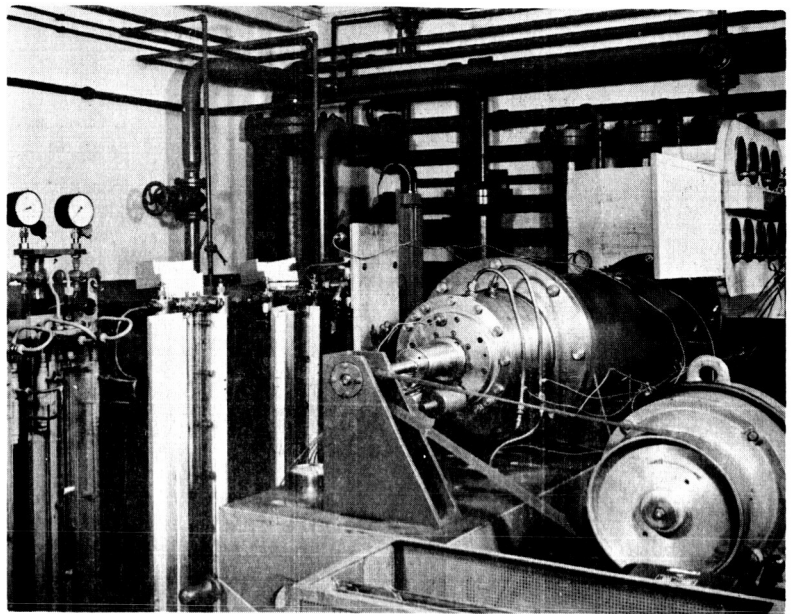

Fig. 6. View of the side of the thrust bearing. Left back: Valves for the admission of compressed air. Left front: High pressure difference manometer for measuring the amount of throughput. Front center: connections of the 12 measuring pressure taps for determination of the pressure distribution.

Fig. 7. Thrust bearing disc with collet and nut on the shaft. In the back, fixed bearing disc with compressed air duct and feeding elements.
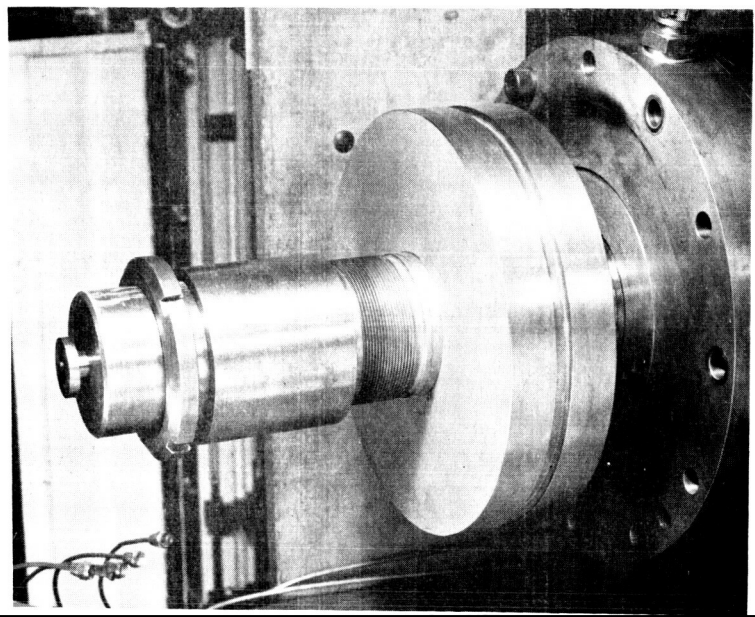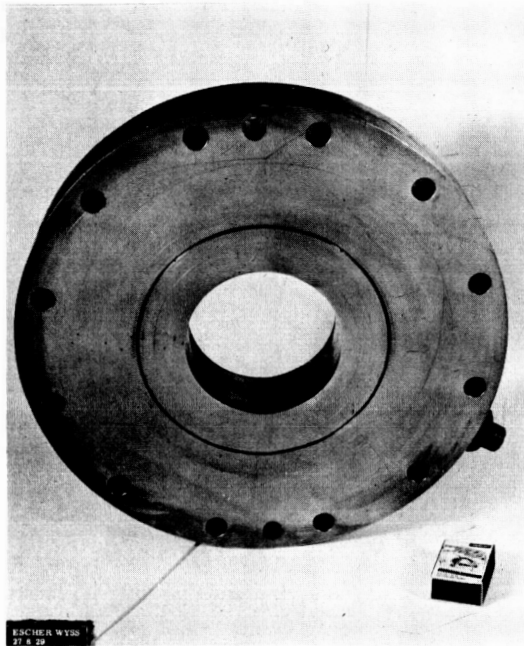
Fig. 8. Stationary bearing disc with annular channel. Twenty feeding nozzles and 12 measuring boreholes on different radii.
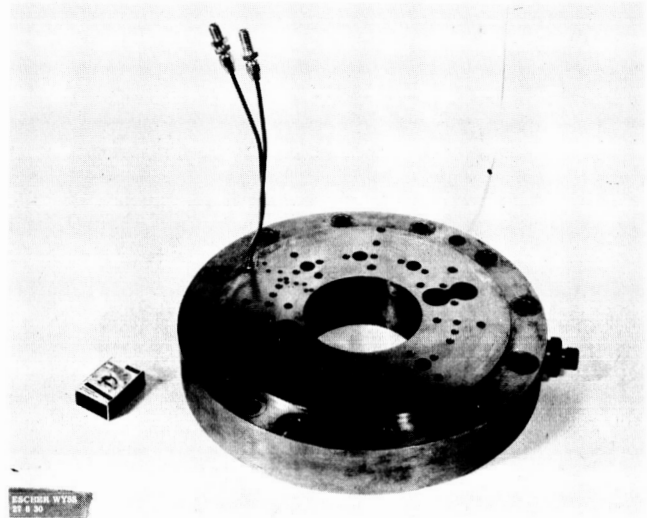

Fig. 9. Stationary bearing disc (back side) with the lid removed. The boreholes of the nozzles, the measuring connections and 10 resonators, equal in pairs, are clearly visible.
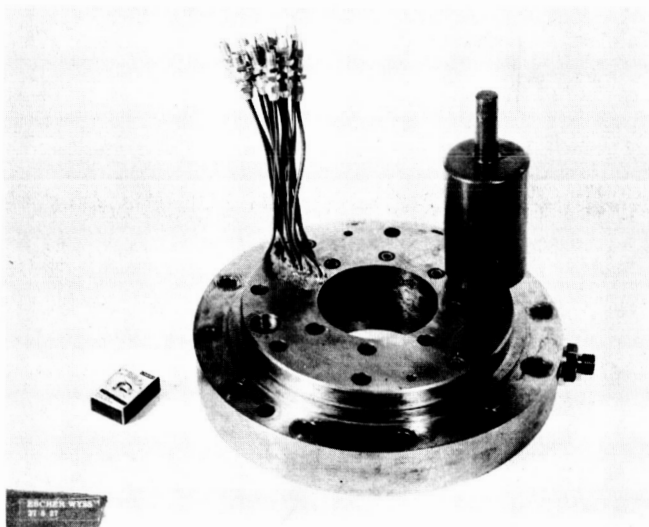

Fig. 10. Stationary bearing disc with mounted lid. Left: Connections of the pressure distribution measurement. Right: Resonator, arranged outside the disc for increasing the volum..

Fig. 11. Stationary and rotating bearing disc after mutual contact at 13,000 r. p. m. On account of thermal deformation, the damage occurred only on the interior portion of the bearing surface.
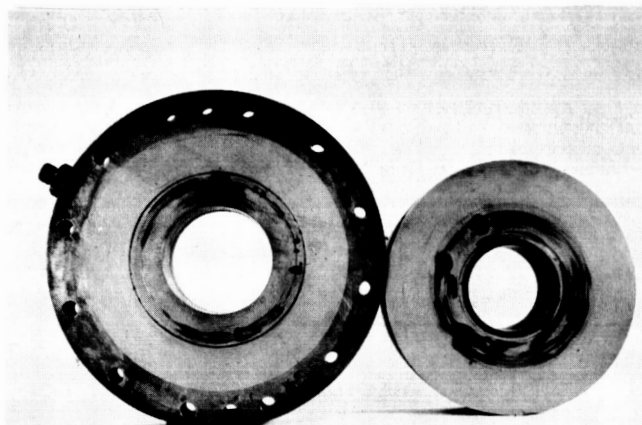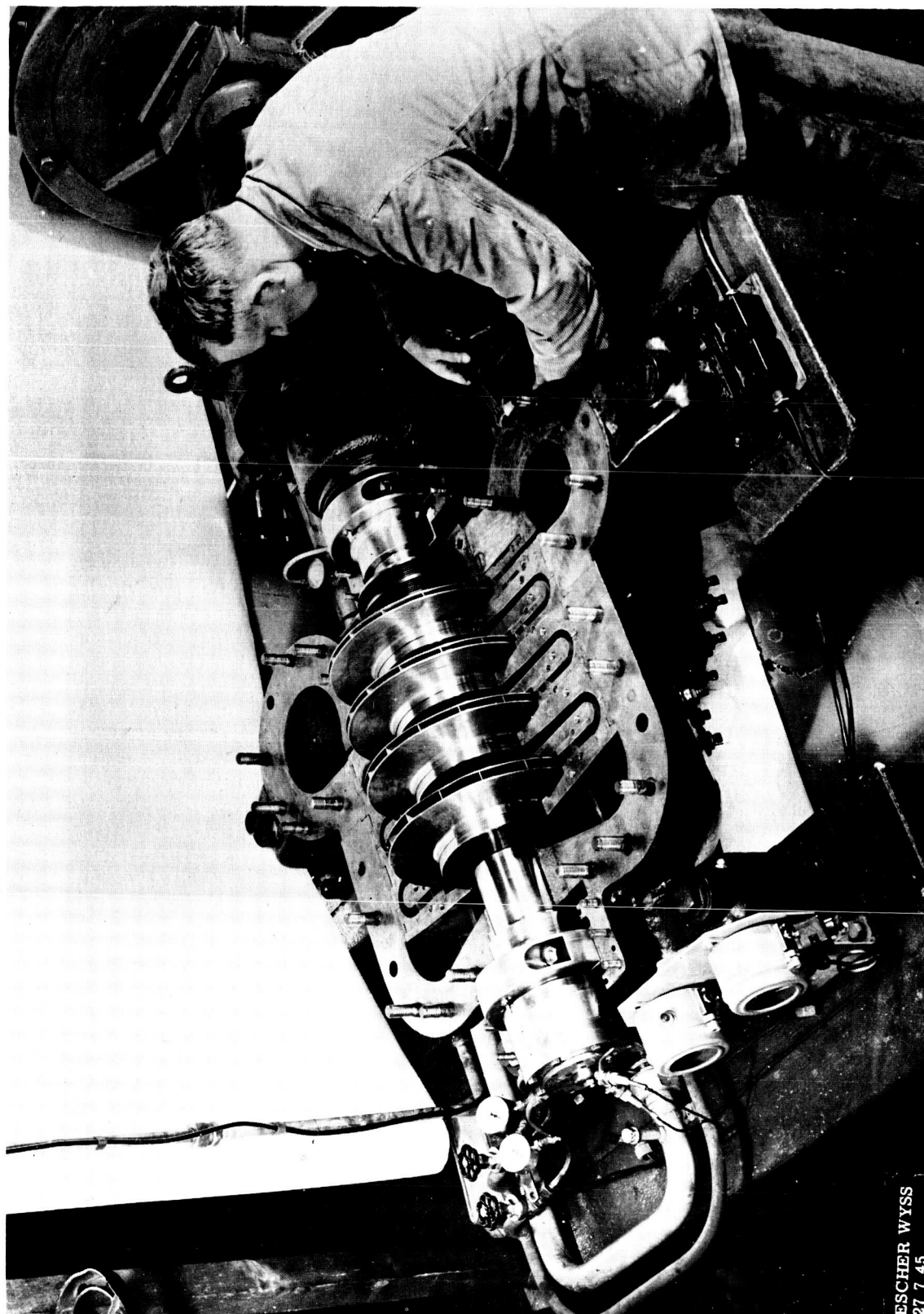
Fig. 12. Four-stage radial compressor "Zurich 52" rebuilt on static air bearings. The removed casing lid makes the rotor, the two radial bearings and, on the far left, the thrust bearing visible. Weight of the rotor: 165 kp (V_1 = 4000 m^3/hr, P_2/P_1 = 3.5, P_1 = 1 atmosphere (absolute), n= 12,500 r. p. m., N $\cong$ 300 HP).

ESCHER WYSS
27 7 45

DISTRIBUTION LIST

Chief of Naval Research
Department of the Navy
Washington 25, D.C.
Attn: Code 438 (3)
            429
            463

Commanding Officer
Office of Naval Research
Branch Office
495 Summer Street
Boston, Massachusetts 02110

Commanding Officer
Office of Naval Research
Branch Office
219 S. Dearborn Street
Chicago, Illinois 60604

Commanding Officer
Office of Naval Research
207 West 24th Street
New York, New York 10011

Commanding Officer
Office of Naval Research
London Branch Office
Box 39
Fleet 39
Fleet Post Office
New York, New York 09510 (25)

Commanding Officer
Office of Naval Research
Branch Office
1030 East Green Street
Pasadena 1, California

Commanding Officer
Office of Naval Research
Branch Office
1000 Geary Street
San Francisco 9, California

Office of Naval Research
Resident Representative
University of Pennsylvania
3636 Walnut Street
Philadelphia, Pennsylvania 19104

Chief, Bureau of Ships
Department of the Navy
Washington 25, D.C.
Attn: Code 305 (Dr. J. H. Huth)
            342 (E. A. Bukzin)
            644 C (R. M. Petros)
            1500 (J. A. Gorman)

Chief, Bureau of Naval Weapons
Department of the Navy
Washington 25, D. C,
Attn: Code RAPP-41 (S. M. Colligemna)
            RREN-4 (M. R. Walter)

Director
Naval Research Laboratory
Washington, D. C.
Attn: Code 2000
            5230 (6)

Special Projects Office
Department of the Navy
Washington 25, D. C.
Attn: Code SP230 (D. Gold)
            SP-001 (Dr. J. P. Craven)

Commanding Officer and Director
U. S. Navy Marine Engineering Laboratory
Annapolis, Maryland
Attn: Code 850
            852 (Watt V. Smith)

Material Laboratory Library
Building 291, Code 912B
New York Naval Shipyard
Brooklyn 1, New York

Superintendent
U. S. Naval Postgraduate School
Monterrey, California
Attn: Library, Technical Reports Section

Commanding Officer
U. S. Naval Avionics Facility
Indianapolis 18, Indiana
Attn: J. G. Weir

Commanding General
U. S. Army Materiel Command
Research & Development Directorate
Research Division
Washington, D. C. 20315
Attn: Mr. Norman L. Klein

Chief of Research and Development
Office of Chief of Staff
Department of the Army
Pentagon Building
Washington 25, D. C.

Commanding General
U. S. Army Engineer R&D Laboratories
Fort Belvoir, Virginia
Attn: W. M. Crim, Nuclear Power
        Field Office
        Technical Documents Center (2)

Commander
Army Rocket & Guided Missile Agency
Redstone Arsenal, Alabama
Attn: Technical Library

ESD - AROD
Box CM, Duke Station
Durham, North Carolina

a

Chief of Staff
U. S. Air Force
The Pentagon
Washington 25, D. C.
Attn: AFRDR-AS/M

Commander
Air Force Office of Scientific Research
Washington 25, D. C.
Attn: SRHM

Commander
Research and Technology Division
of the Air Force Systems Command
Wright-Patterson AF Base, Ohio
Attn: APEL (Mr. M. A. Sheets) (3)
      APIP-1 (B. L. McFadden, Jr.)
      AVNE (R. W. McAdory)
      FDEM (P. C. Hanlon)

Defense Documentation Center
Cameron Station
Alexandria, Virginia (20)

Mr. Clarence E. Miller, Jr.
Office of Assistant Director
(Army Reactors)
Division of Reactor Development
U. S. Atomic Energy Commission
Washington 25, D. C. (2)

Headquarters Library
U. S. Atomic Energy Commission
Washington 25, D. C.

U. S. Atomic Energy Commission
Oak Ridge Operations Office
P. O. Box E
Oak Ridge, Tennessee 37831
Attn: Charles A. Keller

U. S. Atomic Energy Commission
Portsmouth Area Office
Piketon, Ohio 45661
Attn: Dr. Malone

Chief, Division of Engineering
Maritime Administration
GAO Building
Washington 25, D. C.

Library
Cryogenic Engineering Laboratory
National Bureau of Standards
Boulder, Colorado

Director of Research, Code RR
National Aeronautics and Space Adm.
600 Independence Avenue
Washington, D. C. 20546

Scientific and Technical Information Facility
P. O. Box 5700
Bethesda, Maryland 20014
Attn: NASA Representative (SAK/DL) (2)

Mr. Edmund E. Bisson, Chief
Lubrication and Wear Branch
Lewis Research Center
National Aeronautics and Space Adm.
21000 Brookpark Road
Cleveland, Ohio

Mr. P. H. Broussard, Jr.
Gyro-Stabilizer Branch
Guidance and Control Division
National Aeronautics & Space Adm.
George C. Marshall Space Flight Center
Huntsville, Alabama (5)

Mr. H. W. Savage
Oak Ridge National Laboratory
Post Office Box Y
Oak Ridge, Tennessee

Chief, Technical Information Service Extension
Post Office Box 62
Oak Ridge, Tennessee
Attn: Melvin S. Day

Aerojet General Nucleonics
P.O. Box 86
San Ramon, California
Attn: Document Custodian

Aerospace Corporation
P.O. Box 95045, Los Angeles, California
Attn: Library, Reports Acquisitions Group

AiResearch Manufacturing Company
P.O. Box 5217
Phoenix, Arizona 85010
Attn: Mrs. J. F. Mackenzie, Librarian

American Institute of Aeronautics
and Astronautics
Technical Information Service
750 Third Avenue
New York, New York 10017

American Society of Lubrication Engineers
838 Bussee Highway
Park Ridge, Illinois 60068

Chairman
Research Committee on Lubrication
The American Society of Mechanical Engineers
United Engineering Center
345 East 47th Street
New York 17, New York (2)

Dr. W. A. Gross
Ampex Corporation
401 Broadway
Redwood City, California 94063 (2)

Mr. L. Licht
Department of Mechanical Engineering
Columbia University
New York, New York 10027

Mr. Stanley L. Zedekar
Department 244-2, Building 71
Autonetics
P. O. Box 4181
Anaheim, California 92803

C. D. Flanigen
Director of Engineering
Lycoming Division, AVCO Corporation
Stratford, Connecticut

Dr. Russell Dayton
Battelle Memorial Institute
505 King Avenue
Columbus 1, Ohio

Mr. Ralph H. Larson
Research Laboratories Division
Bendix Aviation Corporation
Southfield, Michigan

Walt Tucker
Nuclear Engineering Department
Brookhaven National Laboratory
Upton, Long Island, New York

Jet Propulsion Laboratory
California Institute of Technology
4800 Oak Grove Avenue
Pasadena, California
Attn: Library

Dr. F. Osterle
Mechanical Engineering Dept.
Carngie Institute of Technology
Pittsburgh, Pennsylvania 15213

Proffessor M. C. Shaw, Head
Department of Mechanical Engineering
Carnegie Institute of Technology
Pittsburgh, Pennsylvania 15213

Dr. W. T. Sawyer
Department of Mechanical Engineering
Catholic University
Washington, D. C.

Mr. C. W. Synder, Manager of Engineering
Defense Engineering
Defense Operations DIVISION
Chrysler Corporation
P. O. Box 757
Detroit, Michigan 48231

Robert H. Josephson, Manager
Commercial Development
Clevite Corporation
Mechanical Research Division
540 East 105th Street
Cleaveland, Ohio 44108

Professor V. Castelli
Department of Mechanical Engineering
Columbia University
New York, New York 10017

Professor H. Elrod
Department of Mechanical Engineering
Columbia University
New York, New York 10017 (2)

Mr. Gerald B. Speen
Division Manager
Conductron
P.O. Box 844
Northridge, California

Mr. J. W. Lower, Chief
Engineer-Inertial Components
Honeywell Aero Division
2600 Ridgway Road
Minneapolis, Minnesota

Mr. J. Levine
Ford Instrument Company
31-10 Thomson Avenue
Long Island City 1, New York

Mr. Adolf Egli
Ford Motor Company
Engineering and Research Staff
P.O. Box 2053
Dearborn, Michigan

Dr. John E. Mayer, Jr.
Applied Research Office
Research and Engineering Center
Ford Motor Company
P.O. Box 2053
Dearborn, Michigan

Professor D. D. Fuller
Laboratories for Research and Dveelopment
The Franklin Institute
Philadelphia, Pennsylvania (3)

Mr. Jerry Glaser
Senior Project Engineer (Dept. 37)
AirResearch Manufacturing Division
The Garrett Corporation
9851 S. Sepulveda Boulevard
Los Angeles, California

Library
General Atomic Division
General Dynamics Corporation
P.O. Box 608
San Diego, California 92112

Mr. G. R. Fox, Manager
Bearing and Lubricant Center
General Engineering Laboratory
General Electric Company
1 River Road
Schenectady, New York

Mr. C. C. Moore, Specialist
Advanced Bearing & Seal Technology
ARADC-AETD, H-55
General Electric Company
Flight Propulsion Division
Cincinnati 15, Ohio

Mr. E. Roland Maki
Mechanical Development Department
Research Laboratories
General Motors Corporation
General Motors Technical Center
12 Mile and Mound Roads
Warren, Michigan

Mr. Walter Carow
Kearfott Division
General Precision Incorporated
1150 McBride Avenue
Little Falls, New Jersey

Mr. David Craig, Jr.
Mechanical Design Section
Grumman Aircraft Engineering Corporation
Bethpage, Long Island, New York

Hydronautics, Incorporated
Pindell School Road
Howard County
Laurel, Maryland

Professor L. N. Tao
Illinois Institute of Technology
Chicago 16, Illinois

Mr. Stanley Abramovitz, Director
Industrial Tectonics, Inc.
Fluid Film Bearing Division
New South Road and Commercial Street
Hicksville, Long Island, New York

Dr. W. E. Langlois
International Business Machines Corporation
Research Laboratory
San Jose, California

The Johns Hopkins University
Applied Physics Laboratory
8621 Georgia Avenue
Silver Spring, Maryland
Attn: Fenton L. Kennedy

Mr. B. A. Napier
Director of Engineering
Lear Siegler, Inc.
Power Equipment Division
P.O. Box 6719
Cleveland 1, Ohio

Mr. R. C. Blaylock
Vice President - Technical Director
Ling-Temco-Vought, Inc.
P. O. Box 5003
Dallas, Texas

Dr. J. S. Ausman
Litton Systems, Inc.
5500 Canoga Avenue
Woodland Hills, California   (2)

Mr. Don Moors
Litton Systems
5500 Canoga Avenue
Woodland Hills, California   (2)

Lockheed Aircraft Corporation
Missiles and Space Division
Technical Information Center
3251 Hanover Street
Palo Alto, California

Massachusetts Institute of Technology
Instrumentation Laboratory
68 Albany Street
Cambridge, Massachusetts 02139
Attn: Library, IL1-109

Dr. R. W. Mann (Room 3-459A)
Engineering Projects Laboratory
Massachusetts Institute of Technology
Cambridge 39, Massachusetts

Professor Herbert H. Richardson
Room 3-461
Massachusetts Institute of Technology
Cambridge 39, Massachusetts

McDonnell Aircraft Corporation
Post Office Box 516
St. Louis, Missouri 63166
Attn: Library, Dept. 218

Dr. Beno Sternlicht
Mechanical Technology Incorporated
968 Albany-Shaker Road
Latham, New York   (3)

Mr. Carl F. Graesser, Jr.
Director of Research
New Hampshire Ball Bearings, Inc.
Peterborough, New Hampshire

Professor A. Charnes
The Technological Institute
Northwestern University
Evanston, Illinois

Mr. R. A. Minard
Assistant Product Manager
Gas Bearing Technology Div. MPB Inc.
Precision Products Division
Keene, New Hampshire

Mr. E. L. Swainson, Chief of Research
Precision Products Department
Nortronics
A Division of Northrop Corporation
100 Morse Street
Norwood, Massachusetts

Northrop Norair
3901 W. Broadway
Hawthorne, California 90250
Attn: Technical Information 3924-32

Professor P. R. Trumpler
Towne School of Civil and Mechanical
Engineering
University of Pennsylvania
Philadelphia, Pennsylvania

Mr. Ralph A. Lowry
Research Laboratories
For Engineering Sciences
University of Virginia
Charlottesville, Virginia

Radio Corporation of America
Camden 2, New Jersey
Attn: Library, Building 10-2-5

Mr. Robert S. Siegler
Rocketdyne
Nucleonics Subdivision
6633 Canoga Avenue
Canoga Park, California

Dr. Ralph A. Burton
Southwest Research Institute
San Antonio, Texas

Mrs. Florence Turnbull
Engineering Librarian
Sperry Gyroscope Company
Great Neck, New York

W.G. Wing
Sperry Gyroscope Company
2T120
Great Neck, New York

Mr. O. Decker
Thomson Ramo Wooldridge
TAPCO Group
New Devices Laboratory
7209 Platt Avenue
Cleveland 4, Ohio

Union Carbide Nuclear Company
Division of Union Carbide Corporation
P.O. Box P
Oak Ridge, Tennessee 37831
Attn: R. G. Jordan

Professor J. Modrey
Department of Mechanical Engineering
Purdue University
Lafayette, Indiana

Ralph F. DeAngelias, Technical
Librarian
Norden Division of United Aircraft Corp.
Helen Street
Norwalk, Connecticut 06852

Unidynamics/St. Louis Division Library
Universal Match Corporation
472 Paul Avenue
St. Louis, Missouri 63135

Mr. J. M. Gruber, Ch. Engrg.
Waukesha Bearings Corporation
P. O. Box 798
Waukesha, Wisconsin

John Boyd
Westinghouse Research Laboratories
Churchill Boro
Pittsburgh, Pennsylvania 15235

Mr. H. Walter
Vice President - Research & Development
Worthington Corporation
Harrison, New Jersey

Dr. Calus G. Goetzel, D/52-30
Bldg. 201, Plant 2, Palo Alto
Lockheed Missiles & Space Company
P. O. Box 504
Sunnyvale, California

Mr. Egar J. Gunter, Jr.
University of Virginia
School of Engineering &
Applied Science
Charlottesville, Virginia 22903

General Dynamics/Convair
P.O. Box 1128
San Diego, California 92112
Attn: Library & Information Services (126-00)

Science & Technology Division
Library of Congress
Washington, D. C. 20540

Admiraldy Compress Observatory
Ditton Park
Slough, Bucks, England
Attn: Mr. Henri J. Elwertowski

The University of Southampton
Department of Mechanical Engineering
Southampton, England
Attn: Dr. H. S. Grassam

Mr. N. Grossman, Chief
Engineering Development Branch
Reactor Development Division
US Atomic Energy Commission
Washington 25, D. C. (2)